INTERACTIONS AT THE HEAD-TAPE INTERFACE OF A LINEAR TAPE SYSTEM

MARK ANDREW WILD

Doctor of Philosophy

THE UNIVERSITY OF ASTON IN BIRMINGHAM

August 2001

Interactions at the Head-Tape Interface of a Linear Tape System

MARK ANDREW WILD

Doctor of Philosophy

August 2001

SUMMARY

Many of the recent improvements in the capacity of data cartridge systems have been achieved through the use of narrower tracks, higher linear densities and continuous servo tracking with multi-channel heads. These changes have produced new tribological problems at the head/tape interface. It is crucial that the tribology of such systems is understood and this will continue since increasing storage capacities and faster transfer rates are constantly being sought.

Chemical changes in the surface of single and dual layer MP tape have been correlated to signal performance.

An accelerated tape tester, consisting of a custom made cycler ("loop tester"), was used to ascertain if results could be produced that were representative of a real tape drive system. A second set of experiments used a modified tape drive (Georgens cycler), which allowed the effects of the tape transport system on the tape surface to be studied. To isolate any effects on the tape surface due to the head/tape interface, read/write heads were not fitted to the cycler.

Two further sets of experiments were conducted which included a head in the tape path. This allowed the effects of the head/tape interface on the physical and chemical properties of the head and tape surfaces to be investigated. It was during the final set of experiments that the effect on the head/tape interface, of an energised MR element, was investigated.

The effect of operating each cycler at extreme relative humidity and temperature was investigated through the use of an environmental chamber.

Extensive use was made of surface specific analytical techniques such as XPS, AFM, AES and SEM to study the physical and chemical changes that occur at the head/tape interface.

Results showed that cycling improved the signal performance of all the tapes tested. The data cartridge drive belt had an effect on the chemical properties of the tape surface on which it was in contact. Also binder degradation occurred for each tape and appeared to be greater at higher humidity. Lubricant was generally seen to migrate to the tape surface with cycling. Any surface changes likely to affect signal output occurred at the head surface rather than the tape.

Key Words: Tribology, Linear, Metal Particle, Magneto-Resistive Magnetic Recording.

Acknowledgements

Thank you to my supervisor, Professor Sullivan for his support in both personal and work related matters.

I would also like to thank Imation for supporting the project financially and by supplying the test drives and media samples. I would particularly like to thank Mike Sharrock and the Imation team for helpful discussions throughout the project.

Thank you to Dr. Sayah Saied for her help in the Esca Lab, Mathew Harrisson for his help in the AFM lab and particularly to Andy Abbot, a technician whose time and effort ensured that the project kept on track.

Special thanks must go to Dr. Mike Hempstock the research assistant assigned to co-ordinate the project. His advice and assistance were invaluable throughout the project.

Finally thank you to my partner Jill Collins for support and assistance throughout the project.

Contents

List of Figures

List of Tables

Glossary of Acronyms

ABS	Air Bearing Surface
ADR	Advanced Digital Recording
AES	Auger Electron Spectroscopy
AFM	Atomic Force Microscopy
ATOMM	Advanced super Thin layer high Output Metal Media
BOT	Beginning Of Tape
CPV	Critical Pigment Volume
DDS	Digital Data Storage
DWT	Double-layered Web Tensioned
EOT	End Of Tape
GMR	Giant Magneto-Resistive
HCA	Head Cleaning Agent
HDMR	High Density Magnetic Recording
IMFP	Inelastic Mean Free Path
ME	Metal Evaporated
MIG	Metal In Gap
MP	Metal Particle
MR	Magneto-Resistive
PTR	Pole Tip Recession
QIC	Quarter Inch Cartridge
SEM	Scanning Electron Microscopy
XPS	X-ray Photoelectron Spectroscopy

CHAPTER 1 Subject Background/Literature review

1.1 Introduction

In the competitive personal computer market, much emphasis is placed on the capacity of the hard drive. The Internet boom has led to an unprecedented demand for increased storage capacities on PC's[1]. Data intensive software programmes and applications such as films, music and high resolution photos are today commonplace. The capacity of the largest commercially available hard drive was until recently at 40 GB, but a 75 GB drive was released, both drives are manufactured by IBM. As hard drive capacities increase so to does the need for a high-density back-up media ideally at low cost. Tape technology remains the most efficient and cost-effective means to back up a system, whether it's for a personnel user, small business or global operation[2].

C.D.Mee[3] states that, the attributes of storage capability, at very high density in practical environments, combined with continuously lower cost, allowed magnetic recording media to be seen as the ideal storage vehicle in analogue and digital recording applications in both consumer and data storage arenas.

The main application of data cartridge tape drives is the backing-up of data from computer hard drives. It is essential that the storage capacity of a single tape cartridge is greater than, or at the very least equal to, the capacity of the latest hard drives. This has been achieved to date by the use of narrower track widths, higher linear densities and by using multi-channel heads. A further way of increasing capacity is to make the tape thinner so that a greater amount will fit into the cartridge, however this has its limitations since the tape becomes more fragile and thus more likely to deform/break as its thickness decreases.

As recording densities increase, the tribological contact problems inherent in data cartridges, will be the crucial factors if further substantial increases are to be made. It is therefore essential to fully understand and improve the tribology of the system.

The main area of concern in high-density magnetic recording (HDMR) is minimising the head/tape spacing, since too great a space would lead to signal loss and errors. The tribology

of the head/tape interface is such that spacing can increase automatically during running through various processes, including

- Pole Tip Recession (PTR) wear which occurs through differential wear rates of head materials
- Head stain occurs as a result of transferred tape material, which can also be loose causing unpredictable increases in the head/tape spacing.

The aim of this project was to study the tribological effects of cycling magnetic tape against a magnetic recording head using quarter inch data cartridges (QIC's) loaded with particulate tape. The effects of temperature and humidity on the head /tape interface were also studied.

1.2 Magnetic Recording Theory

It has been known since 1831 that a current carrying coil will induce lines of magnetic flux in a suitable material placed within the coil. At the same time, it was proven that it was possible to detect a current induced in a coil of wire, due to the rate of change of magnetic lines of flux. This simple experiment is the basis for the recording and reading of information using a magnetic medium.[4,5,6,7,8,9,10,11]

1.2.1 General Magnetic Recording Principles

The aim of the magnetic recording process is to record an electrical signal onto a magnetic medium. This is achieved using a transducer, which in magnetic recording systems is called the head. A basic inductive head is designed as in Figure 1.1, where the ring core is effectively an electromagnet.

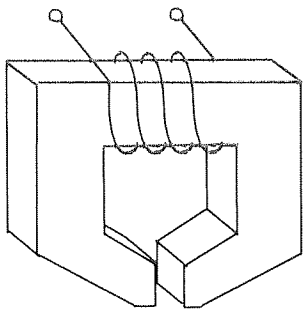

Figure 1.1 Ring Core Magnetic Recording Head.

When current flows through the coil, it induces lines of magnetic flux in the head core, which acts as a guide path for the flux lines. Introducing the gap has the effect of disrupting the flow of the lines of flux which then have to jump the gap, giving rise to a fringing field.

This fringing field present at the gap is well defined, and will leave a remanent magnetisation, M_r , in a suitable media placed within it. With the media moving through the fringing field at constant velocity, a current which is variations in magnitude of a signal with respect to time, is transformed into variations in magnitude with respect to distance, along the medium. The remanent magnetisation is directly proportional to the original signal and therefore allows the signal to be recovered, i.e. read by the same or another head.

During the read process, the lines of flux from the remanent magnetisation in the passing medium move through the head and induce a voltage in the coil. This voltage (or pulse) is

representative of the original signal allowing the written information to be retrieved. The shape of the pulse is characterised by the PW_{50} value and is defined as the width of the pulse at half the maximum amplitude.

Figure 1.2 shows how pulses vary with the magnitude of the fringing field, the depth to which the field penetrates the media effects the width and height of the pulse.

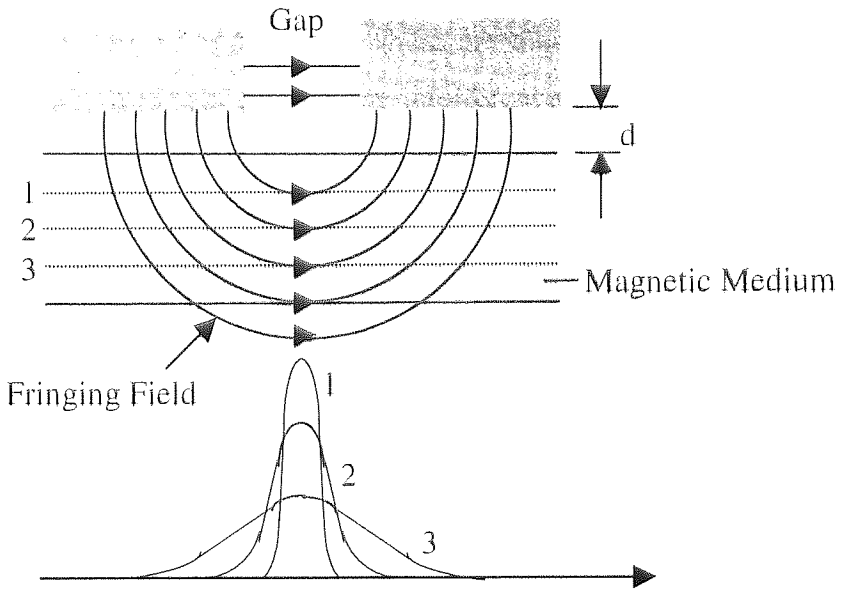

Figure 1.2 Dependance of the output pulse shape on the magnitude of the fringing field depth

Information stored on the media is in the spatial domain, and has a characteristic wavelength λ, the current signal is in the time domain and has a characteristic frequency, f. The two domains are related by equation 1.1:-

$$V = f\lambda \qquad 1.1$$

V - relative head/medium velocity

If the pulse is considered as a bit of information then it is obvious that for high recording densities the pulse should be as narrow as possible. The transition between pulses should ideally be sharp with no overlap occurring. It is advantageous for a system to produce a large output voltage during playback so that the transitions are easily identified. In reality, the parameters associated with the head geometry along with the magnitude of the signal current, place restrictions on the sharpness of the transitions and pulse widths. For an inductive ring head, the PW_{50} value is given by equation 1.2.

$$PW_{50} = 2\sqrt{d(d+\delta)} \qquad 1.2$$

Where

d = Head-media spacing

δ = Media thickness

The head-media separation and media thickness must be kept to a minimum for a narrow PW_{50} value and hence higher data density.

Noise will be inherent in the written signal. There are many factors that contribute toward this, such as head noise, cross talk (defined as interference either between adjacent bits or between adjacent tracks) and electrical circuit noise (collectively termed system noise). Limited smoothness of the tape surface will result in variation of the head to tape spacing whilst non-perfectly distributed magnetic particles in the magnetic layer can contribute to tape noise[12]. It is essential to have a large signal output compared to this system noise. A measure termed the signal to noise ratio (SNR) is used to quantify this. The SNR of a system is of prime importance and is one of the limits to the density at which information can be stored in a magnetic medium[13].

1.2.2 Head/Media Magnetic Properties

To optimise the performance of a system, the head and media must be manufactured with specific properties particular to their roles within the system. Properties relevant to magnetic recording materials can be determined from the B-H hysteresis loop of a material (Figure 1.3).

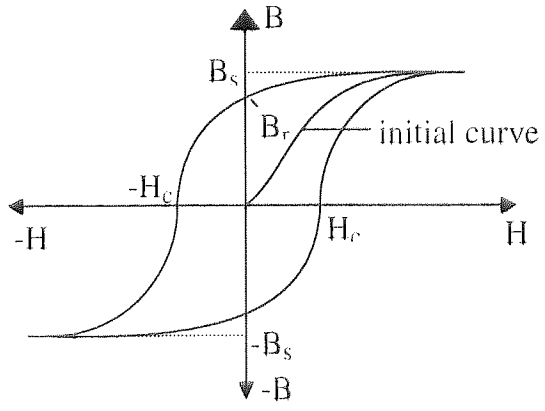

Figure 1.3 B-H hysteresis Loop

A magnetic material will, when subjected to an external magnetic field of strength H, have a B-H hysteresis loop similar to that in Figure 1.3. For an unmagnetised sample, the flux

density B, will increase with the applied magnetic field H, until the saturation flux density, B_s is reached. This is the maximum flux density that a magnetic material will sustain, before an increase in the applied field has no further effect.

The flux that remains when the field is reduced to zero is known as the remnant flux, B_r or remanence. To reduce the flux density back to zero the magnetic field must be applied in the reverse direction. The field strength required to do this is known as a materials coercivity H_c.

A media material requires high remanence (to provide a good read signal), it would be ideal if it retained the saturated value B_S. A media material's ability to retain magnetisation is expressed by the parameter s^*, its squareness ratio. This is the ratio of remanent flux density to saturation flux density B_r/B_s, which would ideally be 1. For a media to be overwritten it is necessary to remove the existing signal, so its coercivity should be low enough for the head to achieve this but high enough so that stray magnetic fields do not erase the stored data.

The following properties are desirable in magnetic media, and heads.

Media

High coercivity, so that stray magnetic fields do not corrupt the recorded data.

High remanence, so that a large amount of flux is available to provide a good play back signal.

Head

For the writing process, a high saturation flux density, B_s, is desirable so that the magnetic media saturates before the head itself.

For reading, the initial permeability should be large. Materials with a high permeability will produce a substantial increase in lines of flux and hence a higher induced current.

Low coercivity, so that changes in the media's magnetisation can be followed quickly.

A suitable head material would produce a narrow hysteresis loop with steep initial curve and is classed as a soft magnetic material. A wide hysteresis loop indicates a hard magnetic material from which a media would ideally be manufactured (Figure 1.4).

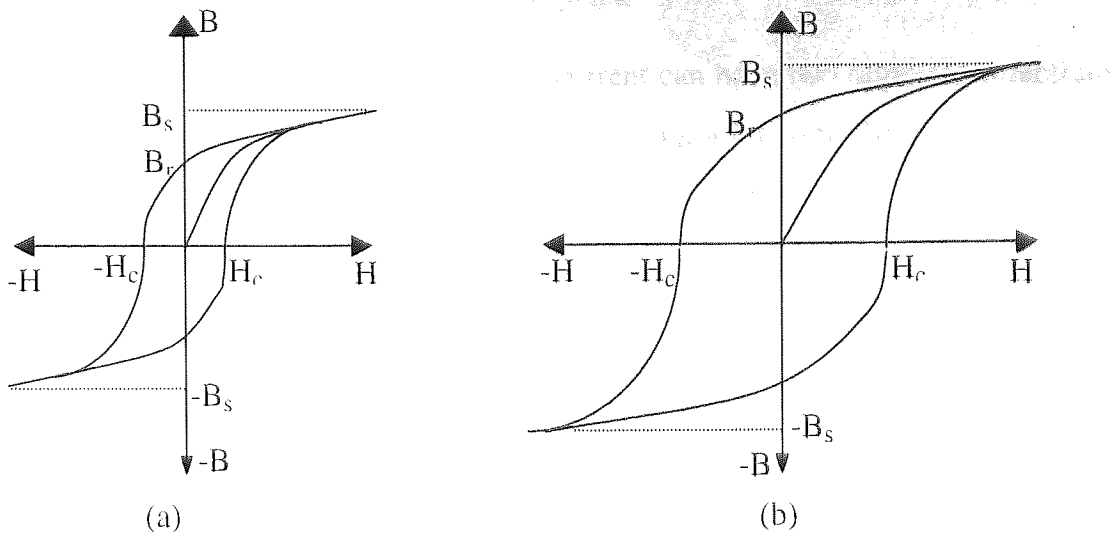

Figure 1.4 B-H Loops for (a) Soft and (b) Hard Magnetic Materials

1.2.3 Modes of recording

There are two modes for the recording of information, these are analogue and digital. Analogue involves the recording, and reading of a continuous input signal waveform. When the media approaches the head gap it encounters a field of increasing strength. As it passes over the gap, the magnetisation within the particles of the media flips backwards and forwards according to the direction of the saturated field.

Digital recording involves the handling of discrete units of information. The magnetisation process in this mode of recording involves complete saturation of the media. This method results in one of two well-defined states of opposing magnetisation, which naturally leads to the use of binary systems for handling this information. Each binary digit is equal to one bit of information, with eight bits being termed a byte. Each bit must be recognised and interpreted as a direction of magnetisation, Figure 1.5 illustrates the read process.

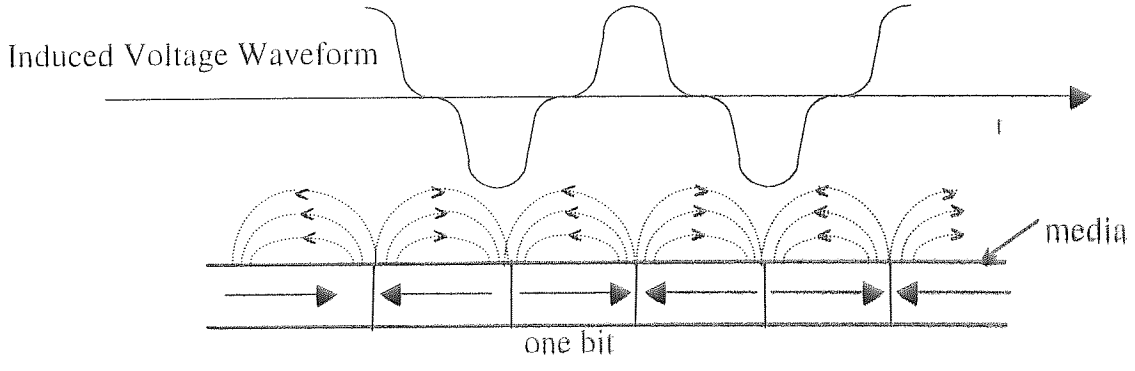

Figure 1.5 Induced Voltage Waveform

Writing is achieved by using the fact that the write current can have two opposing directions. Reading of the stored information is achieved by recognising a bit from the induced voltage waveform, which is related to the rate of change of flux by equation 1.3.

$$v = -N\frac{d\phi}{dt} \qquad 1.3$$

Where

v - Induced voltage

N - number of turns in the coil

$\frac{d\phi}{dt}$ - Rate of change of flux

The type of recording described by Figure 1.5 is known as longitudinal, where the magnetisation lies in the plane of the media, and in the direction of motion. Here an obvious problem is that opposing bits, like opposing magnets, will tend to demagnetise each other, also the transition region between bits is broadened such that the transitions between bits of information are not sharp.

A further demagnetising field (H_d) is present within the media. This is as a result of lines of flux travelling from north to south, not only do they exist externally, but also internally.

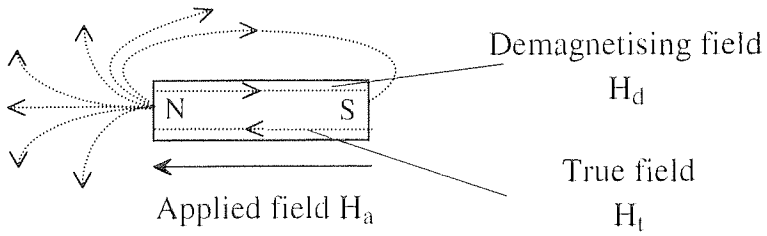

Figure 1.6 Internal Demagnetising Field

The true field H_t is related to the applied field H_a and demagnetising field H_d as follows,

$$H_t = H_a - H_d \qquad 1.4$$

Where

$$H_d = NM_r \qquad 1.5$$

Here M_r is the remanent magnetisation and N is the demagnetisation factor, which takes different values for different shapes (Figure 1.7).

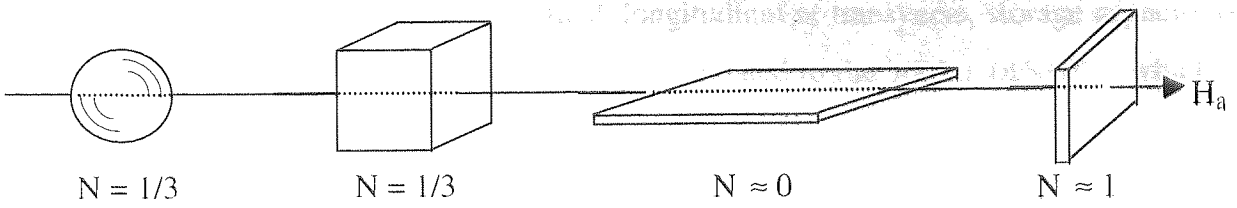

Figure 1.7 The Demagnetisation Factor For Different Shapes

H_d not only increases as M_r increases, but also as wavelength decreases, the result of which is a decrease in M_r's effectiveness[14]. So a large H_c media is also required to counteract H_d at short wavelengths. It is obvious from Figure 1.7 that the material chosen to retain magnetically recorded information should have a high length to height ratio to reduce demagnetisation. Acicular (needle shaped) Fe particles have proved themselves suitable for this purpose[15].

There are two additional types of recording, transverse and vertical/perpendicular. Transverse recording is where the magnetisation lies in the plane of the media, but perpendicular to the direction of motion. This method is almost never used.

Perpendicular recording is when the magnetisation lies perpendicular to the plane of the media. This form of recording sees the external field of adjacent bits reinforcing each (Figure 1.8), rather than opposing, as in longitudinal recording. This has the benefit of reducing losses due to demagnetisation.

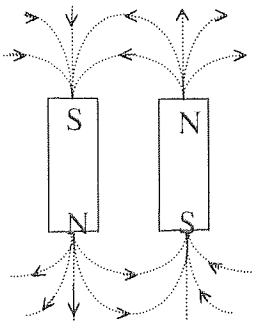

Figure 1.8 Adjacent Bits reinforce each other

Although first proposed about 20 years ago[16] perpendicular magnetic recording is still not being manufactured commercially. Media noise and head induced erasure are both associated with perpendicular recording[17] and until these issues are resolved it will not be viable on the open market.

Whichever mode of recording is used, vertical, longitudinal or transverse, storage capacity of the media is of prime importance. This parameter is related to the 'AREAL DENSITY', which is the product of the following two parameters: -

- The number of bits per unit length of track. (linear recording density).

- The number of tracks per unit width.

There is a constant demand for more data to be stored on magnetic media, preferably in smaller package sizes[18], this means that bit sizes must be reduced. The linear recording density of a media is currently around 4200 bits/mm[19]. The size of a bit is dictated by its length BL, its depth BL/2 and the track width W[20]. A relationship exists between the smallest recordable wavelength and the bit length such that

$$\lambda = 2BL \qquad 1.6$$

Also

$$\lambda = 2BL = V/f \qquad 1.7$$

Therefore, for a high linear recording density it is usual to have a low head to tape speed and record at high frequencies. Speed should however be fast enough to produce a high data transfer rate, an essential requirement when vast amounts of data are to be handled. For example if V is 2.3 ms^{-1} (90ips) and the recorded frequency is 2MHz then the wavelength is 1.15 μm or a bit length of 0.58 μm.

A way of further increasing the storage capability of media is to use narrower tracks allowing more tracks per unit width, and utilising multichannel heads. As track width decreases, so too will the remanent flux needed for reading[21]. To accommodate this, thinner magnetic coatings will be required (to reduce demagnetisation) along with smaller heads and head/media spacing. All of which will introduce new tribological problems that will need to be addressed. These tribological problems will be significant limiting factors in dynamic magnetic storage technology development [18].

1.3 Flexible Magnetic Media

There are two forms of flexible magnetic media in use in the magnetic recording industry. They are particulate and metal evaporated (ME) media, both have the common feature of having a magnetic layer deposited on a flexible substrate. Stiff competition exists between the two formats to produce the leading candidate for high-density magnetic recording. When ME tape was first introduced onto the commercial market its performance was significantly better than the leading particulate tape[22]. With the recording densities of each system increasing by using thin layer metal particulate media or advanced metal evaporated media, the recording characteristics of the latest particulate tapes have surpassed those of ME tapes.

Historically, particulate magnetic recording tapes consisted of iron oxide particles dispersed in a resin binder and coated onto a polyester base film. Such systems were critical for the back-up of mainframe computers which historically was undertaken on an open reel tape system. From the 1980's onwards systems were cartridge based where the tapes were still coated with either chromium dioxide particles (IBM 3480 standard) or cobalt doped γFe_2O_3 pigments. Recently there has been a rapid evolution towards the use of metal particle (MP) technology.

1.3.1 Particulate Media

The basic structure of particulate media is shown in Figure 1.9. The magnetic coating consists of magnetic particles dispersed in polymeric binder resins, ideally, the particles should be dispersed evenly throughout the magnetic coating. The coating also contains solvents, dispersants, lubricants and antistatic agents. The way in which each ingredient interacts with the particles influences the final dispersion characteristics[23]. This dispersion is then applied to a substrate, the particles are then oriented in a magnetic field, the tape dried and finished by calendering (compression rollers) to impart a smooth surface finish. The addition of a back coating is a more recent optional development, added to control friction and wear as the tape passes over drive components, the backcoat is applied to the underside of the substrate.

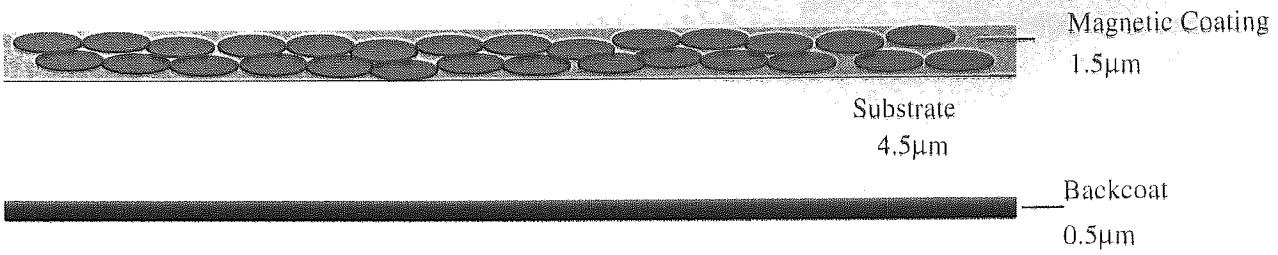

Figure 1.9 Structure of a Particulate Magnetic Tape

1.3.1.1 Magnetic particles

The magnetic particles are probably the most important component in a tape as they retain the stored information. As mentioned earlier for a high output flux during playback, the magnetic particles must have high coercivity and remanence.

As head/tape spacing is an important factor affecting high-density recording, tape smoothness is equally important. This in turn means that particle size and orientation is important, as these, along with substrate roughness and surface finishing techniques, dictate the final surface roughness of a tape. A great deal has been written on the subject of established and possible new magnetic particle materials [4-6, 9,24,25,26]. Important parameters are particle size, distribution, coercivity and remanence. Tapes with multiple layers each a fraction of the total thickness are assessed[27,28].

The development of magnetic particles has gone from oxides to MP, with only four materials being in commercial use [14] as follows.

i. Iron oxide (FeO) including gamma ferric oxide/maghemite (γ-Fe_2O_3), and magnetite (Fe_3O_4). Gamma ferric oxide (γ-Fe_2O_3) was the most common material in use during the early development of the industry. The particle length is between 0.3-1 μm, with a coercivity of around 350 Oe. This is not of sufficient magnitude for high-density recording and is therefore only of any use in low-density applications.

ii. Cobalt modified gamma ferric oxide:- The addition of cobalt to the surface of a gamma ferric oxide particle ensures that the new particle has a higher coercivity of around 1K Oe.

Unfortunately this particle is thermally unstable at high temperatures, and if 300°C is reached cobalt diffuses into the particle [24].

iii. Metal particle (MP):- Standard MP tape uses large acicular Fe particles (~180nm), which are standard iron oxide particles that have been through further processing such as reduction in hydrogen of acicular α-Fe_2O_3 derived from goethite, (α-FeOOH). Again exposure to the environment can be a problem, and the surface consists of a protective oxide or ceramic layer with a thickness of several tens of Å. This oxide layer contributes excellent dispersion characteristics as well as preventing oxidation and sintering.

The coercivity of this particle is around 1550 Oe. MP media are the most commonly used in high-density tape recording applications today. K. Okamoto, et al[25] describe how advanced metal particles, using geothite particles as a starting material, have a mean particle length of less than 100nm. Al, one of the III-group elements or a combination of both were adsorbed onto the geothite particle to prevent sintering during further processing. The partial replacement of aluminium by yttrium was shown to produce a superior anti-sintering agent, plus an improvement in dispersion. The authors suggest that MP tape with advanced particle technology is suitable for the next generation of tape data storage systems.

Advanced metal powders suitable for HDMR are made up of acicular particles with a long axis of about 0.1-1.0 μm[29]. As particle size decreases the passivation layer thickness becomes more critical as it decreases the magnetisation of the media. A future challenge for media manufacturers will be to increase the proportion of actual metal core relative to the oxide passivation layer.

iv. Barium ferrite (BaFe) :- These particles are of particular interest to the magnetic recording industry as they have some attractive properties. They are platelet shaped allowing them to be of use in perpendicular (as well as longitudinal) recording. Generally smaller than other particles they would produce a smoother tape surface. Being chemically stable to the environment means that they do not require a protective layer, hence better head medium spacing. They can also be produced using existing techniques which reduces the cost of developing a new manufacturing technique.

N. Sugita, et al report that the coercivity of BaFe is too high at 3500 Oe, for practical purposes. The samples used were produced using hydrothermal precipitation techniques. The initial compounds used were $FeCl_36H_2O$ and $BaCl_2$. It was shown that by substituting some of the Fe^{3+} for Co^{2+}-Ti^{4+} , the coercivity is lowered to a usable level. Unfortunately, it is temperature dependent, but the substitution of Co^{2+} for Ni^{2+} produces particles with a coercivity of about 1500 Oe that is only slightly temperature dependent.

During production, the magnetic axis of each particle should be oriented in the direction of an applied field. Kotera. H. et-al [30] suggest that this assumed orientation, which predicts the magnetic characteristics of the tape to be constant, may not be correct since there are many kinds of interaction forces involved. These include Coulombs force between particles, torque by the magnetic field and friction force due to particle contact. The understanding of the behaviour of particles when subjected to these forces is of great importance, not only to gain the density of magnetic recording but also to control the characteristics of the magnetic recording device.

1.3.1.2 Substrates

The most common substrate material is polyethylene terephthalate (PET). As the substrate provides the bulk of a tape's thickness, a thinner substrate would allow more tape to be loaded into a data cartridge. This would increase storage capacity, although data access times can increase and the possibility of tape damage (lower mechanical stiffness) during transportation could arise[31]. To overcome this problem, substrates with greater mechanical strength and thermal stability would be required. They must be mechanically and environmentally stable and be very smooth. Higher track densities will mean narrower tracks, therefore lateral contraction due to temperature changes, viscoelastic behaviour and/or shrinkage must be minimised. A substrate should posses a high modulus of elasticity and be of high strength to avoid damage during manufacturing. All of these requirements must be met for high-density magnetic recording (HDMR) to be realised. Some effects of an unsuitable substrate are as follows:-

Long term effects such as uneven tape stack profiles (hardbands)

Instantaneous speed variations

Tape stagger problems can be related to substrate viscoelastic characteristics.

HDMR requires the use of thinner tapes and hence thinner substrates, which show lower mechanical stiffness in general, and hence could easily cause damage to tape edges during tape transportation[31], this could lead to tape deformation. This in turn would increase the head/tape spacing, causing deterioration in the head output signal. Weick B.L. and Bhushan. B[32] report that ultra thin advanced magnetic tape substrates have superior characteristics compared to PET which is typically 14μm thick. Some examples of these along with their thickness are given in Table 1.1.

Poly(Ethylene naphthalate) PEN	4.5 μm
Aromatic polyamide ARAMID	4.4 μm
A polyimide PI	7.6 μm
Poly(Benzoxazole) PBO	5.0 μm

Table 1.1 Advanced Magnetic Tape Substrates

Various tests were carried out to determine the relevant mechanical properties of each material. It was found that when used in a system that produces a typical tape tension of 7 MPa (1K psi), these alternative materials are stressed to a fraction (1/10 to 1/30) of their breaking strength.

PET has a strain of 0.02 to 0.03 at its yield point whereas PEN, ARAMID, PBO don't have yield points, but fail irreversibly only at breaking point. The failure strains at breaking point are all higher than for PET, with PEN having the highest of up to 0.8. Thus three alternative materials are mechanically more suitable than the currently used PET.

When a tape travels over a head, it experiences tension in the longitudinal/machine direction and the transverse direction. Therefore, it is important for a substrate material to possess good mechanical properties in both directions. The most suitable material in this respect was ARAMID, which was shown to be a relatively isotropic material, with an elastic modulus of about 10 GPa regardless of material orientation. PBO possessed the best overall characteristics, but is currently unavailable. The authors ranked each material in order of suitability (most suitable first).

1	PBO - unavailable
2	PEN or ARAMID
3	PI
4	PET

Table 1.2 Suitability of Substrate material (Most suitable first)

1.3.1.3 Binder System

The purpose of the binder is to adhere the particles to the substrate and each other. The binder will usually be of a copolymer type. One polymer will provide flexibility to the tape, whilst the second will provide the adherence properties necessary to hold the particles in place. As particles have decreased in size, the binder has had to cope with increasing packing factors. The critical pigment volume (CPV) of a particulate tape is the maximum non-elastic volume packing factor possible. Gilson[33] studied the effects of the drying process (1.3.1) on particulate media coatings. Before the drying process, the solution is packed below the CPV. During drying, contraction and solvent loss will cause the packing to increase until CPV is reached. At this point, the microstructure cannot be changed, and internal voids are formed Figure 1.10, with the area around the voids being under stress.

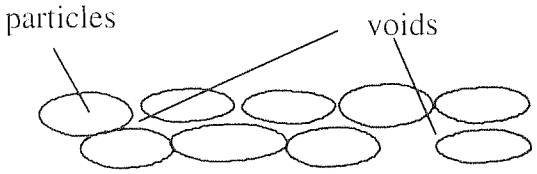

Figure 1.10 Voids in a Binder System

An acceptable binder system must have high flexibility, elasticity, wear resistance and provide good tribological properties such as a low coefficient of friction and low head wear. No one substance can provide all these requirements by itself, therefore several substances are used, with each having properties beneficial to a good binder system. These substances will now be discussed.

1.3.1.4 Wetting agent

In a finished tape the particles must be as evenly distributed throughout the tape surface as possible. To this end, a dispersant known as a wetting agent is used to stop the particles from accumulating in groups. Mechanical energy is still required to break up any groups initially.

This is provided by ball mills, sand mills or kneaders. Jung et-al[34] studied a family of materials called wetting binders. These offer the combined functionality of a dispersant and binder in one. Most are based on copolymers of vinyl acetate and vinyl chloride. It was shown that a wetting binder level of 5% or more by weight of particles produces a dispersion of mostly single particles.

1.3.1.5 Stabilising Agent

By coating particles in a stabilising agent, intimate contact of the particles with each other is prevented. It is important to create a tape with good particle dispersion as this produces an even performance across the length/width of the tape.

1.3.1.6 Lubricant

Essential to reduce friction between the head and tape, a lubricant of monomolecular thickness must be present on the surface of the tape. It will account for approximately 7-15% of the coating. By including the lubricant in the binder system (internal lubrication), it can diffuse to the surface (under pressure from the head) to replace lubricant depleted during use. The lubricant fills voids in the binder, and absorbs the stresses set up in the binder during drying (1.3.1.3). Internal lubrication also reduces loss by evaporation when compared to topical lubrication. Silicon oils, substituted silicon oils, fatty acids, fatty esters, fluorpolyether stearates and natural or synthetic hydrocarbons are all suitable lubricant materials.

Though the magnetic pigment is the major ingredient in the bulk of the tape it is covered by the binder and the solid fatty acid and liquid fatty ester lubricant layer at the tape surface. It is therefore important that these components are chosen to protect the pigment. Hegel[35] showed that excess acid lubricant levels and increased humidity created more debris and coating damage whilst increased ester lubricant level did not.

1.3.1.7 Antistatic Agents

During use the tape is likely to pick up an electrostatic charge which creates running problems (tape adhering to tape path components) and, if the charge is dissipated at the head/tape interface, a distortion in the recorded signal. Quarternary ammonium salts or polyalkylene ether are added to keep the resistivity of the coating at an acceptable level.

1.3.1.8 Back Coating

As an alternative to antistatic agents it is now more common to produce a tape with a backcoat whose job it is to reduce the amount of antistatic charge that accumulates on a tape during use[36]. A back coat is usually produced using the same formulation as the magnetic coating with conductive carbon black replacing the magnetic pigment. When wound onto the cassette spools, the tapes are subject to stresses. The back coating can also help prevent damage during this period. It has been suggested that the backcoat can cause the roughness of the magnetic coating to increase, which increases the head/tape spacing and hence signal loss occurs[76].

The formulation of a particulate magnetic tape coating involves balancing the properties of many ingredients to achieve the optimum electromagnetic and durability performance. The magnetic pigment plays a primary role in determining dispersion quality, since it is the main ingredient. In addition, the binder chemistry must be matched with the pigment to get the peak dispersion quality.

1.3.2 *Metal Evaporated Media*

In particulate tapes, the particles themselves only account for about 50% by volume of the magnetic layer. Which means that only half of the layer is available to retain information. Sony addressed this problem, and in 1989 introduced the first commercial ME tape for the Hi-8 video system [37]. A continuous thin film is deposited, directly on to a substrate by a vacuum evaporation technique. Atoms of a magnetic alloy are vaporised in a vacuum where they amass onto a polymer substrate to form a thin film. Now approximately 80% of the magnetic layer is available to store information, this increases the storage density of tapes by a substantial amount.

1.3.2.1 Metal film

In the early ME tapes Co-Ni-O was the material used for the thin film, whereas more recently Co or $Co_{80}Ni_{20}$ have been employed [38]. Figure 1.11 shows the structure of a typical ME tape. During deposition of the thin metal film, a controlled amount of oxygen is introduced. This has the effect of increasing the hardness and corrosion resistance (oxide layer) of the metal film[39].

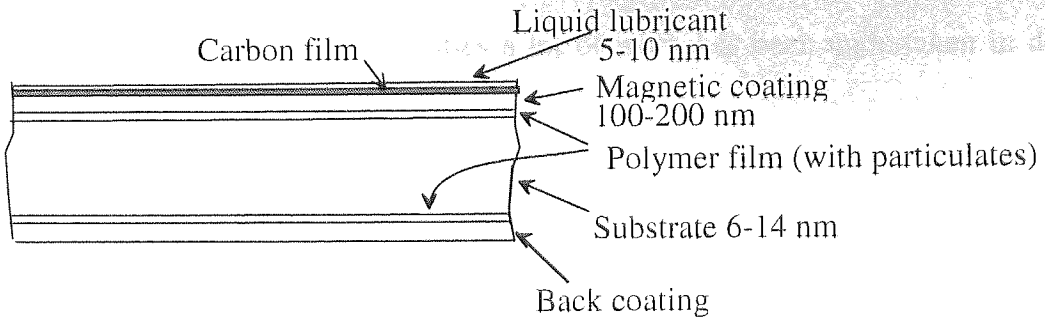

Figure 1.11 Structure of a Metal Evaporated Tape.

1.3.2.2 Lubricant

The metal film is highly reactive with the environment, the incorporation of a topical lubricant stops this reaction, as well as providing a barrier between head and media. The lubricant is often a fluorocarbon organic film.

1.3.2.3 Carbon film

A carbon film improves the tribology of magnetic media and has been proven in the hard disc industry[40]. The carbon film (frequently diamond like carbon) is included for two reasons:- To improve the wear resistance of the tape and to protect the magnetic layer from corrosion due to the environment[41].

1.3.2.4 Substrate

The substrate consists of a base film coated on either side with a polymer film, with additives beneficial to the coating applied[42]. At the metal film side for instance, a smooth surface is required to keep the recording head and magnetic layer in close contact. On the backcoat side a rougher surface is required for ideal running properties and tape storage. For this reason, particles are added to the substrate to control the real area of contact. Base film materials such as PET are used with ME tapes as in MP tapes. PEN films are also used as they have a greater mechanical strength. W. Goerlitz and A. Ito[43] report that ME tapes with ARIMID base films as thin as 2μm will be technically possible.

1.3.3 Multilayer Tapes

As mentioned earlier (1.2.1) high-density recording media need to have a high signal to noise ratio. Also fine particle sizes, with a very high coercivity (~ 3000 Oe) and squareness ratio are required. These properties can be found in multilayer tapes. By creating a tape of multiple layers each a fraction of the total thickness, very fine grain size can be promoted. In the race

for ever increasing data storage capacities a lot of work has been undertaken in developing and studying multilayer structures.

1.3.3.1 Particulate Tapes

By reducing the thickness of the magnetic layer, loss by demagnetisation is expected to decrease. An undesired effect of thinning the magnetic layer is that the media surface becomes rougher and dropouts (attenuation in reproduced signal amplitude[44]) due to surface defects tend to increase[45]. Saitoh et al[46] studied thin film particulate recording media with a nonmagnetic under layer (Figure 1.12). A newly developed method is reported for producing Advanced super Thin layer and high Output Metal Media (ATOMM). Two dispersions are simultaneously coated onto the substrate, using a Double-layer Web Tensioned die coater (DWT), Figure 1.13.

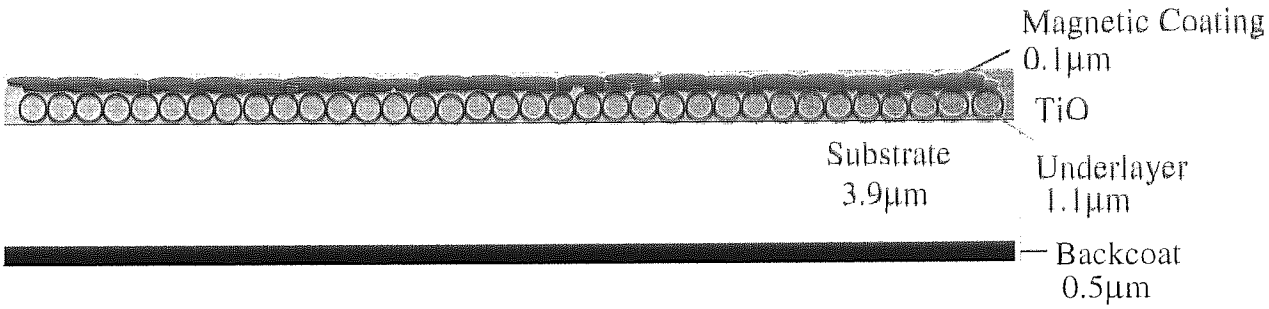

Figure 1.12 Multilayer MP Tape

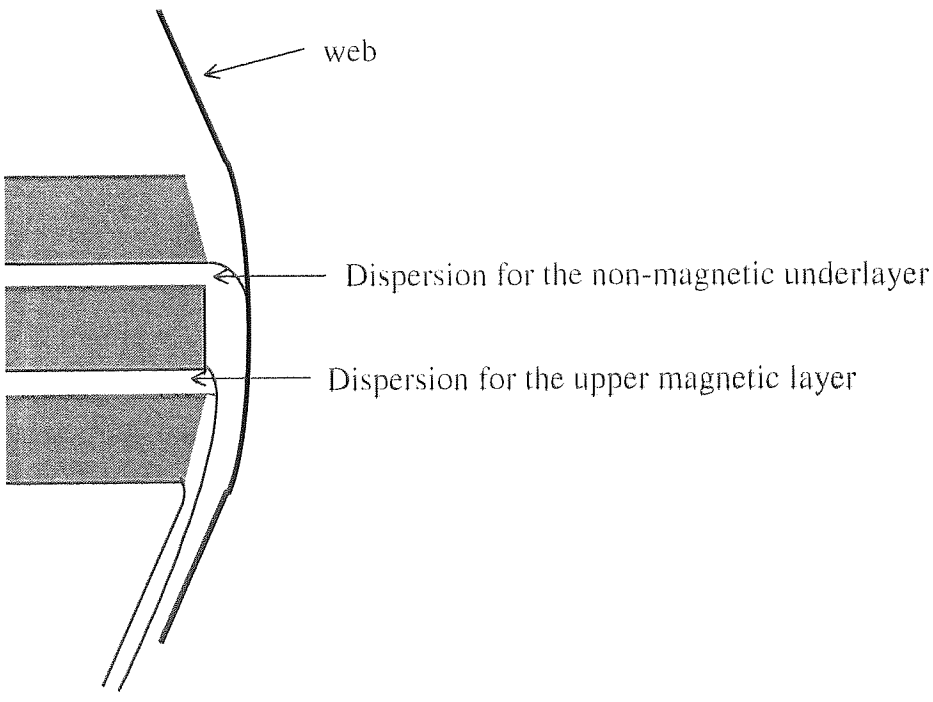

Figure 1.13 DWT die coater

ATOMM are reported to have a smooth surface due to smoothness of the underlayer, and less demagnetisation due to the thinness of the magnetic layer. They also produce a sharp and symmetrical isolated pulse waveform. The structures studied used barium ferrite or MP for the upper layer coatings, with titanium oxide (TiO_2) or alpha ferric oxide (αFe_2O_3) for under layer coatings. Surface roughness is said to decrease as the magnetic layer thickness decreases. The advantages of the underlayer are as follows:-

Adjustment of head-contact by controlling the underlayer strength.
Reduction in static by adding conducting agents.
Improvement of durability by replenishing the surface with lubricant from the underlayer.

The authors[46] conclude that these multilayer structures have the combined magnetic and structural properties required for the ultra-high magnetic recording density of 10 Gbits/inch^2.

1.3.3.2 Metal Evaporated Tape

A single magnetic layer has the characteristic columnar structure shown in Figure 1.14, which is due to the angle of deposition. As a result of this structure, output pulse asymmetry occurs where the height and width are clearly different for each direction of travel[47]. For video systems in which recording and playback are in the forward tape direction pulse asymmetry is not a significant problem. However this is not true for linear applications such as data cartridge systems where data is written and read in both tape directions.

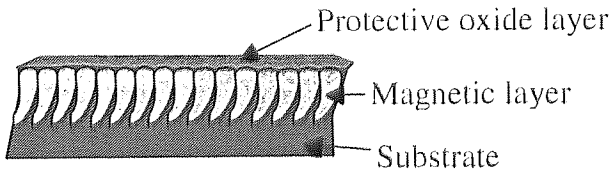

Figure 1.14 The Collumnar Structure of a Single Magnetic Layer.

As well as sharing the advantages of multilayer MP tape, multilayer ME tape can also overcome the problem of directional output characteristics. Figure 1.15 shows the structure of a double layer ME tape. The magnetic layers are oriented in opposite directions and the lower magnetic layer is thicker than the upper layer to compensate for spacing loss.

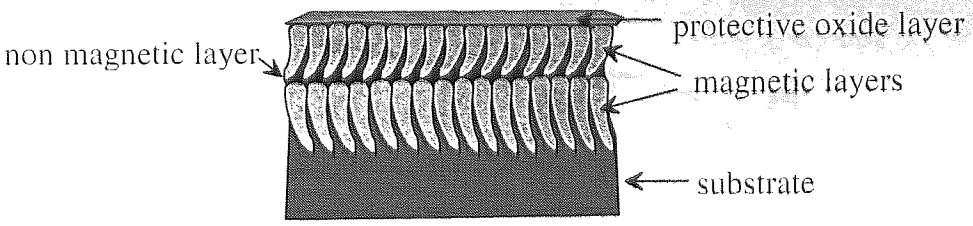

Figure 1.15 The Structure of a Double Layer ME Tape.

1.4 Heads

There are only two types of head in use in the area of magnetic recording, these are inductive and magnetoresistive (MR) type heads. It has been mentioned that an increase in media coercivities is needed for HDMR. The ability of a head to produce enough magnetic flux (saturation flux density, B_s) to magnetise such a media is limited by the performance of the head materials. Hence, a great deal of work is being done on high B_S head materials to be used with these media[48,49].

Some systems use separate heads for reading and writing, in this way materials and parameters can be chosen to maximise the performance of the heads for their specific function. If however one head is to perform both operations, a compromise must be made between functions. This read/write design is the most common in use in modern systems. Further, the high performance expected of today's systems requires that multi-track heads be employed[50]. Capable of writing up to eight tracks simultaneously, the multi-track design allows for faster data read/write operation.

1.4.1 Inductive Heads

The principles of inductive heads have already been dealt with in section 1.2.1, so only the design and materials will be dealt with here. The design of a metal in gap (MIG) inductive head typically used for helical scan systems is as shown in Figure 1.16.

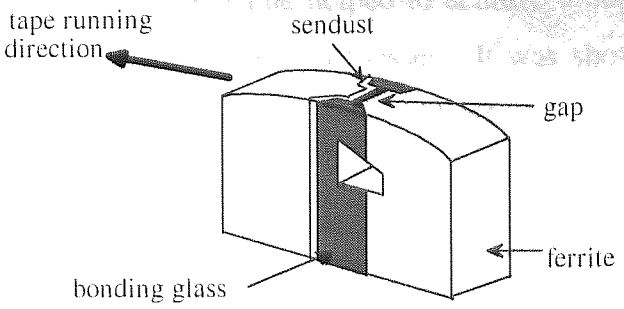

Figure 1.16 Inductive Head Design

Magnetic core materials are usually molybdenum permalloy, Al-Si-Fe alloys such as sendust, Ni-Zn-Fe or Mg-Zn-Fe ferrites. The deposition of sendust or FeAl Si on the ferrite core gives the structure a higher saturation magnetisation M_s. However, at the interface between the ferrite core and the deposited layer a magnetically dead layer is formed which is detrimental to the recorded signal.

When the relative velocity between head and tape is high enough an air gap will be formed between the two. Although it will reduce wear and friction, this gap degrades the performance of the system. To this end flutes can be incorporated into the design of a head which allow the air to bleed away[51].

T. Maegawa et al [52] carried out research into achieving optimum and stable head/tape contact. Parameters used in the experimental work were as follows: -

Tape stiffness, in the longitudinal and transverse directions.

Radius of the head, where R is the radius in the longitudinal direction and r the radius in the transverse direction. (Figure 1.17) .

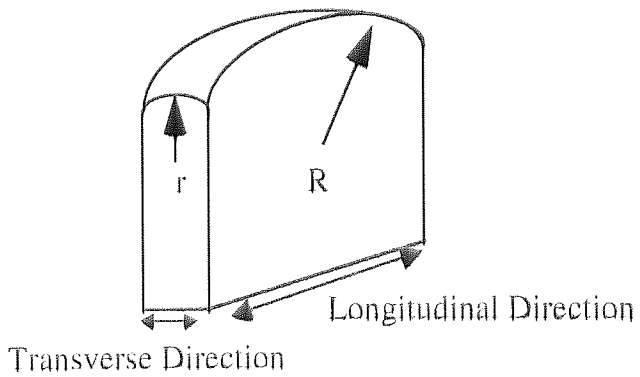

Figure 1.17 Parameters used in the Head/Tape Interface Modelling.

The results showed that a smaller r/R value helped to achieve a better head to tape contact. This applied to all tapes regardless of their stiffnesses. It was shown that for a head to be suitable for a high-density magnetic recorder, it should have

r = 1.0mm,

R = 5.0mm

1.4.1.1 Thin Film Heads

As previously mentioned (1.2.2) the pole material must have a high M_S value, low H_C, and high initial μ. The search for these properties has led to the development of thin film heads. Many publications exist on the study of materials for thin film heads.

K. Hayashi et al[53] looked at the addition of a fourth element to sendust (FeAlSi). They found that the addition of ruthenium (Ru) provides an improvement of the following:-

- Soft magnetic properties.
- Thermal stability
- Control of the film internal stress.
- Thermal expansion coefficient.
- Corrosion resistivity.
- Wear resistivity.

All these improvements are at the expense of an acceptably small drop in M_S.

H. Sakakima[54] studied alloy films of Co-Nb-T, where T represents one of the following elements Fe, Zr, Ru, Mo, Cr. A specially developed annealing process helped to produce an alloy with a very high M_S. An alloy containing Zr was reported to have the best corrosion and wear properties.

F. Roozeboom[55] studied the rapid thermal annealing (RTA), in a static magnetic field, of Co-Nb-Zr and nanocrystalline Fe-Nb-N. It is reported that RTA allows Co-Nb-Zr alloys to be heated to 125°C higher than conventional annealing. This extends the temperature range for further head manufacturing. RTA of Fe-Nb-N alloys at temperatures 100°C higher than conventional, at short times (10s), leads to Fe grains of < 20 nm.

T. Okamura et al[56] tested laminated Fe-Ta-N heads to be used in conjunction with high-density television (HDTV), though the material may be of use in other magnetic recording heads. The heads were shown to have superior recording ability to sendust heads. They exhibited high permeability at high frequencies. A slightly lower reproducing capability was reported. In addition, sufficient wear resistance at high tape speed was reported for this head material. Fe-Ta-N films were found to be more resistant to wear than the more conventional NiFe films[57].

1.4.2 Magneto Resistive Heads

Whereas the inductive type head relies on the rate of change of magnetic flux, MR heads respond to flux magnitude and direction and are therefore speed independent. This type of head uses the fact that the resistance of a material will change with a change of magnetisation direction, ie a change in flux direction. The current through the MR sensor will change with resistance, and hence the information on the media can be read. This material is said to be a magnetoresistive material. MR heads have no facility for creating magnetic flux and are therefore only capable of reading information.

The MR element will be shielded to protect it from stray magnetic fields. The thickness and width of MR shields must be designed to minimise crosstalk as reported by Suzuki et al [58]. A design that optimises the use of materials, is one in which the read and write elements are formed over each other (Figure 1.18). This type of head, which shares common material layers, is known as a merged head and is commonly used in hard drive and linear tape systems.

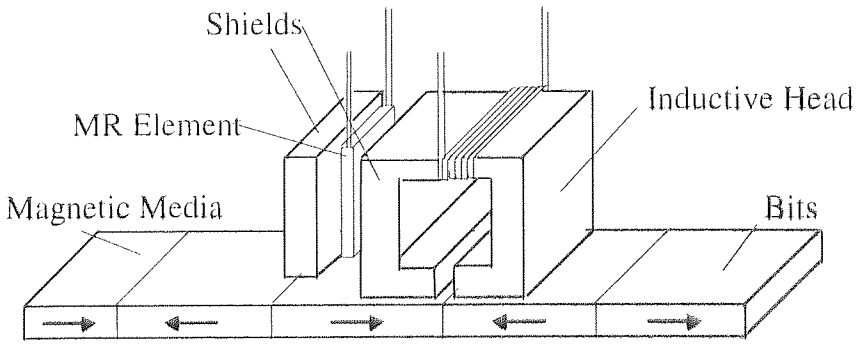

Figure 1.18 A Merged Head Design

Figure 1.18 shows how the pole of the inductive head acts as one shield for the MR head. This type of head is easier to build than inductive heads that perform both read and write operations, this is as a result of fewer manufacturing processes and head tolerance controls

being required. The saving in materials and manufacturing time means that the cost of the final product can be kept low. In an industry that produces millions of heads per year, this is a very important feature.

As track widths decrease, there will be a corresponding decrease in flux available from the magnetic media. For this reason, an increase in the magnetoresistance of head materials is required. As in the case of inductive heads, thin film structures have been studied, in the search for materials capable of providing high-density data storage.

One design of a MR head element is that of a spin valve sensor (Figure 1.19) in which the flux from the media rotates the magnetisation in the sense film, which changes the relative angle between the two directions of magnetisation.

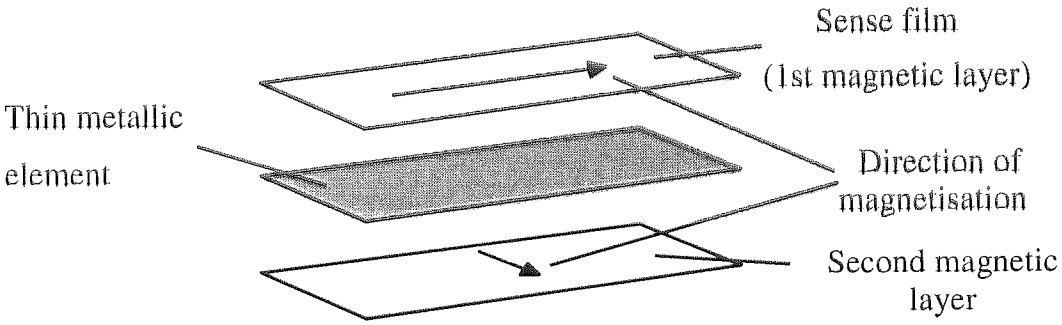

Figure 1.19 Spin Valve Element.

Dee [59] reports that the resistance of the element, ρ, is scaled as the cosine of this angle as shown below.

$$\rho = \rho_o + \Delta\rho \cos^2\theta \qquad 1.8$$

Where θ is the angle between the sense current and element magnetisation direction, Δρ the magnetoresistivity and ρ_0 the initial resistivity.

A similar idea is one that utilises a soft adjacent layer (SAL). As the current passes through the MR sensor, a magnetic field is set up that interacts with the magnetisation of the adjacent SAL[60]. It is expected that as the need for higher areal densities increases, thinner magnetic films and narrower MR sensors will evolve to satisfy the requirements.

J.A. Brug et al[61] investigated changing parameters such as the gap width, head/tape spacing etc, to increase the performance of MR heads. He concluded that the greatest increase in performance would be due to an increase in the magnetoresistance of head materials, Luitjens et al[21] also stated this as an important aspect for increasing density. This has also been a key issue in increasing areal density of hard disc drives. There was a shift from the 40% per annum increase in density to 60% per annum due to the introduction of a MR read-head by IBM in 1992. The recent increase to 100% per annum in laboratory demonstrations has been similarly driven by the introduction of giant magnetoresistive (GMR) spin-valve heads, again initially by IBM in 1998[13]. A GMR material will undergo a significant change in resistance when exposed to the small amount of flux available from bit transitions in HDMR. Typical MR element materials are Ni-Fe, Ni-Co and Co-Fe. One high sensitivity GMR multilayer is Ta/Ni-Fe/Cu/NiFe/Fe-Mn, which was four times more sensitive than a Ni-Fe MR head[62].

1.5 Tape Data Storage Platforms

Competition in the marketplace exists for all technologies and P.C. data backup is no exception. Cost-effective data storage has to incorporate such parameters as fast data recording and access, high storage densities as well as reliability. Various systems are available each with a niche in the market.

Two competing drive formats are those of helical scan and linear. Helical scan systems operate in the same way as a home video cassette recorder (VCR). When a tape cartridge is inserted into the drive, the drives internal mechanism pulls tape out from the cartridge and wraps it around the drum containing the read/write heads. The tape moves across the drum at an angle whilst the drum rotates. In this way data tracks are written at an angle across the width of the tape. Linear systems such as an audiocassette player, have the tape running across a stationary head in such a way that data tracks are written along the length of the tape. These systems can be much simpler in design and hence cheaper to produce.

Whilst helical scan systems have exploited their capacity advantage, linear based systems are associated with low cost and high performance.

The leading competitors are discussed here with the main emphasis being placed on the Travan system, on which the project was focussed.

1.5.1 Digital Data System (DDS)

Produced by Hewlett Packard (HP), this system is a helical scan format. Relatively small cassette and drive size makes the system compact. The VCR like loading system makes loading and unloading a cartridge more time consuming than for most linear systems. The current issue is the DDS-4 cartridge with a capacity of 40Gb at 6 Mb/s (2-1 compression)[63]. The price of a DDS-4 drive is currently around £585 with a data cartridge costing approximately £16[64].

1.5.2 Advanced Digital Recording (ADR)

A linear tape system, produce by Onstream the format is based on eight read/write sensors which allow eight tracks to be written/read at once, this obviously increases the speed at which data can be written and read back. The cartridge is a relatively large one, which permits greater amounts of tape to be utilised (compared to the smaller cartridges of competitors). This increases the storage capacity but will also increase the data access time. The currently available cartridge offers 30 Gb at up to 2Mb/s (2:1 compression)[65]. The price of currently available ADR drives is approximately £315 with a data cartridge costing about £23.

1.5.3 Travan

The Travan QIC system was introduced by 3M (now Imation corporation) to address the needs of the data backup market. The Travan linear tape system, when introduced in 1995, broke old storage capacity records for minicartridge systems[66]. It went on to sell four times the number of drives of all competing tape technologies combined placing it as a market leader[67]. With ten leading manufacturers supporting Travan technology, it was considered an ideal platform on which to base this research.

Each generation of the Travan QIC met the needs of its time with the latest network series (NS) 20 QIC having a capacity of 20 GB (assuming 2:1 compression). Current prices for the drive and tape respectively are £295 and £23[19].

The Travan QIC is of a belt driven design (Figure 1.20) . A polymeric belt in contact with the magnetic surface of the tape is used to control tension in the tape by driving the supply and take-up reels. To eliminate the problem of trapped air, the polymeric drive belt has a micro texture imparted to the surface in contact with the magnetic coating of the tape[68]. The effects of the belt on the tape surface have been reported in earlier works[69,70].

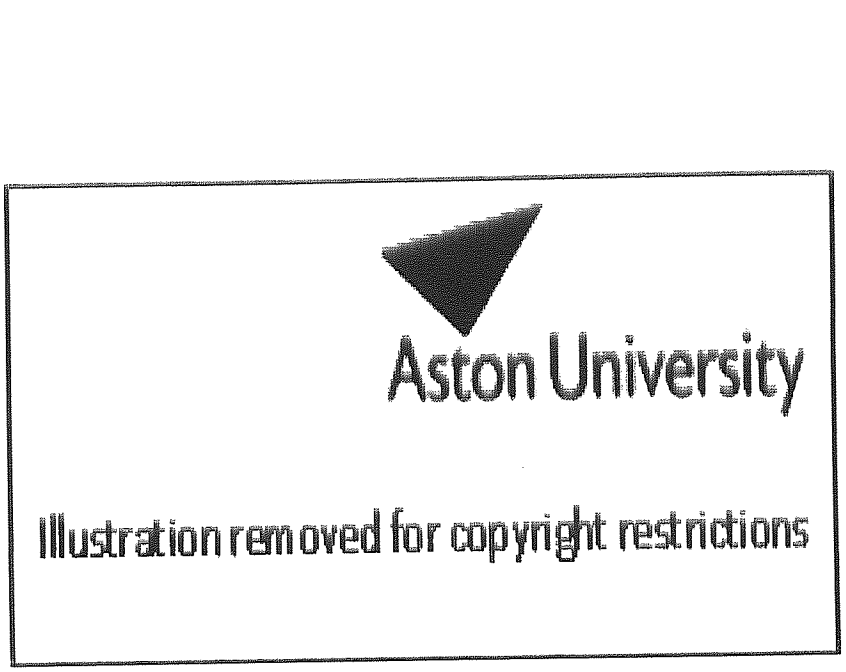

Figure 1.20 Components of a Travan NS20 QIC

1.5.3.1 Drive Components

During running, the tape encounters a number of tape path components. The front side of the tape is in immediate contact with the drive belt and read/write head, while the backside of the tape contacts the cartridge guide pins. The frontside and backside of the tape are in contact with each other when they are wound onto the supply or take up reel in the cartridge. Tape and indeed cartridge wear is likely to occur as a result of such contacts, which could affect the system performance.

Peformance characteristics of the three Tape drive systems discussed are summarised in Table 1.3.

	Capacity/ MB (2:1 Compression)	Data Transfer Speed/ MBs^{-1}	Drive Cost/ £	Cartridge Cost/ £
DDS-4	40	6	585	16
ADR	30	2	315	23
Travan NS-20	20	2	295	23

Table 1.3 Peformance characteristics of three leading tape drive systems

1.6 Tribology- The science and technology of interacting surfaces in relative motion.

The term tribology was introduced in 1966 to cover the study of friction, lubrication and wear[71]. Sullivan[18] reports that in the past, tribological problems arising in magnetic recording have been solved by a combination of good design, and using harder and more wear resistant materials. As the trend continues towards reducing the dimensions of the magnetic recording head, track width and head/tape spacing, it is essential that the tribological behaviour of the component materials is understood. Tribology as applied to magnetic recording, involves the study of the apparently smooth surfaces of tapes and heads in contact with each other. In practice, at the microscopic level these surfaces are uneven, consisting of asperities, which are the interacting elements.

1.6.1 wear

The wear between head and tape can be due to one of five mechanisms, with the possibility of interaction between them.

1. Abrasive wear :- This occurs when a harder material cuts into a softer material when the two materials are in relative motion with each other. This mode of wear occurs gradually, and is not likely to be the cause of sudden changes in surface topography [72]. This type of wear can be divided into two categories,

Two body abrasion, in which a hard rough surface and a softer one are in sliding contact. The harder surface will cause damage to the softer one in the form of grooves.

Three body abrasion, is a situation in which a hard particle becomes entrapped between the two surfaces in sliding contact, and abrades one or both according to their relative hardness',

A reduction in the abrasivity of tapes due to improved binders, surface finish, lubricants and magnetic particles has led to a decrease in this type of wear of heads.

2. Adhesive wear :- When asperities on tape and head meet, they adhere to each other via chemical bonding (Van der Waals). It is far more pronounced if the head and tape have been in stationary contact for an extended period. This form of wear can result in the transfer of material, this was observed by Pugh[73]. In practice, this is the transfer of tape material to the head, which can form a thin film called stain.

3. Fatigue wear :- Continuous stressing of opposing asperities as they interact can cause fatigue cracks to form at their base and eventually wear particles to form. Often there will be no indication of wear until delamination occurs, when deterioration of the surface is likely to accelerate [73]. Once a wear particle is formed due to delamination, three-body abrasion will occur.

4. Corrosive wear :- This is simply the effect of the atmosphere on the tape or head. The polymers in magnetic tape can degenerate due to attack by oxygen and water vapour, while the head elements can oxidise. Bhushan[10] reports that head wear increases by a factor of 4-7, at 30-80% humidity. Problems with corrosion and wear of head components in magnetic tape drives have led the industry to consider the use of protective ultra-thin diamond-like carbon (DLC) coatings for tape heads and metallic tapes [74].

5. Erosion :- In MIG heads, the metal may wear at a greater rate than the surrounding ferrite. This can lead to the situation where a particle can become entrapped in the area between the head and tape. This particle will then repeatedly impact the head and tape causing damage.

The Archard wear law [75]applies in a wide range of situations:

$$\omega = \frac{kW}{p_m} \qquad 1.9$$

ω - Wear rate of material.

k – Non-dimensional wear coefficient which depends on the materials in contact and the degree of cleanliness of the contact. It is usually interpreted as the probability that a wear particle is formed during a given asperity interaction[10].

W - Normal load.

p_m - Hardness of the material being worn away.

This law shows that the volume of wear material is proportional to the distance of travel, load and inversely proportional to the yield stress or hardness of the softer material.

1.6.2 Friction

Friction between dry components follows the general rule that the force is proportional to the coefficient of friction (μ) multiplied by the normal applied load (N).

$$F = \mu N \qquad 1.10$$

Once a lubricant is applied, this rule no longer holds. The frictional force now becomes proportional to the normal load and the relative velocity (V). When the velocity is low, there may be isolated contact points where the lubricant is missing. This leads to high friction (Figure 1.21). At higher velocities, air drawn along with the tape initiates an air bearing[76] which reduces the friction force.

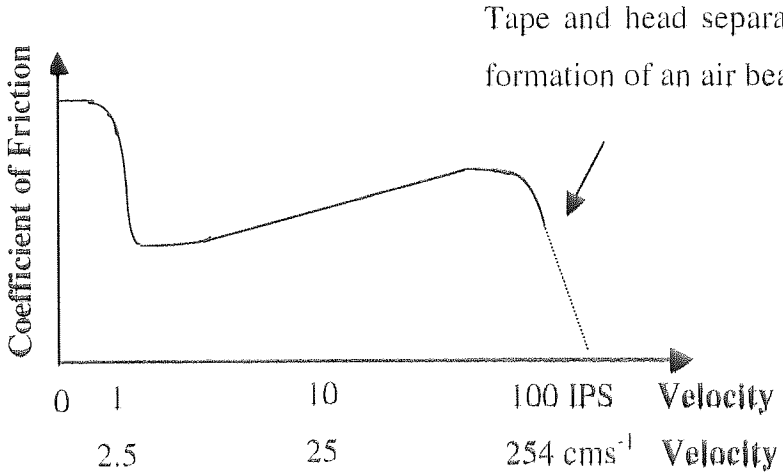

Figure 1.21 Coefficient of Friction Versus Velocity for a Typical Tape Drive

Values vary with tape makeup and all show an upward trend with increased passes and also with high humidity supported by Bhushan[10] and Jorgensen[36].

There are two forms of friction which occur in the area of magnetic recording.

1. Static friction: - This is defined as the force required to initiate sliding. This is most noticeable when head-tape contact has been at rest. This gives the chemical bonding mechanisms time to take effect. In addition, as the magnetic layer is viscoelastic the real area of contact between tape and head will increase with time, this in turn will increase the static friction. Hegal [77] reported that at high humidity the static friction effect can be very high. Also with too thick a lubricant layer, a meniscus effect can increase the static friction of a system[78].

2. Dynamic friction :- This is defined as the force resisting motion between two bodies. It can be split into two components, adhesive and deformation. It is known that the deformation component is negligible, allowing the frictional force due to adhesion to be written as:

$$F \approx \tau A_r \qquad 1.11$$

τ - Interfacial shear stress, which is temperature and pressure dependant.

A_r- Real area of contact, where

$$A_r \approx 3.2 \frac{W}{\Psi Y} \qquad 1.12$$

Y - Tensile yield strength of the polymer.

ψ - Plasticity index.

$$\Psi = \left(\frac{E^*}{Y} \right) \left(\frac{\sigma}{r_a} \right)^{\frac{1}{2}} \qquad 1.13$$

E^* - Complex modulus of elasticity.

σ - Standard deviation of asperity heights.

r_a- Mean radius of asperity peaks.

If $\psi < 1.8$ the contact is elastic and the interacting bodies will regain their initial shape when the contact is over, whereas if $\psi > 2.6$ the contact is plastic and the interacting bodies will be deformed plastically. For a sliding interface requiring near-zero friction and wear, contact stresses should be below the hardness of the softer material to minimise plastic deformation.

If lubricant is present Equation 11 becomes:

$$F = A_r\{\tau(1-\alpha)+\tau_l\alpha\} \qquad 1.14$$

Where

τ_l - Shear stress in the lubricant and α the fractional areal coverage of the lubricant.

Frictional force does not change appreciably when a lubricant is applied. This implies that friction is related to the properties of the magnetic layer. Therefore, from Equation 11 a small A_r is required for a low frictional force. This in turn requires ψ, Y or both in Equation 1.12 be as large as possible. As can be seen from equation 1.13, if Y is large, ψ will decrease, so for this reason E^* should also be large.

As a tape moves over a head, a temperature increase occurs due to friction, which is distributed amongst the contacting asperities. It is possible that one asperity can receive the total temperature increase resulting in a very high temperature at that point. The effect of this temperature rise can be to oxidise media polymers and organic lubricants, which with ensuing polymerisation can form friction polymers (stains). These can be beneficial to head wear, but detrimental to signal performance through spacing loss. The effect of asperity (tip) radius and relative humidity have been shown to affect coefficient of friction and adhesive force at the head/media interface[79].

1.7 Head, tape and signal performance

The characteristics of virgin tapes can alter dramatically during use. Not only in the way that they retain and reproduce a recorded signal, but also in their physical and chemical make up.

In the worst case, the tape degrades to a point that it breaks. Interactions at the head/tape interface can cause the chemical state of the tape to change. A head is not as fragile as a tape, but non the less can undergo changes detrimental to its performance. Alterations in the tape and/or the head can greatly effect the recorded signal.

1.7.1 Signal Loss

In order to analyse the read signal, three signal loss expressions can be derived by Jorgensen F [36].

$$\text{Coating thickness loss} = (1 - e^{\frac{2\pi\delta_{rec}}{\lambda}}) / (\frac{2\pi\delta_{rec}}{\lambda}) \qquad 1.15$$

$$\text{Read gap loss} = \frac{\sin(X)}{X} \qquad 1.16$$

$$\text{Spacing loss} = e^{\frac{-2\pi d}{\lambda}} \qquad 1.17$$

$$\text{Where } X = \frac{\pi g}{\lambda} \qquad 1.18$$

Where λ is the recorded wavelength, δ_{rec} the recorded thickness, g the gap length and d the head/tape spacing.

Since the wavelength will be constant it can be seen that these losses are dependant on dimensions only, which means that they can be controlled, as far as manufacturing tolerances will allow.

The coating loss formula arises due to the fact that the residual magnetisation pattern resides deep into the tape and not just at the surface. The deepest part of this pattern is therefore at an unacceptable distance from the head. Equation 16 can be reduced to one that uses an effective coating thickness δ_{eff}. This is characterised as the thickness from which 75 % of the playback flux emanates and is given as:-

$$\delta_{eff} = 0.44 \ BL \qquad 1.19$$

There is no advantage to be gained in making the coating any thicker than δ_{eff}, as this could lead to demagnetisation losses.

The spacing loss formula results in signal attenuation. By manipulating equation 16 using logarithms, it can be written as Wallace's equation[80],

$$\text{Spacing loss} = -54.6\, d/\lambda \qquad 1.20$$

If spacing loss is detrimental to the system performance, then ideally in contact operation is desired. This requires the tape to be very smooth, which gives rise to new tribological concerns. The use of smoother and thinner tapes could possibly lead to deterioration in head output due to their deformation, as mentioned earlier (1.3.1.2) which would introduce spacing losses as the damaged region passed beneath the head.

Gap loss leads to a simple relationship between the required gap length and the bit length. The signal output becomes zero when the gap length is equal to two bit lengths (Equation 18) Therefore, the gap length is made equal to, or less than one bit length.

Anderson and Bhushan[81] studied dropouts in two S-VHS magnetic tapes. Dropouts are attenuation in reproduced signal amplitude[82] and are categorised by depth and width. The depth is measured as a signal loss in dB, whilst the width is the period of time for which the dropout occurs. According to the size of the dropout, errors in the written signal can result in a loss of information (hard error), smaller dropouts can be endured without such a loss.

Three categories of dropout were identified and it was reported that the friction force at the head/tape interface either spikes, or remains unchanged during each. They are:-

1. Intermittent (friction force spikes)
2. Permanent (friction force spikes)
3. Permanent (friction force unchanged)

Intermittent dropouts only occur in a single pass and are thought to be due to debris stuck to the head gap. Permanent (friction) dropouts occur during every tape pass. These are thought to be due to the magnetic layer having been removed. It is also possible that the manufacturing process may have left regions without magnetic particles. As the head passes over the damaged region, the signal drops due to the lack of magnetic particles and the

friction spikes as the head contacts the substrate. Permanent (unchanged) dropouts are thought to be due to debris covering the write gap during recording.

Initially the number of dropouts was the sum of the intermittent and permanent type, with the intermittent ones decreasing with increasing number of passes. This is probably due to the head reaching its equilibrium state of contact during running in. Also during this period contacting asperities shear allowing new contacts to be formed. This will also reach an equilibrium state. They concluded that for both tapes permanent dropouts dominated.

Patton. S. T. Bhushan. B[83] investigated ME and MP tapes in the Hi-8 VCR system whilst in streaming mode which simply means the tape continuously passing the head. Heads were run in for two days to get past the initial stage of large dropouts due to tape and head conforming to each other. For MP tape at a given dropout depth, dropout frequency always decreased with increasing width. Increasing the wavelength decreased the dropout frequency in every class. This suggests that spacing loss is a cause of dropouts (equation 16). MP tape improved considerably with use until the dropout level reached a minimum level.

The dropout measurement in many recorders, under varying conditions, reveals that dust particles are a cause of dropouts[12,36]. Also defects left as a result of tape calendering are a cause of dropouts[84]. Such defects included shed material adhering to the calendering rollers and being redeposited onto the tape.

If an old data pattern is not completely erased before the area of tape is rewritten, system performance will be degraded. Stek et-al[85] reported that the residual pattern interferes with the original. Residual signals are due to patterns deep in the tape that are not completely overwritten. Possible reasons are variations in the write current, and/or deterioration of head performance.

1.7.2 Stain

As contact recording becomes essential to reach the required high densities, the formation of contaminants on the head is now more of a problem than head wear. They can lead to a temporary or permanent loss of signal as previously mentioned (1.7.1). Arudi & MacCracken[86] reported that debris can occur as a result of abrasive, adhesive and impact wear

mechanisms. It can consist of binder, magnetic particles, small amounts of lubricant, substrate material from slitting and other manufacturing debris. Organic deposits include tape binder, lubricant, foreign organic deposits. Inorganic deposits include magnetic particles, chemically altered (oxidised) head and tape materials and compacted unaltered head and tape materials plus tape path components.

Bhushan and Hahn[87] studied stains on magnetic heads run against γ-FeO tapes. Stain thickness' ranged from 10 - 30 nm as measured with an atomic force microscope (AFM). It has been reported that stains consisting of iron and oxygen (γ-FeO and MP tapes) could be removed by the application of an acidic solution[86]. However this method caused the head materials to be etched thus abrasive cleaning with a relatively rough tape is preferable. Kamei et al[88]also reported that stain could be removed from heads by the addition of a chelating agent to tape surface. Applied by dip-coating the agent – known as 1,10-phenathroline reduced stain by reacting with the iron oxide component to form metal complexes which were easily removed by tape motion. The amount of stain evident on tapes following a test was proportional to the amount of chelating agent applied.

A suggested method of stain formation is that organic materials chemically bond to the head followed by a build up of oxidised material. If the stain is found to be inorganic it is possible that the organic component has thermally decomposed and depleted. Organic stains are known as friction polymers. They are not the same as any surrounding material, as they are a result of tribochemical reactions such as repolymerisation.

Stains start as small spots and can spread into patches or a continuous film and are readily formed in scratches and recessed areas. Lauer and Blanc[89] found polyester polyurethane binder chemically attached to video heads run against FeO tapes. Owen [90] made a surprise discovery in that friction coefficient was unchanged by staining of the head. Stains investigated were composed of organic and iron, oxygen constituents [87,81].

It has been reported that humidity below 35-45% is usually necessary for staining to occur, whereas at higher humidities head wear is more pronounced, which is equivalent to abrasive cleaning. It is also known that high interface temperatures may encourage the growth of

stains due to frictional heating/sintering of magnetic particles. This was also confirmed by Kamei et al[88] who reported that little or no stain formed under ambient conditions, whereas stain was abundant on heads cycled in 40°C/10% RH.

1.7.3 Heads

The electrical characteristics of a head changes as it wears. Reduced gap depth increases the efficiency. This means that a lower write current is required. In addition, the playback voltage is higher from a worn head. A magnetic recording system must be robust enough to deal with these changes, or be calibrated from time to time.

It is possible to predict the shape of a head after it has been worn, and to optimise a head's contour. It is possible that two different drives may have different wrap angles (Figure 1.22). For multichannel heads, this problem is overcome by using outriggers to remove wrap angle error.

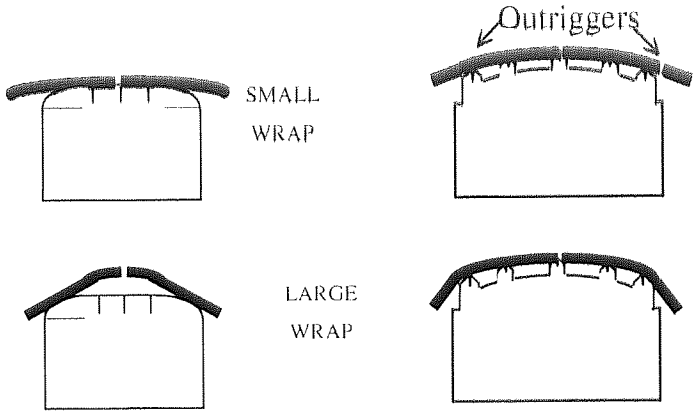

Figure 1.22 Different Drives produce Different Wrap Angles

Abrasive wear of the head can cause the destruction of an initially very straight gap. It has been known for material to be dragged across the gap causing a magnetic short. Head cores manufactured using Al - Fe alloys wear about ten times slower than Ni -Fe cores. This also holds for amorphous MetGlass cores which have very high hardness.

NiZn is widely used for shields and tape bearing surfaces in MR heads as it has high wear resistance. N. Ishiwata et al[91] investigated methods of suppressing the temperature rise that occurs in these shielded MR heads when the current is increased to improve head output. The result was that the thermal conduction of the shields and gap layers should be improved to dissipate this heat. Also the crystallinity of the Ni-Fe films used in this design could be improved to suppress Joule heating.

Tian. H. Lee[92] reports that electrostatic damage (ESD of MR heads will usually cause the resistance of the MR sensor to change. This could result in a head which is unusable. Two mechanisms of damage have been observed, these are the electrothermal failure of the MR sensor and dielectric breakdown of the MR shields. Electrothermal failure is due to a concentrated current flow causing localised joule heating of the MR sensor. Dielectric breakdown takes place between the leads and the shields and is due to a high voltage build up. The MR sensor is also melted during this failure mechanism, but it is not known whether the dielectric breakdown causes high current flow into the MR sensor, or if the sensor melts first.

1.7.3.1 Ceramic Region (ABS)

The ceramic region of a magnetic recording head is commonly know as the Air Bearing Surface (ABS) since it supports the load of the passing tape via air which becomes entrapped between the tape and head during tape motion. The properties of these ceramic regions can influence the wear properties of the overall head and hence signal performance. The choice of ceramic is therefore an important one when manufacturing heads.

After being manufactured residual stresses are present in a ceramic material and are greatest at the roots of small cracks in the surface of the ceramic. Fracture stress of ceramics is known to reduce at high humidities (moisture-assisted fracture or static fatigue)[93]. The wear of head materials by tape is negligible or gradual with relative humidities up to about 40-45% RH. Above this level, the wear becomes significant. Static fatigue is due to a reaction between the environment and residual stresses in the ceramic.

Different systems use different ceramics for the ABS. Of two popular helical scan systems, the Hi-8 video system uses $CaTiO_3$ while DDS uses MnZn ferrite. The most commonly used ceramic in linear tape systems is two phase Al_2O_3-TiC, used by the ADR and Travan systems.

The addition of 30% by weight TiC to the Al_2O_3 ceramic has two beneficial results. The grain size of Al_2O_3 is limited which results in a material of higher hardness and strength. Secondly crack propagation is restricted. The wear of this ceramic and methods for improving such properties has been the topic of much research.

Gong et-al[94] studied the effects on fracture toughness of varying the TiC grain size in Al_2O_3-TiC ceramic. TiC grain sizes between 0.5 and 8.2 μm were examined using Vickers indentation tests. It was found that fracture toughness of the ceramic increases with increasing TiC particle size. The same authors performed Knoop hardness tests on the same samples and concluded that as the average size of TiC particles increased, the true hardness of Al_2O_3-TiC ceramic increased slightly[95].

Li et al[96] studied the effects of adding Co to the Al_2O_3 and TiC powders before they are mixed and sintered. The erosion wear resistance of the new ceramic was found to be better than that of Al_2O_3-TiC ceramic. The bridging and anchoring effect of cobalt dispersing at the grain boundaries was very important. Microcutting and brittle fracture were found to be the dominant wear mechanisms for the ceramic generating powder and flakes of material[97].

Flakes of material resulting in three-body damage to the head surface has been reported by Harrison[98]. Experiments performed with a Hi-8 video system allowed the material to be identified as grain pullout from the $CaTiO_3$ ceramic.

Research involving ADR and Travan linear tape systems resulted in the identification of grain pullout from the TiC phase of the Al_2O_3-TiC ceramic[99]. Cycling experiments against MP tapes were performed at various environmental conditions. For both systems, the removed particles were seen to be a cause of PTR. Cyclic stressing of the TiC grains from repeated contact with passing tape, causes grain boundary cracks to propagate. At some point, the cracking will be such that the grain (or part of it) then breaks free. These grains/flakes then become trapped between the head and tape, where they continually impact against the head in the manner of three-body abrasive wear.

An amorphous hydrated surface layer may form by tribochemical reaction and act as a solid lubricant[97]. Bhushan and Khatavkar[100] report that moisture at high RH affected the grain boundaries of a Mn-Zn ferrite sample. Abrasive wear was also seen to increase at high RH. For Mu-metal, increased wear was due to adhesive wear bought on as a result of high meniscus forces, also three body abrasion due to debris present at the interface. For Mn-Zn ferrite, the wear mechanism at high relative humidities was due to moisture assisted crack formation, loose particles shed in the static test supported this.

To combat wear and PTR in magnetic recording heads, manufacturers use a diamond like carbon (DLC) coating to protect the head components from wear.

The adhesion of the coating to the ceramic may require the development of new ceramics to improve adhesion.

1.7.4 Tapes

Morioka et-al[101] produced a computer simulation that clarifies the relationship between tape surface roughness, head/tape spacing loss and output voltage level. The roughness of the head was assumed to be substantially less than that of the tape. A stable contact between head and tape was also assumed. Under these conditions, tape surface roughness was a main factor determining tape to head spacing. It is for this reason that smoother tapes are required for HDMR to reduce the head/tape separation.

Bhushan and Lowry[102] showed how MP, ME and BaFe tapes exhibited promising friction and wear performance compared to the more conventional Co-γ-Fe_2O_3 and CrO_2 tapes. Previous work had shown that Co-γ-Fe_2O_3 and BaFe tapes inflicted the least damage to an Al VCR drum and to themselves exhibiting a low and stable coefficient of friction[103]. The durability of ME tape was considered to be questionable due to the adherent wear debris that it deposited on the head. Further investigation by Bhushan and Patton[104] using a helical scan system, concluded that particulate tapes exhibited greater wear lifetimes than the ME, with eventual failure being due to the following mechanisms:

i Particulate Tape

Mild continuous adhesive wear followed by catastrophic failure possibly due to tape fatigue.

ii ME

Damage introduced at high 'bumps' resulted in localised delaminations of the tape coating.

This failure mechanism has also been reported by Hempstock and Sullivan[105]. Following this, a paste like deposit film, consisting of the delaminated debris, formed on the head leading

edge. This film passed to the head gap causing greater adhesion and hence friction. The increase in friction then caused the removal of the entire magnetic coating.

It was also reported that during the initial running in of a new tapes where the head and tape are worn to a "desired Equilibrium State of contact" ie the longitudinal contour of the head matched that of the tape, head wear and friction force were large, along with head output and tape durability being poor. These all improved as the equilibrium state was reached. The ME tape being stiffer, also contoured the head in its lateral direction.

Using a modified AFM/FFM (friction force microscope), Bhushan and Koinkar[106] were able to perform microfriction, microscratching, microwear and nanoindention tests on ME, MP and BaFe tape samples. They concluded that ME tapes were superior in hardness, scratch and wear resistance when compared to MP and barium ferrite tapes. However the fact that ME tape fails catastrophically is again reported, with MP and BaFe tapes being deemed more durable. A further interesting result is that micro-scale friction values of all tapes are comparable, as are macro-scale values, with micro-scale values being smaller than macro-scale. Further to this, Fujiwara et al[107], show that for ME tapes the microscopic effective friction coefficient (MEFC) is not dependent on the surface roughness, unlike the macroscopic coefficient. They conclude that the MEFC describes the intrinsic friction properties of the lubricant.

Bhushan. B. and Khatavkar[108], using MP tape, investigated the effects of various head cleaning agent, critical pigment volume (CPV) and lubricant levels on the head/tape interface. The HCA was Al_2O_3 particles of 0.2-0.4 μm in diameter. It was noted that the CPV needs to be as high as possible to maximise the signal, but if it is too high the result is a brittle and inflexible tape. This complements Gilson's[33] work and shows that the CPV needs to be deduced with the drying process in consideration to avoid inflexible tapes.

Tape debris generated during use consists of binder, magnetic particles plus other additives and is caused by adhesive abrasive and impact wear. The surrounding polymer is softer than the embedded particles and is therefore more likely to deform at the head/tape interface. For this reason, tapes with lower CPV tend to wear more. Magnetic particles break free of the coating which leads to a loss of recorded signal. Low frequency recorded signals can allow

some loss of magnetic pigment due to the wavelength of these being longer. Whereas with high frequencies, a loss of magnetic pigment creates a greater loss of the recorded signal.

The investigated HCA levels showed that a cleaner head/tape interface was produced at the higher levels. 1% wt HCA is the limit for improving signal playback, any further increase would simply increase head wear. Within the range studied, variation in HCA, CPV, and lubricant levels under similar conditions left the coefficient of friction unchanged.

Dual and single layer MP tapes were found to have similar wear characteristics[102] with uncalendered single layer tape being 3 orders of magnitude greater than the calendered tape. This shows the importance of smooth tapes, they would generate less debris, a known cause of dropouts.

1.8 Environmental Effects

Temperature and/or humidity can significantly affect the performance of magnetic tape[109,110] and heads[111, 112]. Elements likely to degrade the head and tape are present in the atmosphere. Oxygen can lead to oxidation of elements in the head surface whilst water vapour can cause the formation of hydroxides. The polymeric binder present in tapes can breakdown in the presence of high humidity through hydrolysis and chain scission [113].

At low humidities (<35% RH) stain formation occurs which is possibly due to higher friction based contact temperatures due to the absence of cooling provided by humidity[111]. High humidities (>50% RH) may allow for the formation of stain but at such conditions the higher head wear encountered removes any stain and hence keeps the head clean.

Harrison[114] performed cycling tests using the Hi-8 video platform. Two sets of environmental conditions were studied - 30°C/90% RH and 22°C/80% RH. Both ME and MP tape types were studied for each condition. These were commercially available Sony Hi-8 ProME and Sony Video8 MP tapes. At the higher temperature of 30°C abrasive wear of the head materials was found to be greater than at 22°C.

Xu et-al[109] studied friction and wear of ME tape at a range of temperatures and relative humidities using pin on disc equipment. The friction coefficient (μ) showed different

characteristics within two temperature ranges, above 10°C and below 5°C. It was shown that at temperatures lower than 5°C, the friction coefficient increased with increasing humidity until a maximum was reached (in the range of 50% – 80 % RH). Above 80% RH the friction coefficient was seen to decrease. Above 10°C, μ decreased until a minimum was reached (around 50%-80% RH). Above 80% RH μ increased with increasing relative humidity, probably as a result of high meniscus force[115]. The conclusion was that the boundary lubricant changed its dynamic phase state from solid to amorphous or liquid with increasing temperature or humidity. The solid and liquid phases produced low friction whilst the amorphous state produced high friction.

Hempstock and Sullivan[116] investigated the effects of stop motion and cycling tests on the head/tape interface of a Hi-8 video system. MP and ME tapes were studied. The MP tape was less durable at higher humidity (80% RH) than at ambient humidity (40% RH) whilst for ME tape the opposite was true. It was shown that at high humidity, binder depletion had occurred for the MP tape this corresponded with an increase in the number of dropouts recorded. For ME tape, the water molecules present at the head/tape interface were unable to penetrate the PFPE film and hence they formed an additional layer between the head and the tape. Although the water layer would be detrimental to signal performance, it reduced friction and wear (ME tape) by acting as an additional lubricant.

Hegel[35] performed cycling experiments using a custom-built tape cycler. The cycler was capable of mimicking the tape path of a typical data cartridge. By cycling short loops of MP tape (1m) at ambient and high humidity conditions whilst monitoring friction at the tape/guide pin interface, Hegel was able to asses the impact of different lubricant levels. It was shown that the high humidity conditions increased the formation of iron carboxylate salt (pigment adsorption of lubricant), which in turn accelerated the increase in tape friction as the magnetic coating degraded.

CHAPTER 2 Experimental Procedure

2.1 Introduction

The research consisted of two distinct processes, sample generation and surface analysis. Generation of samples was itself subdivided into three phases. The first part entailed a comparison of two tape cycling methods. This was necessary to ascertain if one method (loop tester) was suitable for generating samples that were characteristic of those generated in a standard Travan™ data cartridge used in production drives available on the open market. The remaining two phases both involved the cycling of tape samples loaded into Travan™ data cartridges. The difference between the two groups being the type of head utilised in the drive unit.

Each phase of sample generation was performed using one common set of environmental conditions but with at least one set of conditions unique to the particular phase. The reason for utilising different environmental conditions between phases was as a result of analysis of results from the previous phase. If the results of one phase did not show a significant degradation in tape performance then the environmental conditions were changed to try and promote such degradation.

Surface analysis by X-ray Photoelectron Spectroscopy (XPS) (2.5.5) and Auger Electron Spectroscopy (AES) (2.5.6), Atomic Force Microscopy (AFM) (2.2.3) and Scanning Electron Microscopy (SEM) (2.5.8) was employed to investigate the chemical and/or physical changes of the samples as a result of the cycling experiments.

2.1.1 Tapes

The type of tape, and where known its formulation, is presented in this section. Only one tape, MP1, was examined in each series of experiments throughout the research. Where possible the remaining tapes were compared in composition to this benchmark tape. The experimental tapes used in the first phase of this study comprised of 3 tapes, two 1650 Oe MP tapes (1.3.1.1), MP1 and MP2, and a 900 Oe Co-modified iron oxide tape, tape A. MP2 was deemed to be the least durable of the three with tape A being the most durable.

Information regarding the elemental composition of the three tapes was provided by Imation and is summarised in Table 2.1–Table 2.3. The numbers given in the "Material Quantity" columns refer to the solid weight of material for each component relative to a "100" weight of pigment. Table 2.4 lists the quantity of pigment, carbon and HCA incorporated into each of the tapes.

	Material Quantity	C%	H%	O%	N%	Cl%
Dispersion C	2	50.3	3.0	38.3	8.4	
Binder C	6.53	85.1	7.1	1.1	6.4	0.2
Binder D	6.53	62.7	6.8	26.3	4.3	
Lubricant A	1	73.7	12.3	14.0		
Lubricant B	1	77.7	12.9	9.4		
Activator B	7.32	60.7	6.7	25.5	6.8	

Table 2.1 Elemental Composition of Tape MP1

	Material Quantity	C%	H%	O%	N%	Cl%	S%
Binder E	7.52	83.6	7.5	5.1	3.4	0.4	
Binder F	11.28	62.6	7.8	26.1	3.4		0.1
Lubricant A	2.0	73.7	12.3	14.0			
Lubricant B	2.0	77.7	12.9	9.4			
Act A	2.19	60.4	4.9	21.9	12.8		

Table 2.2 Elemental Composition of Tape MP2

	Material Quantity	C%	H%	O%	N%	Cl%	S%	P%	Cl%	%Vinyl Chloride
Disp A	2.07	54.2	6.5	33.4				3.9		
Disp B	0.07	60.0	10.0	28.1	0.6			1.2		
Bind A	10.62	64.0	8.0	24.0	3.9		0.3			
Bind B	10.62								48.0	85.0
Lube A	1.25	73.7	12.3	14.0						
Lube B	1.00	77.7	12.9	9.4						
Act A	8.22	80.4	4.9	21.9	12.8					

Table 2.3 Elemental Composition of Tape A

	MP1	MP2	tape A
Pigment	100	100	100
Carbon	0.5	0	0
HCA	12	12	7

Table 2.4 Quantity of Pigment, Carbon and HCA in tapes MP1, MP2 and tape A

The 2nd and 3rd phases of the project focussed entirely on MP1 plus four different types of experimental media, used in conjunction with drives that were fitted with either a TR-4 or TR-5 head. The five different types of experimental media were:

MP1 - 1650 Oe MP tape to determine test protocol and provide a baseline
Alumina not well dispersed so abrasive tape
MP3 - MP tape with the same formulation as MP1, but higher lubricant concentration
MP4 -Same as MP3 but with a lower pigment loading
MP5 -Single layered MP tape
MP6 -Dual layered MP with same magnetic coating as MP5

Tapes MP3 and MP4 are similar to tape MP1 although they posses a different pigment loading. This, however, was considered to be an important factor in affecting the durability of

the system, since it is believed the thickness of the polymer layer at the surface can vary significantly with only a small change in the absolute volume loading.

Tapes MP5 and MP6 allowed a comparison to be made between the durability of a dual layered tape (thin magnetic coating over non-magnetic particles) and a full (thick) coat of identical magnetic dispersion.

No detailed information regarding the elemental composition of tapes MP3, MP4, MP5 and MP6 was available to the project.

The situation arose in the section using a TR-5 head in which each tape identity was being stated repeatedly, to avoid this tapes MP1, MP3 and MP4 were designated as group A tapes while tapes MP5 and MP6 were termed group B tapes.

2.1.2 Heads

Figure 2.1 shows a schematic diagram of a Travan 4 (TR-4) and Travan 5 (TR-5) head with their main constituent parts. The basic structure of each head is identical, each being distinguished by its pole materials and the type of mount used to secure the head. TR-4 heads utilise NiFe for the pole, pole/shield and shield whereas the TR-5 head utilises CoZrTa. For both heads the insulator and gap regions consist of Al_2O_3 while the ceramic is manufactured from Al_2O_3-TiC.

Each head contains two distinct read/write structures, one located on the left of the head and the other on the right. These will be referred to during the course of this thesis as the left and/or right read/write structures. In order to clarify the precise location of the two structures, the left read/write structure is positioned on the left when viewed from above the head with the poles facing the observer.

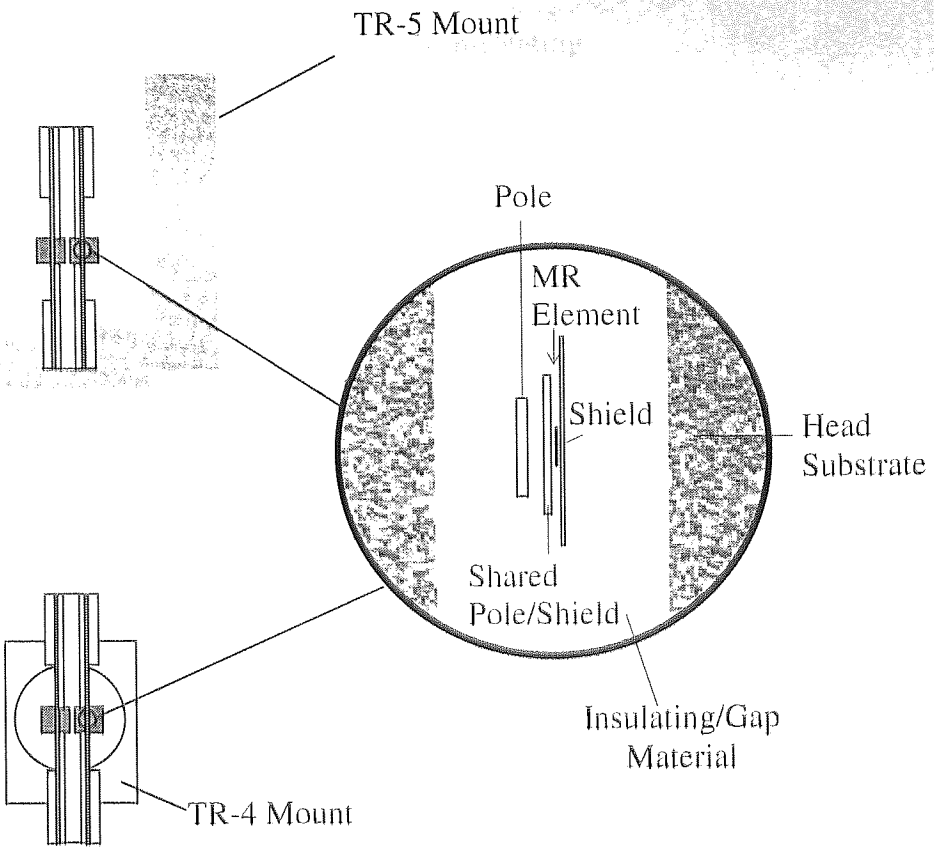

Figure 2.1 Schematic diagram of a TR-4 and TR-5 head

2.2 Loop Tester Cycling Experiments

2.2.1 Loop Tester

The first test involved an accelerated wear tester, consisting of a custom made cycler ("loop tester"), which enabled small lengths of tape (~ 1m) to run for up to several thousand passes in a relatively short period of time. It was possible to vary the speed of the loop tester but for the experiments reported in this thesis, all tapes were cycled at 2.29 ms^{-1}. A Schematic diagram of the loop tester is illustrated in Figure 2.2.

The tension in the tape was set via a mass, which remained constant throughout the experiments (50 ± 2 grams).

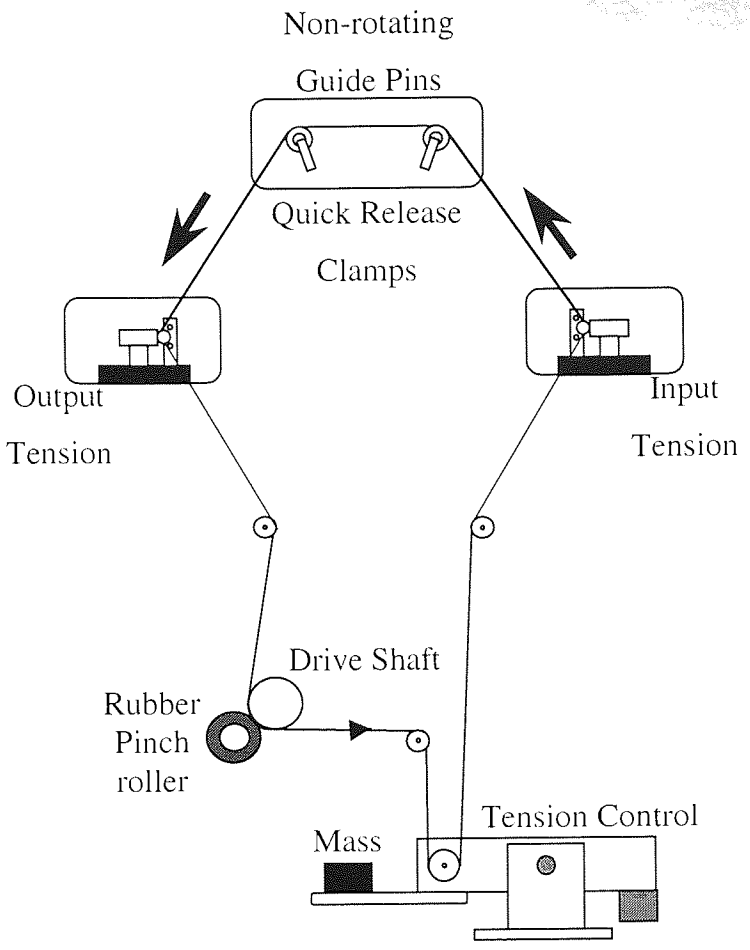

Figure 2.2 Schematic diagram of the loop tester

2.2.2 *Humidity Chamber*

The humidity chamber available for this section of the research was of a very basic design. A Perspex box was constructed in which to house the loop tester Figure 2.3. To initiate high humidity conditions, a compressor was used to pass air through two flasks of water, which allowed wet air to be fed into the Perspex enclosure. To create low humidity conditions, it was necessary to replace the two water filled flasks with one containing anhydrous $CaSO_4$ drying crystals. This allowed the humidity of the air to be reduced.

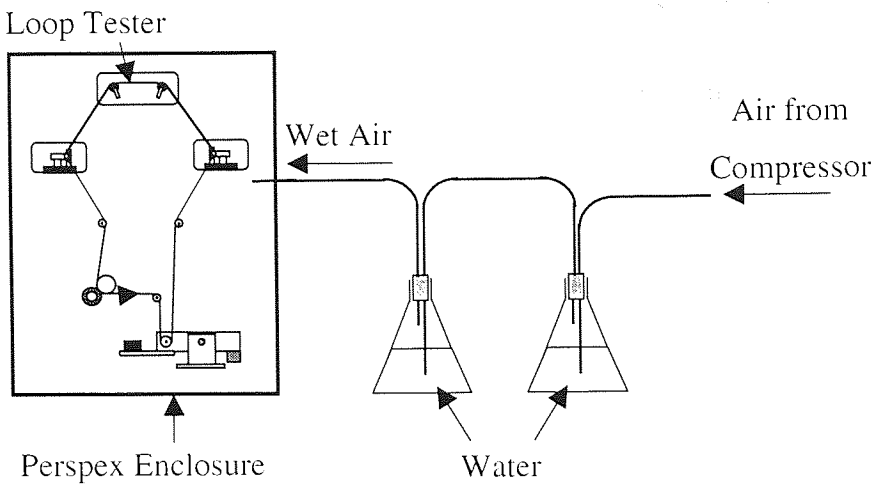

Figure 2.3 Schematic of the Humidity chamber

2.2.3 *Cycling Experiments*

The two ends of a section of tape, approximately 1m in length, were spliced together to form a loop. The loop was then placed onto the loop tester as shown in Figure 2.2. White cotton gloves were worn during hand to tape contact to avoid the transference of contaminants to the tape.

Each tape was cycled at 2.29 ms^{-1} for 100, 250, 500, 1K, 5K, 10K and 20K passes, a fresh loop of tape being installed for each number of passes. The tests were performed at controlled conditions of 22°C, 40% Relative Humidity (RH) and the pins which formed the tape guide system were replaced after each test to ensure no cross-contamination could occur. The 1 m lengths of sample tape were all taken from the same cartridge, which meant that sample to sample variability was negligible.

Following the 22°C, 40% condition, experiments were performed at high humidity conditions, namely 22°C, 80% RH. However the loop tester was housed in an enclosure that took several minutes to reach the required high humidity conditions which meant that it was only possible to perform experiments for 5K and 10K passes at these conditions.

2.3 Georgens Cycler Experiments (No Head)

2.3.1 Georgens Cycler

The Georgens cycler (Model 2K-04) comprised of four individual units, each of which could be used to cycle tape loaded into a Travan cartridge. Each unit included a pass counter, mode selector switch and firmware to provide over 40 tape motion patterns. These included end-to-end passes, short length passes and shuffle modes at speeds of 1.1, 1.5, 2.3 and 3.0 ms^{-1}.

Each of the four modules was supplied with a standard head mount (MCD2) to allow the inclusion of a read/write head. The modules were also modified by Georgens to include additional circuitry in order to provide a current source to turn a MR head stripe on or off.

During this first phase of experiments the effects of the tape transport system on the tape surface were studied. To isolate any effects on the tape surface due to the head/tape interface, no read/write heads were fitted to the Georgens cycler (Figure 2.4).

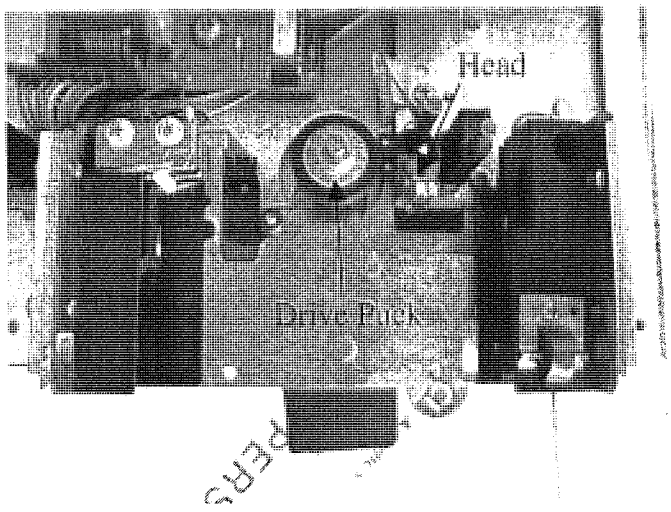

Figure 2.4 Georgens Cycler (head included to indicate its position)

2.3.2 Humidity Chamber

A commercial Heraeus Votsch VLK 04/300 environmental chamber was used during the remainder of the project. The independent temperature and humidities in the range of 10 to 95% RH to be achieved in the temperature range of 10 to 90°C. It was necessary to modify the chamber for one set of conditions that fell outside of the above range. In order to achieve a low temperature and low humidity simultaneously the following modifications were made.

The cycler was enclosed in a Perspex box before being placed into the chamber (Figure 2.5). A 20m length of copper tubing was also placed into the chamber with one end inserted into the Perspex box. A dryer unit (Zander Adsorption Dryer KE 12) was then used in conjunction with a compressor (Jun Air 2K-40 B) to blow dry air into the remaining end of the copper tubing. This had the effect of cooling the dry air before it arrived at the enclosed cycler.

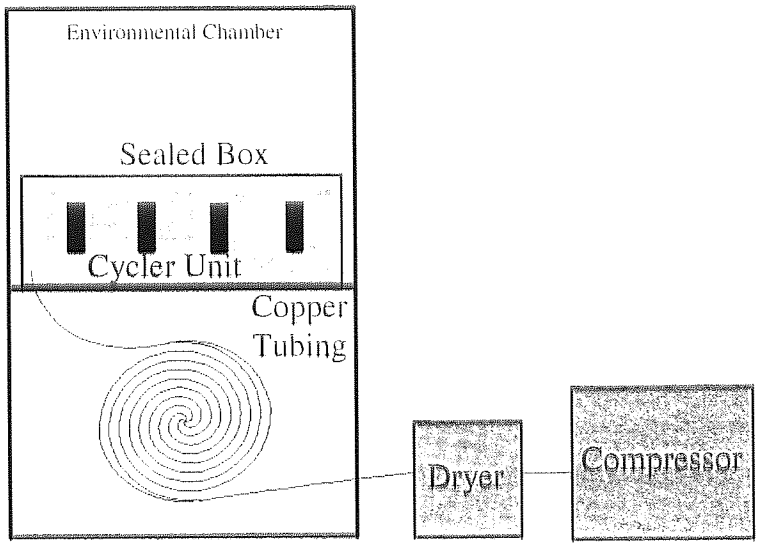

Figure 2.5 Schematic of Humidity Chamber Modifications

2.3.3 Drive Unit

This was custom built by Imation Minneapolis. It comprised of two standard Travan QIC drives that had been modified to allow a signal to be measured for dropouts. The signal was written and read during the same pass. The drive allowed two tapes to be run simultaneously.

2.3.4 Oscilloscope

A Tektronix TDS 120 oscilloscope was used throughout this research. This up-to-date model included features that were useful to the project. The oscilloscope display could be paused which then allowed images to be viewed or stored.

2.3.5 P.C.

To allow communication with the drive unit employed for dropout measurement, a Victor 433D P.C. was utilised.

2.3.6 *Dropout Tester*

The Deradus E20 Dropout Tester was initially provided by 3M Minneapolis, for a project based on videocassettes. A small modification ensured the tester was compatible with the linear tape system. Figure 2.6 presents a schematic of the equipment used for dropout measurement.

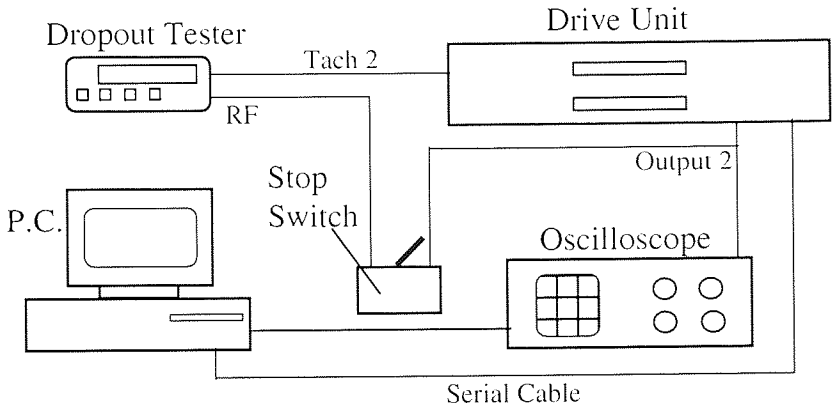

Figure 2.6 Schematic of equipment used for Dropout Measurement

The procedure for dropout frequency measurement was initiated via a P.C. and was as follows: -

I. A user response was required to select the number of tracks to be utilised. This was always one

II. A user response was needed as to whether to initiate a tensioning run or not. A tensioning run was initiated when a tape was first inserted into the drive (2.3.3). The tape ran through to the end of the tape (EOT), before rewinding back to the beginning of the tape (BOT). This set the tape tension in the cartridge, which was repeatable for each cartridge. This guaranteed that any differences between cartridges were not due to tensioning effects.

III. The head automatically moved to track one (centre of tape). A user response was required to change the head current. This was kept at the default value of 10mA.

IV. The tape moved forward for 200 feet before a write head was activated which wrote a signal to the tape. The signal used was a 300 mV (p-p) 2 MHz sinewave (set via an oscilloscope (2.3.4)), which enabled the dropout rate in a given section of tape to be determined. The signal was read immediately after being written, to determine the dropout rate. After a one-minute interval the stop switch was activated which stopped

information from the drive and hence the dropout count, allowing the measurements to be logged. The tape carried on to EOT and then back to BOT.

V. Steps II through to V were repeated in order to obtain a second set of measurements which were used to check the reproducibility of the first set. The dropout rates quoted in this thesis are an average of the two sets of measurements.

The classes of dropout used during this phase were 6 dB, 10 dB and 16 dB by 3 μs, 10 μs, 20 μs, 50 μs and 100 μs. Every time the signal temporarily decreased by a given depth for a given length of time, the relevant class of dropout would increment by one so that over a minute, a representative dropout rate for a given tape was obtained.

2.3.7 Cycling Experiments

The Georgens cycler was placed into the environmental chamber in which the conditions were set at 22°C, 40% RH. Tapes MP1, MP2 and tape A were loaded into Travan cartridges, allowing them to be cycled in the Georgens cycler. So that a comparison could be made with like samples from the loop tester experiments, it was necessary to produce samples in the Georgens cycler having been cycled for an equal number of passes as those from the loop tester. Due to the fact that tape loaded into a cartridge was approximately 750m in length, it was impractical, from a time perspective, to cycle a tape up to 20K passes. For this reason, tapes were cycled for the following pre-determined number of passes, 100. 250, 500, 1K, 5K and 10K passes. The tape speed during cycling was $2.3ms^{-1}$. The same experiments were performed at environmental conditions of 22°C, 80% RH; 32°C, 80% RH and 40°C, 15% RH for MP1 and tape A only. The four conditions used gave a wide range of operating conditions of high and low humidity/temperature. In order to ensure the media components were at equilibrium, the tapes were placed in an environmental chamber, at the designated test condition, for a minimum of 100 hours prior to the commencement of the cycling experiments

Single cartridges (dropout cartridges) of tapes MP1, MP2 and tape A were used to monitor the dropout rate at each of the above pre-determined number of passes. However, when the durability tests were performed at 32°C, 80% RH and 40°C, 15% RH, it was intended that the tapes would be cycled beyond 10K passes in order to try to reach a stage at which the dropout rate significantly increased.

Analysis required the tapes to be cut in order for the tape samples to be properly mounted. Once a tape had been cut, it was not possible to continue to use this tape for further cycling and thus a new tape in a new cartridge was used to generate each tape sample for analysis. All the tapes came from the same batch and hence sample to sample variability should have been negligible.

2.4 Georgens Cycler with TR-4 Head

The Georgens cycler, as described in section 2.3.1, was fitted with a TR-4 head (section 2.1.2, Figure 2.1). This allowed the effects of the head/tape interface on the physical and chemical properties of the tape surface to be investigated.

2.4.1 Cycling Experiments

To investigate the significance of the environment on the head/tape interface, a more severe condition, likely to promote chemical/physical changes to the head and/or tape, was employed, namely 5°C, 10% RH. The conditions of 32°C, 80% RH and 40°C, 15% RH were also utilised.

The classes of dropouts to be monitored were refined slightly from those used in previous experiments. The 20 classes of dropout monitored in subsequent experiments were 4 dB, 5 dB, 6 dB and 10 dB by 3 μs, 6 μs, 10 μs, 20 μs and 50 μs. It was intended to cycle the single dropout cartridge until significant dropout growth occurred. The procedure for the cycling of the dropout cartridge was as described in section 2.3.7 for tapes MP1 and tape A at each of the aforementioned environmental conditions. Due to the limited number of TR-4 heads available it was only possible to generate one cartridge, the dropout cartridge, for tape analysis.

2.5 Georgens Cycler with TR-5 Head

2.5.1 Georgens Cycler (TR-5)

At this stage of the project the TR-4 head was replaced by the next generation TR-5 head (section 2.1.2, Figure 2.1). It was also at this stage that the effect on the head/tape interface, of an energised MR element, was investigated. Custom-built cyclers supplied by Imation were necessary for the TR-5 heads due to the mount design being different to that of the TR-4

head (Figure 2.1). These cyclers will be referred to as TR-5 cyclers to distinguish them from the cycler used in previous experiments. All cycling experiments were controlled via a P.C. The firmware provided various tape motion patterns which included end-to-end passes, short length passes and shuffle modes at speeds of 1.1, 1.5, 2.3 and 3.0 ms^{-1}. The number of passes available were between 50, and 10K allowing any number of passes (in multiples of 50) to be set. The firmware allowed a running total of the number of passes to be kept for each drive.

2.5.2 Personal Computer (P.C.)

An Amstrad P.C., model PC9486 DX2/50 was used to communicate with the TR-5 cyclers while an Epson LQ 550 printer allowed printouts of experimental data to be obtained.

2.5.3 Cycling Experiments

Development tapes MP3, MP4, MP5 and MP6 were introduced at this final stage of the project. Environmental conditions were set at 32°C, 80% RH and 5°C, 10% RH, with the four tapes being cycled at each condition. The procedure for sample generation was similar to that in section 2.3.7, the difference being the number of passes each cartridge was cycled for. The dropout cartridge (single cartridge) was cycled up to 10K passes, with the dropouts being measured at the previously described intervals (2.3.7). Three cartridges (multiple cartridges) were used with a second head, the first being cycled for 500 passes the second for 1500 passes and the third for 3000 passes.

In total the samples generated for analysis were tapes at 500, 1500, 3000 and 10K passes plus heads that had seen 5K (multiple cartridges) or 10K passes (single cartridge) of tape. For two experiments a fourth cartridge was cycled for 5K passes after the initial 500, 1500 and 3000, this produced a head that had seen 10K passes but with multiple cartridges. This allowed a comparison between a head having been run against one cartridge with a head having been run against four.

The type of tape and experimental conditions are summarised for each cycler at the end of this section.

2.5.4 *Surface Analytical Techniques*

As all the interactions studied were surface specific it was essential that surface analytical techniques were used. They were thus a feature of the programme.

An essential requirement for a surface analysis instrument is that it is sensitive to the top few atomic layers of the sample being analysed. It is also desirable for the technique to be able to determine atom type, chemical state and structure. The distance that an electron may travel before undergoing an inelastic (loses energy) collision is known as its Inelastic Mean Free Path. For electrons in the energy range 100 - 1K electron volts (eV) this distance may be of the order of 1nm or less. Any technique that performs energy analysis of electrons in this energy range is therefore going to be surface sensitive.

The two most common ways of exciting an electron are by X-ray bombardment and bombardment by electrons. These two techniques are called X-ray Photoelectron Spectroscopy (XPS) and Auger Electron Spectroscopy (AES) respectively. Both were available as a part of the Fisons instruments VG ESCALAB 200D spectrometer equipped with a HSA energy analyser, which was used throughout this research. XPS was used for chemical analysis of the tapes, but due to the relatively large spot size (150μm in diameter) it was unsuitable for the individual component parts incorporated into the heads. For this reason AES was used to investigate the surface of the heads. AFM was used to obtain topographical information whereas SEM provided a visual aid only to any physical changes to the samples.

2.5.5 *X-ray Photoelectron Spectroscopy (XPS)*

Low energy X-ray photons, usually Al Kα or Mg Kα are directed at a sample where they interact with the sample material's electrons. If a core electron within the sample surface is given enough excess energy it will become excited and leave its orbital. The energy of photoelectrons leaving the sample is determined using a concentric hemispherical analyser (CHA). These photoelectrons are detected and counted according to their energy which will be characteristic of a specific element, Equation 2.1 [117]describes the process.

$$KE = h\nu - BE - \phi \qquad 2.1$$

KE - Kinetic energy of the emitted photoelectron.

hv - Energy of the photon.

BE - Binding energy for the emitted photoelectron.

ϕ – work function of sample and analyser

KE is measured in the ESCA experiment, hv is known and so BE can be calculated, which is the characteristic energy of a specific element.

Each element detected has a characteristic set of peaks in the photoelectron spectrum. The presence of a peak at a particular energy therefore indicates the presence of a specific element within the sample. The concentration of the element within the sampled, is related to the intensity of the peaks. Thus, peak areas can be used to quantify the composition of the materials surface.

Since photoelectrons, in the range up to about 1000 eV, are strongly attenuated by passage through the sample material itself, the information obtained comes only from the sample surface with sampling depth (d) on the order of 10 nm [118]. The sampling depth is directly linked to the angle (θ) between the sample and analyser by Equation 2.2 where θ is defined as being 0 when the analyser is normal to the sample, as is illustrated in Figure 2.7.

$$d = 3\lambda \text{ Cos } \theta \qquad 2.2$$

Where λ is the Inelastic Mean Free Path (IMFP), which is the distance covered by an electron between two inelastic collisions. When an electron undergoes a collision, its energy changes randomly and it contributes to the background noise build up. The electrons which leave the sample without inelastic collisions, form the peaks.

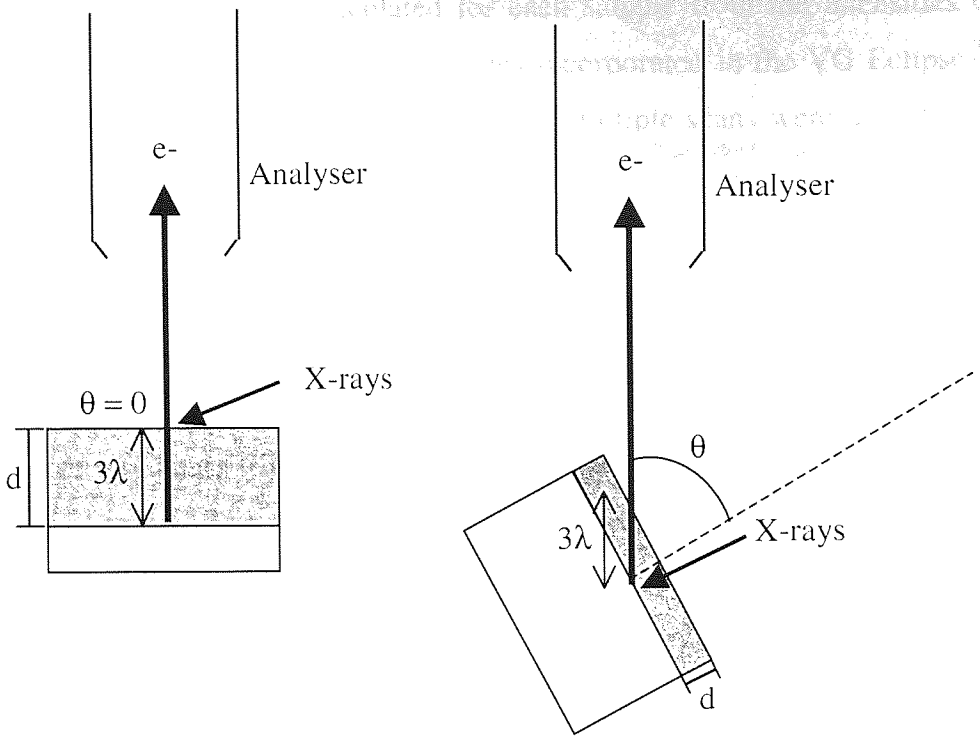

Figure 2.7 Effect of take off angle (θ) on sampling depth (d)

Mg K_α X-radiation was employed for the XPS examination of all tapes, at a source excitation energy of 15 KeV and emission current of 20 mA. The initial area of analysis was chosen to be 2 mm x 3 mm and was superseded by 1mm^2 for each analysis. The change was due to belt/tape interaction, it was required that the tape be analysed at two separate areas, one where the belt contacted the tape and one where it did not.

Survey scans were first recorded for all samples at analyser take-off angles of 0° (normal to the analyser) and then narrow region energy scans were collected for all the elements identified on the surface at 0° take-off angle. An analyser pass energy of 20 eV with step size of 0.1 eV and dwell time of 100 ms was used throughout. The XPS spectra were smoothed for ease of peak identification, however, a minimal amount of smoothing was carried out to avoid possible peak distortion. The amount of smoothing used was directly related to the concentration of the element, as a more abundant element would have a better-defined peak and as such would require little smoothing. The smoothing method used by Eclipse is that of Proctor and Sherwood which works by fitting a $4^{th}/5^{th}$ order polynomial to spectrum data.

Relative atomic concentrations were calculated for each sample from the intensities of the major photoelectron spectral lines by means of codes incorporated in the VG Eclipse V 2.0 instrument data system using Schofield cross sections. Multiple scans were used for all the constituents in the surface, in order to improve statistics and in the case of tape A, the Cl 2p peak was always collected first since this was most vulnerable to radiation induced loss.

It was important to monitor the thickness of material covering the magnetic pigment, this was termed the overlayer and consisted of binder, lubricant and carbonaceous contamination from the air. An overlayer thickness (d) was calculated using the value of the saturated Fe signal obtained after several stages of etching the tape. The relative atomic percentage of Fe at this point was found to be 42%.

$$I = I_0 \exp(-d / \lambda \cos\theta) \qquad 2.3$$

I - signal intensity of Fe at the time of overlayer measurement

I_0 - signal intensity at saturation.

TOA θ - 0°

λ (mean free path length) - 25 Å

By substituting known/measured values into Eq 2.3 allowed d to be calculated.

2.5.6 Auger Electron Spectroscopy (AES)

Electrons of energy 3-10keV are incident upon a sample. These electrons cause core level electrons from atoms contained in the sample to be ejected resulting in an atom with a core hole. The atom then relaxes via electrons with a lower binding energy dropping into the core hole. The energy thus released can be converted into an X-ray or emit an electron (Auger electron). The energy of the Auger electron is characteristic of the element that emitted it, and can thus be used to identify the element. Since the width of the Auger electron peak is large, little chemical state information is available.

AES allows a map of a particular element to be obtained. Once an element has been identified by its peak (as above), the system can be set to collect data for that particular element. By setting the kinetic energies of the centre position of the peak and the position at which the background starts the system then scans for the set energy range. As the electron

beam is rastered across the sample surface, emitted Auger electrons that fall within the set energy range are detected. This builds up an image indicating the position of the element being detected on the sample surface. The element being detected appears as the bright against the background on the final image.

When scanning, ultra high vacuum (UHV) conditions are required to prevent filament burn out and collision of electrons with the gas molecules. Normally, when a sample was brought into the UHV environment from air, it was coated with carbon and oxygen contamination layer. This contamination had to be removed by sputtering before the surface could be investigated. Sputtering involved directing a beam of Ar ions at between 500eV and 5keV at the sample for no longer than one minute to prevent damage to the surface under investigation.

All heads were mounted on a standard ESCA stub using a carbon conductive paste, a small amount was used to reduce contamination of the chamber.

Whilst setting up the ESCALAB 200 to perform AES on a sample, it was necessary to tilt and/or pivot the sample relative to the electron gun to avoid charging of the sample and to obtain the best viewing position on the monitor. Charging is alleviated when the number of electrons entering the surface is counterbalanced by the number ejected. With the take off angle (TOA) (sample relative to analyser) at 0°, the full intensity of the electron beam was focussed onto the sample surface. Tilting the sample relative to the electron gun allowed the charge intensity at the sample surface to fall. Tilting and change in the electron energy was used to balance secondary electron emission to eliminate charging.

Once a sample had been pivoted for the best viewing position, tilting of the sample produced a greater degree of charging according to the particular direction of tilt. It is thought that the non-uniform nature of the TR-5 head array did not produce a gaussian distribution of the electron beam intensity.

A further consequence related to the tilting of the sample was one of perspective. To compare an AFM image with an elemental AES map they would both need to be seen from the same perspective. Obviously if the sample is tilted and/or pivoted for AES work then it is not seen

from the same perspective as the AFM image and correlation of results was made more difficult.

To investigate the effects of charging and perspective of sample positioning during AES work, SEM images at a number of positions were acquired. To avoid excessive charging of the sample with maximum incident electrons, a low voltage of 2 keV was used during image acquisition. Starting at 250° and moving at 5° intervals through to 335° a series of images was collected.

2.5.7 Atomic Force Microscope (AFM)

AFM was performed using a Topometrix Explorer scanning probe microscope in non-contact mode. The Topometrix SPMLab V.3.06 software was used to control the instrument, for all data processing and image generation.

An AFM (Figure 2.8) relies on the interaction between a mechanical probe and a sample, to relate topographical information to a computer, which then allows 2D and 3D images of the sample's surface to be generated via software. The probe/sample interaction is on the atomic level. The atomic force between the atoms of the tip and sample is the parameter that is monitored during image acquirement. The silicon nitride tip, mounted on a cantilever (Figure 2.8), interacts at the atomic level with the sample in the attractive force range.

The tip or sensing probe, works in conjunction with a piezoelectric ceramic and feed back circuit to keep the force between sample and tip constant which allows the production of computer-generated images.

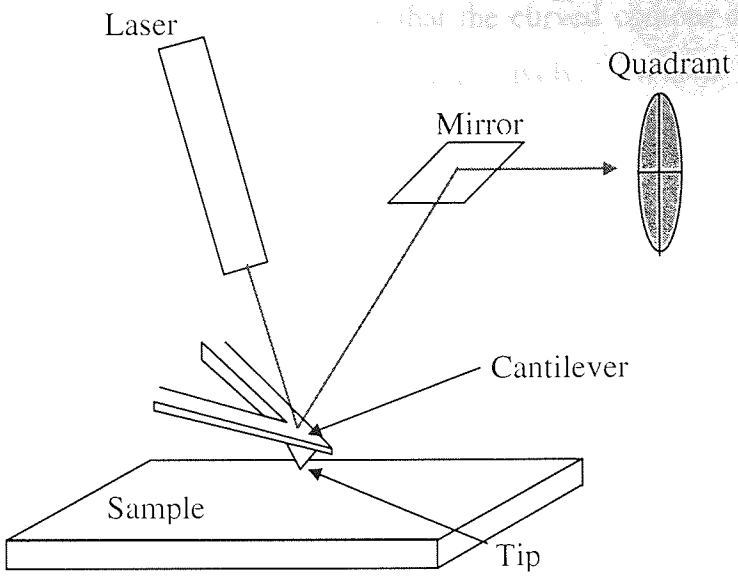

Figure 2.8 AFM Components

A piezoelectric ceramic can be manufactured with an expansion coefficient as low as 1 angstrom/volt, which means that with a 100-millivolt potential source applied, the ceramic will move 0.1 angstrom. This makes AFM an ideal tool for sub micron work.

The feedback circuit monitors the force between the tip and sample to ensure that it remains constant. Deflections of the cantilever, as it maps the surface of a sample, cause the laser to move across the face of the quadrant photo detector (Figure 2.8). The magnitude of the tip's deflections can then be calculated from the difference in light intensities on these four sectors. This information can be used to adjust the piezoelectric ceramic to maintain a constant force between tip and sample. It is this adjustment that is used to produce an image.

The analysis software allowed a number of techniques to be applied to an acquired image to best fit the data to the sample. The first step was always levelling, this was necessary to remove experimental tilt from the height data. For the heads 2^{nd} order plane levelling was used, this fitted the data to a curved plane (the head has a curved surface ref2). For tapes first order plane levelling was performed which fitted the data to a flat plane. Care was taken when deciding the order of levelling to use on the head, after some experimentation with the possible orders, 2^{nd} was chosen.

A comparison of first, second and third order levelling (Figure 2.9-Figure 2.11) as applied to data processing of an AFM image was made. The following images are to the same scale in both the X and Y directions and are of the exact same position on a virgin TR-4 head. It can

be seen from Figure 2.10 and Figure 2.11 that the curved contour of the head was retained during second and third order levelling respectively. Which radius of curvature is representative of the actual curvature was unknown.

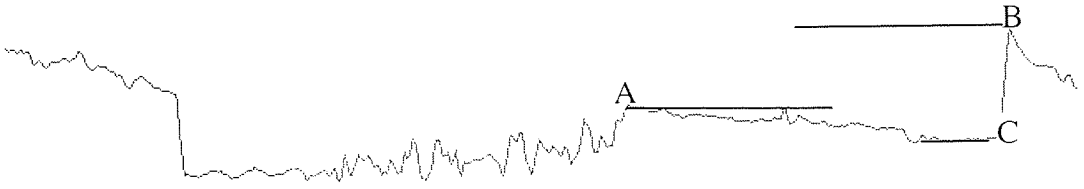

Figure 2.9 First Order Levelling

Figure 2.10 Second Order Levelling

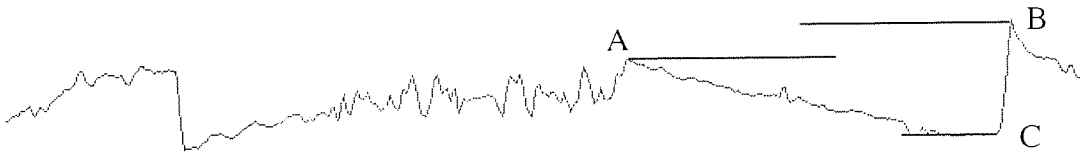

Figure 2.11 Third Order Levelling

It was obvious from points A and B in the above figures that there was a difference in height measurements when two points at too great a distance apart were compared. For this reason it was decided to restrict height measurements to neighbouring points along the head contour, such as B and C. The relative heights between the following components of each read/write structure were measured.

- Ceramic – Insulator (Shield side and Pole side)
- Insulator - Shield
- Shield - Read Gap
- Read Gap - Shared Shield/Pole
- Shared Shield/Pole - Write Gap
- Write Gap - Pole
- Pole - Insulator

2.5.8 *Scanning Electron Microscopy (SEM)*

Scanning electron microscopy is made possible when an electron beam is accelerated by a high voltage, and formed into a fine probe by a series of electromagnetic lenses. The electron beam is rastered across the surface of the specimen by means of a series of deflection coils. Secondary electrons emitted from the sample are typically detected by a photomultiplier system, amplified and displayed on a Cathode Ray tube that is rastered in synchronisation with the electron beam scan. The more electrons a particular region emits, the brighter the image at that point.

As with AES (2.5.6), SEM is a technique that suffers with sample charging. During initial attempts to image tape samples, they were gold sputtered to relieve charging problems. Unfortunately the gold sputtering obscured surface detail of the tape. A second method was considered, that of conductive paint. The stub to which the sample was to be fixed was coated with the conductive paint, the tape sample was immediately affixed to the stub, using the paint as a glue. A further addition of paint from the surface of the tape to the stub, ensured maximum sample conduction.

The tape type, cycling condition and analysis technique used for each sample is summarised in Table 2.5 through to Table 2.8.

All Tapes-XPS

All Heads- AFM, AES and SEM

Loop Tester		
Environmental Conditions	22°C, 40% RH	22°C, 80% RH
Tape type : MP1	✔	✔
MP2	✔	✔
tape A	✔	✔

Table 2.5 Summary of tape and cycling conditions for the loop tester

✔ - XPS

Georgens Cycler – No Head Installed				
Environmental Conditions	22°C, 40% RH	22°C, 80% RH	32°C, 80% RH	40°C, 15% RH
Tape: MP1	✔	✔	✔	✔
MP2	✔	N/A	N/A	N/A
tape A	✔	✔	✔	✔

Table 2.6 Summary of tape and cycling conditions for the Georgens cycler with no head installed

✔ - XPS

Georgens Cycler – TR-4 Head Installed			
Environmental Conditions	32°C, 80% RH	40°C, 15% RH	5°C, 10% RH
Tape: MP1	11K Passes XPS	After 4K Passes Cartridge Failed XPS	20K Passes XPS
tape A	11K Passes XPS	After 2K Passes Cartridge Failed XPS	N/A XPS
Heads	AFM, AES	AFM, AES	AFM, AES

Table 2.7 Summary of analysis techniques for head and tape for samples generated in the Georgens cycler with a TR-4 head installed

Georgens Cycler – TR-5 Head Installed				
Environmental Conditions	32°C, 80% RH		5°C, 10% RH	
Tape: MP1	✔	✔✔✔	✔	✔✔
MP3	✔	✔✔✔	✔	✔✔
MP4	✔	✔✔	✔✔✔✔	✔✔✔✔✔
MP5	✔✔✔✔✔	✔✔	✔	✔✔
MP6	✔✔✔✔✔✔	✔✔✔✔✔	✔	✔✔

Table 2.8 Summary of tape and cycling conditions for the Georgens cycler with a TR-5 head installed

✔- Dropout Cartridge cycled for 10K passes.

✔✔ - Three cartridges cycled for 500, 1500 and 3K passes, XPS

✔✔✔ - Four cartridges cycled for 500, 1500, 3K and 5K passes, XPS

✔✔✔✔ - Dropout cartridge which broke after 7K passes

✔✔✔✔✔ - Three cartridges cycled for 500, 1500 and 2K passes, the third failed after 2K passes

✔✔✔✔✔✔ - Dropout cartridge which broke after 2K passes.

CHAPTER 3 Results

3.1 Loop Tester Cycling Experiments

Three tapes, MP1, MP2 and tape A were cycled at 22°C, 40% RH and 22°C, 80% RH for predetermined numbers of passes (2.2.3). After the completion of each predetermined number of passes, the front side of the tape was analysed using XPS.

3.1.1 MP1

3.1.1.1 22°C, 40% RH

3.1.1.1.1 XPS

Figure 3.1 shows the relative atomic concentrations of elements detected in the surface of the tape as a function of increasing number of passes. The elements detected were Fe, O, N, C and Al. The Fe originates from the magnetic pigment, O from the binder, lubricant, Fe oxide and Al oxide. The presence of N is due entirely to the constituents of the binder whereas C arises mainly from the binder and lubricant but also from a hydrocarbon contamination layer on the outer surface of the tape. Al was present in the tape as a head-cleaning agent.

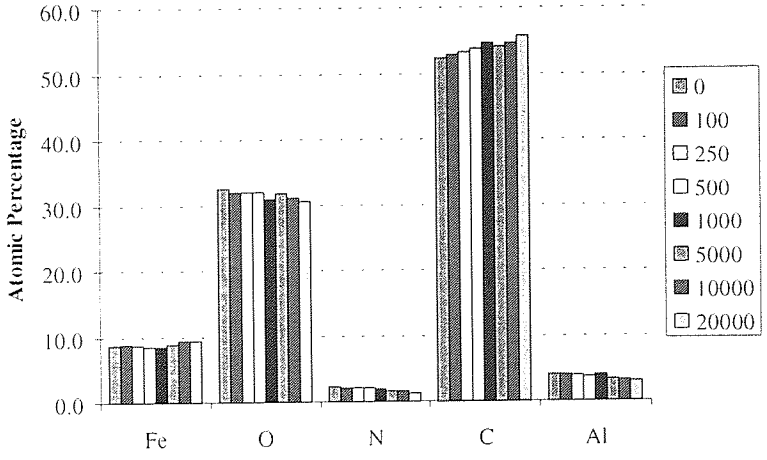

Figure 3.1 Atomic Concentration of Elements as a Function of Increasing Number of Passes for Tape MP1 at 22°C, 40% RH

Figure 3.1 shows that for tape MP1 the Fe signal decreased and then increased again at higher passes, whereas the C signal steadily increased and N decreased up to 20 000 passes.

Synthesis of the C peak revealed that 4 different chemical states contributed to the total C peak as shown in Figure 3.1. The major energy peak of C-C (and C-H) occurred at a binding energy of 284.6 eV and was used as a reference point for the other peaks.

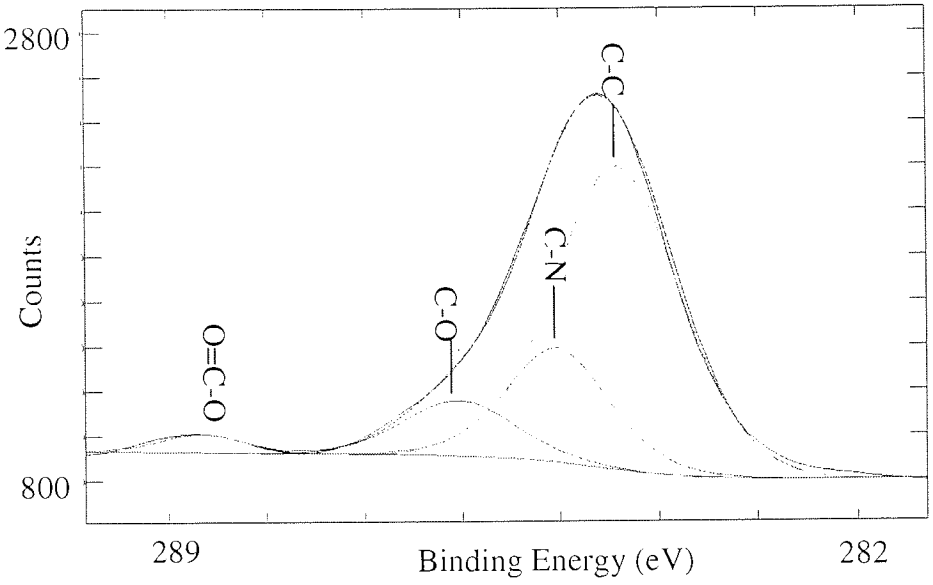

Figure 3.2 Example of Peak Synthesis of C for Tape MP1

The C-N and C-O bonds occur within the binder and were therefore good indicators of any change occurring within it. The carboxyl peak, O=C-O was present in both the lubricant and the binder, for this reason it did not provide useful information regarding near surface changes.

Figure 3.3 shows the result of cycling on the synthesised C peak. The C-O and C-N bonds decreased while the C-C/C-H bond increased with cycling. The carboxyl bond showed no trend throughout cycling.

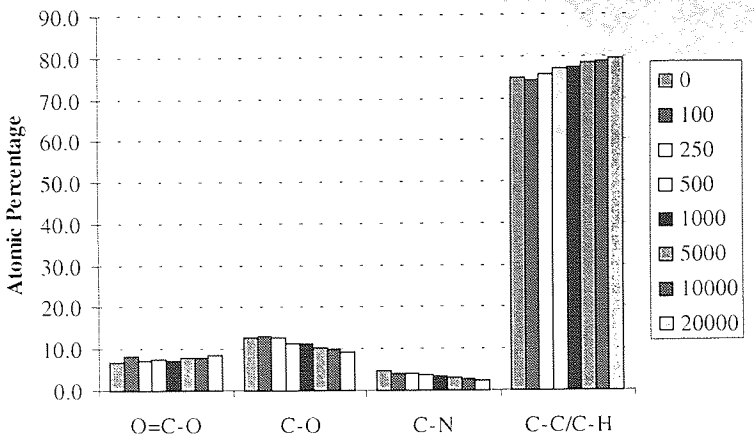

Figure 3.3 Synthesis of C for Tape MP1 at 22°C, 40% RH

It is not possible to ascertain if the near surface region of one tape is particle rich in comparison to another tape by simply comparing relative concentrations. For instance two tapes could have the same pigment loading but different lubricant levels resulting in different relative concentrations for Fe. A better method is to compare the ratio of one element to another, particularly relative to the concentration of Fe.

Figure 3.4 and Figure 3.5 show the ratio of Fe:C, Fe:N and N:C .

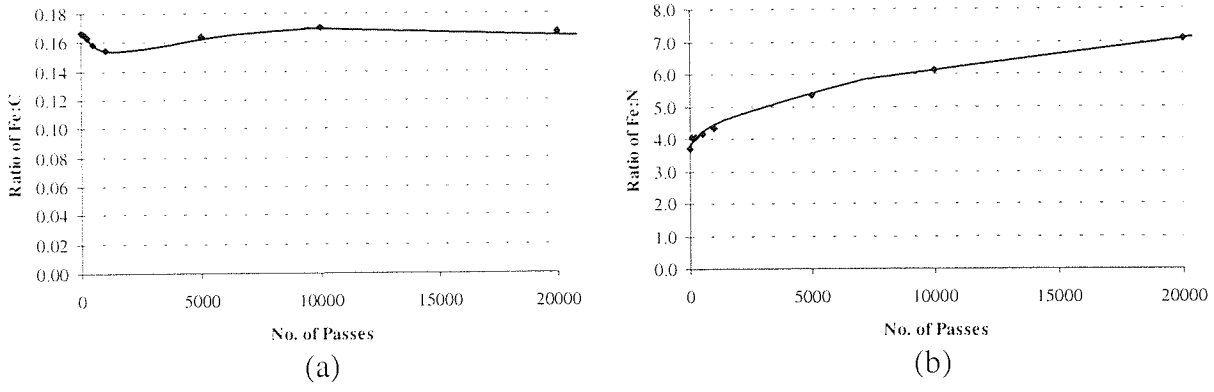

Figure 3.4 Ratio of (a) Fe:C and (b)Fe:N for Tape MP1 at 22°C, 40% RH

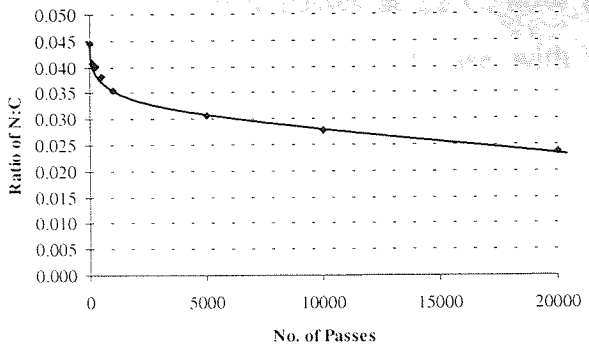

Figure 3.5 Ratio of N:C for Tape MP1 at 22°C, 40% RH

The variation in overlayer thickness with increasing number of passes is presented in Figure 3.6.

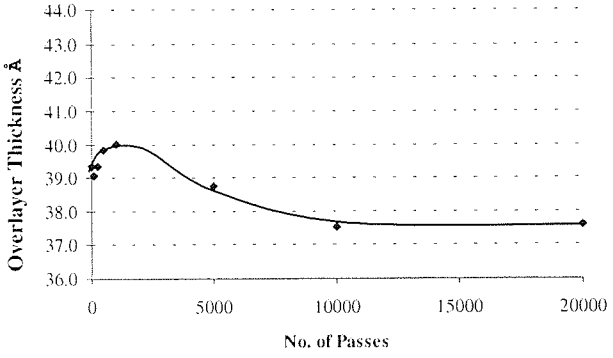

Figure 3.6 Variation in Overlayer Thickness as a Function of increasing number of Passes for Tape MP1 at 22°C, 40% RH

The change in the Fe:C ratio showed no discernible trends (Figure 3.4) and could be considered to be stable with increased cycling. This was not the case for the ratios containing N.

Figure 3.4 and Figure 3.5 both provide evidence of N depletion with increasing number of passes. Overall a decrease of the overlayer thickness was noted with increased cycling, this was consistent with a loss of binder material.

3.1.1.2 22°C, 80% RH

3.1.1.2.1 XPS

XPS analysis was performed on samples of tape MP1 run at high humidity conditions for 5K and 10K passes only. Figure 3.7 shows the relative atomic percentage of elements detected in

the surface of tape MP1 at 0, 5K and 10K passes at 22°C, 80% RH. The trends for the elemental concentrations were similar to the ambient case with exception of Fe, which decreased at the higher number of passes at high humidity.

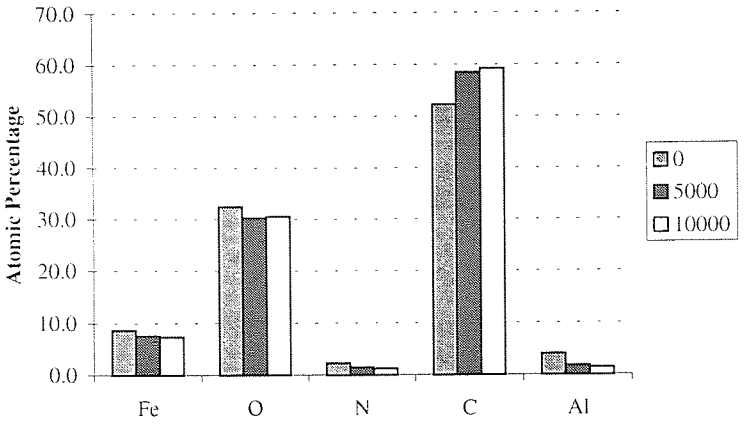

Figure 3.7 Atomic Concentration of Elements as a Function of Increasing Number of Passes for Tape MP1 at 22°C, 80% RH

Synthesis of the C1s peak (Figure 3.8) revealed the same trends at high humidity as those at ambient conditions, namely an increasing C-C/C-H component with decreasing C-O and C-N components showing that at high humidity, binder depletion was still evident.

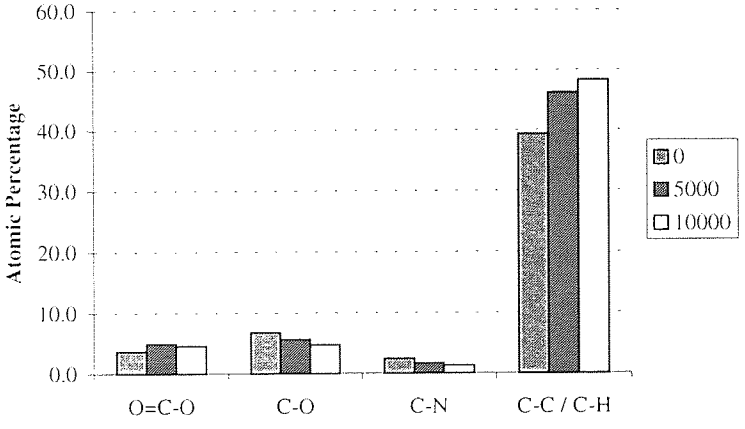

Figure 3.8 Synthesis of C for Tape MP1 at 22°C, 80% RH

Figure 3.9 shows how the ratios containing Fe and N altered with increaseing number of passes. The largest change was for the Fe:N ratios, which showed a significant increase with increased cycling, possibly due to binder depletion.

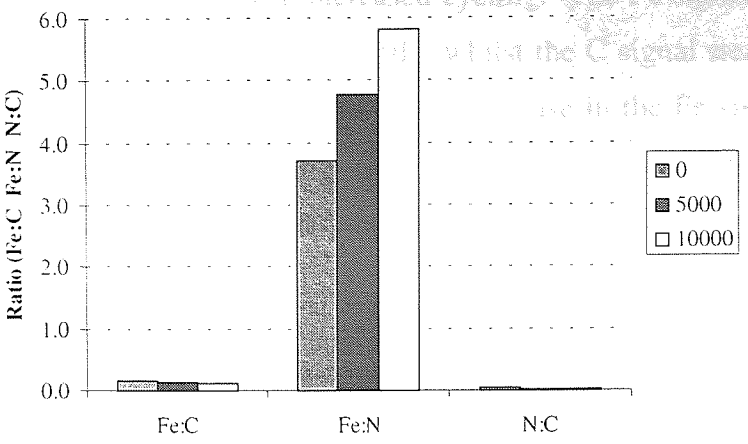

Figure 3.9 Ratio of Fe:C, Fe:N and N:C and for MP1 at 22°C, 80% RH

3.1.2 MP2

3.1.2.1 22°C, 40% RH

3.1.2.1.1 XPS

Tape MP2 produced the same trends for elemental changes as for tape MP1. The Fe signal decreased at a greater rate than MP1 up to 500 passes, indicating that the different makeup of tape MP2 had some effect on its performance during cycling. The synthesised C1s peak also produced similar results.

3.1.2.2 22°C, 80% RH

The same XPS related trends were observed as for tape MP1.

3.1.3 Tape A

3.1.3.1 22°C, 40% RH

3.1.3.1.1 XPS

XPS analysis in the surface region of tape A was performed on a sample from each predetermined number of passes. The elements detected were Co, Fe, O, N, C, Cl, and Al. The presence of Co was due to the nature of the tape, it being a Co modified Fe oxide tape (2.1.1). The Cl content of the tape was due to the use of a Cl based binder (Table 2.3). Exposure to the primary X-ray beam caused a decrease in concentration of chlorine, for this reason the Cl 2p peak was always collected first.

The N and Cl signals both decreased with increased cycling. The Fe signal was more or less stable, although it increased then decreased slightly, whilst the C signal steadily increased up to 20 000 passes after an initial decrease. The slight increase in the Fe signal was probably due to the overall layer thickness decreasing. A possible mechanism for this is removal of a carbonaceous contamination film, hence the initial drop in the detected C signal.

Synthesis of the C1s peak revealed 5 chemical states contributing to the total peak, as shown in Figure 3.11. The C-Cl bonds occurred at two separate energies one of which coincided with the binding energy of the C-N bond. Since the two Cl peaks were known to be of equal magnitude, it was possible to separate the C-N/Cl bond into C-Cl and C-N bonds.

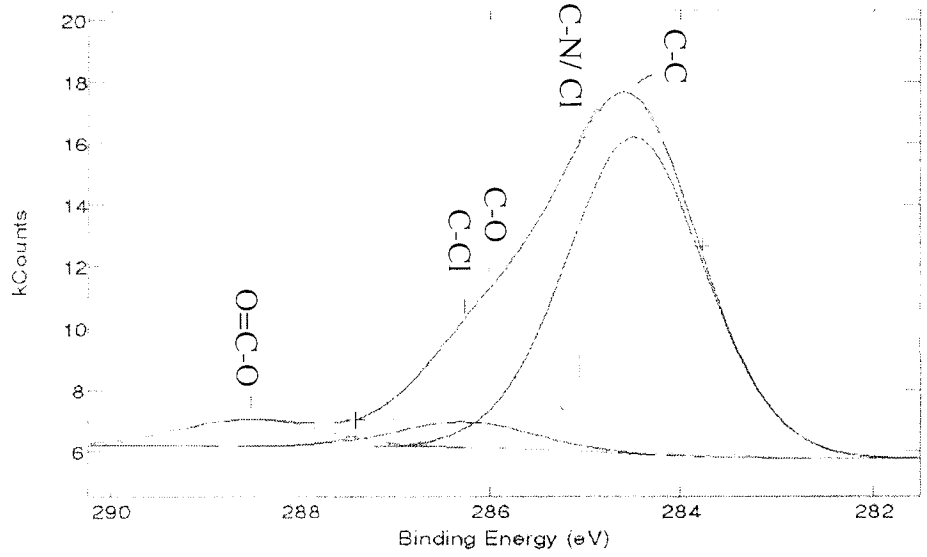

Figure 3.10 Example of Peak Synthesis of C for Tape A

Figure 3.11 shows the effect of cycling on the synthesised C peak. The C-N, C-Cl and C-O bonds decreased. The C-C/C-H bond increased with cycling after an initial decrease up to 100 passes. This decrease corresponded to the decrease in the C signal and therefore corroborates the idea of the removal of a carbonaceous contamination film.

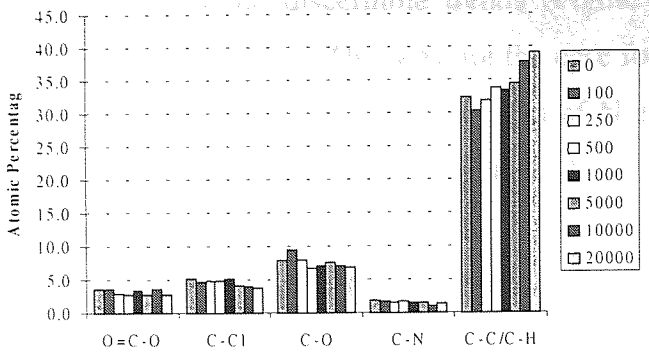

Figure 3.11 Synthesis of C for Tape A at 22°C, 40% RH

Figure 3.12 shows how the ratios of Fe:C, Fe:O, Fe:N, N:C, Cl:C, and Fe:Cl respectively were affected by cycling of the tape.

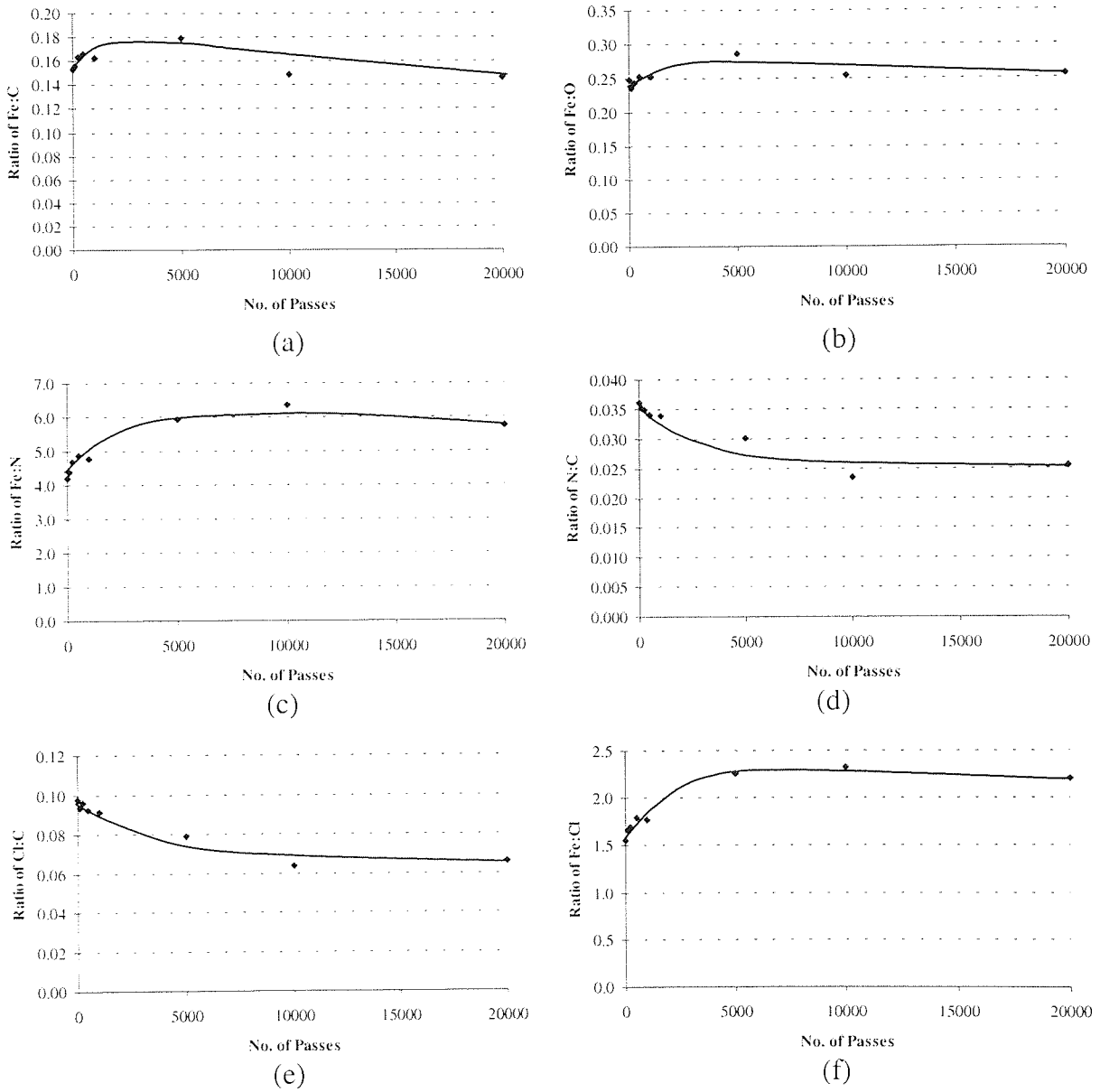

Figure 3.12 Ratio of (a) Fe:N (b) N:C (c) Fe:C and (d) Fe:O (e) Cl:C and (f) Fe:Cl for Tape A at 22°C, 40% RH

The change in the Fe:C ratio showed no discernible trends (Figure 3.12c) and could be considered to be stable with increased cycling. This was not the case for the ratios containing N and Cl. Figure 3.12 (a, b, e and f) provide evidence of loss of N and Cl with increasing number of passes. Figure 3.11 mirrors the results for tape MP1 in that the C-C/C-H component of the C signal increased with cycling. A brief initial decrease of the overlayer thickness was noted before increasing to a stable situation with increased cycling (Figure 3.13).

The variation in overlayer thickness with increasing number of passes is presented in Figure 3.13. After an initial decrease the overlayer thickness recovered to the virgin state.

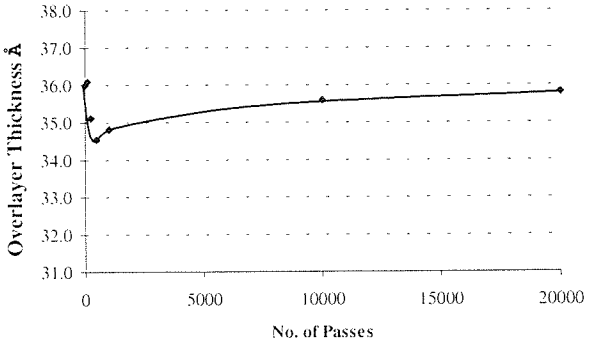

Figure 3.13 Variation in Overlayer Thickness as a Function of increasing number of Passes

3.1.3.2 22°C, 80% RH

3.1.3.2.1 XPS

Cycling experiments were performed for 5K and 10K passes at high humidity conditions. Figure 3.14 shows the relative atomic percentage of elements detected in the near surface region of tape A at 0, 5K and 10K passes at 22°C, 80% RH. The trends for the elemental concentrations (Figure 3.14)and synthesised C peak (Figure 3.15) were similar to the ambient case.

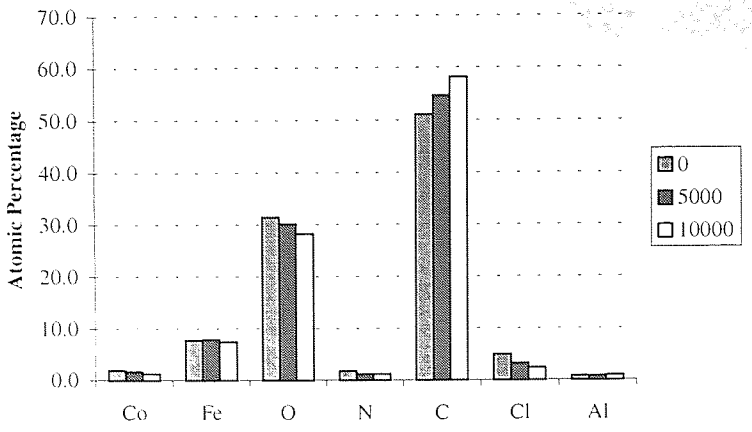

Figure 3.14 Atomic Concentration of Elements as a Function of Increasing Number of Passes for Tape A at 22°C, 80% RH

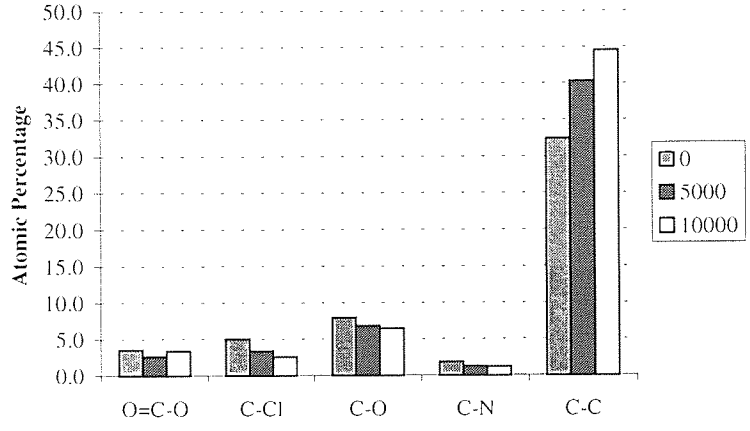

Figure 3.15 Synthesis of C for Tape A at 22°, 80% RH

Figure 3.16 shows how the ratios of interest altered with increased number of passes. As for tape MP1, the largest change was for the Fe:N ratios, similarly for the Fe:Cl ratios which showed a significant increase with increased cycling.

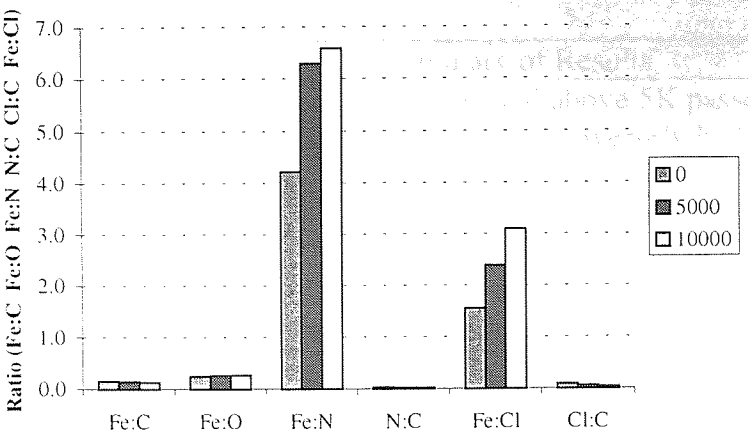

Figure 3.16 Ratio of Fe:C, Fe:N, N:C abd Fe:O for tape A at 22°C, 80% RH

The results for this section are summarised in Table 3.1.

Tape	Condition	Summary of Results	
MP1	22°C/40% RH	XPS	Increase in Fe signal above 5K passes, C increased with pass number. Conversely N decreased with increasing passes.
		Synthesis of C	C-O and C-N components both decreased throughout cycling whereas C-C/C-H increased.
		Ratios	Fe:C initial decrease then increased, Fe:N increased throughout. N:C decreased.
	22°C/80% RH	XPS	Similar to 22°C/40% RH results, except for Fe which decreased above a higher number of passes.
		Synthesis of C	As for 22°C/40% RH test.
		Ratios	As for 22°C/40% RH test except Fe:C decreased throughout cycling.
MP2	22°C/40% RH	XPS	As for MP1, however the Fe signal decreased at a greater rate up to 500 passes.
		Synthesis of C	As for MP1.
		Ratios	As for MP1.
	22°C/80% RH	XPS	As for MP1.
		Synthesis of C	As for MP1.
		Ratios	As for MP1.
tape A	22°C/40% RH	XPS	N and Cl both decreased with cycling. Slight increase in Fe signal. Overall C increased throughout the test.
		Synthesis of C	C-N, C-Cl and C-O decreased, C-C/C-H increased after an initial decrease at 100 passes.
		Ratios	Fe:C showed no discernible trends. Fe:N and Fe:Cl increased with cycling. N:C and Cl:C decreased.
	22°C/80% RH	XPS	As for 22°C/40% RH test.
		Synthesis of C	As for 22°C/40% RH test.
		Ratios	As for 22°C/40% RH test.

Table 3.1 Summary of Results for the Loop Tester Experiments

3.2 Georgens Cycler Experiments (No Head)

Tape MP1 was loaded into a QIC and cycled in a Georgens cycler with no head installed. This allowed any effects that the tape path components may have had on the tape surface to be observed.

3.2.1 MP1

3.2.1.1 22°C, 40% RH

3.2.1.1.1 XPS

Near identical results were produced for the Georgens cycled tapes and those cycled on the loop tester. The Fe signal decreased and then increased slightly at higher passes, whereas the C signal increased overall up to 10K passes. N was seen to decrease with cycling.

Figure 3.17 shows the result of cycling on the synthesised C peak. The C-O and C-N bonds decreased while the C-C/C-H bond increased with cycling.

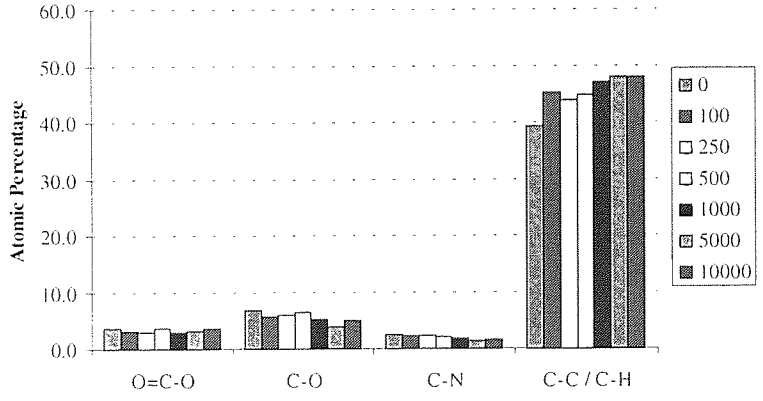

Figure 3.17 Synthesis of C for Tape MP1 at 22°C, 40% RH

The ratios of Fe:C, Fe:N and N:C are presented at the end of this section so that the results for all four environmental conditions can be compared, one graph for each ratio.

3.2.1.1.2 Dropout Analysis

The effects of cycling on the dropout frequency of the 6, 10 and 16 dB categories are shown in Figure 3.18. In each case the frequency dropped up to 1K passes then levelled off to a constant rate.

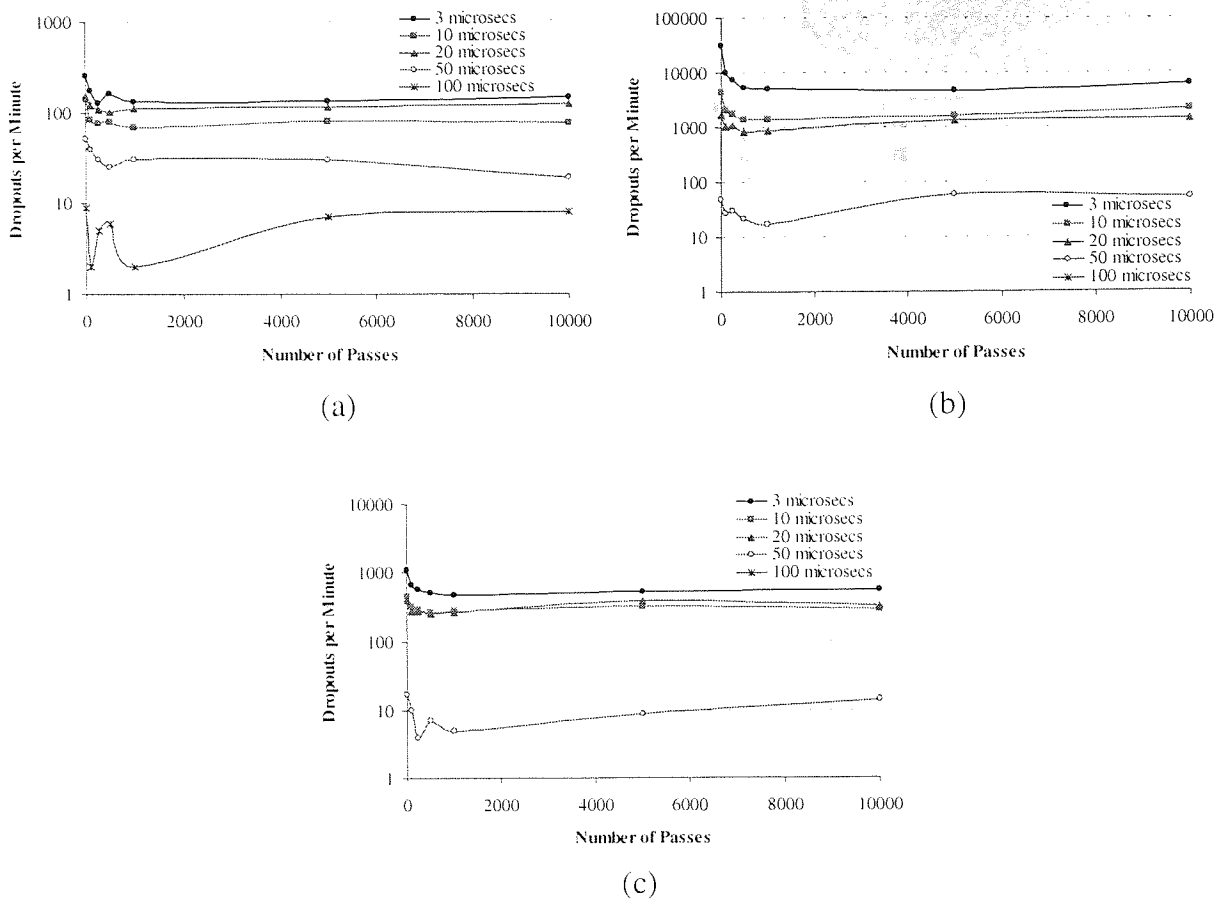

Figure 3.18 (a) 6 dB (b) 10 dB and (c) 16 dB Dropout Growth for Tape MP1 at 22°C 40%RH

3.2.1.2 22°C, 80% RH

3.2.1.2.1 XPS

Figure 3.19 shows how the relative atomic concentrations of elements found in the surface of the tape varied as a function of increasing number of passes. The Fe signal remained constant until it increased at the higher number of passes, whereas the C signal increased overall up to 1K passes where a significant decrease was noted.

The synthesised C peak (Figure 3.20) showed that the C-O and C-N components decreased with cycling. The C-C/C-H component mirrored the trend of the C 1s signal in that it increased up until 1K passes then decreased at 5K and 10K passes.

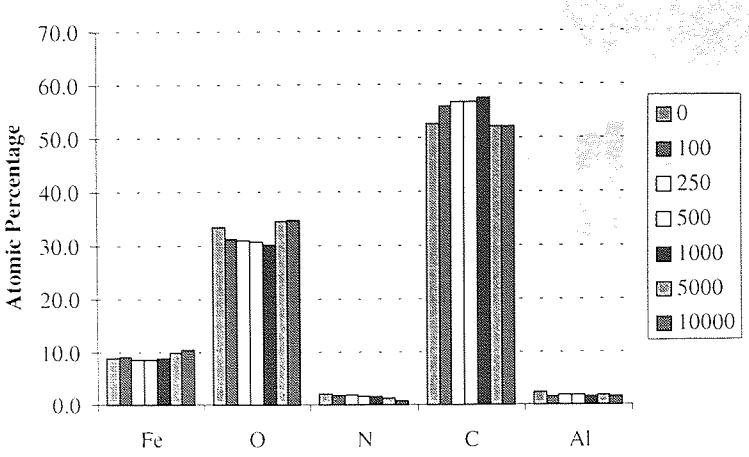

Figure 3.19 Atomic Concentration of Elements as a Function of Increasing Number of Passes for Tape MP1 at 22°C, 80% RH

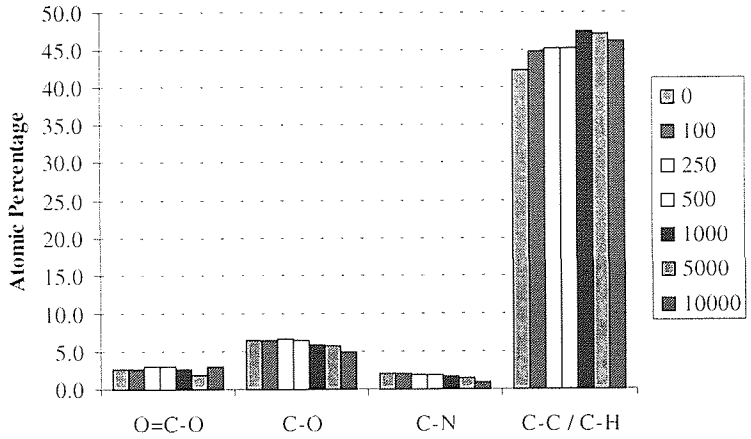

Figure 3.20 Synthesis of C for Tape MP1 at 22°C, 80% RH

3.2.1.2.2 Dropout Analysis

The effects of cycling on the dropout frequency of the 6, 10 and 16 dB categories were similar to those at 22°C, 40% RH (3.2.1.1.2). In each case the frequency dropped sharply up to 1K passes then levelled off to a constant rate.

3.2.1.3 32°C, 80% RH

3.2.1.3.1 XPS

The same elemental trends were observed as for the 22°C, 80% RH case. At this condition the synthesised C peak (Figure 3.21) showed that overall, the C-C/C-H component of the C 1s signal increased throughout cycling. The C-O and C-N components decreased with cycling.

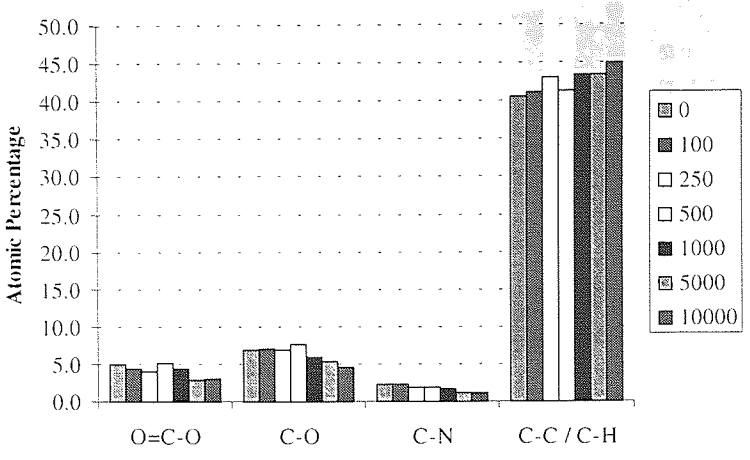

Figure 3.21 Synthesis of C for Tape MP1 at 32°C, 80% RH

3.2.1.3.2 Dropout Analysis

The effects of cycling on the dropout frequency of the 6, 10 and 16 dB categories were the same as for the two previous cases (3.2.1.1 and 3.2.1.2) and as such will not be presented. In each case the frequency dropped sharply up to 1K passes then levelled off to a constant rate.

3.2.1.4 40°C, 15% RH

3.2.1.4.1 XPS

Identical trends were observed as for the 22°C, 80% RH and 32°C, 80% RH cases but to a lesser degree. The C signal increased slightly up to 1K passes before decreasing at 5K and 10K passes. At this condition the synthesised C peak (Figure 3.21) showed that overall, the C-C/C-H component of the C 1s signal decreased throughout cycling until an increase occurred at 10K passes. The C-O component remained relatively stable throughout cycling only exhibiting a decrease at 10K passes. The C-N components decreased with cycling.

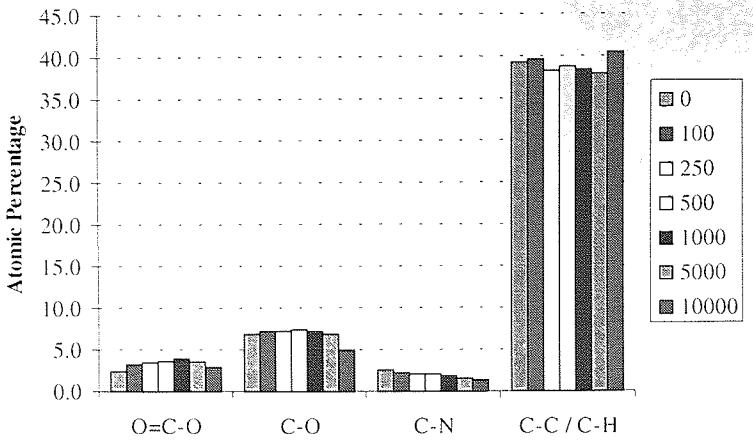

Figure 3.22 Synthesis of C for Tape MP1 at 40°C, 15% RH

3.2.1.4.2 Dropout Analysis

The effects of cycling on the dropout frequency of the 6, 10 and 16 dB categories were the same as for the three previous cases (3.2.1.1, 3.2.1.2 and 3.2.1.3) and as such will not be presented. In each case the frequency dropped sharply up to 1K passes then levelled off to a constant rate.

The ratios of Fe:C, Fe:N and N:C for each environmental condition are presented in Figure 3.23 and Figure 3.24.

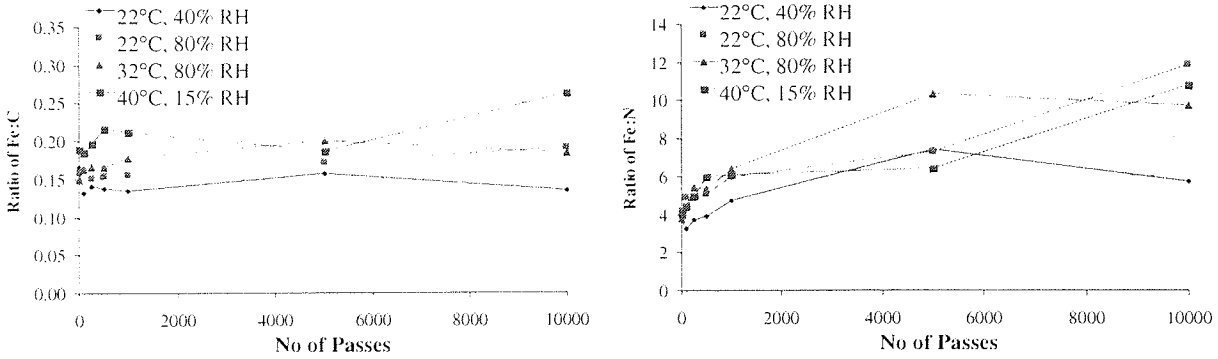

Figure 3.23 Ratio of (a) Fe:C and (b) Fe:N for Tape MP1

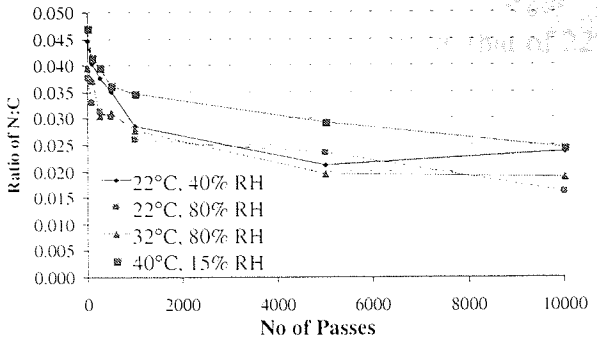

Figure 3.24 Ratio of N:C for Tape MP1

The change in the Fe:C ratios showed a slight increase with increased cycling (Figure 3.23). This was not the case for the ratios containing N, both provided evidence of N depletion with increasing number of passes (Figure 3.23 and Figure 3.24).

The effects of cycling on the dropout frequency of the 6, 10 and 16 dB categories were the same as for the three previous conditions (3.2.1.1, 3.2.1.2 and 3.2.1.3) and as such will not be presented. In each case the frequency dropped sharply up to 1K passes then levelled off to a constant rate.

The variation in overlayer thickness with increasing number of passes is presented in Figure 3.25. The overlayer thickness appeared to decrease as a function of temperature.

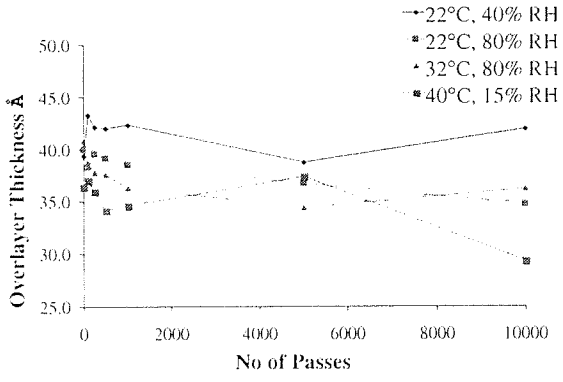

Figure 3.25 Variation in Overlayer Thickness as a Function of increasing number of Passes for tape MP1

3.2.2 MP2

Tape MP2 was only utilised for one experimental condition, that of 22°C, 40% RH (2.3.7)

3.2.2.1 22°C, 40% RH

3.2.2.1.1 XPS

Figure 3.26 shows how the relative atomic concentrations of elements found in the surface of the tape varied as a function of increasing number of passes.

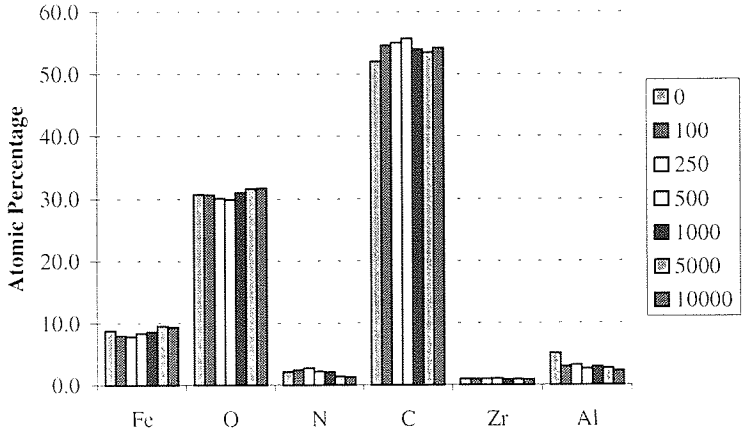

Figure 3.26 Atomic Concentration of Elements as a Function of Increasing Number of Passes for Tape MP2 at 22°C, 40% RH

Two phases seemed to have occurred during cycling, initially, Fe and O decreased whilst C and N increased. The next phase had C and N decreasing whilst the O and Fe signals increased for the remainder of cycling. Figure 3.27 shows how the C-C/C-H component increased throughout cycling. The C-O and C-N components increased and then decreased at the higher number of passes.

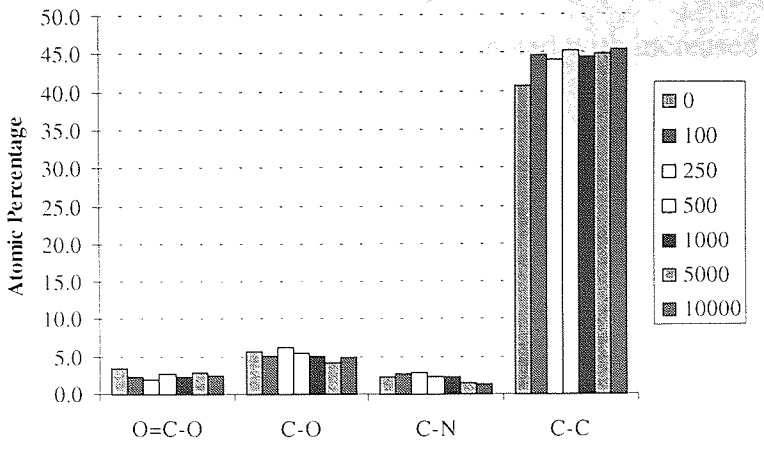

Figure 3.27 Synthesis of C for Tape MP2 at 22°C, 40% RH

Figure 3.28 present the ratios of Fe:C, Fe:N and N:C respectively.

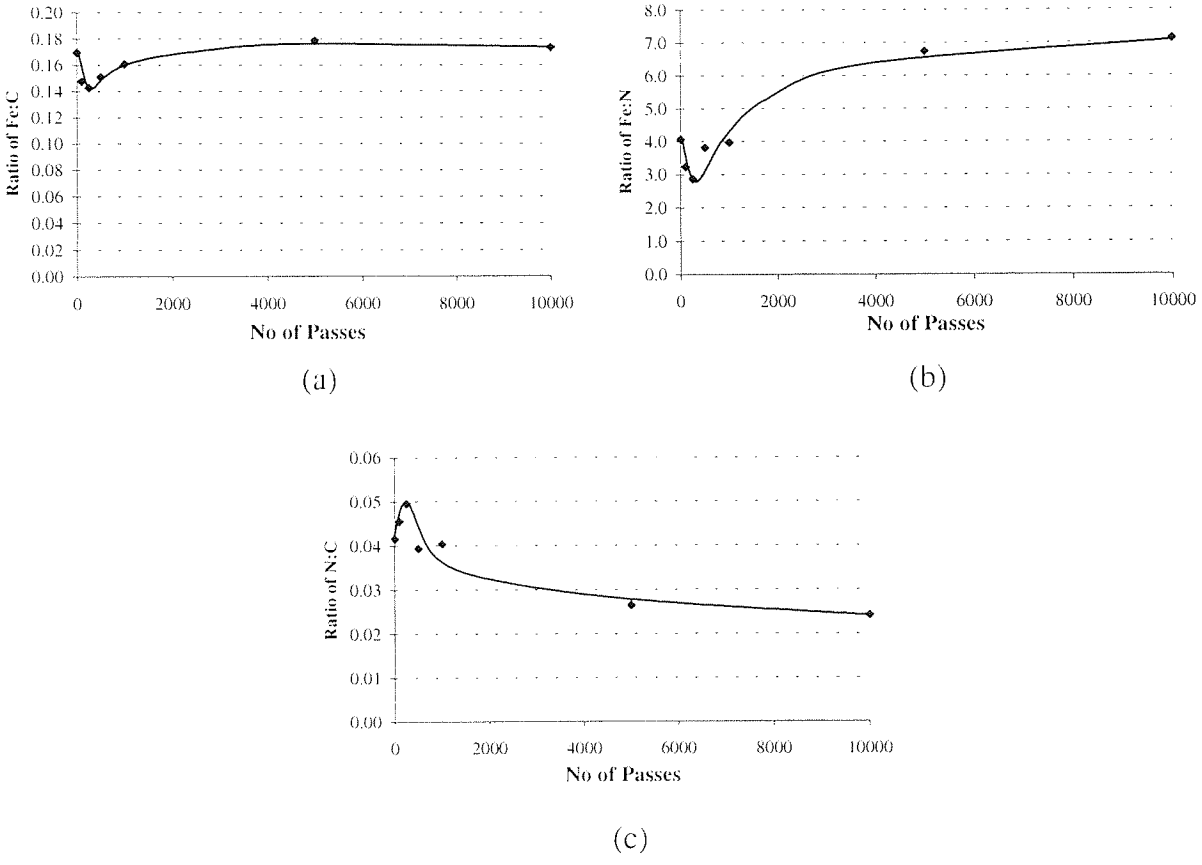

Figure 3.28 Ratio of (a) Fe:C (b) Fe:N and (c) N:C for Tape MP2 at 22°C, 40% RH

The change in the Fe:C ratio showed a slight decrease in the initial stages of cycling. For the ratios containing N (Figure 3.28 b and c), both provided evidence of depletion at the higher number of passes.

The variation in overlayer thickness with increasing number of passes is presented in Figure 3.29. Overall a decrease of the overlayer thickness was noted with increased cycling.

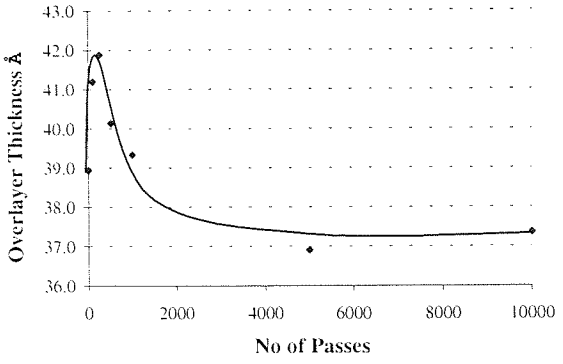

Figure 3.29 Variation in Overlayer Thickness as a Function of increasing number of Passes

3.2.2.1.2 Dropout Analysis

The effects of cycling on the dropout frequency of the 6, 10 and 16 dB categories are shown in Figure 3.30. As for tape MP1, in each case the frequency dropped sharply up to 1K passes then levelled off to a constant rate.

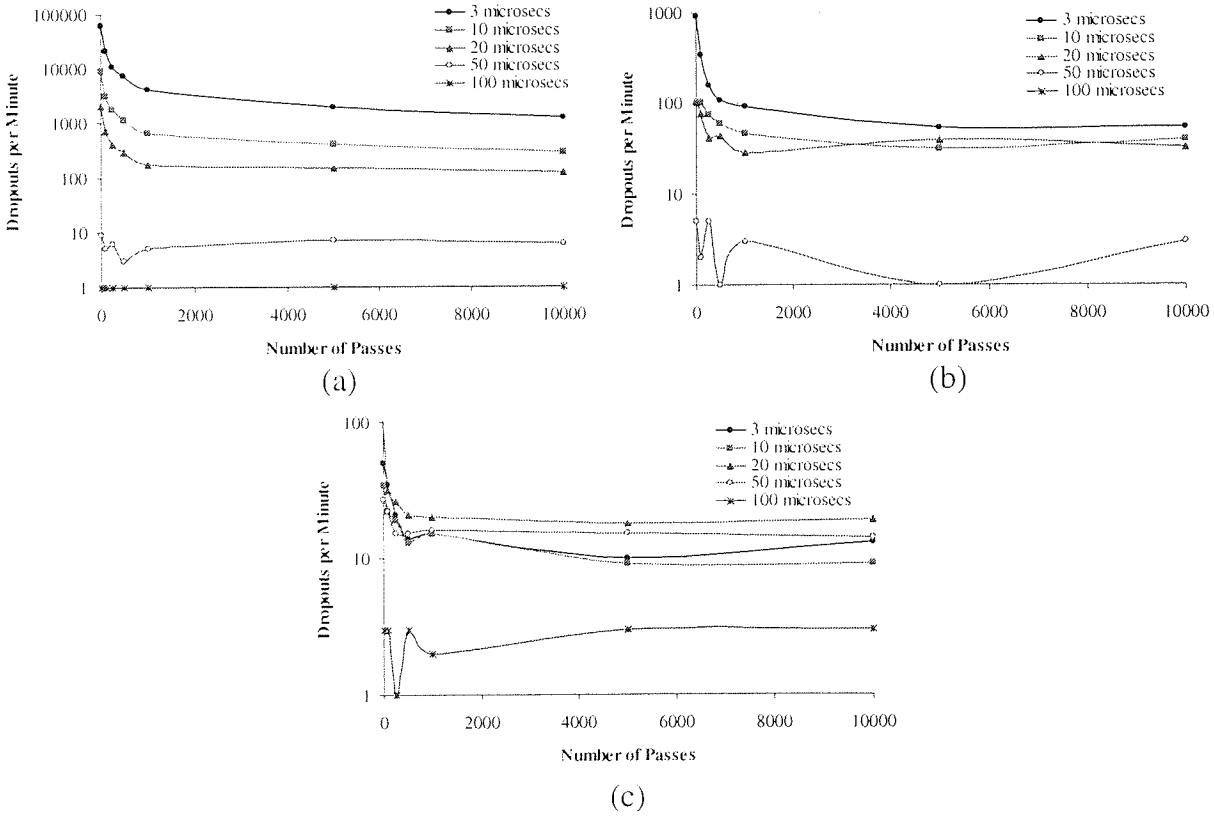

Figure 3.30 (a) 6 dB (b) 10 dB and (c)16 dB Dropout Growth for Tape MP2 at 22°C 40%RH

3.2.3 Tape A

3.2.3.1 22°C, 40% RH

3.2.3.1.1 XPS

Similar results were produced for the Georgens cycled tapes and those cycled on the loop tester. The Fe signal remained relatively stable with cycling, whereas the C signal increased up to 10K passes. N and Cl decreased with cycling.

Figure 3.31 shows the result of cycling on the synthesised C peak. The C-O, C-Cl and C-N bonds decreased while the C-C/C-H bond increased with cycling.

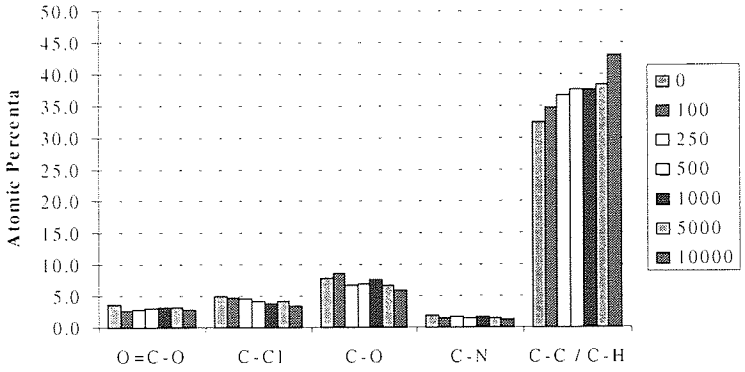

Figure 3.31 Synthesis of C for Tape A at 22°C, 40% RH

3.2.3.1.2 Dropout Analysis

The effects of cycling on the dropout frequency of the 6, 10 and 16 dB categories are shown in Figure 3.32. As for tape MP1 and MP2, an initial sharp decrease in the frequency occurred which levelled off to a constant rate.

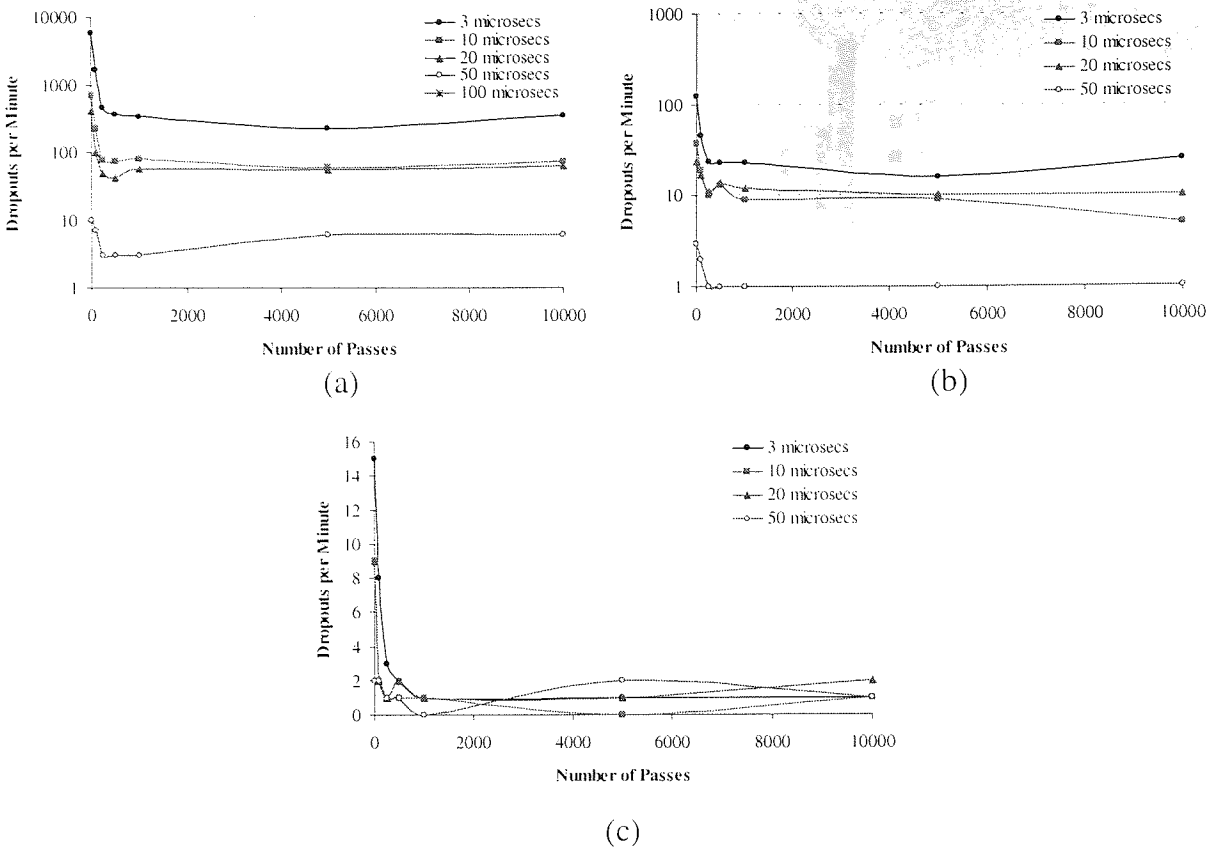

Figure 3.32 (a) 6 dB (b) 10 dB and (c) 16 dB Dropout Growth for Tape A at 22°C 40%RH

3.2.3.2 22°C, 80% RH

3.2.3.2.1 XPS

Similar results were produced for the condition of 22°C, 40% RH. The Fe signal exhibited a slight increase with cycling, whereas the C signal increased distinctly up to 10K passes. N and Cl decreased with cycling.

Figure 3.33 shows the results of cycling on the synthesised C peak. The C-O, C-Cl and C-N bonds decreased while the C-C/C-H bond increased with cycling.

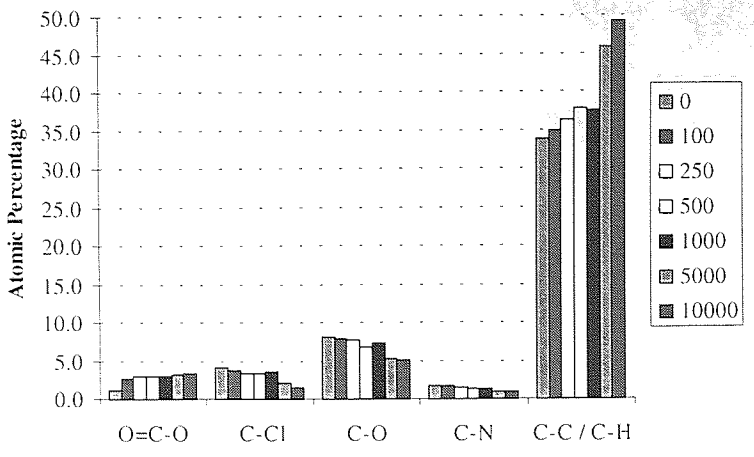

Figure 3.33 Synthesis of C for Tape A at 22°C, 80% RH

3.2.3.2.2 Dropout Analysis

The effects of cycling on the dropout frequency of the 6, 10 and 16 dB categories were similar to those at 22°C, 40% RH and as such will not be presented graphically.

3.2.3.3 32°C, 80% RH

3.2.3.3.1 XPS

Similar results were produced for the conditions of 22°C, 40% RH and 22°C, 80% RH. The Fe signal exhibited an increase with cycling, as did the C signal. Co and Cl decreased with cycling, but N only appeared to decrease after 10K passes.

Figure 3.34 shows the results of cycling on the synthesised C peak. The C-O, and C-Cl bonds decreased overall while the C-C/C-H bond increased overall with cycling. The C-N bond showed no definite trend with cycling although a decrease was noted at the higher numbers of passes.

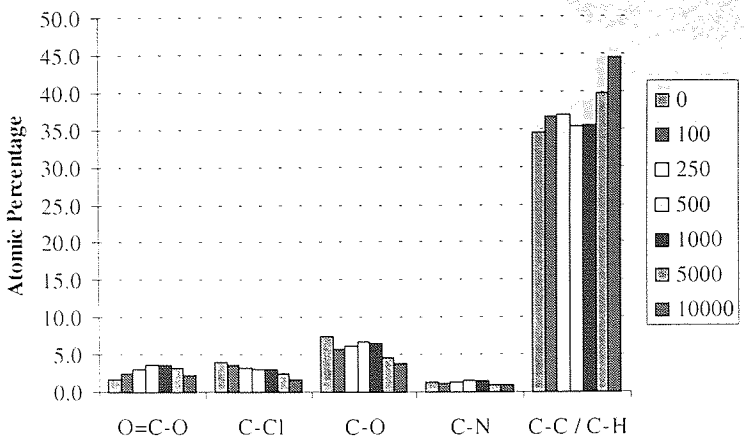

Figure 3.34 Synthesis of C for Tape A at 32°C, 80% RH

3.2.3.3.2 Dropout Analysis

The effects of cycling on the dropout frequency of the 6, 10 and 16 dB categories were similar to the conditions of 22°C, 40% RH and 22°C, 80% RH. An initial sharp decrease in the frequency occurred which levelled off to a constant rate until 16000 passes were completed. A slight increase occurred after 12K passes for the 100μs class for the 10 dB and 16 dB categories.

3.2.3.4 40°C, 15% RH

3.2.3.4.1 XPS

The results produced were similar to those at the conditions of 22°C, 40% RH and 22°C, 80% RH. The Fe signal exhibited an increase with cycling, as did the C signal. Co, N and Cl decreased with cycling.

Figure 3.35 shows the results of cycling on the synthesised C peak. The C-O, and C-Cl bonds decreased overall while the C-C/C-H bond increased with cycling. The C-N bond showed no definite trend with cycling although a decrease was noted at the higher number of passes.

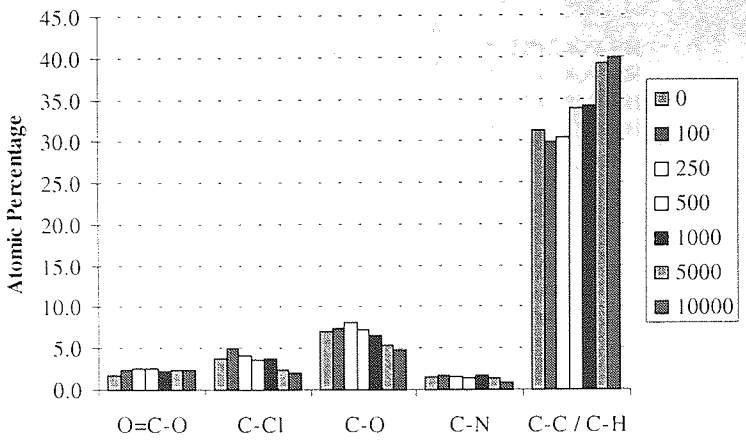

Figure 3.35 Synthesis of C for Tape A at 40°C, 15% RH

3.2.3.4.2 Dropout Analysis

The effects of cycling on the dropout frequency of the 6, 10 and 16 dB categories were similar to the conditions of 22°C, 40% RH, 22°C, 80% RH and 32°C, 80% RH. An initial sharp decrease in the frequency occurred which levelled off to a constant rate. A slight increase was noted for the smallest category of 3μs for all classes of dropout the 6dB class also showed an increase in the 10μs category of dropout.

The ratios of Fe:C, Fe:N, Fe:Cl, N:C and Cl:C are presented in Figure 3.36.

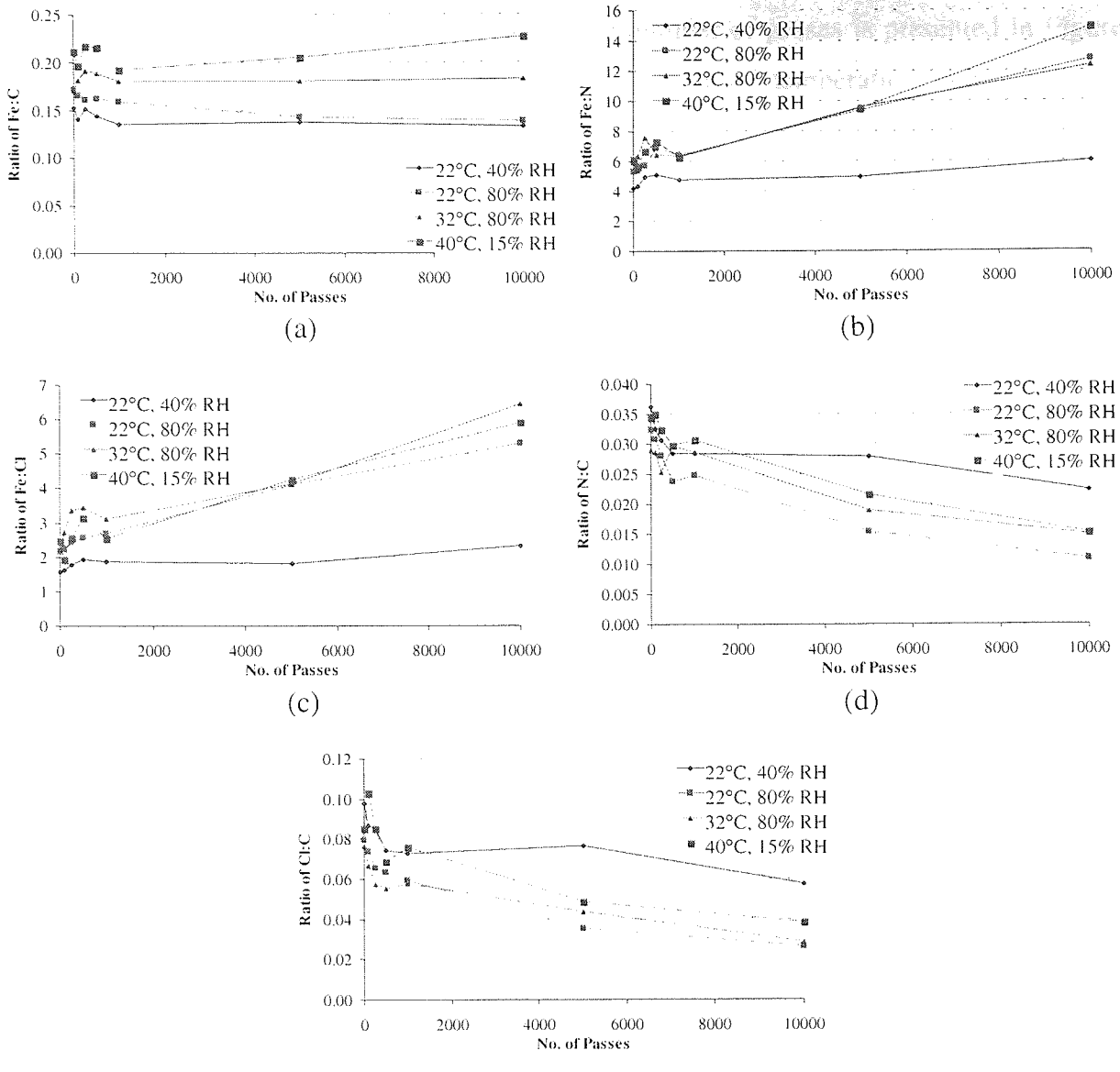

Figure 3.36 Ratio of (a) Fe:C (b) Fe:N (c) Fe:Cl (d) N:C and (e) Cl:C for Tape A at 40°C 15%RH

The change in the Fe:C ratios showed little change with increased cycling (Figure 3.36a). This was not the case for the ratios containing N and Cl, which provided evidence of N and Cl depletion with increasing number of passes.

The elemental ratio plots suggest the change in surface concentration was dependent on the environmental operating conditions. For the cases of Fe:N and Fe:Cl (Figure 3.36b and c respectively), the spread of data points for the virgin tape and the tape that had been cycled for just a few hundred passes was relatively small. However, after 10K passes the spread of data points for each condition was much wider.

The variation in overlayer thickness with increasing number of passes is presented in Figure 3.37. The overlayer thickness decreased as a function of temperature and/or relative humidity.

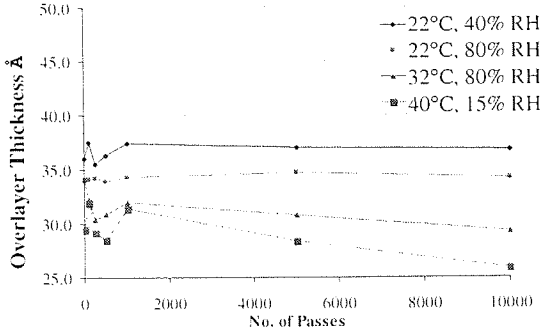

Figure 3.37 Variation in Overlayer Thickness as a Function of increasing number of Passes for Tape A

The results for this section are summarised in Table 3.2.

Tape	Condition	Summary of Results	
MP1	22°C/40% RH	XPS	Increase in Fe signal above 5K passes, C increased with pass number. Conversely N decreased with increasing passes.
		Synthesis of C	C-O and C-N components both decreased with cycling whereas C-C/C-H increased.
		Ratios	Fe:C initial decrease then increased, Fe:N increased throughout. N:C decreased.
	22°C/80% RH	XPS	Similar to 22°C/40% RH results except C decreased above 5K passes.
		Synthesis of C	As for 22°C/40% RH test.
		Ratios	As for 22°C/40% RH test.
	32°C/80% RH	XPS	Similar to 22°C/80% RH results
		Synthesis of C	As for 22°C/80% RH test.
		Ratios	Fe:C increased slightly with cycling, Fe:N increased throughout whilst N:C decreased.
	40°C/15% RH	XPS	Similar to 22°C/40% RH results but C remained stable up to 5K passes where it decreased up to 10K passes.
		Synthesis of C	As for 22°C/40% RH test.
		Ratios	As for 32°C/80% RH test.
MP2	22°C/40% RH	XPS	As for MP1, however the Fe signal decreased at a greater rate up to 500 passes.
		Synthesis of C	As for MP1.
		Ratios	As for MP1.
	22°C/80% RH	XPS	As for MP1.
		Synthesis of C	As for MP1.
		Ratios	As for MP1.
tape A	22°C/40% RH	XPS	N and Cl both decreased with cycling. Slight increase in Fe signal. Overall C increased throughout the test.
		Synthesis of C	C-N, C-Cl and C-O decreased, C-C/C-H increased after an initial decrease at 100 passes.
		Ratios	Fe:C showed no discernible trends. Fe:N and Fe:Cl increased with cycling. N:C and Cl:C decreased.
	22°C/80% RH	XPS	As for 22°C/40% RH test.
		Synthesis of C	As for 22°C/40% RH test.
		Ratios	As for 22°C/40% RH test.

Table 3.2 Summary of Results for the Georgens Cycler Experiments (No Head)

3.3 Georgens Cycler with TR-4 Head

3.3.1 MP1

3.3.1.1 XPS

3.3.1.1.1 32°C, 80% RH

Since only one tape was cycled (due to a lack of heads) there remained only two samples for analysis at the end of each experiment, a virgin tape and one which had reached the end of the designated number of passes. At the end of 11 000 passes, the front side of the tape was analysed using XPS in order to determine whether any significant chemical changes had resulted from interactions with the TR-4 head. The analysis was performed at the edge of the tape and in the centre (at a position relative to the location of the drive belt). The results, together with those when tape MP1 was cycled for 10K passes at 32°C, 80% RH with no head present, are listed in Table 3.3.

32°C, 80% RH	Fe	O	N	C	Al
No Tr-4 head (10K passes)	12.5	34.9	1.0	49.5	2.1
Centre (with Tr-4 head)	13.1	38.1	1.1	45.7	2.0
Edge (with Tr-4 head)	10.4	32.4	2.1	52.3	2.8

Table 3.3 Elemental concentrations on front side of tape MP1 after 10K passes at 32°C,80% RH

In previous experiments (before heads were installed into the cycler units), the area of analysis chosen for XPS experiments was 3×2 mm^2, and was concentrated mainly in the centre region of the tape. After the introduction of a TR-4 head, analysis of the tape was performed at two distinct positions - an area beneath the drive belt (centre) and an area off the belt position (edge). The area of analysis was also reduced to 1×1mm^2 to keep regions discrete. Any comparisons with earlier XPS results should be made with those from the centre region of the tape. Results suggest the addition of a (permanently unenergised) TR-4 head to the cycler did not lead to significant chemical changes to the surface of the tape.

Indeed, the Fe:N ratio for the surface of the tape prior to the addition of a head was 12.5 whereas after the head had been included, the Fe:N ratio at the centre of the tape was 11.9. However, when comparing these values with those from the edge of the tape, there are significant differences. The percentage of Fe had reduced to 10.4 whereas the N content had increased to 2.1 which yielded a Fe:N ratio of 4.9 . Note that for the virgin tape, the Fe:N ratio was 3.8 which showed that although the ratio was greater at the centre when compared to the edge of tape, a reduction in N and/or an increase in Fe had occurred at both positions. Similarly the Fe:C ratio had increased from the virgin condition (0.17) but was greater at the centre of tape.

	Centre		Edge	
	Fe:N	Fe:C	Fe:N	Fe:C
32°C, 80% RH	11.9	0.29	4.9	0.20

Table 3.4 Fe:N and Fe:C ratios for tape MP1 run at 32°C, 80 RH with a TR-4 head installed

The difference between the centre and edge of tape was obvious (Table 3.3 and Table 3.4). There was clearly an abundance of Fe at the centre of tape whereas there was a higher N and C content at the edge.

The effects of cycling on the dropout frequency of the 4 dB, 5 dB, 6 dB and 10 dB categories are shown in Figure 3.38. An initial sharp decrease in frequency occurred for most classes of dropout, which levelled off to a constant rate. An increase occurred for the 50 μs class for the 4 dB, 6 dB and 10 dB dropout categories.

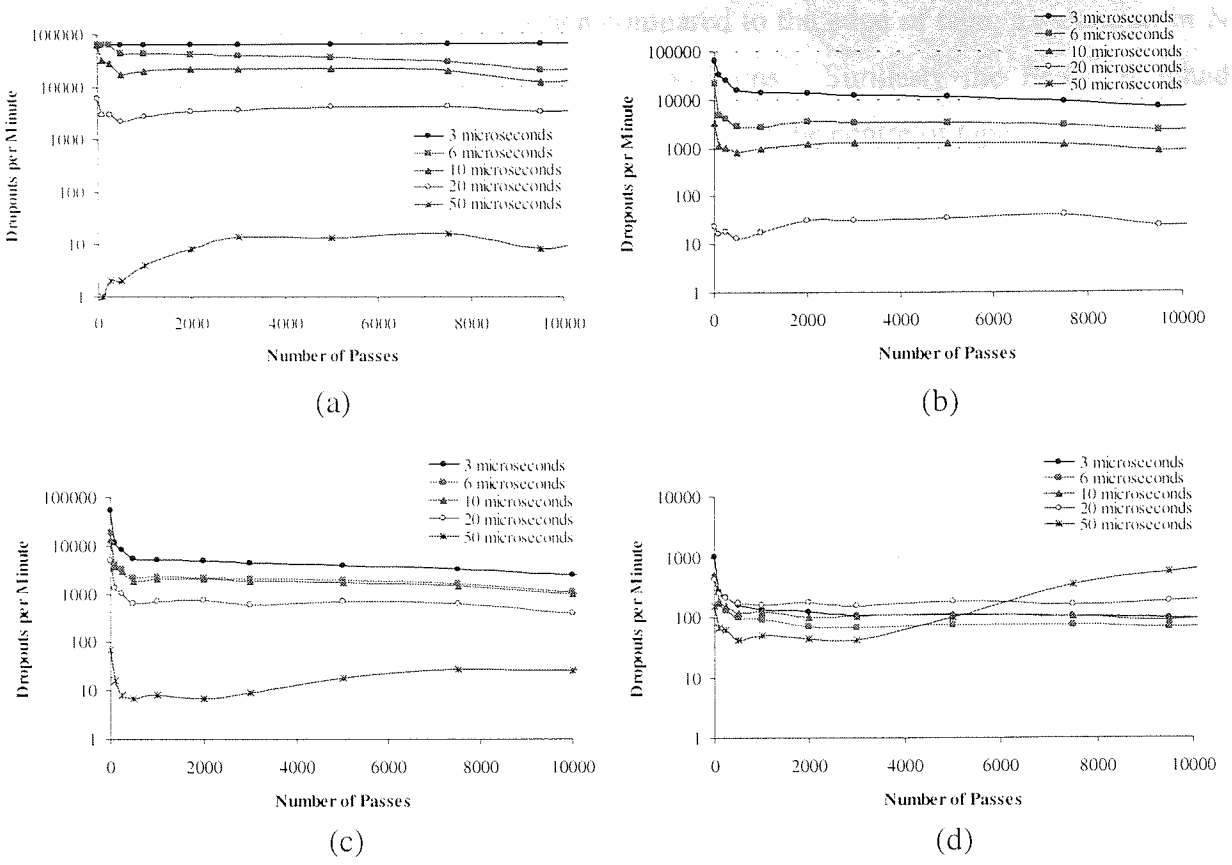

Figure 3.38 (a}4 dB (b) 5 dB (c) 6 dB and (d) 10 dB Dropout Growth for Tape MP1 at 32°C, 80% RH

3.3.1.2 40°C, 15% RH

When tape MP1 was cycled against a TR-4 head at 40°C, 15 % RH cartridge failure occurred after just 4K passes. The mode of failure was that of the tape backcoat adhering to the cartridge guide pins, thus preventing tape motion. XPS analysis of the front side of the tape was carried out at the centre and edge tape positions. The results, together with those when tape MP1 was cycled for 5K passes at 40°C, 15% RH with no head, are listed in Table 3.5.

40°C, 15% RH	Fe	O	N	C	Al
No Tr-4 head (5K passes)	10.4	35.6	1.6	50.1	2.3
Centre (with Tr-4 head)	12.9	34.9	0.8	50.0	1.5
Edge (with Tr-4 head)	10.0	33.3	1.3	52.7	2.7

Table 3.5 Elemental concentrations on front side of tape MP1 after 5K passes at 40°C, 15% RH

The Fe:N ratio was greater at the centre when compared to the edge of tape, a reduction in N and/or an increase in Fe had occurred at both positions. Similarly the Fe:C ratio had increased from the virgin condition (0.17) but was greater at the centre of tape.

	Centre		Edge	
	Fe/N	Fe/C	Fe/N	Fe/C
40°C, 15% RH	16.1	0.26	7.7	0.19

Table 3.6 Fe:N and Fe:C ratios for tape MP1 run at 40°C, 15% RH with a TR-4 head installed

The effects of cycling on the dropout frequency of the 4, 5, 6 and 10 dB categories were similar to the 32°C, 80% RH case up to the point of failure. The frequency dropped sharply up to 1K passes then levelled off to a constant up to 3K passes.

3.3.1.3 5°C, 10% RH

When tape MP1 was cycled against a TR-4 head at 5°C, 10 % RH it was cycled for 20K passes to promote dropout growth. As such there can be no comparison made with a tape cycled without a head present (10K passes). XPS analysis of the front side of the tape was carried out at the centre and edge tape positions. The results are listed in Table 3.7.

5°C, 10% RH	Fe	O	N	C	Al
Centre after 20K passes (with Tr-4 head)	11.1	33.5	0.8	52.4	2.2
Edge after 20K passes (with Tr-4 head)	9.1	32.4	1.2	55.3	2.0

Table 3.7 Elemental concentrations on front side of tape MP1 after 20K passes at 5°C, 10 % RH

As for the two previous environmental conditions the centre and edge of tape produced different results. The Fe:N ratio was greater at the centre when compared to the edge of tape although a reduction in N and/or an increase in Fe had occurred at both positions. Similarly the Fe:C ratio had increased from the virgin condition (0.17) but was greater at the centre of tape.

	Centre		Edge	
	Fe/N	Fe/C	Fe/N	Fe/C
5°C, 10% RH	13.9	0.21	7.6	0.17

Table 3.8 Fe:N and Fe:C ratios for tape MP1 run at 5°C, 10 % RH with a TR-4 head installed

The effects of cycling on the dropout frequency of the 4, 5, 6 and 10 dB categories were similar to the 32°C, 80% RH case. The frequency dropped sharply up to 1K passes then levelled off to a constant level up to 20K passes. No increase was observed for any class of dropout.

3.3.2 Tape A

3.3.2.1 32°C, 80% RH

At the end of 11K passes, the experiment was stopped manually and XPS analysis of the front side of the tape was performed. The results, together with those when tape A was cycled for 10K passes at 32°C, 80% RH with no head, are listed in Table 3.3.

Tape A	Co	Fe	O	N	C	Cl	Al
No Tr-4 head (10K passes)	2.3	10.3	30.2	0.8	53.4	2.0	0.9
Centre (with Tr-4 head)	2.1	9.8	32.0	0.7	52.4	1.9	1.1
Edge (with Tr-4 head)	2.7	8.9	33.4	1.0	48.3	4.7	1.0

Table 3.9 Elemental concentrations on front side of tape A after 11K passes at 32°C, 80% RH

The ratios of Fe:N were similar (compared with the centre of tape) for the tapes cycled with and without a head in the system. The Fe:N ratio for the surface of the tape prior to the addition of a head was 12.9 whereas after the head had been included, the Fe:N ratio at the centre of the tape was 14.0. However, when comparing these values with those from the edge of the tape, there are significant differences. The percentage of Fe had reduced whereas the N content had increased. Note that for the virgin tape, the Fe:N ratio was 6.0 which showed that although the ratio was greater at the centre when compared to the centre of tape, a reduction

in N and/or an increase in Fe had occurred at both positions. Similarly the Fe:C ratio had increased from the virgin condition (0.17) but was slightly greater at the centre of tape.

	Centre			Edge		
	Fe:N	Fe:Cl	Fe:C	Fe:N	Fe:Cl	Fe:C
32°C, 80% RH	19.4	5.1	0.19	8.9	1.9	0.18

Table 3.10 Fe:N Fe:Cl and Fe:C ratios for tape A run at 32°C, 80% RH with a TR-4 head installed

The magnitudes of the 4, 5, 6 and 10 dB dropout categories was an order of magnitude lower than for tape MP1 at the same conditions, though the trends were identical. The frequency dropped sharply up to 1K passes then levelled off to a constant level up to 11K passes. No increase was observed for any class of dropout.

3.3.2.2 40°C, 15% RH

Due to the tapes backcoat adhering to the cartridge guide pins, prohibiting tape motion, cartridge failure occurred just before the completion of 2K passes which meant the dropout count at 2K passes was not collected. The XPS results, are listed in Table 3.11, no comparison with results without a head could be made as the nearest number of passes would be 1K, half the number covered during this experiment.

Tape A	Co	Fe	O	N	C	Cl	Al
Centre (with Tr-4 head)	3.5	9.0	32.2	0.66	50.7	3.4	0.5
Edge (with Tr-4 head)	3.9	8.9	30.8	1.0	49.5	4.6	1.4

Table 3.11 Elemental concentrations on front side of tape A after 2K passes at 40°C, 15% RH

Comparing the Fe:N values for the centre and edge of tape, showed that there were significant differences (Table 3.12). Although the percentage of Fe was similar at both positions, the N and Cl content was greater at the edge. Again, a reduction in N and/or an increase in Fe had occurred at both positions, similarly Cl had reduced at the centre but remained fairly constant at the edge. Although the Fe:C ratio had increased from the virgin condition (0.17) they

remained similar at the two tape positions, possibly due to the low number of passes completed.

	Centre			Edge		
	Fe:N	Fe:Cl	Fe:C	Fe:N	Fe:Cl	Fe:C
40°C, 15% RH	13.6	2.6	0.18	8.9	1.9	0.18

Table 3.12 Fe:N Fe:Cl and Fe:C ratios for tape MP1 run at 40°C, 15% RH with a TR-4 head installed

Similar to the previous condition (32°C, 80% RH), the dropout magnitudes decreased up to 1K passes where cartridge failure occurred.

The results for this section are summarised in Table 3.13.

Tape	Condition	Summary of Results		
MP1	32°C, 80% RH	XPS	Comparison	
			Centre	Edge
			Abundance of Fe detected.	Abundance of C and N detected.
		Ratios	Fe:N and Fe:C higher	
		Dropouts	Sharp reduction up to 1K passes then stable. An increase occurred in the 50 µs class for the 4 dB, 6 dB and 10 dB categories.	
	40°C, 15% RH	XPS	As for 32°C, 80% RH	As for 32°C, 80% RH
		Ratios	As for 32°C, 80% RH test.	
		Dropouts	As for 32°C ,80% RH test but no increases occurred for the 50µs class.	
	5°C, 10% RH	XPS	As for 32°C, 80% RH	As for 32°C, 80% RH
		Ratios	As for 32°C, 80% RH	
		Dropouts	As for 32°C ,80% RH test but no increases occurred for the 50µs class.	
Tape A	32°C, 80% RH	XPS	Abundance of Fe detected.	Abundance of Cl and N detected.
		Ratios	Fe:N and Fe:Cl higher	
		Dropouts	Sharp reduction up to 1K passes then stable.	
	40°C, 15% RH (2K Passes)	XPS	Fe similar	Abundance of Cl and N detected.
		Ratios	As for 32°C, 80% RH	
		Dropouts	A decrease occurred up to 1K passes where dropout analysis terminated due to the tape breaking	

Table 3.13 Summary of Results for the Georgens Cycler Experiments (TR-4 Head)

3.3.2.3 AFM and AES Analysis

3.3.2.3.1 Virgin TR-4 Head

Physical information regarding a virgin TR-4 head was obtained by analysing a head using non-contact AFM techniques. Figure 3.39 illustrates the main areas of interest on the head and the information revealed was used as reference data for subsequent head analyses. Figure 3.40 shows an AFM generated line scan across the pole region of a virgin TR-4 head. The line scan option allows height between features to be established by the use of pointers. The line scan feature is shown in relation to the AFM scan in Figure 3.39 whilst an exploded view (for clarity) is shown in Figure 3.40. The exploded view will be used for the remainder of the thesis.

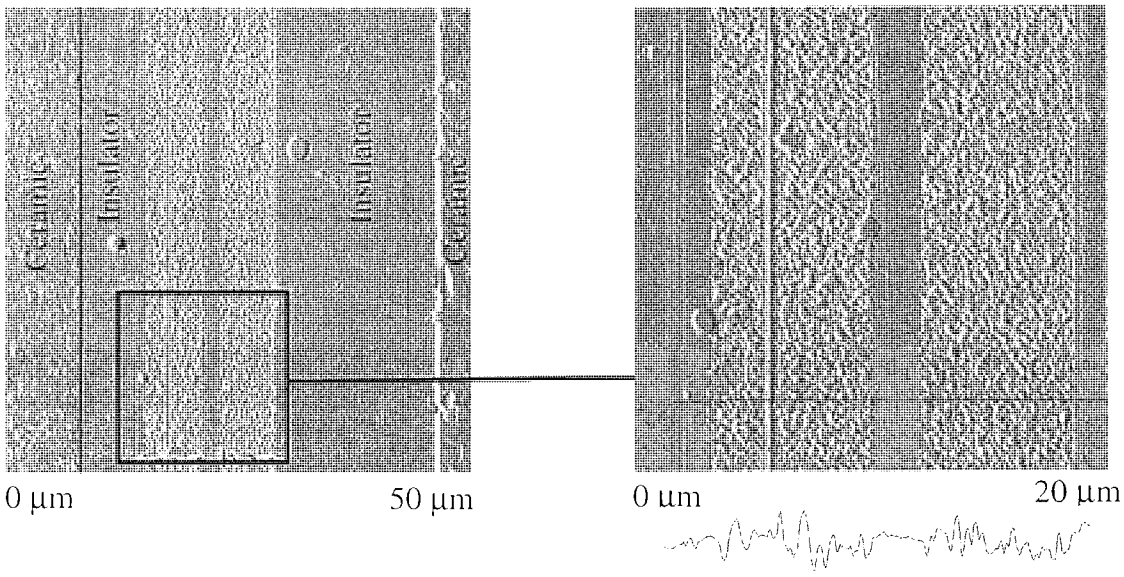

Figure 3.39 AFM images of the surface of a virgin TR-4 head and an example of the line scan option

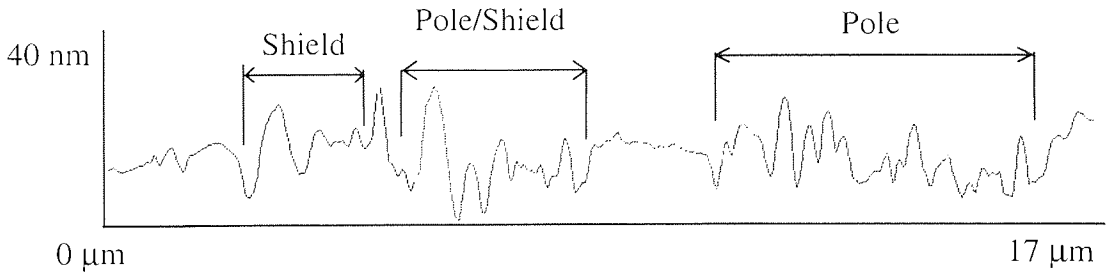

Figure 3.40 AFM line scan of the poles and insulator regions of a virgin head

The heights from the ceramic to the insulator regions on the pole and shield sides of the head were measured six times and the average values were found to be 41.1 nm for the shield side and 45.3 nm for the pole side. Line scan height measurements of the left read/write structure were repeated six times and the average values were found to be:

Insulator – Shield = 15.7 nm

Shield – Read Gap = 17.8 nm

Read Gap – Shared Shield/Pole = 17.8 nm

Shared Shield/Pole – Write Gap = 24.4 nm

Write Gap – Pole = 17.8 nm

Pole – Insulator = 19.0 nm

3.3.2.4 MP1

3.3.2.4.1 32°C, 80% RH

The left read/write structure was examined using AFM to investigate physical changes that may have occurred to the head components during cycling. Figure 3.41 shows the left read/write structure of a TR-4 head after 11K passes of tape.

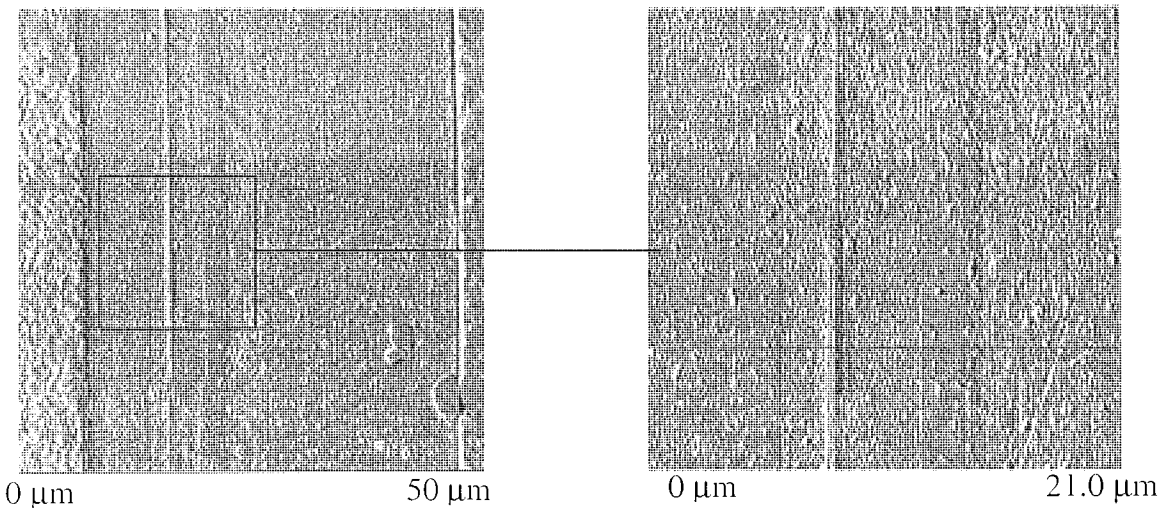

Figure 3.41 AFM image of the left read/write structure after 11K passes of tape MP1

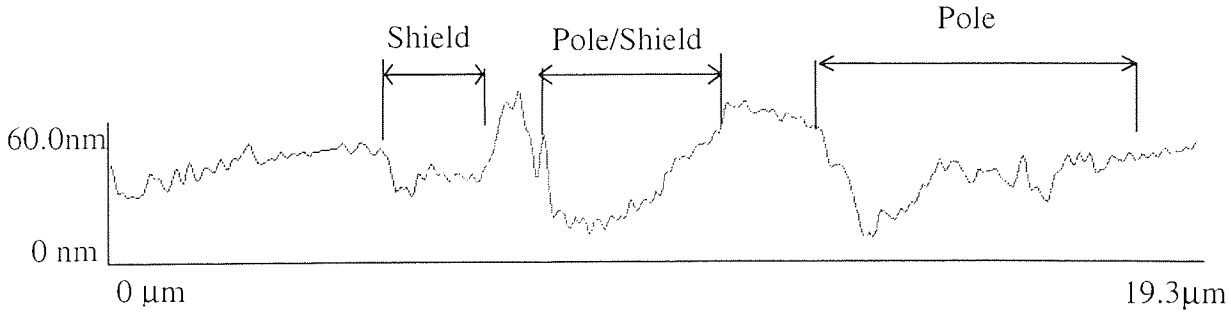

Figure 3.42 line scan of the left head assembly after 11K passes of tape MP1

The heights from the ceramic to the insulator regions on the pole and shield sides of the head were measured six times and the average values were found to be 72.2 nm for the shield side and 59.5 nm for the pole side. Line scan measurements of the left read/write structure were repeated six times and the average values were found to be:

Insulator – Shield = 19.8 nm (maximum)
Shield – Read Gap = 31.2 nm (maximum)
Read Gap – Shared Shield/Pole = 49.2 nm
Shared Shield/Pole – Write Gap = 47.8 nm
Write Gap – Pole = 47.4 nm (maximum)
Pole – Insulator = 49.0 nm

PTR was evident on this structure being greatest on the shared pole/shield and shield, also AES analysis showed that Ti was present on the pole/shield. The right structure produced similar results.

3.3.2.4.2 40°C, 15% RH

AFM analysis was also performed on the TR-4 head despite the early cartridge failure. Figure 3.43 shows an AFM image of the left read/write structure whereas Figure 3.44 shows an AFM generated line scan across the pole area.

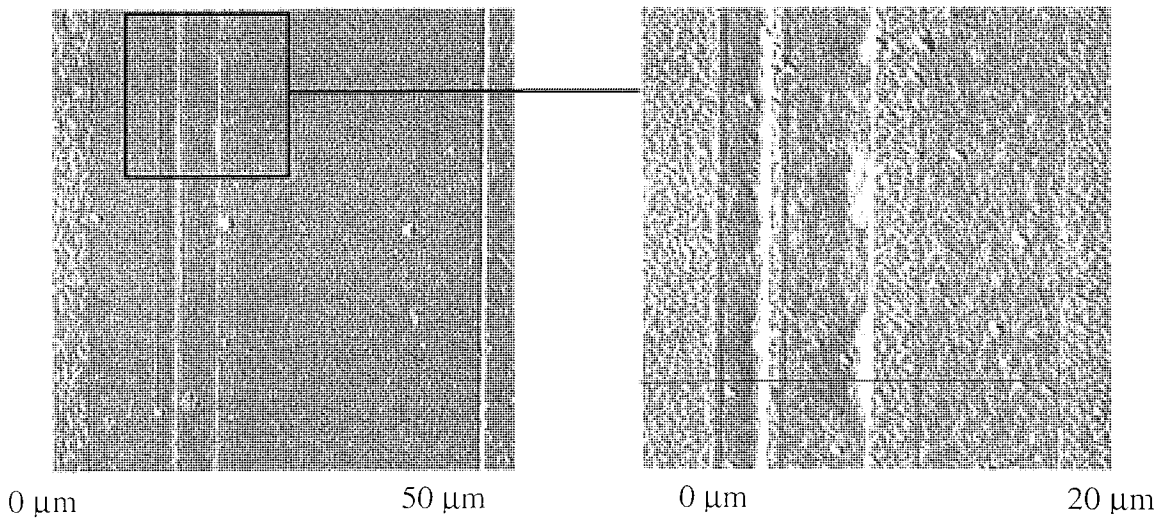

Figure 3.43 AFM image of the left read/write structure of the TR-4 head after 4K passes of tape MP1 at 40°C, 15% RH

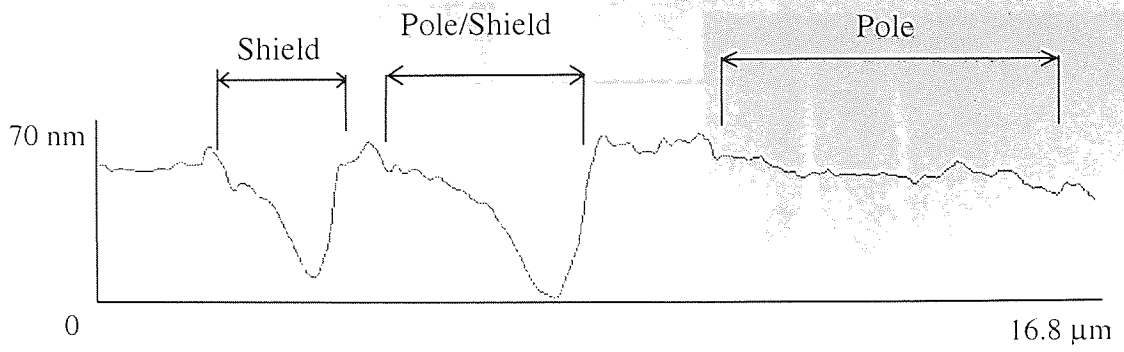

Figure 3.44 line scan of the left head assembly
after 11K passes of tape MP1

For the left read/write structure, the heights from the ceramic down to the insulator, on both the pole side and shield side were measured at six points. The average values were then calculated and these were found to be 37.3 nm for the pole side and 37.7 nm for the shield side. Some pole tip recession was evident on the read/write structure in the shared pole/shield and shield regions. Recession of the glue between the ceramic and the insulator was also evident on the pole side of the read/write structure. The average value of six measurements taken along the length of the glue line indicated a depth of recession from the ceramic to the glue of 100.5 nm. Line scan measurements of the left read/write structure were repeated six times and the average values were found to be:

Insulator – Shield = 48.7 nm (maximum)
Shield – Read Gap = 54.6 nm (maximum)
Read Gap – Shared Shield/Pole = 10.7 nm
Shared Shield/Pole – Write Gap = 66.3 nm (in the deepest pit)
Write Gap – Pole = 8.8 nm (no recession of this pole)
Pole – Insulator = 11.5 nm

AES analysis provided evidence of Fe on all regions of the structure while Ti was detected on the pole and insulator (pole side) regions. The right structure produced similar results.

3.3.2.4.3 5°C, 15% RH

At the completion of 20K passes, the TR-4 head was removed from the cycler in order that AFM and Auger analyses could be performed. Figure 3.45 shows an AFM image of the left read/write structure.

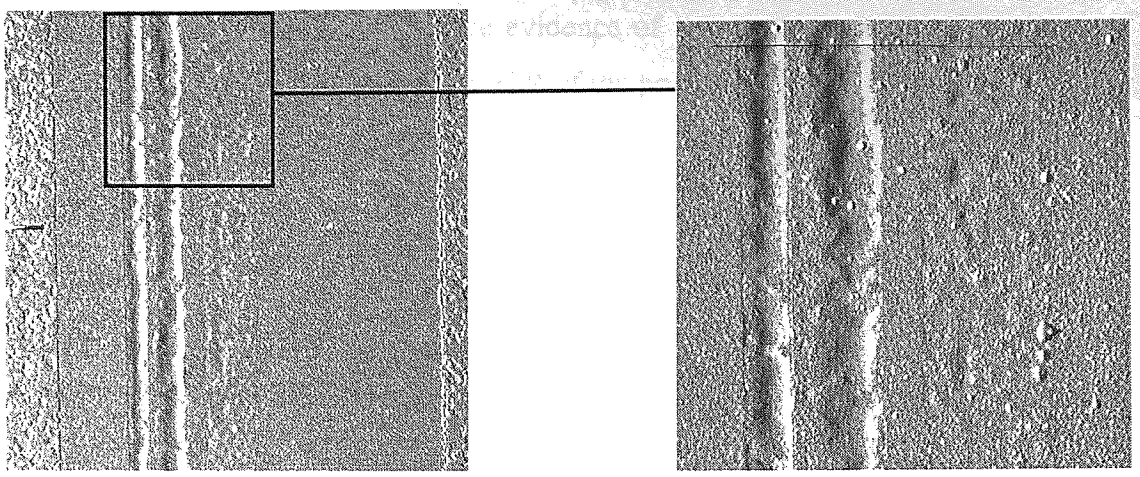

Figure 3.45 AFM image of the left read/write structure of the TR-4 head after 20K passes of tape MP1 at 5°C, 15% RH

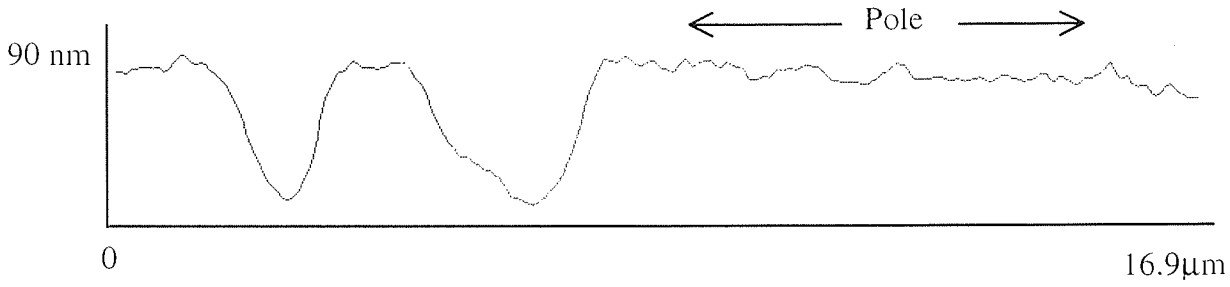

Figure 3.46 line scan of the left head assembly after 20K passes of tape MP1

For the left read/write structure, significant recession of the shared pole/shield and of the shield was evident whereas the write pole only appeared to have suffered minor recession. The heights from the ceramic to the insulator were repeated six times and the average values were calculated as 25.2 nm for the shield side and 24.7 nm for the pole side. Line scan measurements of the left read/write structure were also repeated six times and the average values were found to be:

Insulator – Shield = 60.7 nm (maximum)

Shield – Read Gap = 67.4 nm (maximum)

Read Gap – Shared Shield/Pole = 93.9 nm

Shared Shield/Pole – Write Gap = 87.3 nm (in the deepest pit)

Write Gap – Pole = 30.0 nm (little evidence of wear)

Pole – Insulator = 13.0 nm (little evidence of wear)

AES analysis of the head did not produce evidence of any contamination of the head. The right head showed similar results but with PTR of the pole in evidence.

3.3.2.5 Tape A

3.3.2.5.1 32°C, 80% RH

AFM analysis was performed on the TR-4 head when the cycling had reached 11K passes. Figure 3.47 shows an AFM image of the left read/write structure whereas Figure 3.48 shows an AFM generated line scan across the pole area.

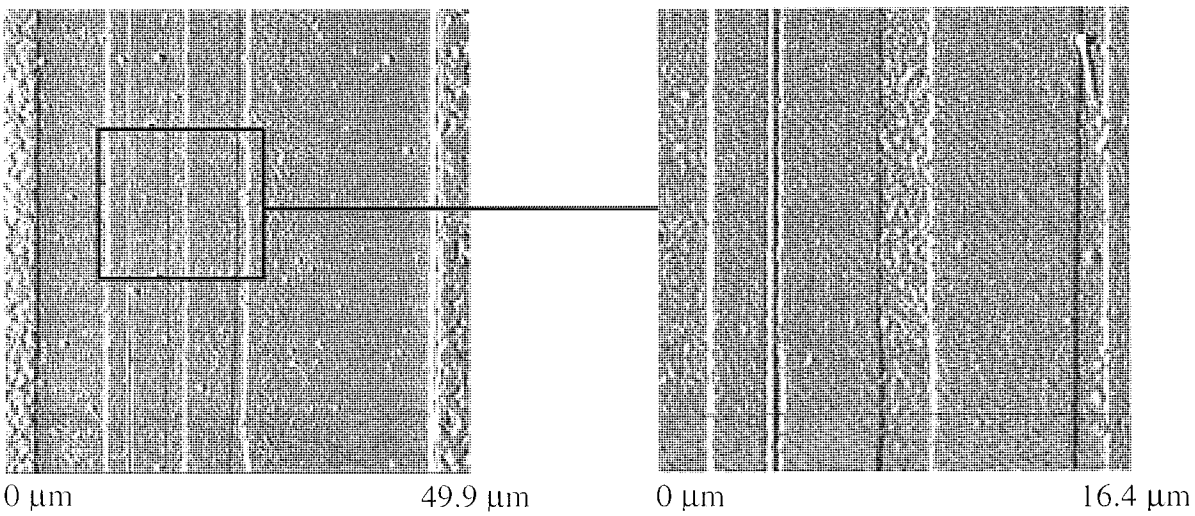

Figure 3.47 AFM image of the left read/write structure of the TR-4 head after 11K passes of tape A

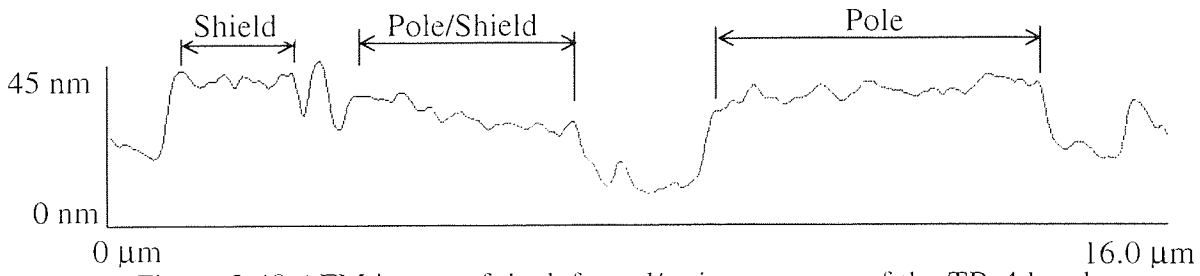

Figure 3.48 AFM image of the left read/write structure of the TR-4 head after 11K passes of tape A

No PTR was evident on this head, the poles had filled with material transferred from the tape, this would have protected the poles from PTR.

3.3.2.5.2 40°C, 15% RH

AFM analysis was performed on the TR-4 head when cycling had stopped due to cartridge failure after 2K passes. Figure 3.49 shows an AFM image of the left read/write structure whereas whereas Figure 3.50 shows an AFM generated line scan across the pole area.

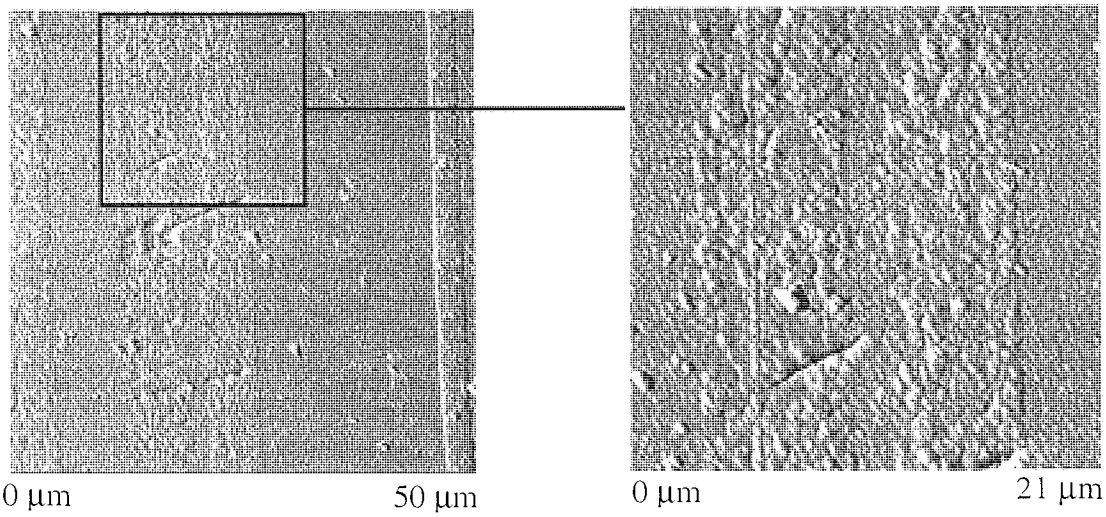

Figure 3.49 AFM image of the left read/write structure of the TR-4 head after 2K passes of tape A

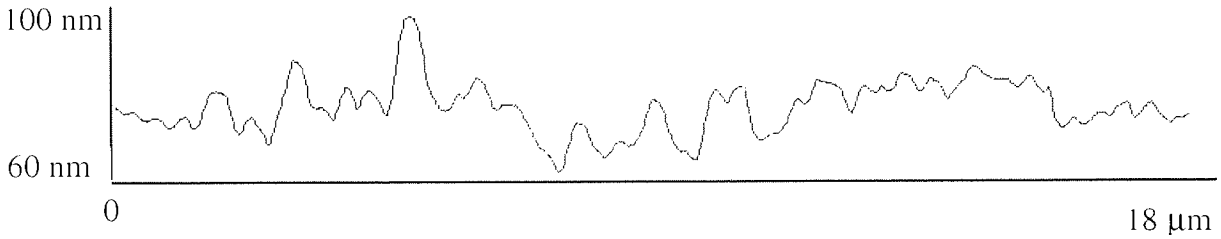

Figure 3.50 AFM image of the left read/write structure of the TR-4 head after 2K passes of tape A at 40°C, 15% RH

No PTR was evident on this head, a transfer of tape material had occurred congregating mainly on the poles. This was confirmed by AES, which showed that Fe was detected at all analysis positions being greater on the pole areas.

3.4 Georgens Cycler with TR-5 Head (Group A Tapes)

3.4.1 32°C 80% RH

3.4.1.1 MP 3

After the completion of 10K passes (dropout cartridge) and 5K passes (three cartridges) with tape MP3 at 32°C 80% RH, cartridge failure had not occurred. Dropout analysis and XPS results are presented in this section.

3.4.1.1.1 Dropout Analysis

Figure 3.51 shows the 4 dB, 5 dB, 6 dB and 10 dB dropout growth as a function of increasing number of passes. For the 5dB category (Part b) the 50 ms class of dropout is zero throughout cycling and as such did not register.

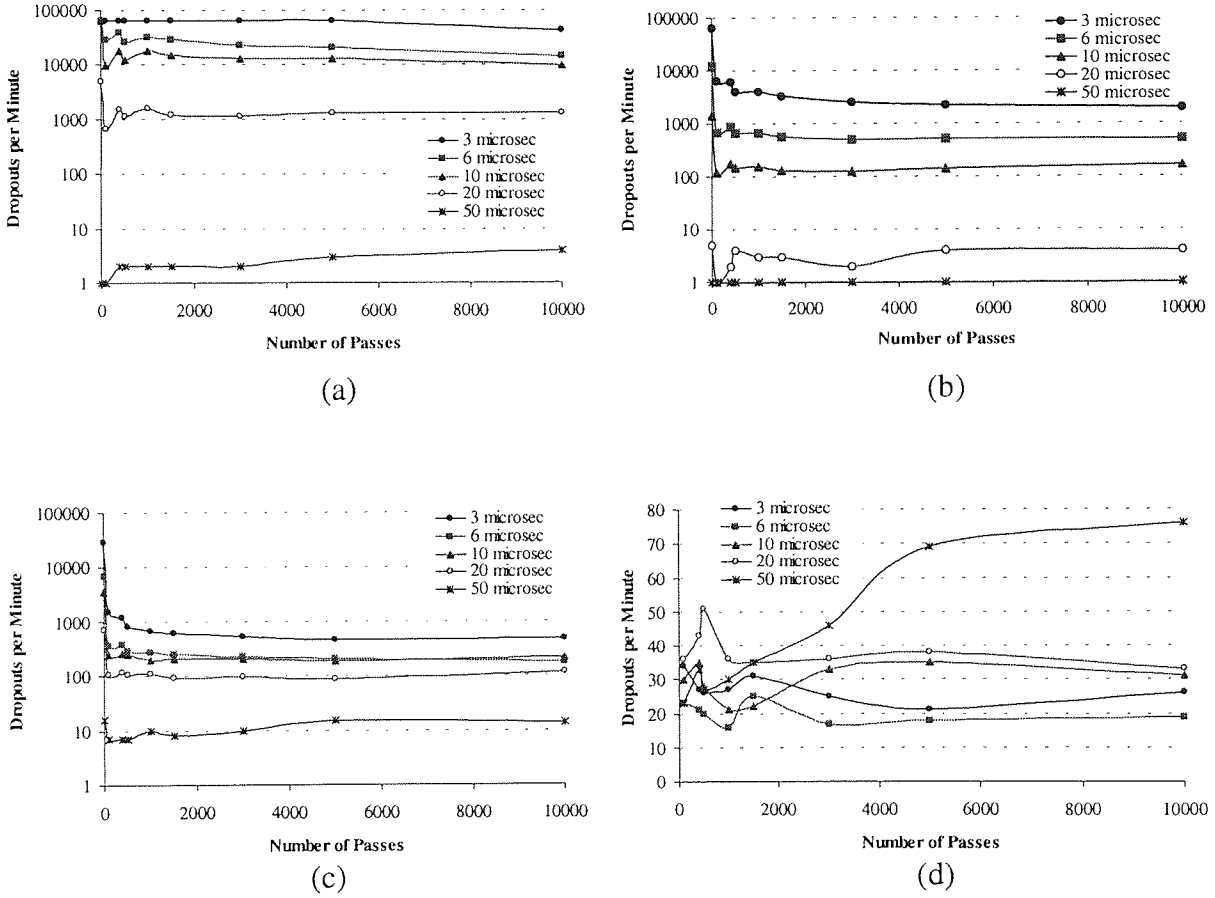

Figure 3.51 (c) (a) 4 dB (b) 5 dB (c) 6 dB and (d)10 dB dropout growth for tape MP3 at 32°C, 80% RH

The dropout growth initially decreased before levelling off for most classes of dropout. The largest dropout width, that of 50 μs was seen to increase with cycling at the 4dB and 10 dB categories.

3.4.1.1.2 XPS

Figure 3.52 and Figure 3.53 show the changes in elemental concentration at the centre and edge regions of tape MP3 at an increasing number of passes, when cycled against a head at 32°C, 80% RH.

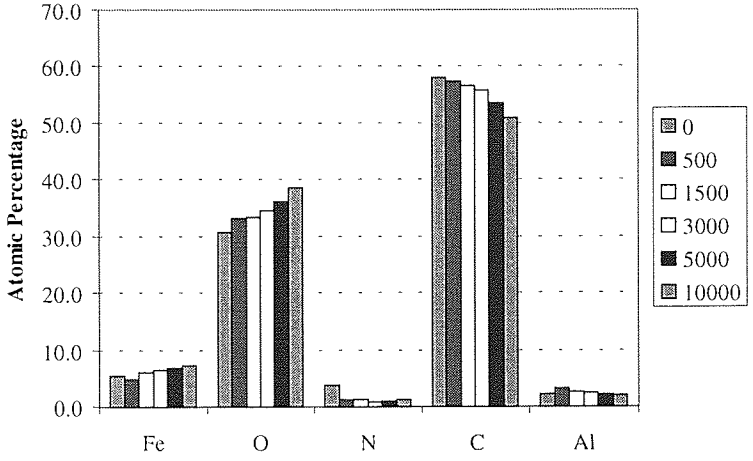

Figure 3.52 Atomic Concentration of Elements as a Function of Increasing Number of Passes for MP3 at 32°C, 80% RH - Centre

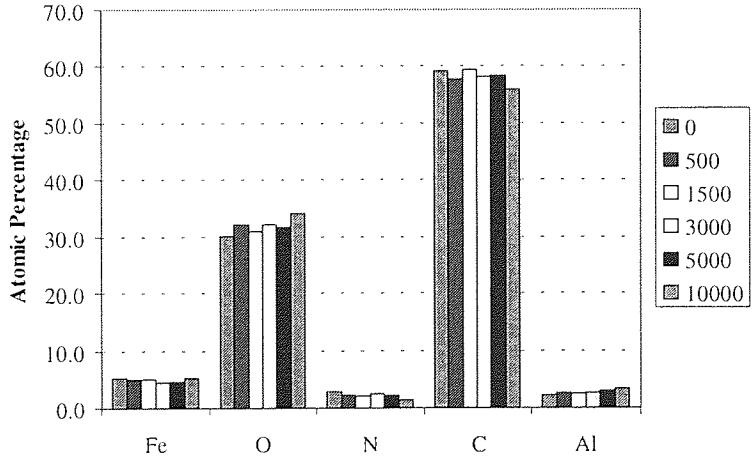

Figure 3.53 Atomic Concentration of Elements as a Function of Increasing Number of Passes for MP3 at 32°C, 80% RH – Edge

It was clear from Figure 3.52, that at the tape centre, Fe and O concentrations increased with cycling whilst the C concentration decreased. The N concentration also decreased overall. The trends at the edge of the tape were similar to those at the centre for N, O and C with the only difference being the rate of change in concentration. The Fe concentration at the edge of the tape was more stable than at the centre, with only a slight decrease being noted.

Synthesis of the C peak confirmed the difference in the severity of changes in elemental concentration between the centre and edge of tape (Figure 3.54 and Figure 3.55 respectively). The centre showed a definite increase in the C-C/C-H bond for the first 1500 passes before decreasing for the remainder of the experiment, being most severe at 10K passes. At the edge of the tape, the increase was of a more subtle nature. Similarly, the C-O bond decreased at a greater rate at the centre of the tape when compared to the edge.

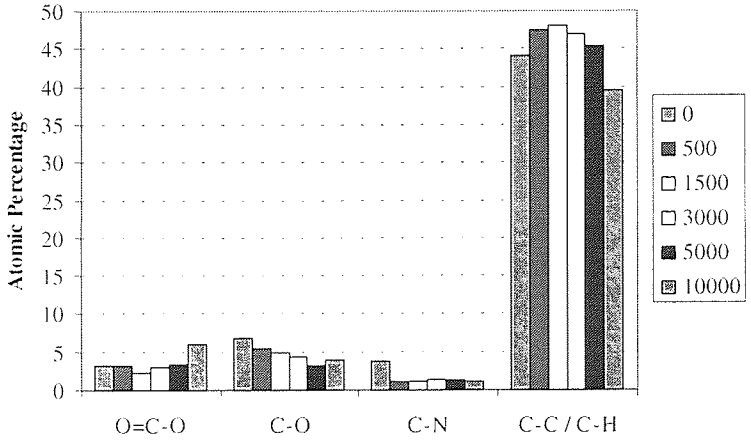

Figure 3.54 Synthesis of C for MP3 at 32°C 80% - Centre

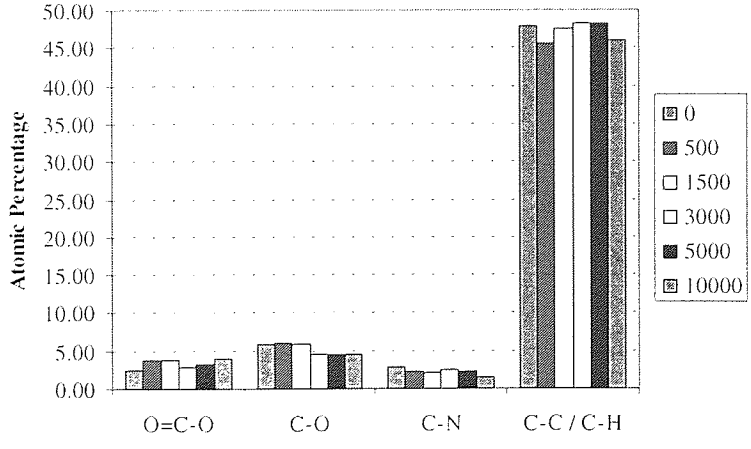

Figure 3.55 Synthesis of C for MP3 at 32°C 80% - Edge

Figure 3.56 shows the difference in elemental composition between the centre and edge regions at the surface of tape MP3 when cycled against a Tr-5 head at 32°C, 80% RH. This was simply the relative percentage at the edge subtracted from the relative percentage at the centre. There is clearly a higher percentage of Fe and O at the centre region of the tape compared to the edge, whereas there is a higher percentage of N and C at the edge compared to the centre region.

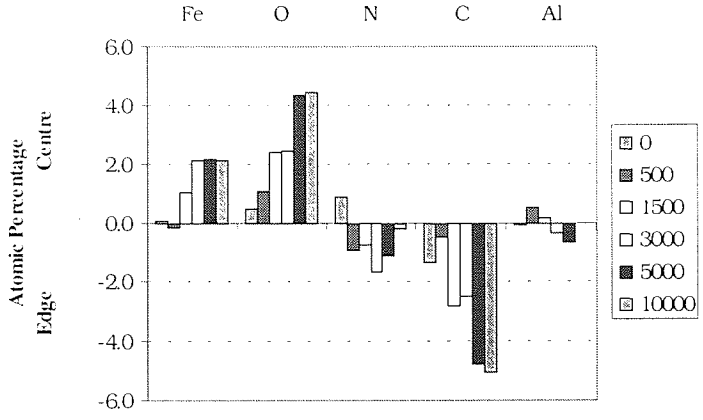

Figure 3.56 Difference between the Centre and Edge of MP3
with increasing number of passes at 32°C 80%

Group A tapes (2.1.1 Tapes) exhibited the same elemental trends at their centre positions. Any differences in behaviour between tapes occurred at their edges and only for the C and O signals though these differences were not pronounced. For MP1 the C signal remained stable throughout cycling whilst the O signal increased up to 500 passes where it also became stable for the remainder of the experiment. Tape MP4 exhibited stable C and O concentrations throughout cycling. The Fe and N concentrations followed the same trend for all three tapes in that a slight decrease was seen throughout cycling.

Synthesis of the C peak showed that the trends for all group A tapes were almost identical, at both tape regions.

Figure 3.57 - Figure 3.59 compare ratios of Fe:C, Fe:N, and N:C respectively for tapes MP1, MP3 and MP4.

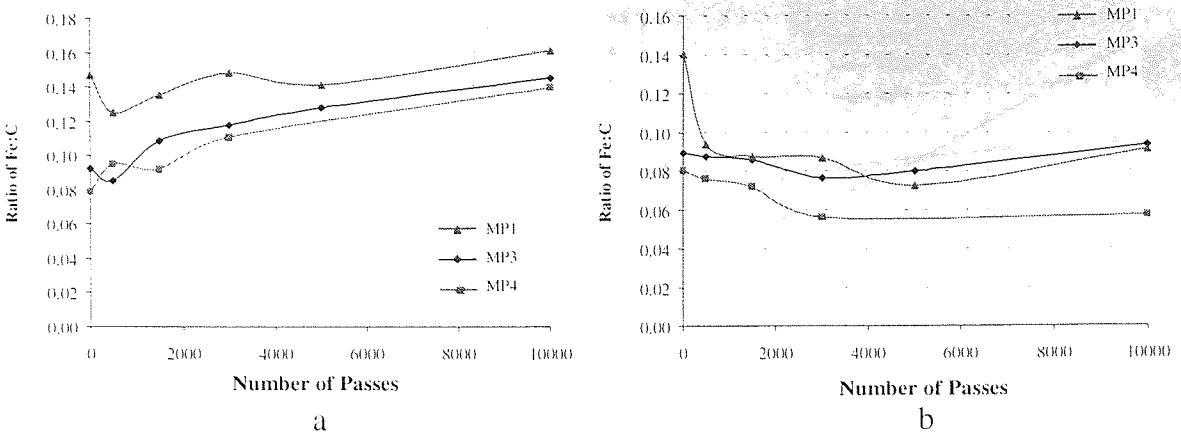

Figure 3.57 Ratio of Fe:C for Group A tapes at 32°C, 80% RH (a) Centre and (b) Edge

It can be seen in Figure 3.57 (a) that at the centre of each tape the ratio of Fe/C increased throughout cycling indicating a loss of C and a gain in Fe (except for the first 100 passes of tape MP1 and tape MP2. The tapes were rated by order of magnitude, from high to low giving

$$MP1 > MP3 > MP4.$$

At the edge of tape, the Fe:C trend was seen to be more stable (Figure 3.57 (b)), with all tapes exhibiting a decrease for the first 3000 passes before stabilising.

The Fe:N ratios in Figure 3.58 produced a similar situation to the Fe:C ratios. As the N signal was small, errors were large, the rogue points at 3000 passes corresponded to changes of just 0.5 and 0.9% in the N signal. Disregarding these points for MP1 and MP3 gave the general trend for as an increase in the Fe:N ratio throughout cycling. For MP4 the ratio increased up to 1500 passes where it then stabilised for the remainder of the cycling. The Fe:N ratios for all three tapes were very similar up to 1500 passes, at which point MP4 became the lowest ratio for the remainder of cycling.

Apart from the 10K point for MP3, the Fe:N ratios at the edge of the tapes showed a more stable situation than at the centre (Figure 3.58 (b)).

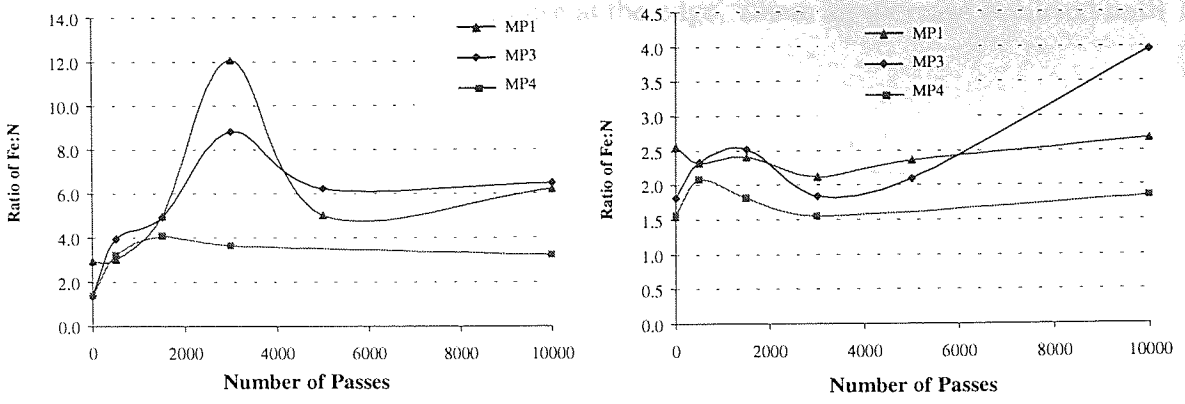

Figure 3.58 Ratio of Fe:N for Group A tapes at 32°C, 80% RH
(a)Centre and (b) Edge

The N:C ratios produced a more stable situation at the edge of the tapes when compared to the centres. At the centre (Figure 3.59), all three tapes showed an initial decrease in the N:C ratio followed by a slight increase for the remainder of cycling. This indicates that N was depleted faster during the first 1500 passes. MP3 displayed the lowest magnitude with that of MP1 and MP4 interchanging as cycling continued.

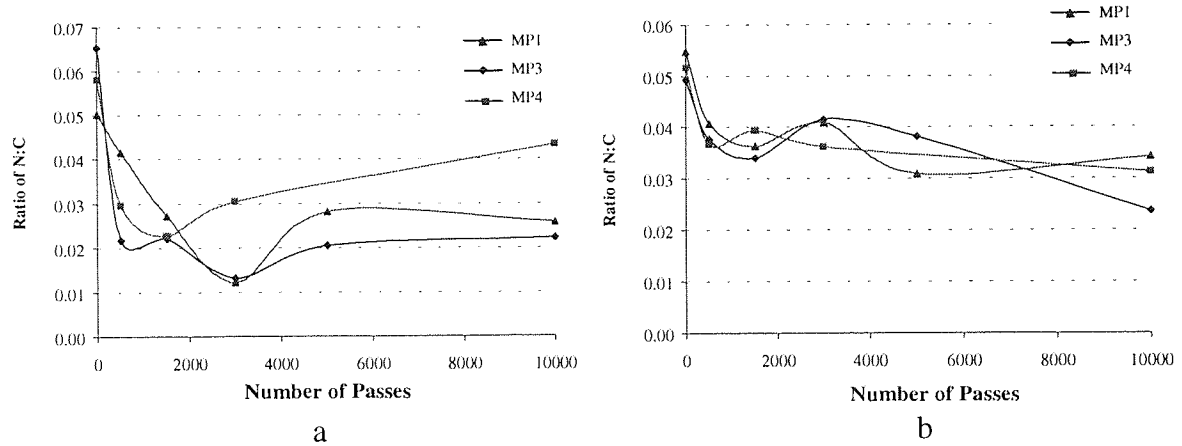

Figure 3.59 Ratio of N:C for group A tapes at 32°C, 80% RH
(a) Centre and (b) Edge

Tape MP4 produced the highest N:C ratio at the centre position. The edge of tape produced a gradual overall decrease throughout cycling (Figure 3.59 (b)). All three tapes displayed similar magnitudes at the edge region.

The overlayer thicknesses were calculated for tape MP3 at the centre and edge positions and are presented in Figure 3.60. The overlayer thickness was seen to decrease at the centre as

cycling commenced. This was not the case at the edge, where an increase occurred until 10 K passes where a decrease occurred.

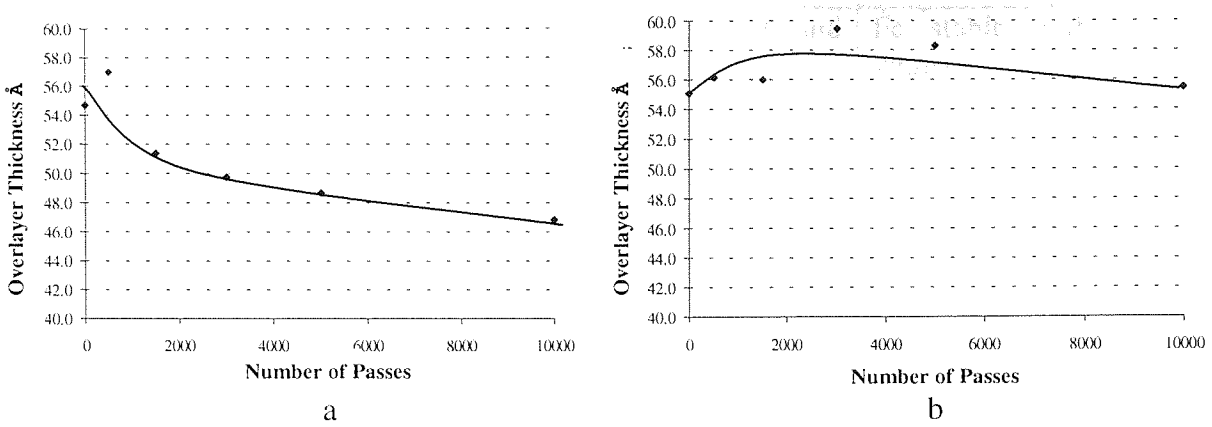

Figure 3.60 Variation in Overlayer Thickness as a Function of Increasing Number of Passes for Tape MP3 at 32°C 80% RH – (a) Centre and (b) Edge

The results for this section are summarised in Table 3.14.

Tape	Condition	Summary of Results		
MP3	32°C, 80% RH	XPS	Comparison	
			Centre	Edge
			Fe increased while C and N showed a decrease with increased cycling	Fe stable with cycling whilst C and N decreased.
		Synthesis of C	C-C/C-H increased for 1500 passes then decreased with cycling. C-N and C-O decreased with cycling.	C-C/C-H increased overall up to 5K passes then decreased at 10K. C-N and C-O decreased with cycling.
		Ratios	Fe:N and Fe:C increased. N:C decreased up to 3K passes then stable.	Fe:N stable, Fe:C decreased up to 1500 passes then stable. N:C decreased overall with cycling.
		Dropouts	Sharp reduction up to 1K passes then stable. An increase occurred in the 50 μs class for the 4 dB, and 10 dB categories.	
MP1	32°C, 80% RH	XPS	As for MP3	As for MP3 but with a stable C signal with cycling.
		Synthesis of C	As for tape MP3	As for tape MP3
		Ratios	As for MP3.	As for MP3.
		Dropouts	Same trend as for tape MP3 with an increase in the 50 ms class for the 4 dB category. Highest number of equilibrium dropouts of the group A tapes.	
MP4	32°C, 80% RH	XPS	As for tape MP3	As for tape MP3 but with a stable C signal with cycling.
		Synthesis of C	As for tape MP3	As for tape MP3 but with no reduction in C-C/C-H at 10K passes.
		Ratios	Fe:N and Fe:C increased. N:C decreased up to 1500K passes then increased.	Fe:N stable, Fe:C decreased up to 3000 passes then stable. N:C decreased overall with cycling.
		Dropouts	As for tape MP3 but with no increase for the 50 μs class. Similar number of equilibrium dropouts.	

Table 3.14 Summary of Results for the Georgens Cycler Experiments (TR-5 Head) using Group A Tapes at 32°C, 80%RH.

3.4.2 *AFM and AES Analysis*

3.4.2.1 Virgin TR-5 Head

Topographical information from a virgin head was obtained using non-contact AFM. Figure 3.61 illustrates the main areas of interest on the head. The information gained was used as reference data for subsequent head analyses. The two black stars in Figure 3.61 denote the position of the write gap, the two white stars the read gap, all other features can be identified with reference to the read/write gaps.

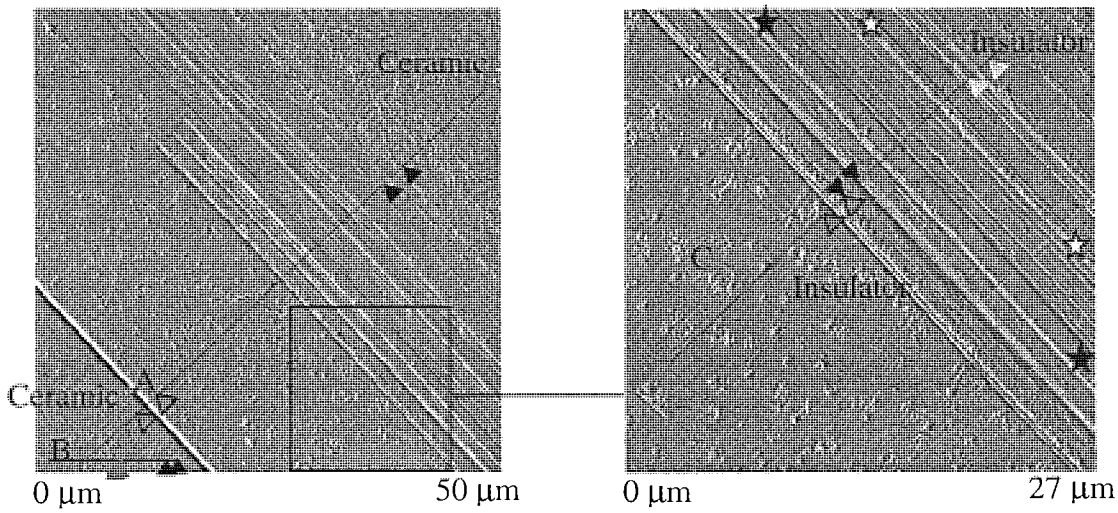

Figure 3.61 AFM images of the surface of a virgin TR-5 head

Relative heights from the ceramic air-bearing surface (ABS) of the head to the insulator regions are shown in Figure 3.62. As the ceramic regions are on either side of the sensor structure, it was necessary to distinguish between them. The ceramic on the pole side of the sensor structure will be referred to as the ceramic (pole side) whereas the ceramic on the shield side will be known as the ceramic (shield Side). From the ceramic (shield side) to insulator, measurements between 18 and 26 nm were noted. From the ceramic (pole side) to insulator, the measurements were wider ranging, being from 11 to 37 nm.

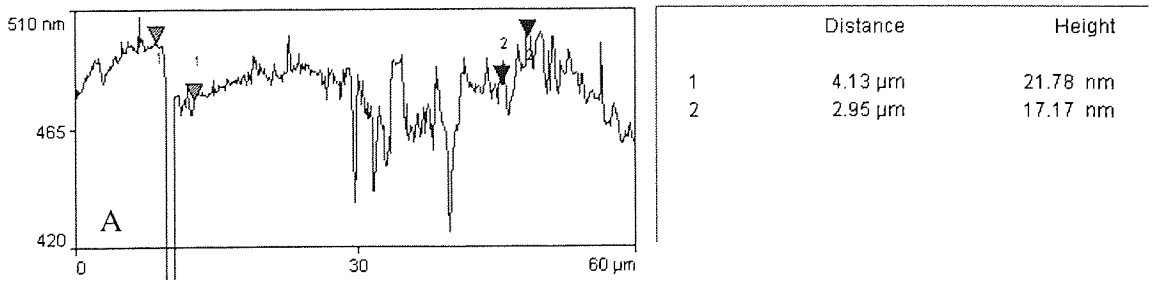

Figure 3.62 AFM line scan of the surface of a virgin TR-5 head (A)

It was interesting to note that relative to the surrounding insulator material, the poles were recessed on the virgin head. Depths of approximately 10 and 15 nm were recorded for the insulator to pole and insulator to shield depths respectively. The read and write gaps (also Al_2O_3 insulator material) were found to be level with the outer insulator regions which meant that they stood proud of the pole areas (Figure 3.63).

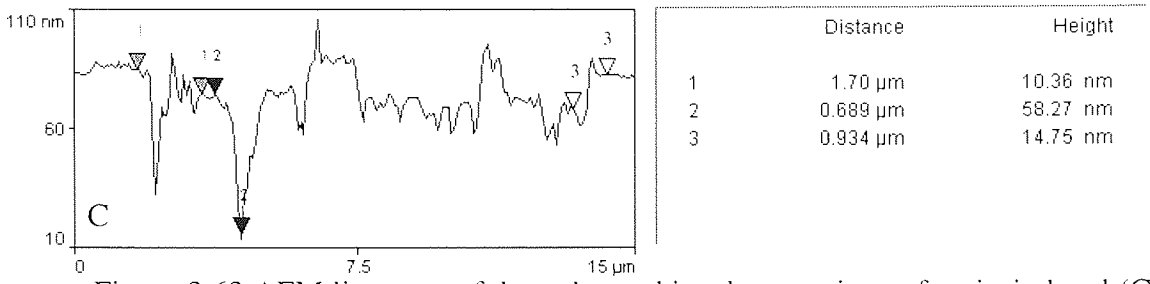

Figure 3.63 AFM line scan of the poles and insulator regions of a virgin head (C)

At both edges of the pole, ridges of around 58nm deep were present. The shield and shared pole/shield were not particularly smooth with ridges up to 20nm being present. Measurements made on the ceramic region of the head showed that the TiC phase of the ceramic was recessed from the Al_2O_3 phase by up to 23 nm (ps-ceramic) (Figure 3.64) and 18 nm (ceramic (shield Side)).

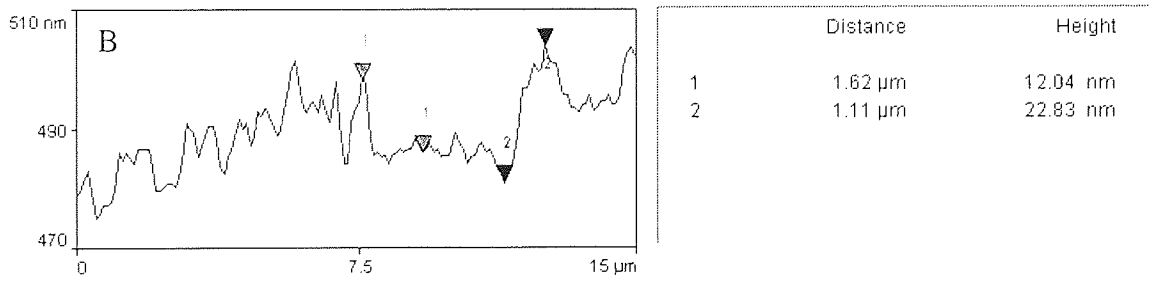

Figure 3.64 AFM line scan of the ceramic region of a virgin head (B)

The two read/write structures of each head were examined using AFM in order to investigate whether any staining and/or relative wear of the individual head components had resulted from the cycling experiments. AES of the head was performed to see if a transfer of material had occurred from tape to head.

3.4.2.2 MP1

3.4.2.2.1 Single (Dropout) Cartridge

3.4.2.2.1.1 Left Structure

Figure 3.65 shows an AFM image of the left read/write structure after 10K passes of tape MP1 at 32°C, 80% RH. Material transfer to the head was so severe that most of the component detail was lost. A line scan across the AFM image revealed the material had reached a height of 952.9 nm, as illustrated in Figure 3.66.

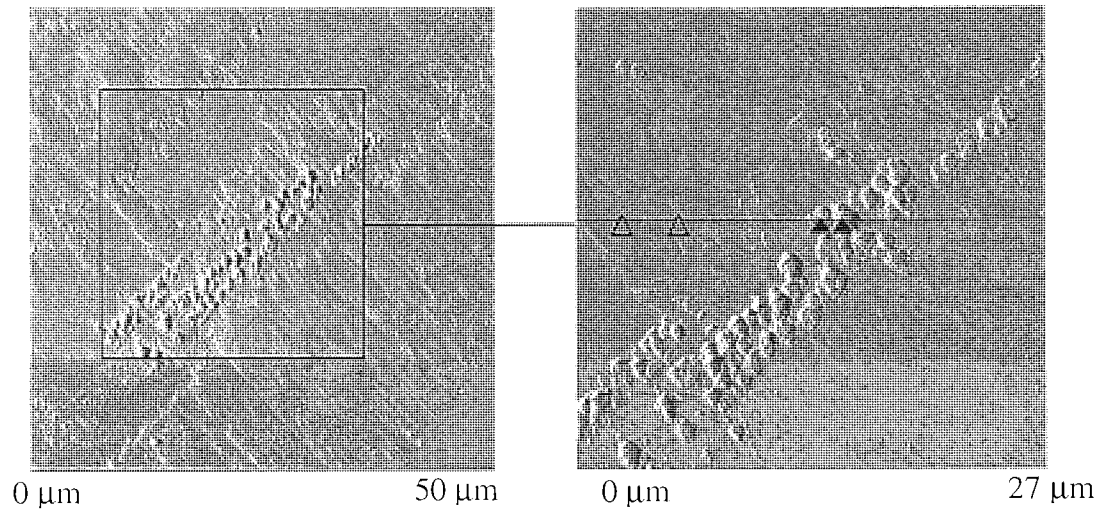

Figure 3.65 Left read/write structure after
10K passes of tape MP1 at 32°C, 80% RH

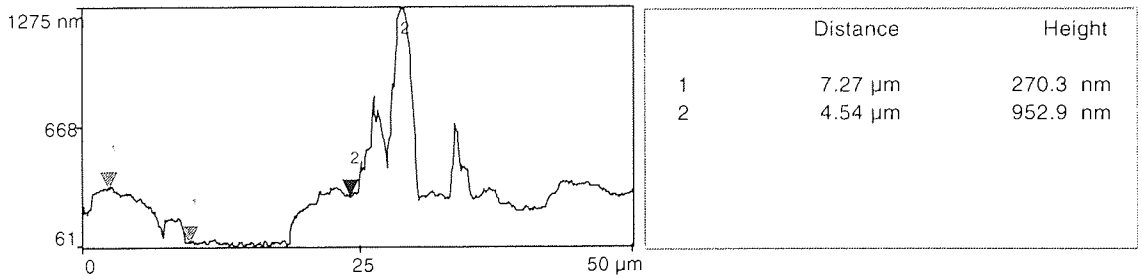

Figure 3.66 Line scan of the left read/write structure of a head after
10K passes of tape MP1 at 32°C, 80%RH

AES analysis of this structure confirmed the presence of Fe on all the component parts. Al was detected on the edge of the pole and at the centre and one edge of the pole/shield. Ti was detected at both points analysed on the pole but only at one point on the shield (arrowed in

Figure 3.65). Cobalt, the main constituent of the poles, was detected on the ceramic (pole side) region of the structure.

3.4.2.2.1.2 Right Structure

Figure 3.67 shows an AFM image of the right read/write structure of a head after 10K passes of tape MP1 at 32°C, 80% RH. Again material transfer to the head was very severe although it was not as prominent as was observed on the left structure since some of the head components could be identified.

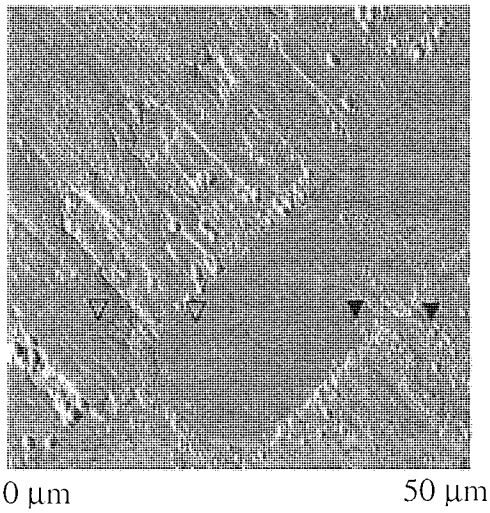

Figure 3.67 Right head assembly after 10K passes of tape MP1 at 32°C, 80% RH

Figure 3.68 presents topographical information across the right head assembly as indicated by the line on the AFM image of Figure 3.68. The stain had reached a height of 257.4 nm.

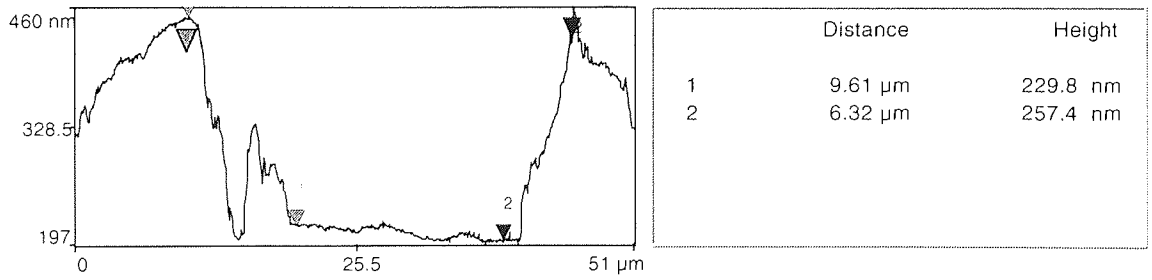

Figure 3.68 Line scan of the right head assembly after 10K passes of tape MP1 at 32°C, 80% RH

Following AES analysis of this structure it was found that Fe and Ti were present on all the component parts. Al was detected on the edge of the pole and at the centre of the shield.

3.4.2.2.2 Multiple Cartridges (x4)

3.4.2.2.2.1 Left Structure

Figure 3.69 shows an AFM image of the left read/write structure after 10K passes (four cartridges) at 32°C, 80% RH. Pole tip recession was evident, as indeed was stain on the Al_2O_3 regions of the head, particularly in the immediate vicinity of the MR element.

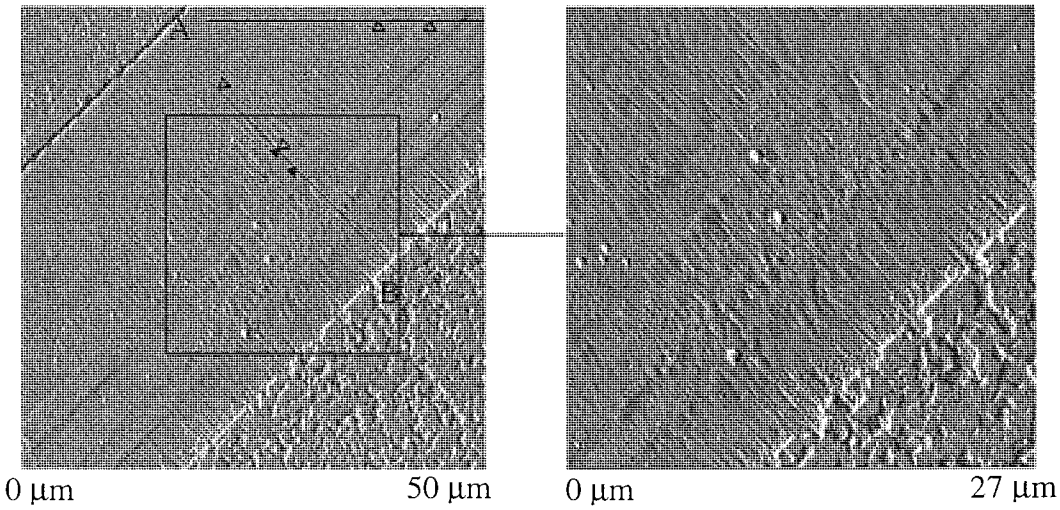

Figure 3.69 Left head assembly after 10K passes
of tape MP1 at 32°C, 80% RH and a close up scan of the pole area

Figure 3.70 , part A, shows that at a position where no stain was present, the height from the insulator to the pole was 39.4 nm. However, in a region where stain was prominent (part B), the distance between the insulator and the stain was 51.5 nm. In addition, the distance between the stain and the pole was 30.9 nm, thus giving a relative height from the insulator to the pole of 20.6 nm. This would indicate pole tip recession had occurred in this region between periods of stain build up.

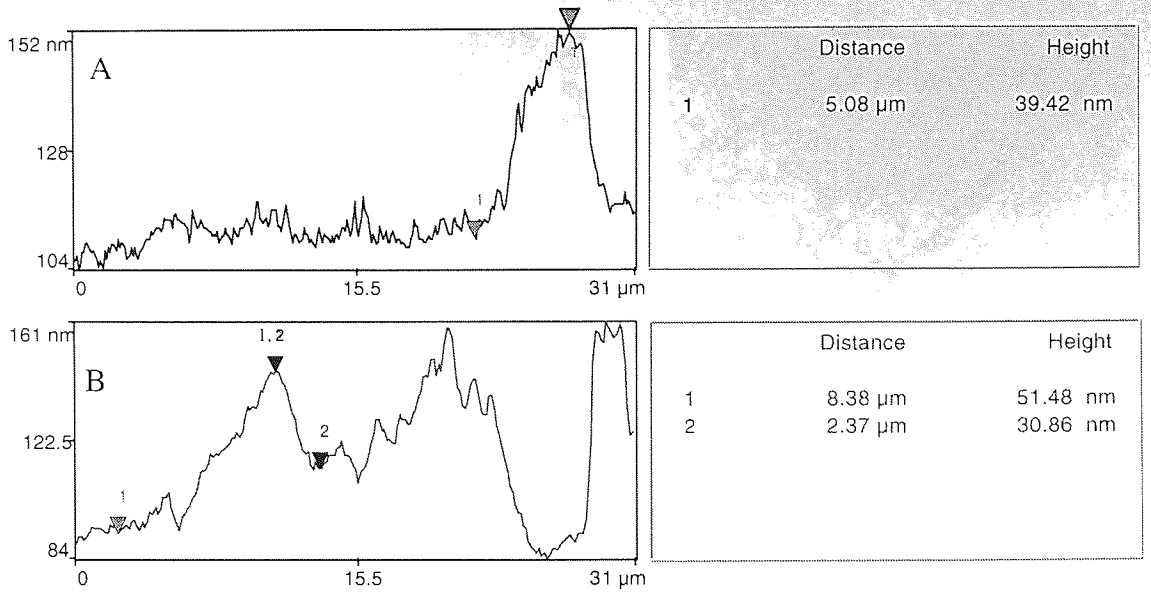

Figure 3.70 Line scan of the left head assembly of a head after 10K passes of tape MP1 at 32°C, 80% RH

AES analysis of this structure confirmed the presence of Fe on all component parts of the structure. Al was detected on the pole/shield. Ti was detected at most points analysed, the exception being the insulator region on the pole side.

3.4.2.2.2.2 Right Structure

Figure 3.71 shows an AFM image of the right read/write structure of the head after 10K passes (four cartridges) at 32°C, 80% RH. Staining of the insulator (pole side) and the write gap can be clearly observed. Recession of the shield had also started, as indicated by the formation of a pit in Figure 3.71. Figure 3.72 shows the corresponding topographical information using a representative line scan.

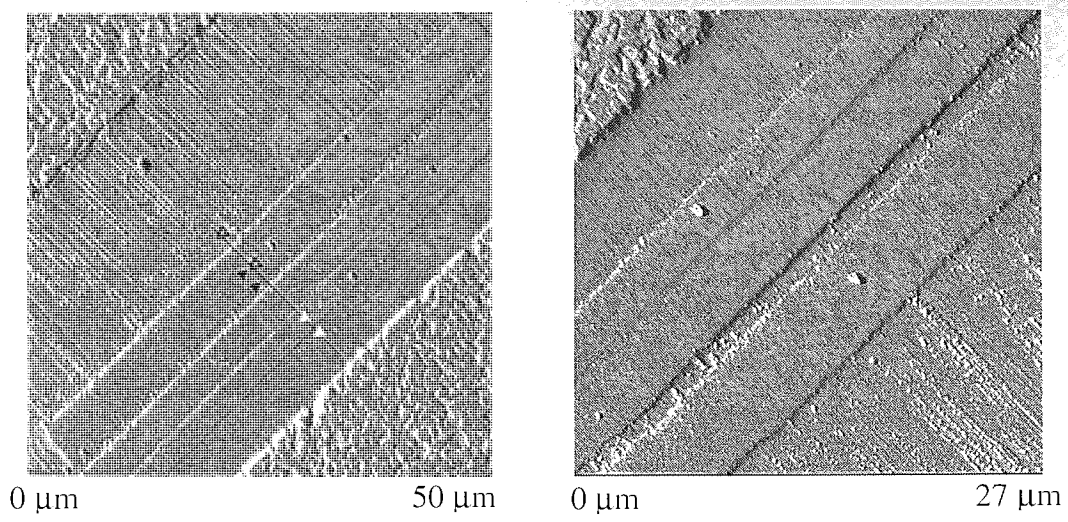

Figure 3.71 Right head assembly after 10K passes
of tape MP1 at 32°C, 80%RH and a close up of the pole area

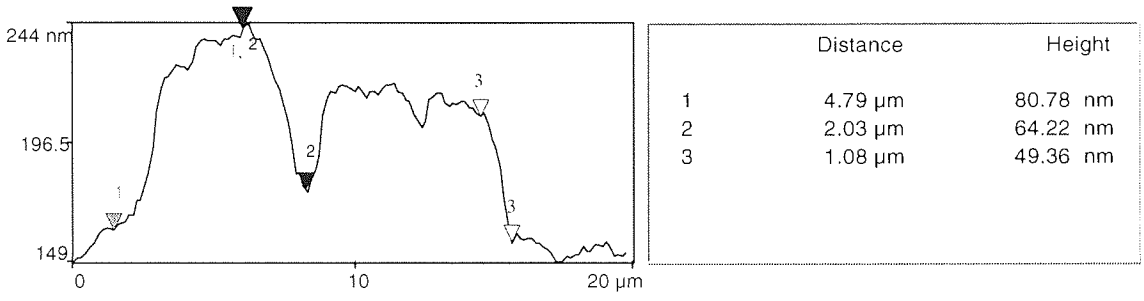

Figure 3.72 Line scan of the right head assembly of a head after
10K passes of tape MP1 at 32°C, 80%RH

AES analysis confirmed the presence of Fe, Ti and Al on all the component parts. Due to the nature of the material transferred to the insulator on the pole side, an area analysis was performed which indicated the presence of Co (pole material). Co was also detected on the ceramic (pole side).

Figure 3.73 shows SEM and AES maps (O, Fe and Ti) of the right read/write structure after 10K passes of tape MP1 at 32°C, 80% RH.

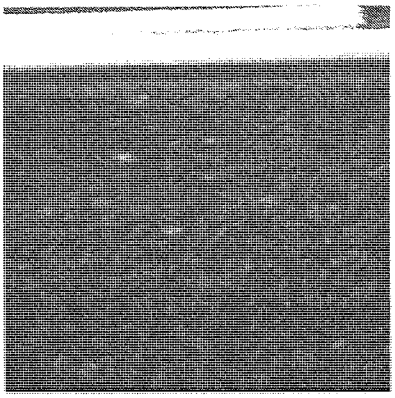

(a) SEM (70μm)

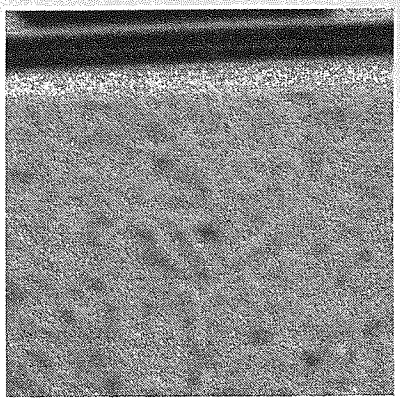

(b) AES – O (70μm)

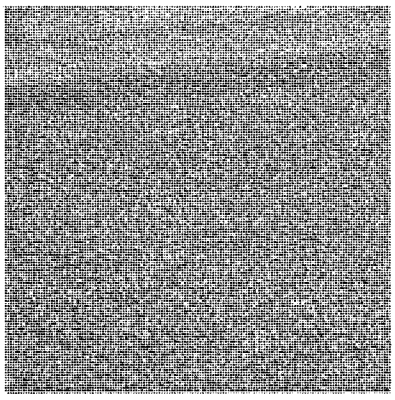

(c) AES - Fe (70μm)

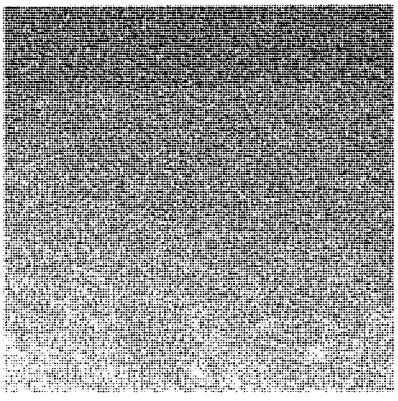

(d) AES – Ti (70μm)

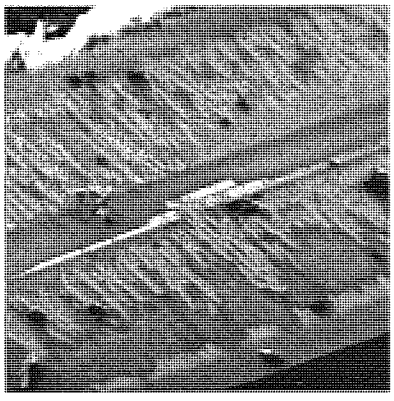

(e) SEM Debris (400μm)

Figure 3.73 SEM and AES maps (O, Fe and Ti) of the right read/write structure after 10K passes of tape MP1 at 32°C, 80% RH.

Fe was seen to be prevalent on the poles and ceramic regions of the head (Figure 3.73 (c)). The scale of transferred material was evident from the SEM image of Figure 3.73 (e).

3.4.2.3 MP3

3.4.2.3.1 Single (Dropout) Cartridge

3.4.2.3.1.1 Left Structure

Figure 3.74 shows an AFM image of the left read/write structure of a head after 10K passes (dropout cartridge) of tape MP3 at 32°C, 80% RH. No pole tip recession was identified on this assembly. Material transfer to the head was severe on the ceramic and pole regions and thus most of the component detail was lost. The thickness of the transferred material was shown to be at least 60.4 nm on the ceramic (shield side), as shown by the line scan in Figure 3.75.

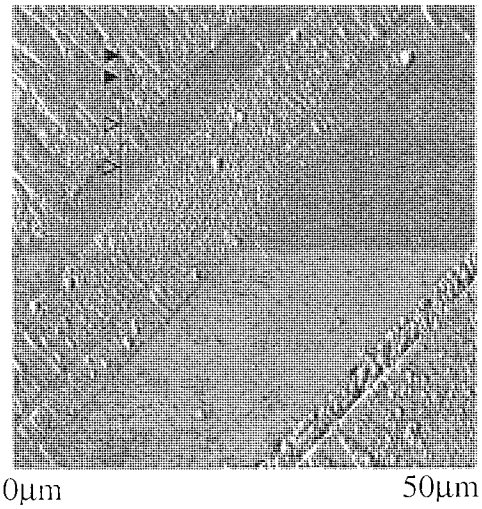

Figure 3.74 Left read/write structure of a head after 10K passes of tape MP3 at 32°C, 80% RH

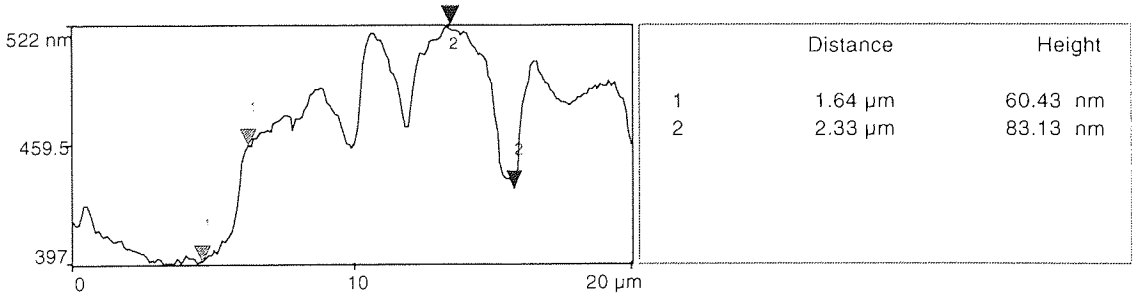

Figure 3.75 Line scan of the left read/write structure of a head after 10K passes of tape MP3 at 32°C, 80% RH to establish transferred material height

AES analysis of this structure confirmed the presence of Fe on all regions of the structure. Traces of Al were found at all points analysed while Ti was detected on all positions of the structure with the exception of the insulator areas.

3.4.2.3.1.2 Right Structure

Figure 3.76 shows an AFM image of the right read/write structure of a head after 10K passes (dropout cartridge) of tape MP3 at 32°C, 80% RH. As with the left structure, material transfer to the ceramic and pole regions was severe and thus most of the component detail was lost. The Al_2O_3 regions of this structure remained relatively free from such material. Figure 3.77 shows a line scan across the right head assembly and from this, the height of the transferred material on the ceramic (shield side) to the insulator was 232.9 nm.

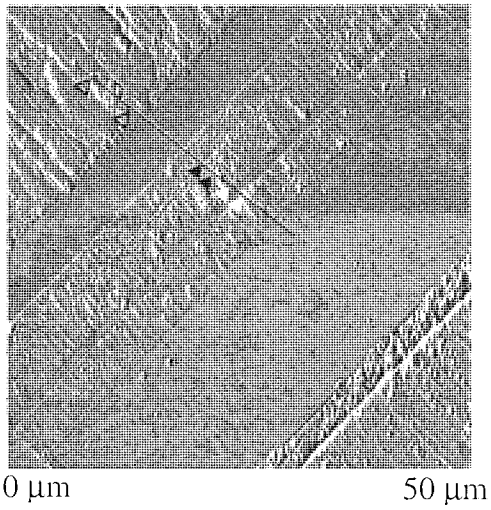

Figure 3.76 Right head assembly of a head after 10K passes of tape MP3 at 32°C, 80% RH

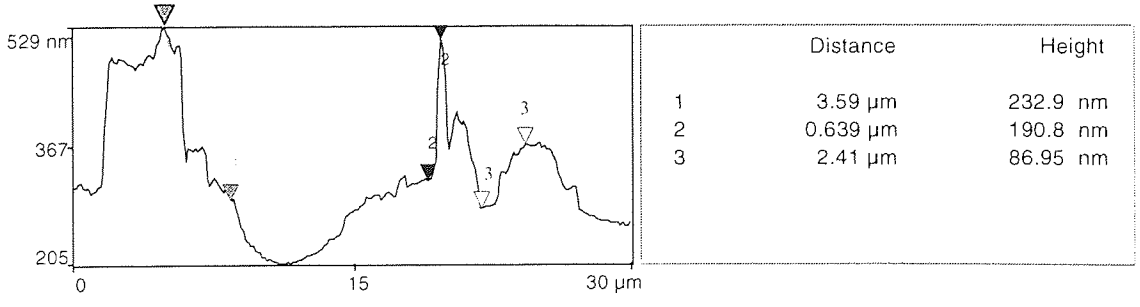

Figure 3.77 Line scan of the right head assembly of a head after 10K passes of tape MP3 at 32°C, 80% RH

The results of AES analysis showed that Fe was present on all regions of the structure with the exception of the insulator area (pole side). Traces of Al were found on all regions of the structure. Ti was found on the insulator (shield side) and the shield.

Figure 3.78 shows SEM and AES maps (O, Fe and Ti) of the right read/write structure after 10K passes of tape MP3 at 32°C, 80% RH. Fe was seen to be dominant on the poles and ceramic regions.

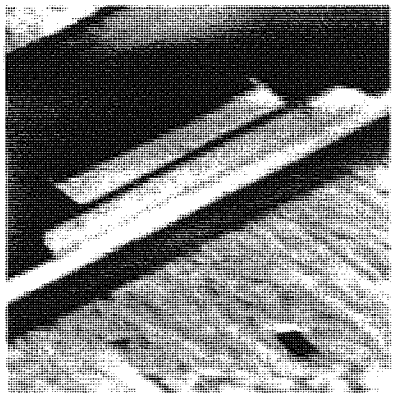

(a) SEM (105μm)

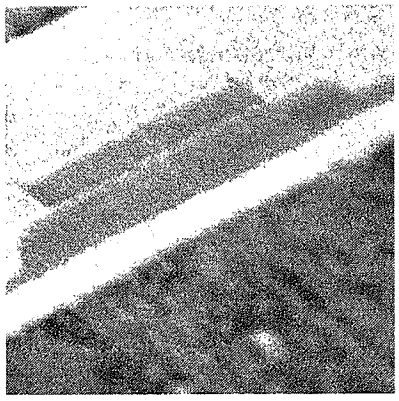

(b) AES – O (105μm)

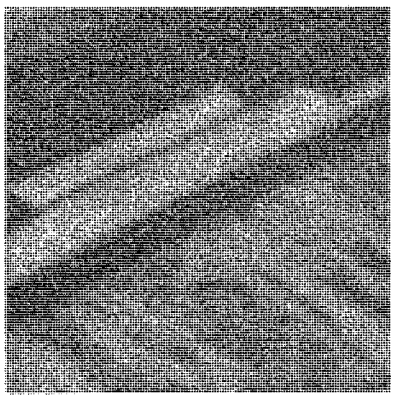

(c) AES - Fe (105μm)

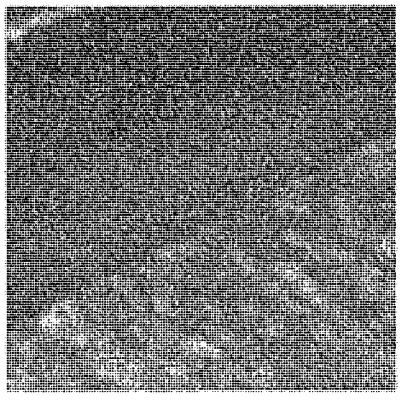

(d) AES – Ti (105μm)

Figure 3.78 (a) SEM and AES maps ((b) O, (c) Fe and (d) Ti) of the right read/write structure after 10K passes of tape MP3 at 32°C, 80% RH.

3.4.2.3.2 Multiple Cartridges (x4)

3.4.2.3.2.1 Left Structure

Figure 3.79 shows an AFM image of the left read/write structure of a head after 10K passes (four cartridges) of tape MP3 at 32°C, 80% RH. No pole tip recession was evident on this assembly. Stain was present on all regions of the structure.

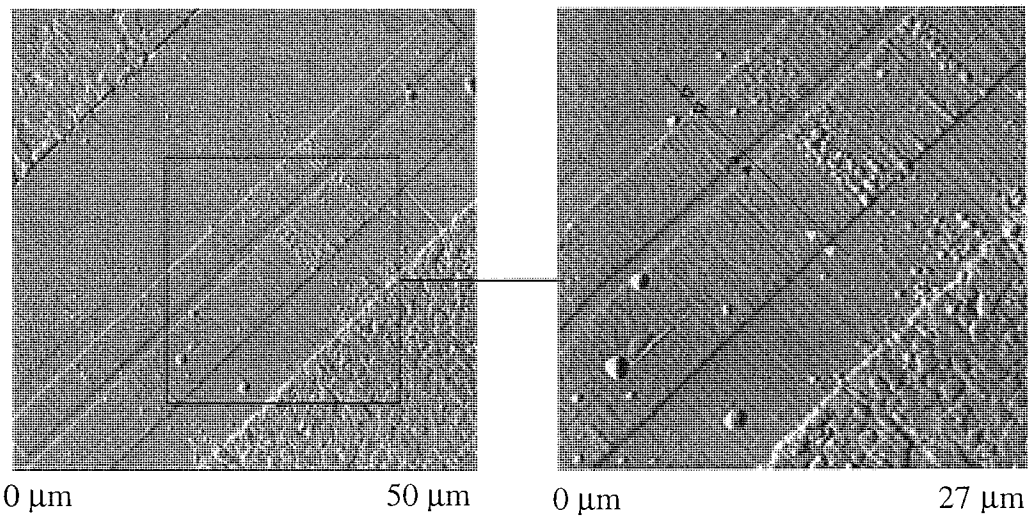

Figure 3.79 Left head assembly of a head after 10K passes of tape MP3 at 32°C, 80% RH with a close up of the pole area

The line scan in Figure 3.80 revealed that the pole and pole/shield had worn by a greater extent at the edge neighbouring the write gap than at the opposite edge. Some heavy scoring across the head was also evident.

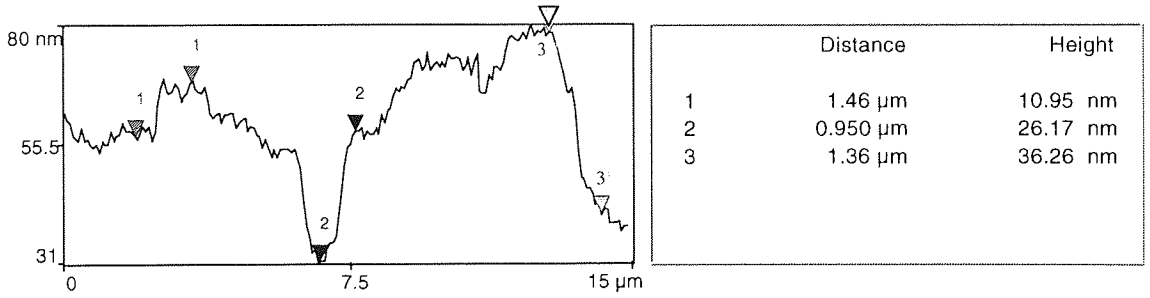

Figure 3.80 Line scan of the left head assembly after 10K passes of tape MP3 at 32°C, 80% RH

AES analysis of this structure revealed the presence of Fe and Al on all areas with the exception of the insulator (shield side). Ti was detected at all positions with the exception of the insulator (shield side).

3.4.2.3.2.2 Right Structure

Figure 3.81 shows an AFM image of the right read/write structure of a head after 10K passes (4 cartridges) of tape MP3 at 32°C, 80% RH. No immediate pole tip recession was evident on this assembly. Stain was present on the insulator region between the ceramic and the pole and on the write gap.

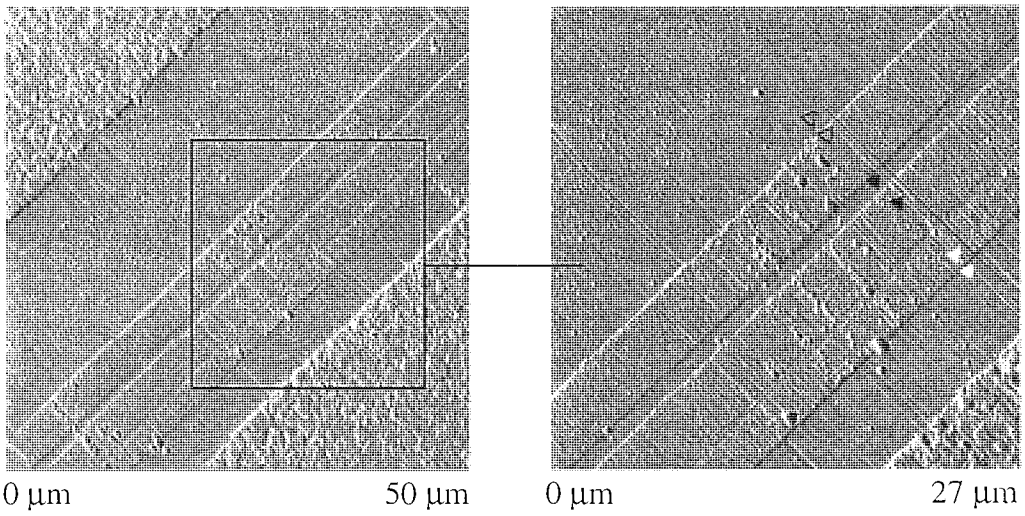

Figure 3.81 Right head assembly of the head after 10K passes of tape MP3 at 32°C, 80% RH and a close up of the pole area

Figure 3.82 shows a line scan across the poles of the right head structure

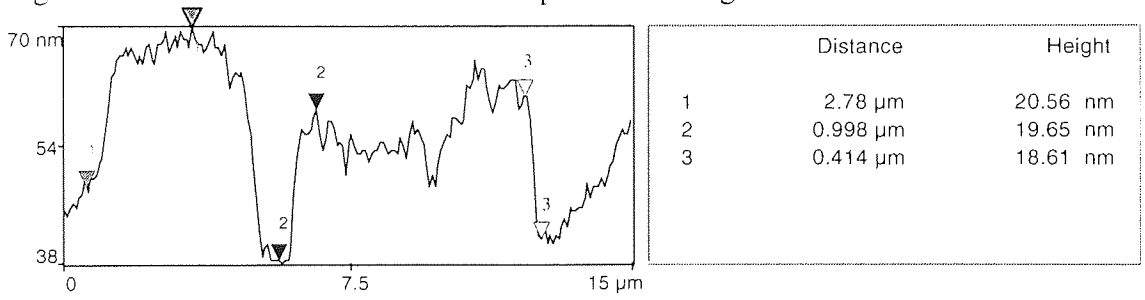

Figure 3.82 Line scan of the right head assembly of a head after 10K passes of tape MP3 at 32°C, 80% RH

AES analysis of this structure revealed the presence of Al at all positions and Fe on all areas with the exception of the insulator (shield side). Ti was detected on the ole and shield whilst Co (pole material) was detected on the insulator (pole side) and on the ceramic (pole side) region of the head.

3.4.2.4 MP4

3.4.2.4.1 Single (Dropout) Cartridge

3.4.2.4.1.1 Left Structure

Figure 3.83 shows an AFM image of the left read/write structure of a head after 10K passes (dropout cartridge) of tape MP4 at 32°C, 80% RH. No pole tip recession was evident on this assembly. Staining of the head appeared to be very heavy on the ceramic and moderately heavy on the poles. Stain appeared to be spreading to the insulator and gap regions from the ceramic and poles respectively. Figure 3.84 shows a line scan across the individual components and a representative area of stain on the insulator (pole side) which was found to have a thickness of 142.5 nm.

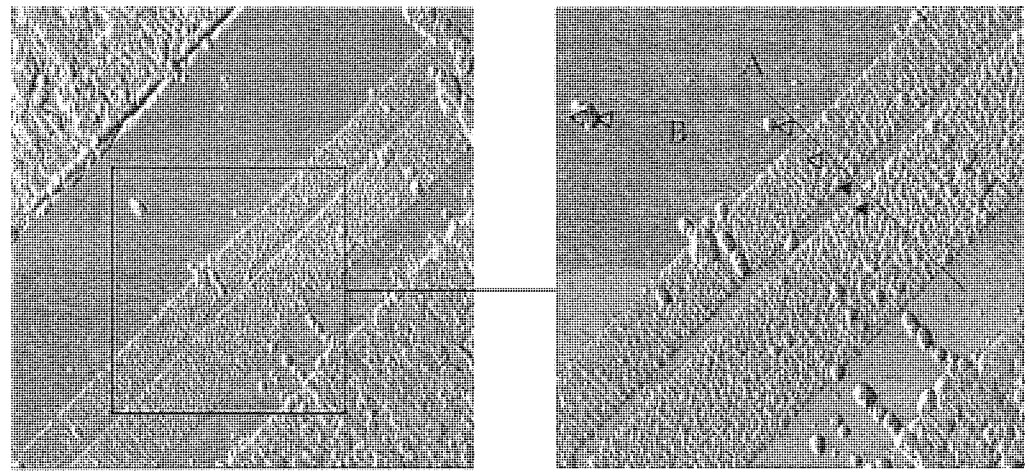

Figure 3.83 Left read/write structure of a head after 10K passes of tape MP4 at 32°C, 80% RH

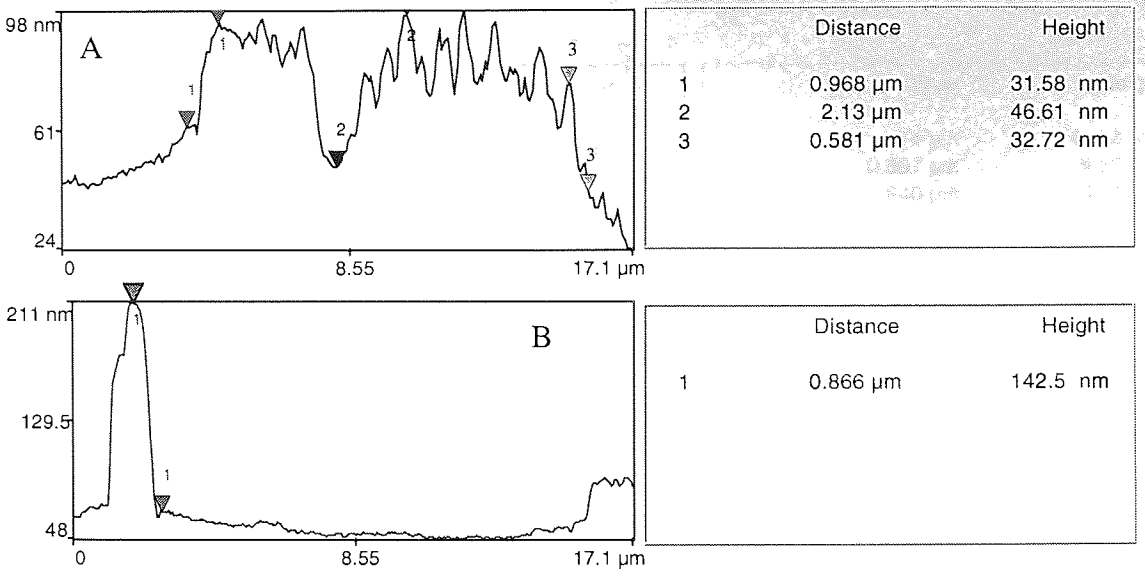

Figure 3.84 Line scan of the left read/write structure of a head after 10K passes of tape MP4 at 32°C, 80% RH

AES analysis of this structure confirmed the presence of Fe and Ti on all the component parts with the exception of the insulator regions. Al was present on all regions. Co, the main element of the poles, was detected on both ceramic regions of the structure.

3.4.2.4.1.2 Right Structure

Figure 3.85 shows an AFM image of the right read/write structure of a head after 10K passes (dropout cartridge) of tape MP4 at 32°C, 80% RH. Staining of the head was at its most severe on the ceramic and pole regions of the structure. Pole tip recession was not evident.

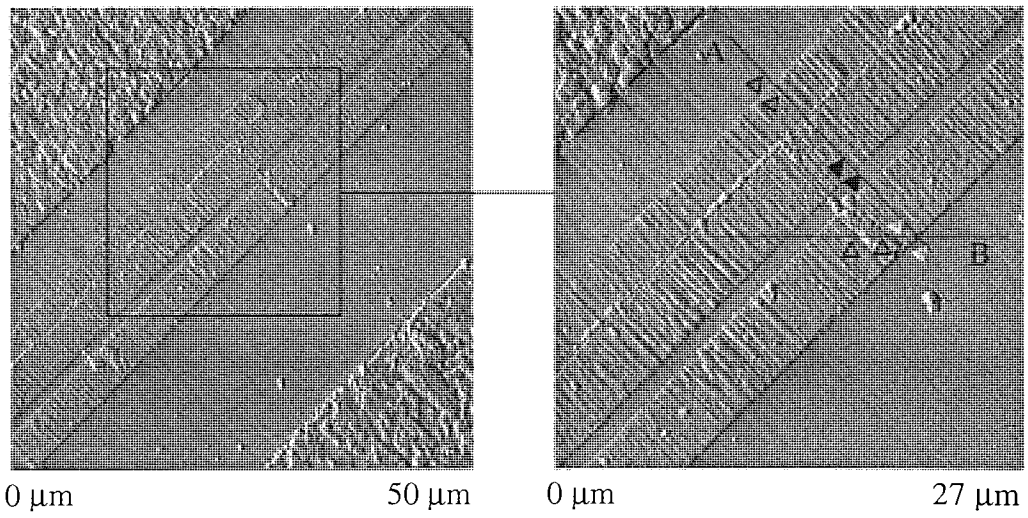

Figure 3.85 Right head assembly of a head after 10K passes of tape MP4 at 32°C, 80% RH

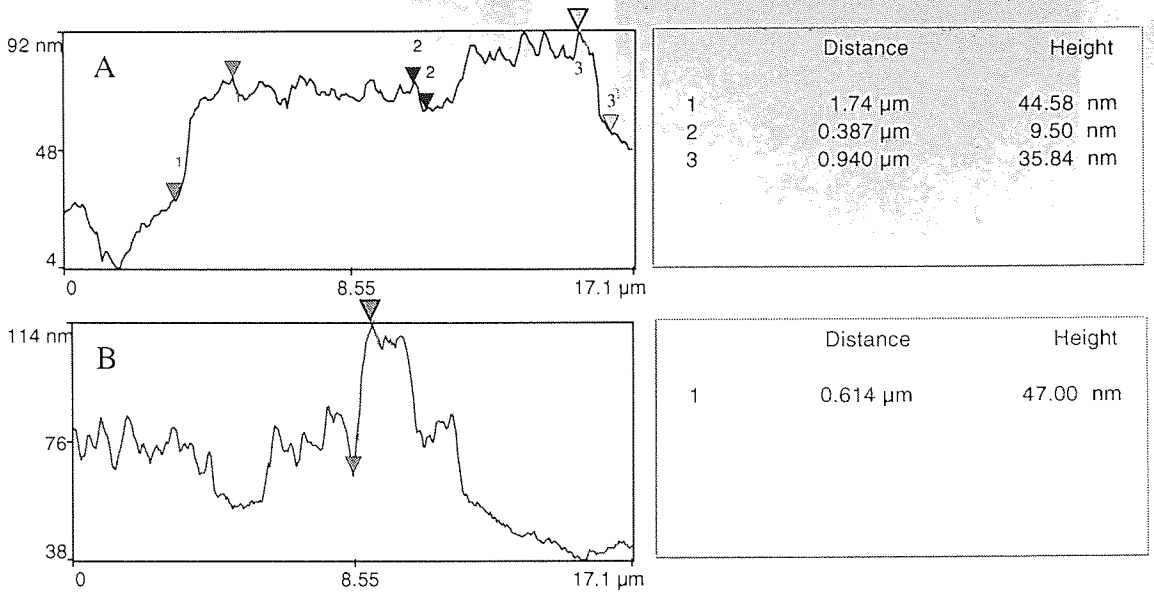

Figure 3.86 Line scan of the right head assembly of a head after 10K passes of tape MP4 at 32°C, 80% RH

The line scan in Figure 3.86 revealed the stain that adhered to the pole had a maximum thickness of 47nm and this was relative to the stain covering the pole surface.

As for the left structure, AES analysis confirmed the presence of Fe and Ti on all the component parts with the exception of the insulator regions. Al was detected at all positions analysed. Co was found on the shield side of the insulator and ceramic regions.

3.4.2.4.2 Multiple Cartridges

3.4.2.4.2.1 Left Structure

Figure 3.87 shows an AFM image of the left read/write structure of head after 5K passes (three cartridges) of tape MP4 at 32°C, 80% RH. Stain was most evident on the shield and shared pole/shield at the region surrounding the MR element. This appeared to have spread to the insulator region, neighbouring the shield.

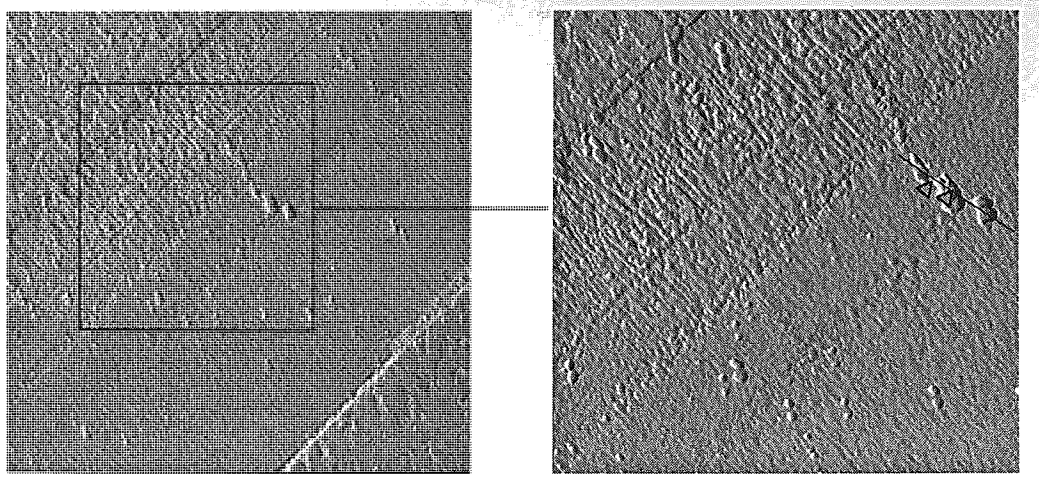

Figure 3.87 Left head assembly of a head after 5K passes of tape MP4 at 32°C, 80% RH with a close up of the pole area

The line scan in Figure 3.88 revealed the maximum thickness of stain on the left head assembly was 95.3 nm.

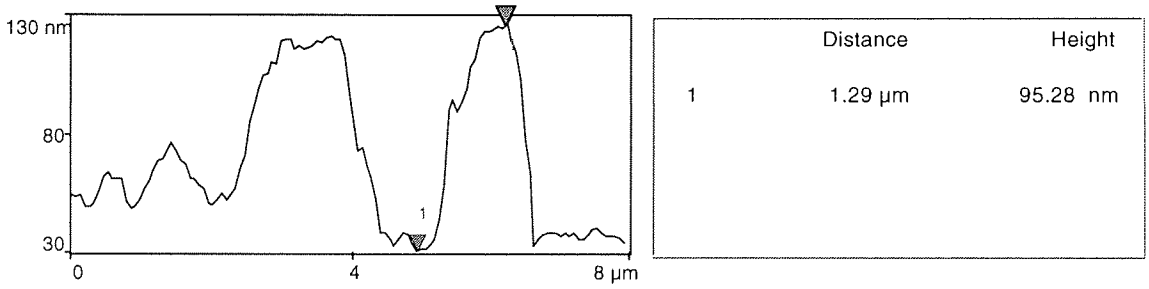

Figure 3.88 Line scan of the left head assembly of a head after 5K passes of tape MP4 at 32°C, 80% RH to establish stain height

AES analysis of this structure confirmed the presence of Fe, Ti and Al on all the component parts. Co was found on all positions analysed with the exception of on the of the insulator pole side.

3.4.2.4.2.2 Right Structure

Figure 3.89 shows an AFM image of the right read/write structure of a head after 5K passes (dropout cartridge) of tape MP4 at 32°C, 80% RH. No immediate pole tip recession was evident on this assembly. Slight staining had occurred across the insulator and pole regions of the structure. Pitting of the insulator on the pole side had occurred.

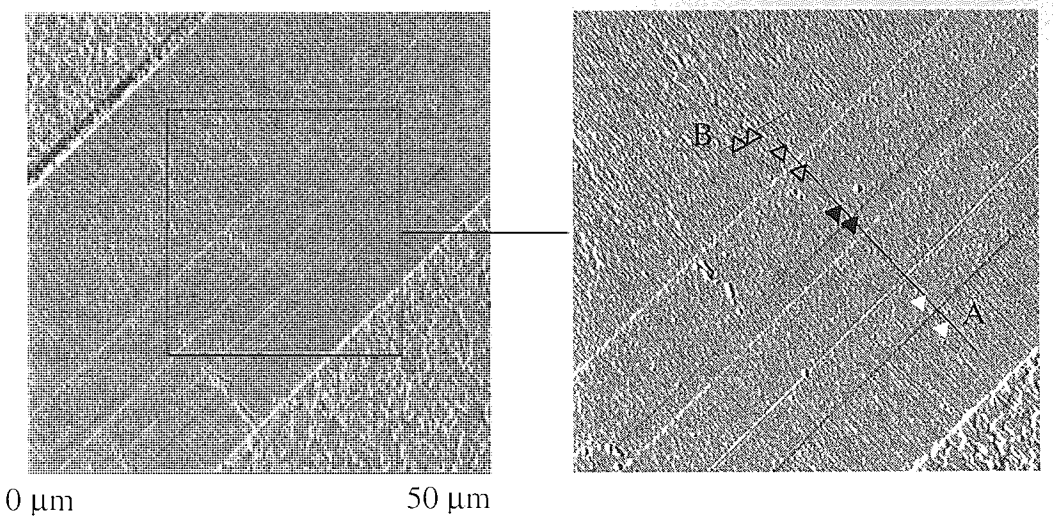

Figure 3.89 Right head assembly of a head after 5K passes
of tape MP4 at 32°C, 80% RH with a close up of the pole area

The line scan in Figure 3.90 shows the pitting detected on the insulator region (pole side) had a depth of at least 18.7 nm

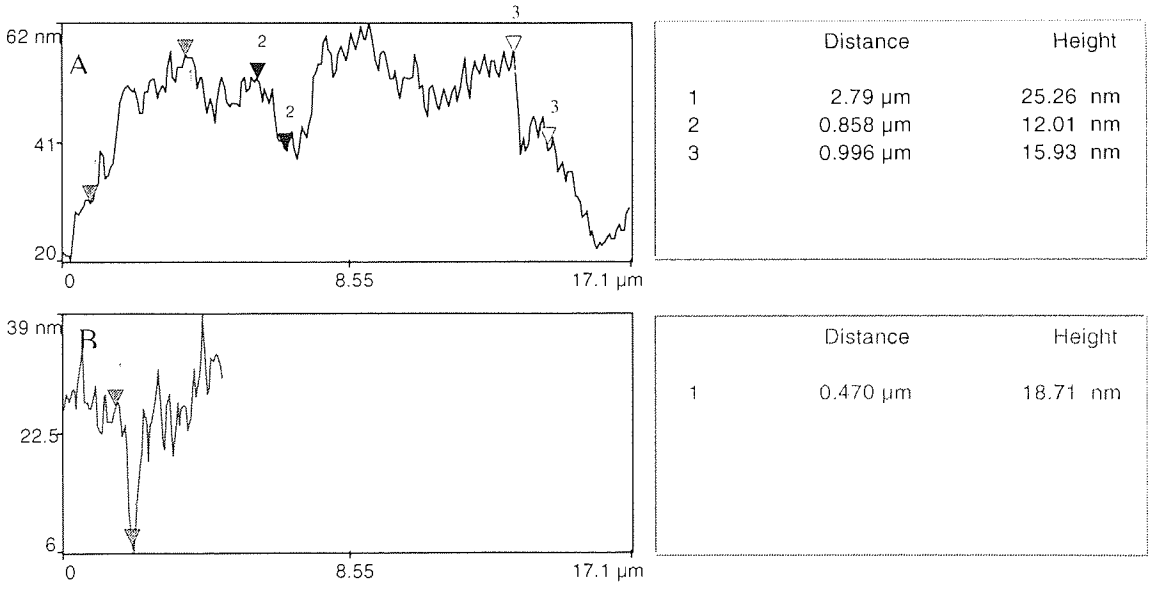

Figure 3.90 Line scan of the right head assembly of a head after
5K passes of tape MP4 at 32°C, 80% RH

AES analysis of this structure confirmed the presence of Fe and Ti on all the component parts. Al was detected at all positions but the shield. Co was detected at most positions analysed with the exception of the pole side of the insulator.

3.4.3 5°C, 10% RH

3.4.3.1 MP3

3.4.3.1.1 Dropout Measurement

Figure 3.91 show the 4 dB, 5 dB, 6 dB and 10 dB dropout growth as a function of increasing number of passes. The 4 dB x 50 µs class of dropout was seen to increase overall throughout the duration of the experiment as indeed did the 5 dB x 20 µs dropouts (Figure 3.91a and b respectively). In every case, dropouts with widths 3 µs, 6 µs and 10 µs consistently decreased with increasing cycling.

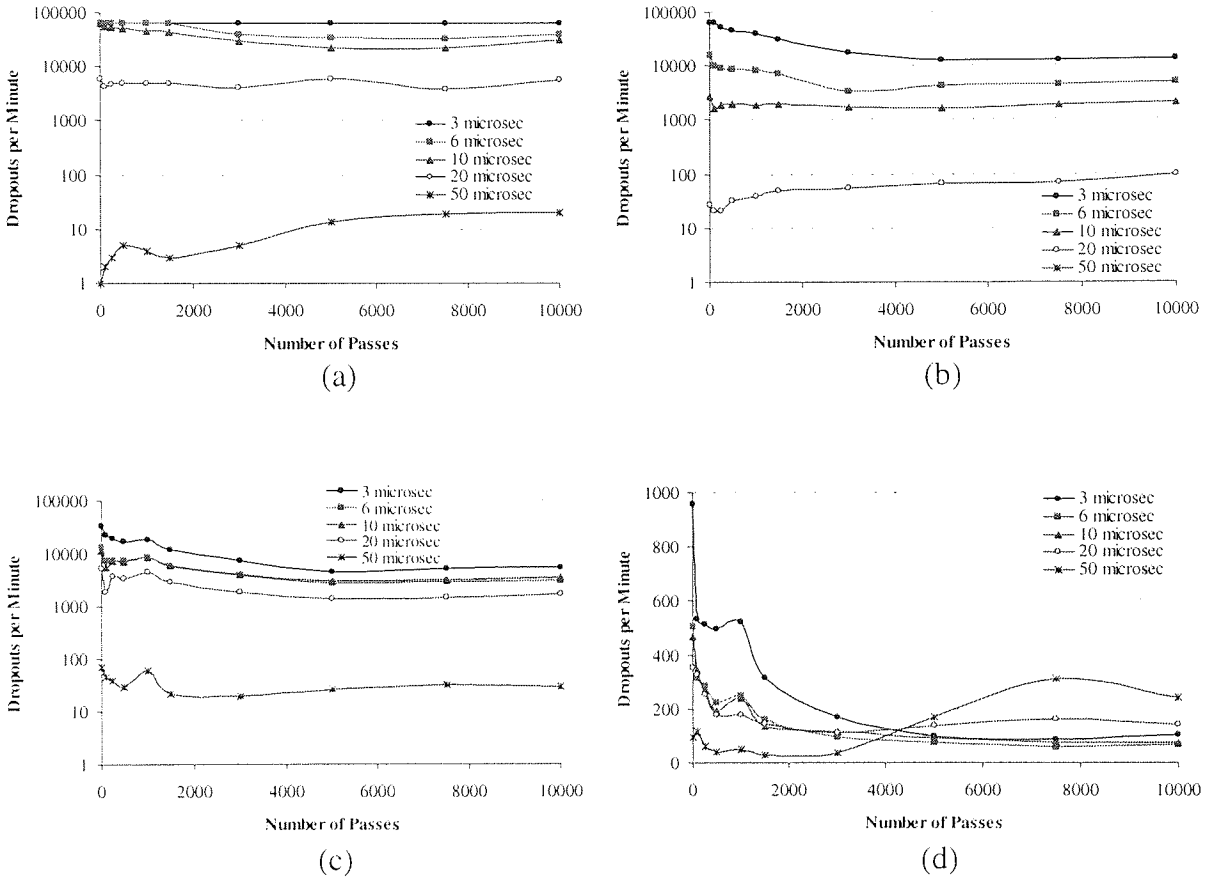

Figure 3.91 (a) 4 dB (b) 5 dB (c) 6 dB and (d) 10 dB dropout growth for tape MP1 at 5°C, 10% RH

3.4.3.1.2 XPS

After the completion of 7K passes of tape MP4 (dropout cartridge) at 5°C, 10% RH cartridge failure occurred. After 5K passes (using three identical cartridges for 500, 1500 and 3000 passes), cartridge failure had not occurred. XPS analysis of the tape at the centre and edge positions was performed.

At the tape centre the Fe concentration increased with cycling whilst that of N decreased. The concentration of O was extremely stable throughout cycling as was that of C which only showed a very slight increase after 1500 passes. The overall trends at the edge of the tape were very similar to those at the centre with the exception of N which remained stable with cycling.

Synthesis of the C peak confirmed the stability of all but the C-N component at the centre and edge of tape (Figure 3.92 and Figure 3.93 respectively). The central tape position produced a definite decrease in the C-N bond throughout cycling although the C-O bond was stable.

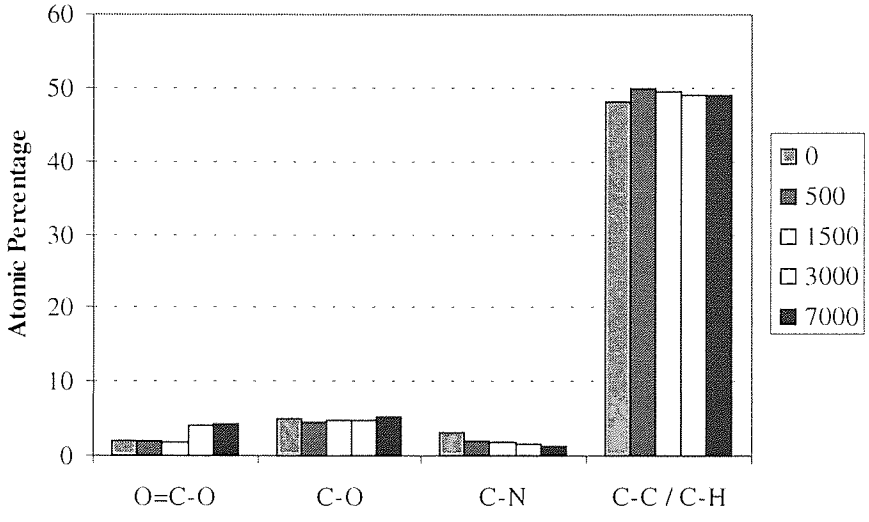

Figure 3.92 Synthesis of C for MP4 at 5°C 10% - Centre

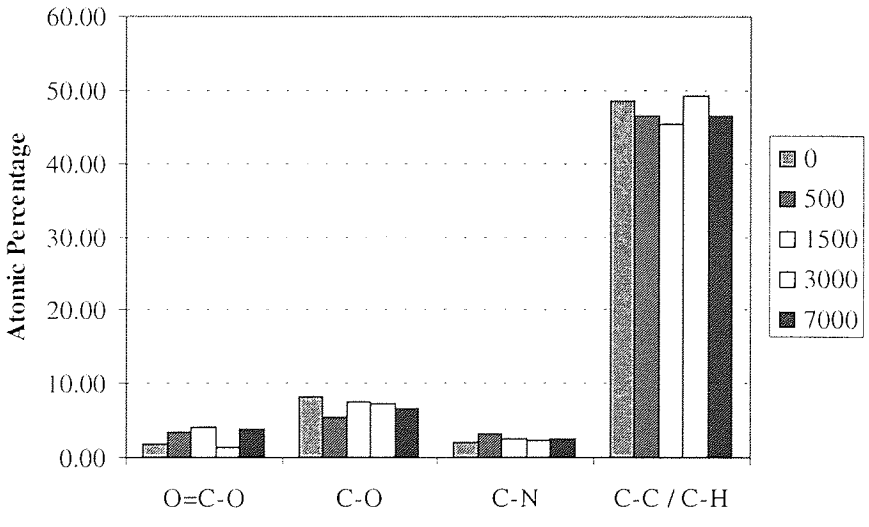

Figure 3.93 Synthesis of C for MP4 at 5°C 10% - Edge

The stability of the C and O signals suggested that little chemical change had occurred at the tape surface.

There were differences in elemental composition between the centre and edge regions at the surface of tape. There was clearly a higher percentage of Fe and O at the centre region of the tape compared to the edge. At the edge, there is an overall higher percentage of N and C when compared to the centre region.

Group A tapes exhibited different elemental trends at their centre and edge positions. For MP1 the C signal decreased up to 500 passes where it then remained stable until 3000 passes and increased at 10K passes. The O signal followed the opposite trend. The Fe and N signals remained reasonably constant throughout cycling at both positions on the tape. Synthesis of the C peak revealed that the C-C/C-H signal increased while the C-O component decreased at both the centre and edge throughout cycling.

Tape MP3 exhibited definite trends for C and O concentrations throughout cycling. At both positions on the tape the C signal decreased with cycling whilst the O signal increased. Fe increased at the centre whereas N decreased, both elements remained constant at the edge. The C-C/C-H signal for the edge and centre of tape showed an increase with cycling. The C-O signal decreased at both tape positions whereas the C-N signal decreased at the centre but remained level at the edge.

Figure 3.94 - Figure 3.96 compare ratios of Fe:C, Fe:N, and N:C respectively for group A tapes.

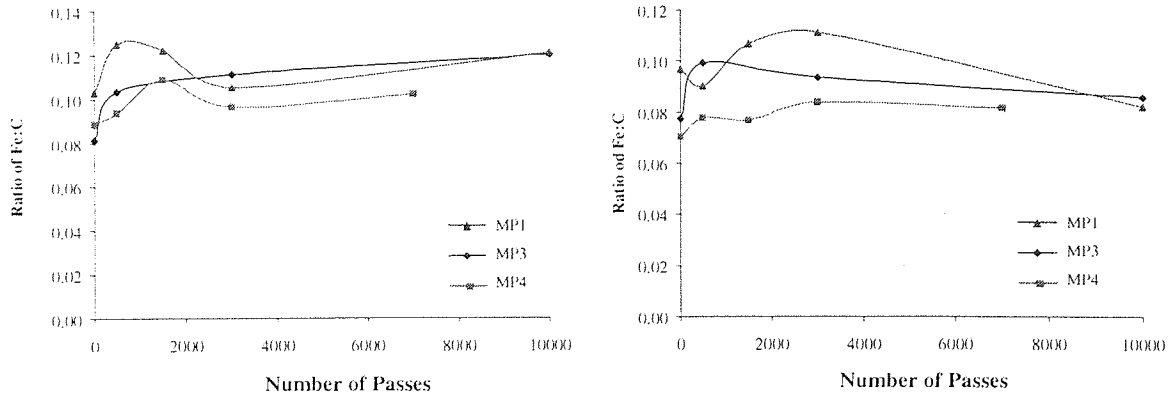

Figure 3.94 Ratio of Fe:C for group A tapes at 5°C, 10% RH (a) Centre and (b) Edge

Figure 3.94 shows that at the centre of tape, the Fe:C ratios had increased between the virgin condition and 10K passes (7K passes in the case of MP4). The situation was very similar to that found at 32°C, 80% RH where the tapes were ordered by magnitude (greatest first) as:

MP1 > MP3 > MP4.

There was a difference in the N:C trends between the centre and edge of tapes for MP3 and MP4. At the centre of tape (Figure 3.95 (a)) there was an overall decrease in the N:C ratio whereas at the edge of tape (Figure 3.95 (b)) there was an overall increase. This suggests that N depletion occurred at a greater rate than the C increase at the centre of tape, with the opposite effect occurring at the edge. Tape MP1 produced a very stable ratio at both positions on the tape.

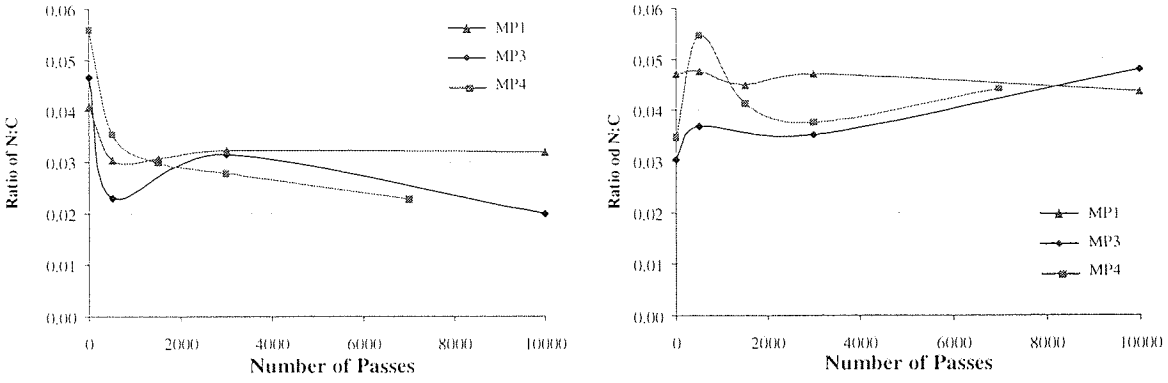

(a) (b)

Figure 3.95 Ratio of N:C for group A tapes at 5°C, 10% RH
(a) Centre and (b) Edge

All three tapes exhibited the same trend for the Fe:N ratios at the centre of tape. The ratio initially increased, decreased slightly then increased again. Fe increased and N decreased throughout cycling which was consistent with the initial and final increases in the Fe:N ratios. The decrease in the ratio was more likely to be due to a decrease in Fe rather than an increase in N.

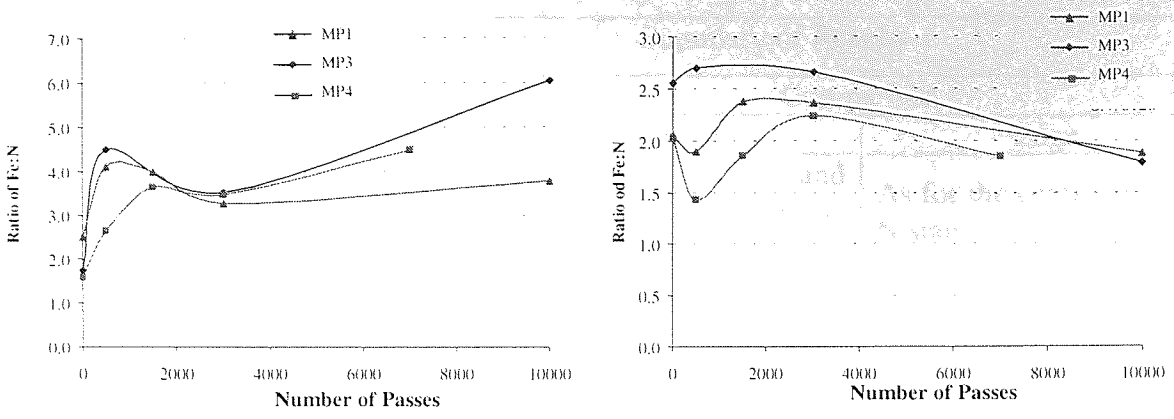

(a) (b)

Figure 3.96 Ratio of Fe:N for group A tapes at 5°C, 10% RH
(a) Centre and (b) Edge

The opposite trend occurred at the edge of tape, after an initial decrease the ratio increased before finally decreasing for tapes MP1 and MP4. These changes were subtler than at the centre as the magnitudes of the ratio were lower. At the higher number of passes, Fe was removed at a greater rate than N.

The overlayer thickness' were calculated for MP4 at the centre and edge positions and are presented in Figure 3.97. The overlayer thickness was seen to decrease at the centre and edge as cycling commenced.

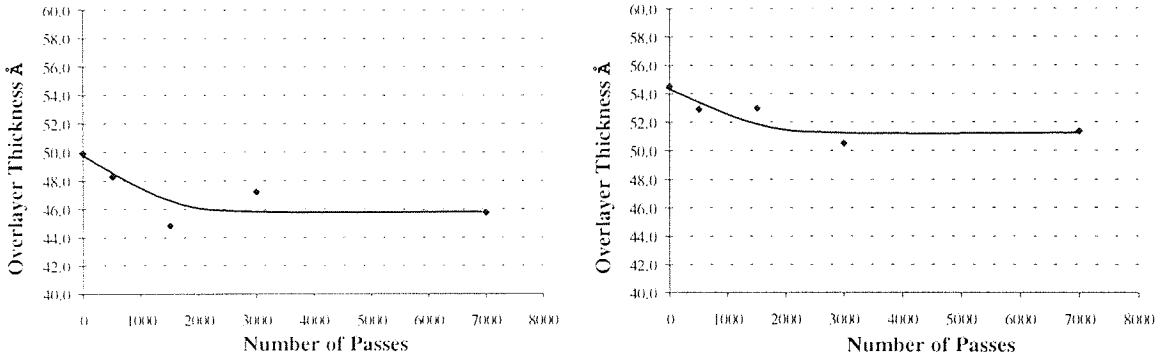

(a) (b)

Figure 3.97 Variation in Overlayer Thickness as a Function of Increasing Number of Passes for MP4 a 5°C 10% RH – (a) Centre and (b) Edge

At the edge, where the situation was again more stable, a more subtle decrease in the overlayer thickness was noted.

The results for this section are summarised in Table 3.15.

Tape	Condition	Summary of Results		
			Comparison	
			Centre	Edge
MP3	5°C, 10% RH	XPS	Fe increased while C and N showed a decrease with increased cycling	As for the centre but with N stable.
		Synthesis of C	C-C/C-H increased for 500 passes then. C-N and C-O decreased with cycling.	C-C/C-H was stable with cycling. C-N and C-O decreased with cycling.
		Ratios	Fe:N and Fe:C increased. N:C decreased up to 500 passes then relatively stable.	Fe:N stable up to 3K then decrease. Fe:C increased up to 500 passes then stable. N:C increased overall with cycling.
		Dropouts	As for tape MP1 but with no increase for the 50 μs class. Lowest number of dropouts of the group A tapes.	
MP1	5°C, 10% RH	XPS	Fe increased while C and N were relatively stable with increased cycling.	As for the centre.
		Synthesis of C	C-C/C-H increased while C-O and C-N decreased.	As for the centre but with a stable C-N component.
		Ratios	Fe:N and Fe:C increased overall. N:C decreased up to 500 passes then stable.	Fe:N stable, Fe:C decreased overall. N:C stable throughout cycling.
		Dropouts	A reduction up to 1K passes then stable. The 50 μs class increased with cycling for the 4 dB and 10 dB category.	
MP4	5°C, 10% RH (7K passes)	XPS	Fe increased while N showed a decrease with increased cycling. C was relatively stable.	Fe increased with cycling whilst C and N remained stable.
		Synthesis of C	All components stable except C-N, which decreased.	Slight reduction in C-C/C-H and C-O with C-N stable.
		Ratios	Fe:N and Fe:C increased. N:C decreased.	Fe:N relatively stable, Fe:C stable. N:C increased overall with cycling.
		Dropouts	A reduction up to 1K passes then stable.	

Table 3.15 Summary of Results for the Georgens Cycler Experiments (TR-5 Head) using Group A Tapes at 5°C, 10%RH.

3.4.3.2 AFM and AES Analysis

3.4.3.2.1 MP1

3.4.3.2.1.1 Single (Dropout) Cartridge

After the completion of 10K passes (dropout cartridge) and 5K passes (three cartridges) using tape MP1 at 5°C 10% RH, cartridge failure had not occurred. The two read/write structures of each head were then examined using AES and AFM techniques in order to investigate for evidence of staining and/or relative wear of the individual components.

3.4.3.2.1.1.1 Left Structure

Figure 3.98 shows an AFM image of the left read/write structure of a head after 10K passes (dropout cartridge) at 5°C, 10% RH.

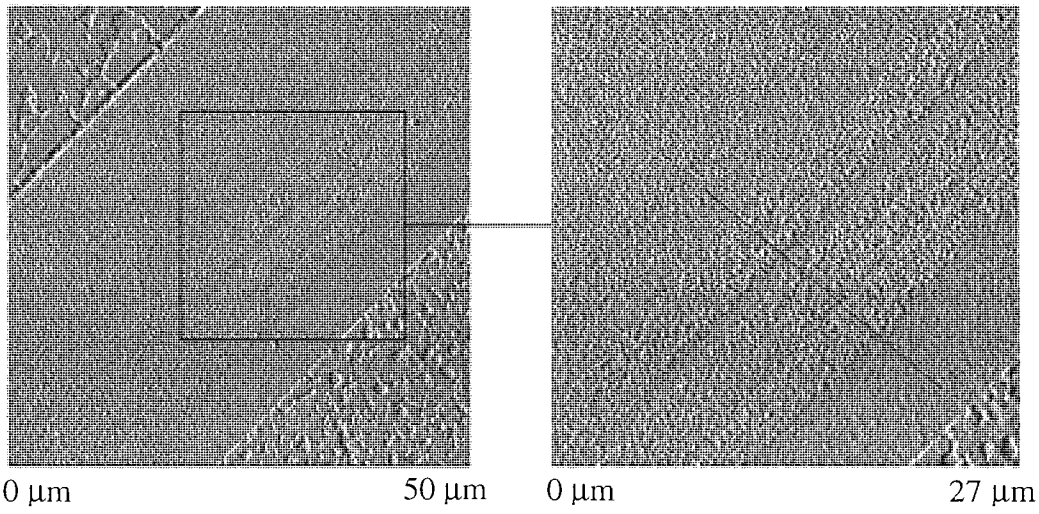

Figure 3.98 Left head assembly of a head after 10K passes of tape MP1 at 5°C, 10% RH and a close up of the pole area

Stain was visible on most regions of this head with the possible exception of the ceramic areas. Heavy staining of the poles made identification of separate regions quite difficult as illustrated in Figure 3.99.

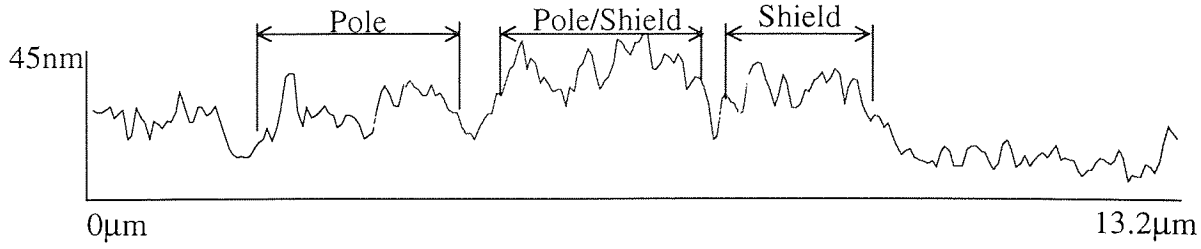

Figure 3.99 Line scan of the left head assembly of a head after 10K passes of tape MP1 at 5°C, 10% R H

AES analysis of this structure confirmed the presence of Fe on most areas of the left head assembly, unusually only the two ceramic regions exhibiting no trace of Fe. The elemental concentration for the pole was obtained from the centre region where the Fe concentration was at its greatest. Al it was also detected on the poles.

3.4.3.2.1.1.2 Right Structure

Figure 3.100 shows an AFM image of the right read/write structure of a head after 10K passes (dropout cartridge) at 5°C, 10% RH. No immediate pole tip recession was evident on this assembly. However, stain was present on the insulator region between the ceramic and the pole, on the write gap and on the poles.

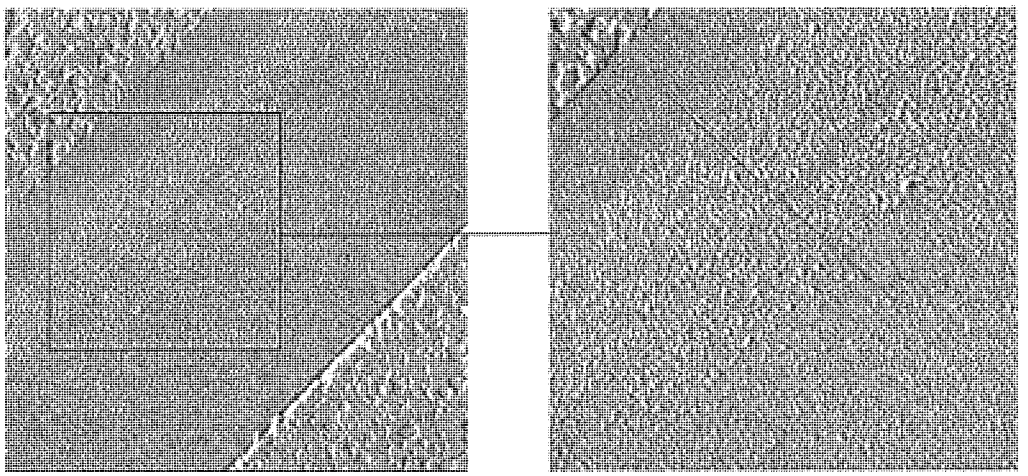

Figure 3.100 Right head assembly of a head after 10K passes of tape MP1 at 5°C, 10% RH with a close up of the pole area

Significant staining of the poles made it difficult to identify the separate regions of the head and in particular, the transition between the shared shield/pole and the shield, as shown in Figure 3.101.

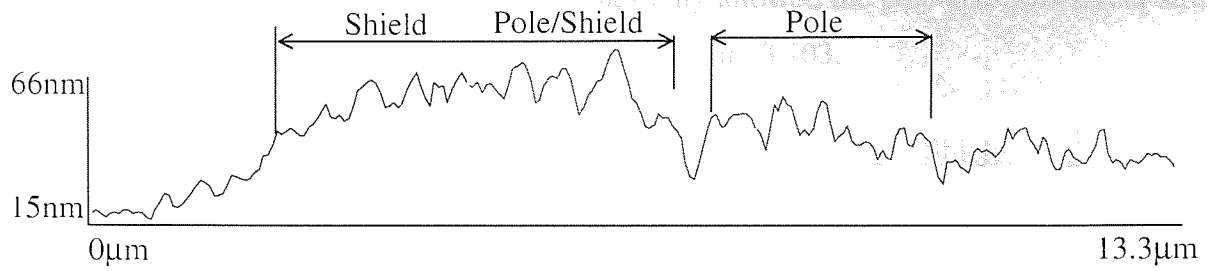

Figure 3.101 Line scan of the right head assembly of a head after 10K passes of tape MP1 at 5°C, 10% RH

After performing AES analysis on this structure it was found that Fe was only present on the pole, pole/shield and shield.

3.4.3.2.1.2 Multiple Cartridges

3.4.3.2.1.2.1 Left Structure

Figure 3.102 shows an AFM image of the left read/write structure of a head after 5K passes (three cartridges) of tape MP1 at 5°C, 10% RH. Some pole tip recession was evident on this assembly, as indeed was some staining of the Al_2O_3 regions and the poles.

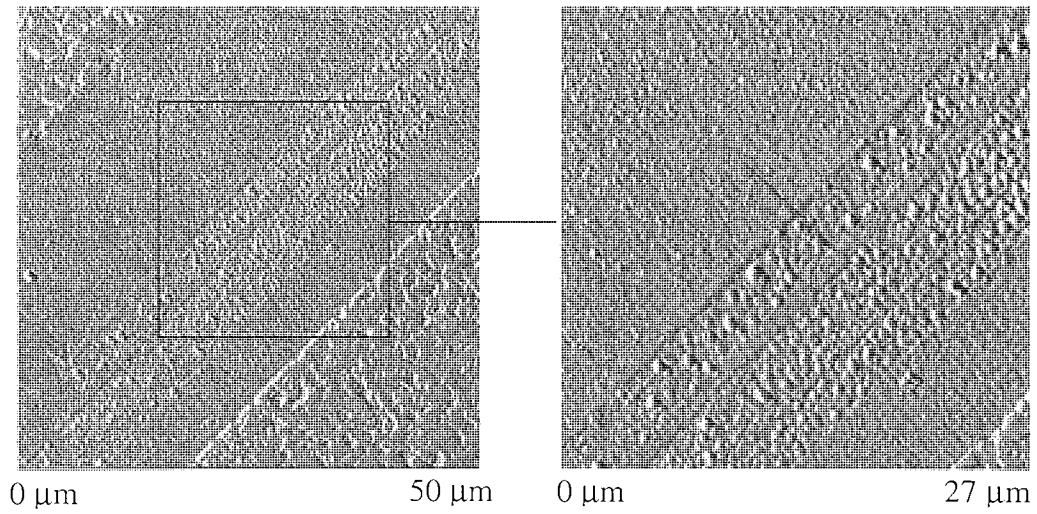

Figure 3.102 Left head assembly of a head after 5K passes of tape MP1 at 5°C, 10% RH with a close up of the pole area

Faint staining was visible on most regions of the head with the possible exception of the ceramic areas. Heavier staining on the poles only allowed the pole and pole/shield structures to be identified from the line scan, as shown in Figure 3.103.

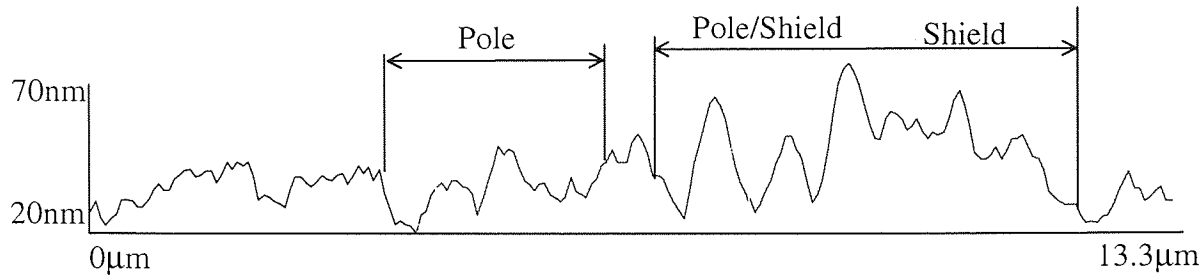

Figure 3.103 Line scan of the left head assembly of a head after 5K passes of tape MP1 at 5°C, 10% RH

AES analysis of this structure confirmed the presence of Fe on the pole areas. Traces of Al were also detected on the pole.

3.4.3.2.1.2.2 Right Structure

Figure 3.104 shows an AFM image of the right read/write structure of a head after 5K passes (three cartridges) of tape MP1 at 5°C, 10% RH. Some pole tip recession was evident on this assembly, as indeed was some staining of the Al_2O_3 regions and the poles. The stain formation on this structure was not as great as on that of the left structure since it was mainly confined to the pole areas. Figure 3.105 shows a line scan across the right head assembly.

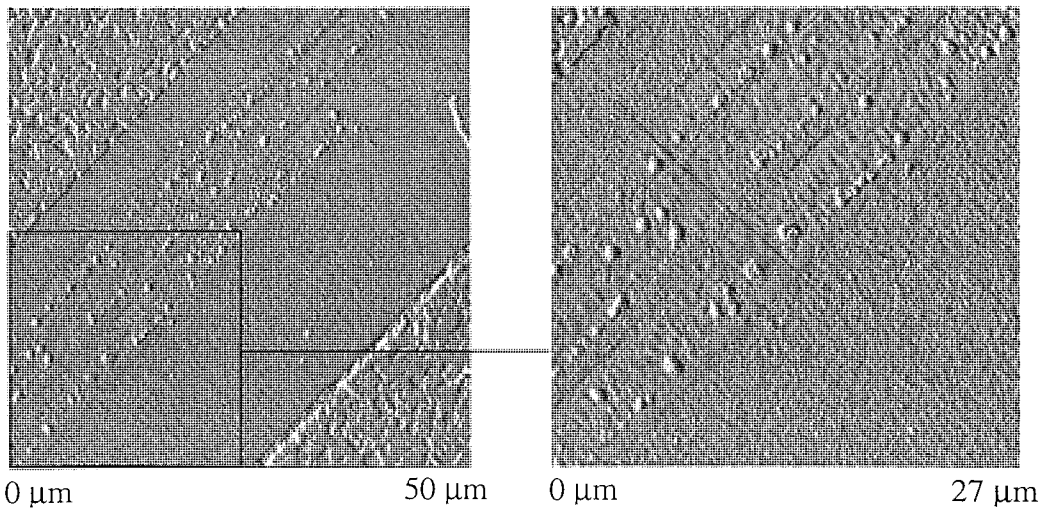

Figure 3.104 Right head assembly of a head after 5K passes of tape MP1 at 5°C, 10% RH with a close up of the pole area

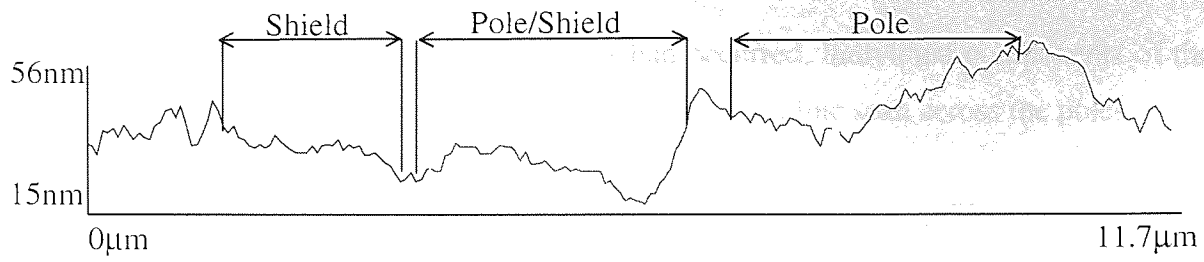

Figure 3.105 Line scan of the right head assembly of a head after 5K passes of tape MP1 at 5°C, 10% RH

Following AES analysis it was established that Fe was present on the poles and a small quantity on the insulator (pole side). Al was found on the pole/shield and shield. Ti was found on the insulator (shield side).

3.4.3.2.2 MP3

3.4.3.2.2.1 Single (Dropout) Cartridge

3.4.3.2.2.1.1 Left Structure

Figure 3.106 shows an AFM image of the left read/write structure of a head after tape MP3 had been cycled for 10K passes (dropout cartridge) at 5°C, 10% RH. No pole tip recession was evident although staining was visible on most regions of the head, with the possible exception of the ceramic areas. The most severe staining occurred on the shield and shared pole/shield, around the area where the MR element is situated.

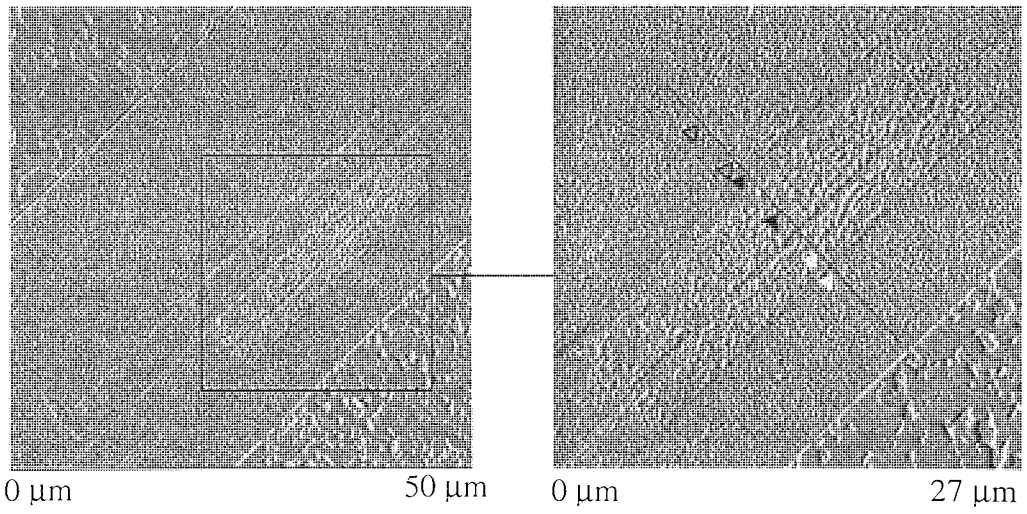

Figure 3.106 Left head assembly of a head after 10K passes of tape MP3 at 5°C, 10% RH and a close up of the pole area

Although quite heavy staining of the poles had occurred, individual components of the head assembly were still clearly visible. Figure 3.107 shows a line scan across the poles.

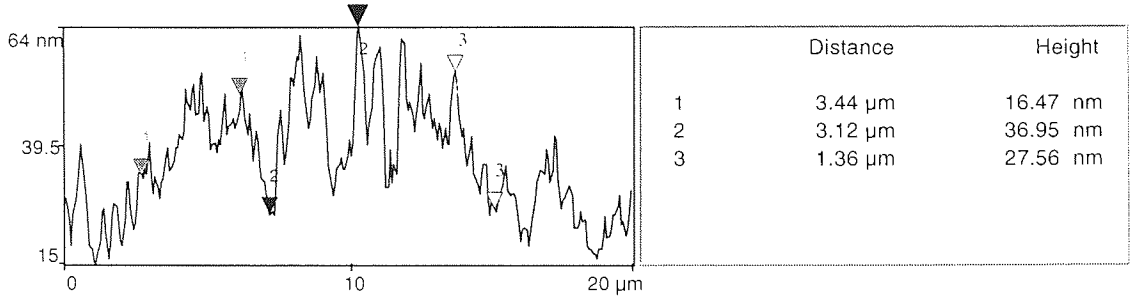

Figure 3.107 Line scan of the left head Assembly of a head after 10K passes of tape MP3 at 5°C, 10% RH

AES analysis of this structure confirmed the presence of Fe on all analysis positions, with the exception of the insulator on the shield side. Ti and Al were detected at all positions whereas Co, other than the poles, was found on the insulator (pole side).

3.4.3.2.2.1.2 Right Structure

Figure 3.108 shows an AFM image of the right read/write structure of a head after 10K passes (dropout cartridge) of tape MP3 at 5°C, 10% RH. No pole tip recession was detected on this structure. Uniform staining was visible on most regions of the head with the possible exception of the ceramic areas.

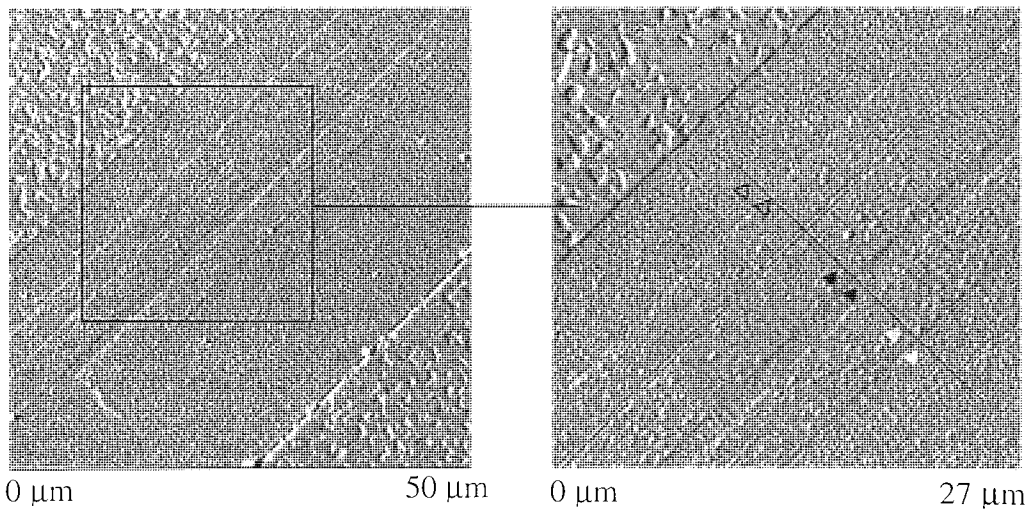

Figure 3.108 Right head assembly of a head after 10K passes of tape MP3 at 5°C, 10% RH with a close up of the pole area

The individual components of the head structure are clearly identifiable despite the slight staining.

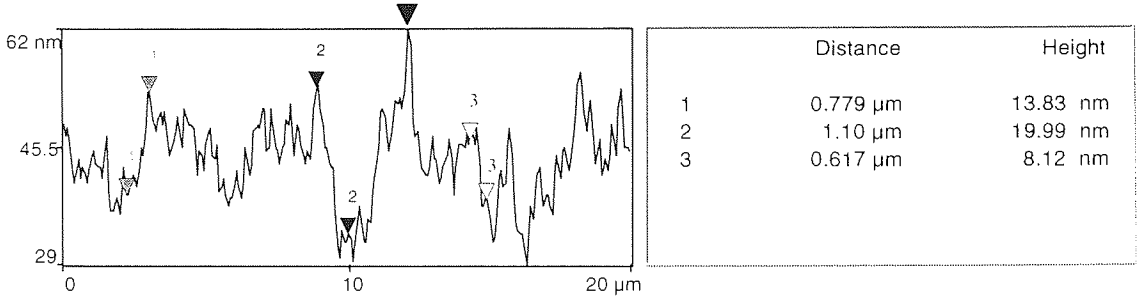

Figure 3.109 Line scan of the right head assembly of a head after 10K passes of tape MP3 at 5°C, 10% RH

Following AES analysis of this structure it was confirmed that Fe, Ti and Al were present on all positions analysed.

3.4.3.2.2.2 Multiple Cartridges

3.4.3.2.2.2.1 Left Structure

Figure 3.110 shows an AFM image of the left read/write structure of a head after 5K passes (three cartridges) of tape MP3 at 5°C, 10% RH. No pole tip recession was evident on the structure, although large areas of stain covered most of the head structure.

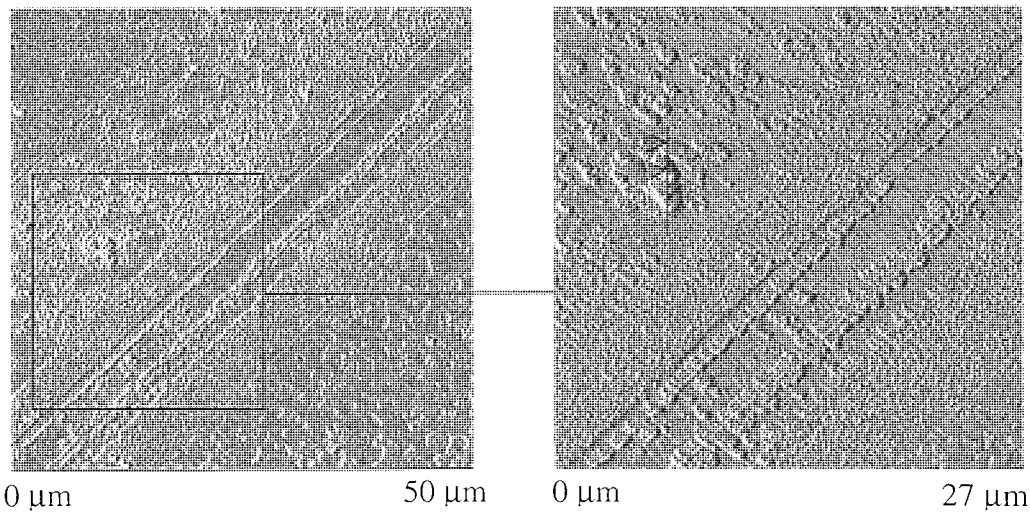

Figure 3.110 Left head assembly of a head after 5K passes of tape MP3 at 5°C, 10% RH with a close up of the pole area

The line scan in Figure 3.111 revealed the stain on the insulator region (pole side) had a thickness of at least 185 nm.

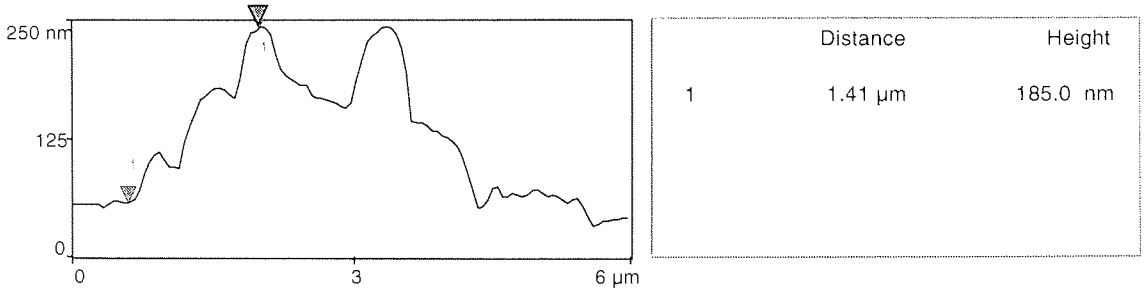

Figure 3.111 Line scan of the left head assembly of a head after 5K passes of tape MP3 at 5°C, 10% RH

AES analysis of this structure confirmed the presence of Fe on all areas. A very high concentration of Fe was found on the pole as was expected due to the heavy staining on this particular region. Al was found on the shield as well as its usual sites.

3.4.3.2.2.2.2 Right Structure

Figure 3.112 shows an AFM image of the right read/write structure of a head after 5K passes (three cartridges) of tape MP3 at 5°C, 10% RH. No immediate pole tip recession was evident on this assembly. Stain was present on all regions of the structure, including the ceramic

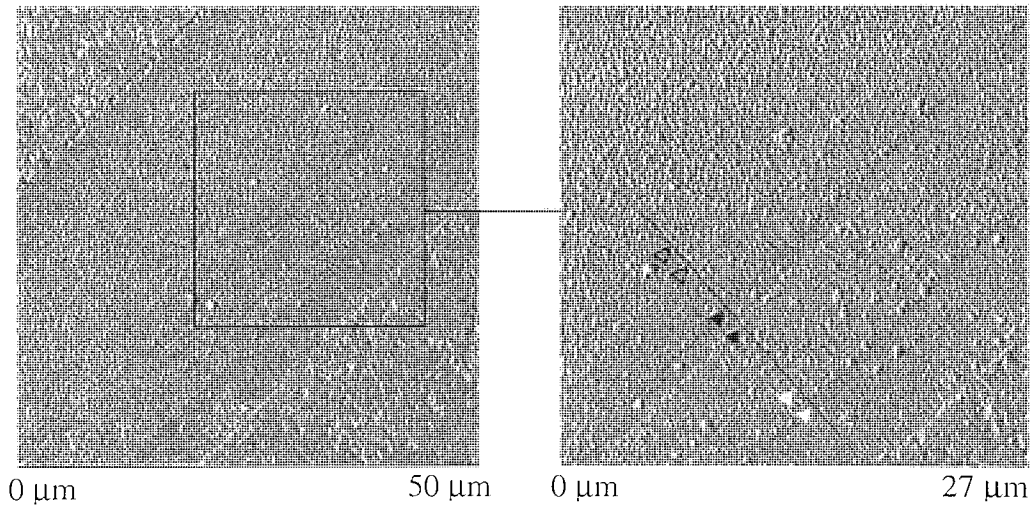

Figure 3.112 Right head assembly of a head after 5K passes of tape MP3 at 5°C, 10% RH with a close up of the pole area

Figure 3.113 shows a line scan across the right head assembly. It is possible to distinguish each component of the head structure although some are slightly obscured by stain.

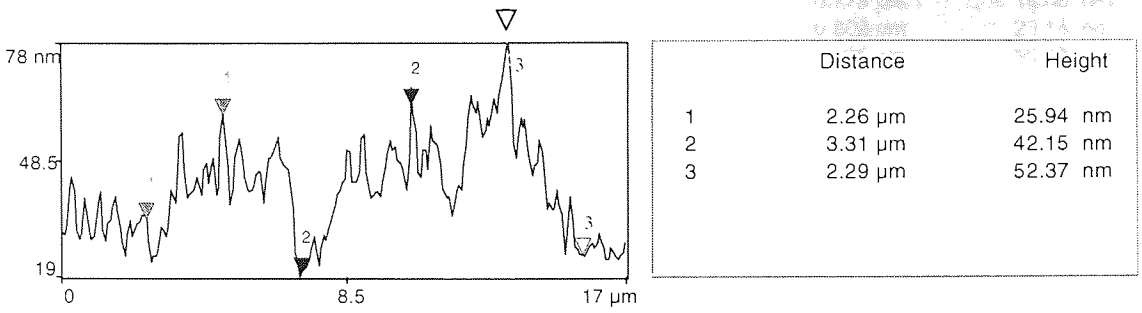

Figure 3.113 Line scan of the right head assembly of a head after 5K passes of tape MP3 at 5°C, 10% RH

AES analysis of this structure confirmed the presence of Fe on the shield and pole only. Al was found on the pole/shield.

3.4.3.2.3 MP4

3.4.3.2.3.1 Single (Dropout) Cartridge

3.4.3.2.3.1.1 Left Structure

Figure 3.114 shows an AFM image of the left read/write structure of a TR-5 head after 7K passes (dropout cartridge) of tape MP4 at 5°C, 10% RH. Slight stain was visible on most regions of this head with the possible exception of the ceramic areas. Figure 3.115 shows a line scan across the pole and shield regions of the left head.

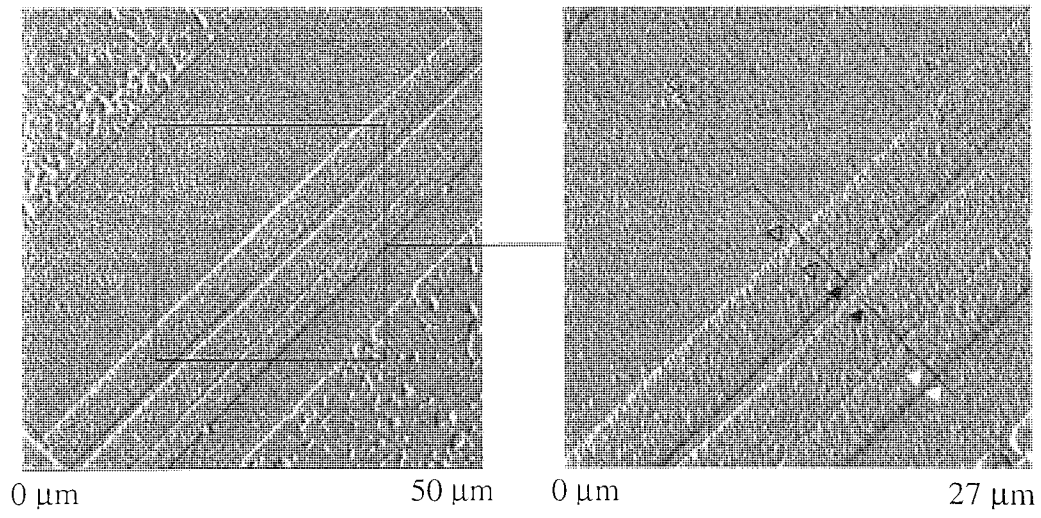

Figure 3.114 Left head assembly of a head after 7K passes of tape MP4 at 5°C, 10% RH with a close up of the pole area

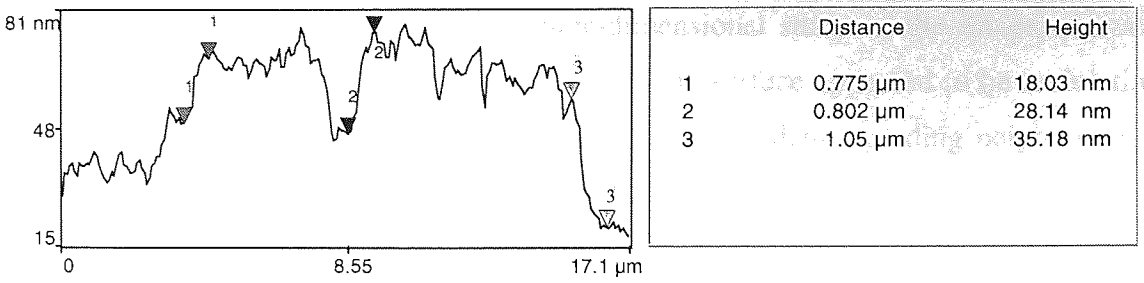

Figure 3.115 Line scan of the left head assembly of a head after 7K passes of tape MP4 at 5°C, 10% RH

AES analysis of this structure confirmed the presence of Fe on all the analysis positions, with the exception of the shield side ceramic. Similarly, Al was found on all positions. Ti was detected at most positions with the following exception; insulator (pole side).

3.4.3.2.3.1.2 Right Structure

Figure 3.116 shows an AFM image of the right read/write structure of a head after 7K passes (dropout cartridge) of tape MP4 at 5°C, 10% RH. No immediate pole tip recession was evident on this assembly. The heaviest staining was present on the insulator region between the ceramic and the pole but additional staining had also occurred on the insulator at other locations and on the poles.

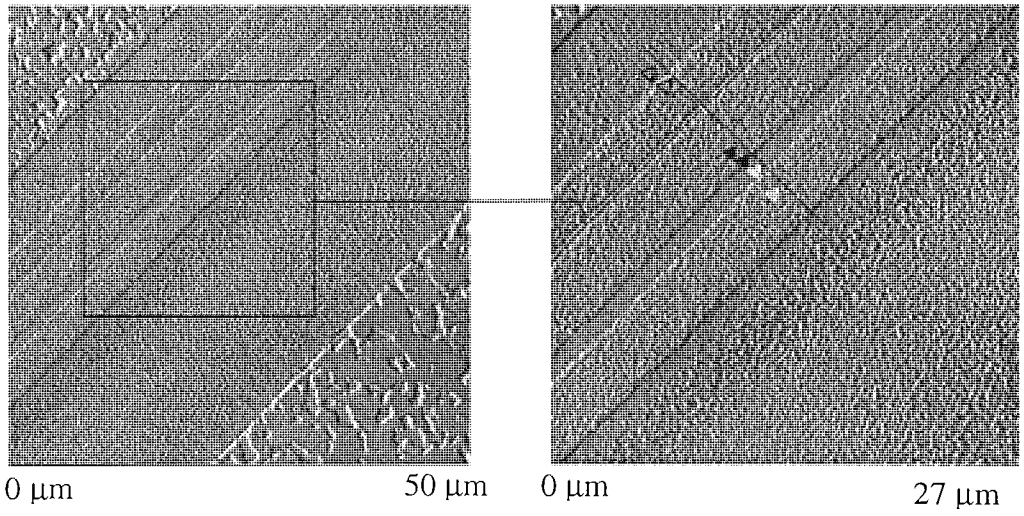

Figure 3.116 Right head assembly of a head after 7K passes of tape MP4 at 5°C, 10% RH with a close up of the pole area

The line scan shown in Figure 3.117 appeared to suggest that the shared pole/shield was lower than the pole and shield. However a three-dimensional study of the image, shown Figure 3.118 provided evidence of a corrupt scan since the surface appeared to be undulating. The visual information regarding the stain in addition to the data regarding neighbouring points should be unaffected and thus still valid.

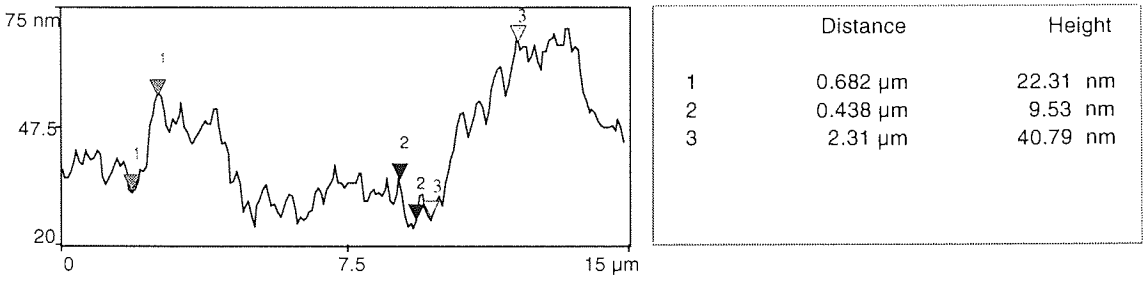

Figure 3.117 Line scan of the right head assembly of a head after 7K passes of tape MP4 at 5°C, 10% RH

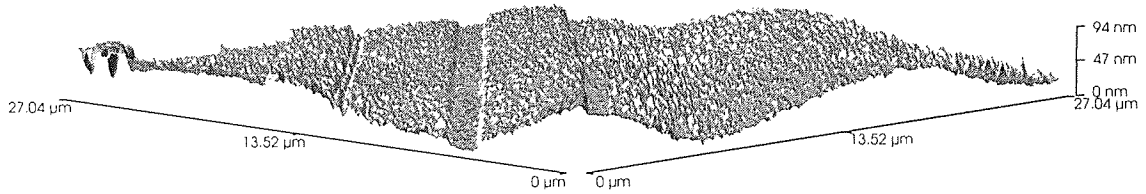

Figure 3.118 Right head assembly of a head after 7K passes of tape MP4 at 5°C, 10% RH (distorted scan)

AES analysis of this structure confirmed the presence of Fe, Ti and Al on all analysis positions. Co was detected on the insulator (pole side).

3.4.3.2.3.2 Multiple Cartridges

3.4.3.2.3.2.1 Left Structure

Figure 3.119 shows an AFM image of the left read/write structure of a head after 5K passes (three cartridges) of tape MP4 at 5°C, 10% RH. Stain was present on all regions of the head, but specifically at the area surrounding the MR element. At the region where the ceramic and insulator (pole side) are bonded together, the glue used to adhere the ceramic and insulator together appears to have seeped out of the joint since it now protrudes above all the other

features on the structure. This is confirmed by the line scan in Figure 3.120 (part A) whereby the height of the glue above the ceramic was 612 nm. Such a large protrusion could be responsible for the excessive amount of debris that was observed on this particular head, as shown in Figure 3.121.

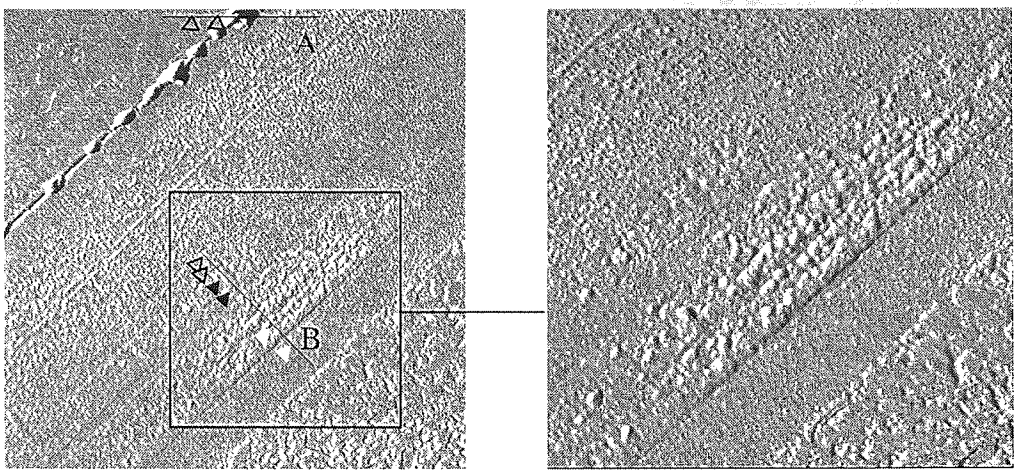

Figure 3.119 Left head assembly of a head after 5K passes of tape MP4 at 5°C, 10% RH with a close up of the pole area

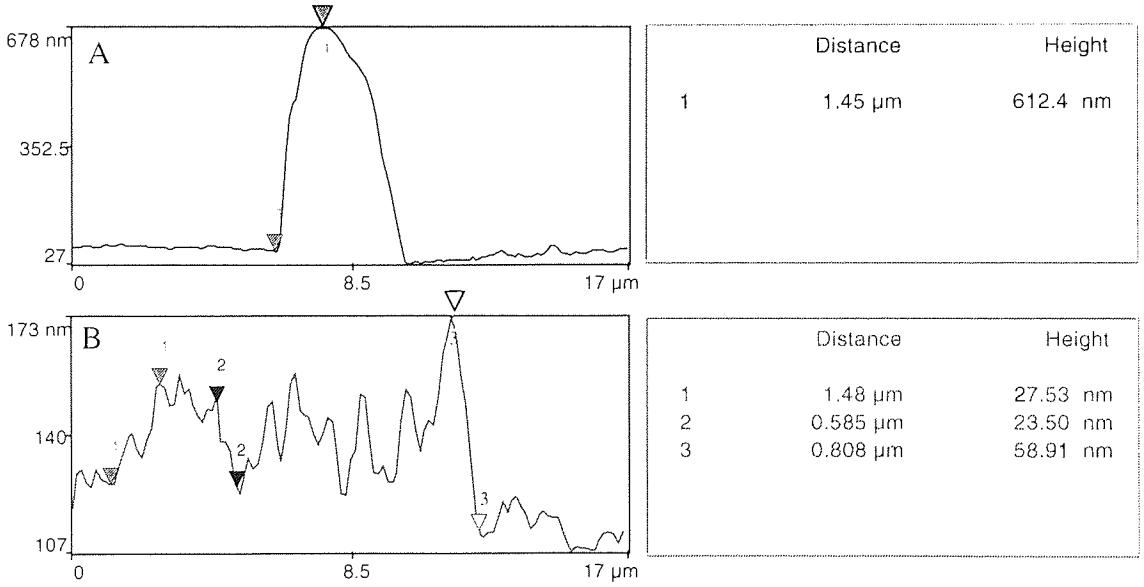

Figure 3.120 Line scans of the left head assembly of a head after 5K passes of tape MP4 at 5°C, 10% RH

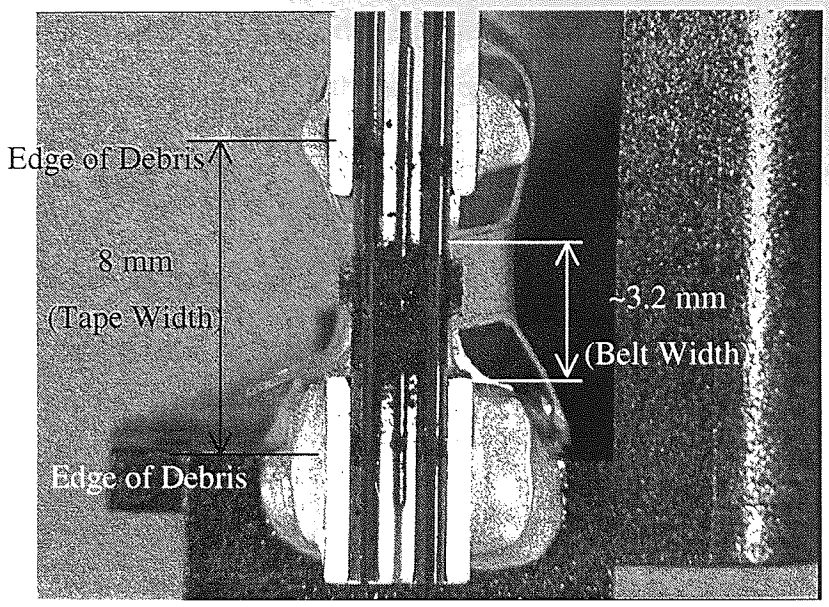

Figure 3.121 Debris on a head after 5K passes of tape MP4 at 5°C, 10% RH
(N.B. Much of the debris is in the same position as the belt)

AES maps (O, Fe and Ti) showed that Fe had deposited itself on the poles and ceramic regions.

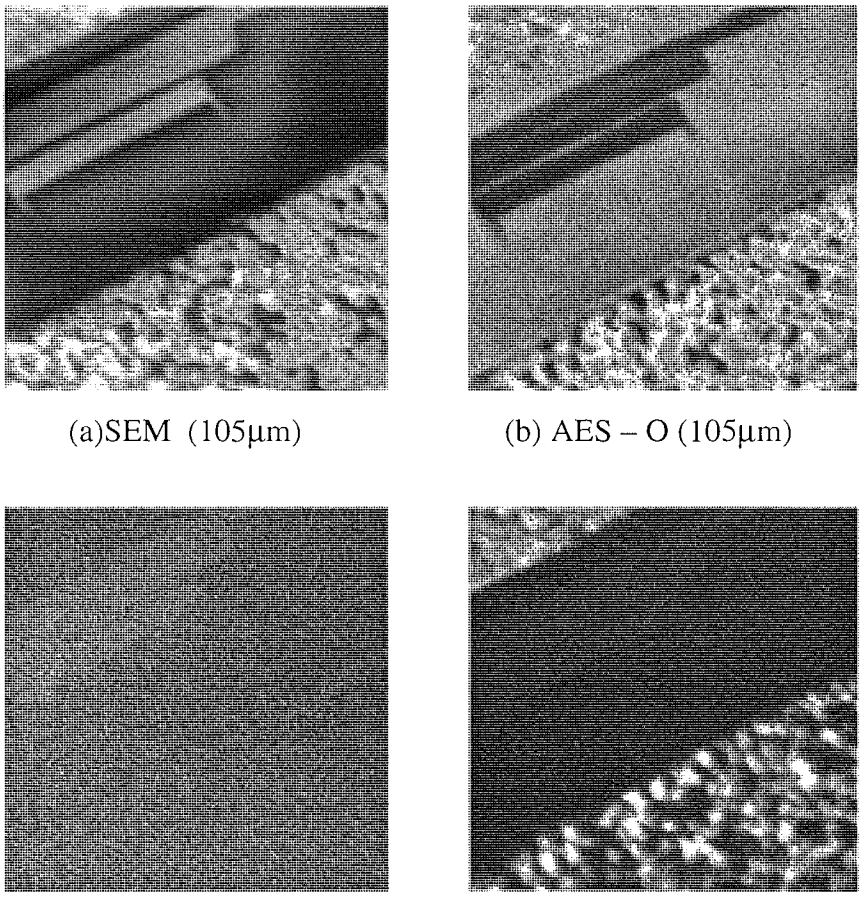

(a)SEM (105μm) (b) AES – O (105μm)

AES – Fe (105μm) AES – Ti (105μm)

Figure 3.122 SEM and AES maps (O, Fe and Ti) of the left read/write structure after 5K passes of tape MP4 at 5°C, 10% RH.

AES analysis of this structure confirmed the presence of Fe and Al on all analysis positions, while Ti was present on all positions with the exception of with the insulator (pole side).

3.4.3.2.3.2.2 Right Structure

Figure 3.123 shows an AFM image of the right read/write structure of a head after 5K passes (three cartridges) of tape MP4 at 5°C, 10% RH. No pole tip recession was evident on this assembly. The stain formation on this structure was not as prevalent as that on the left structure. A representative line scan of the read/write structure of the right head assembly is shown in Figure 3.124.

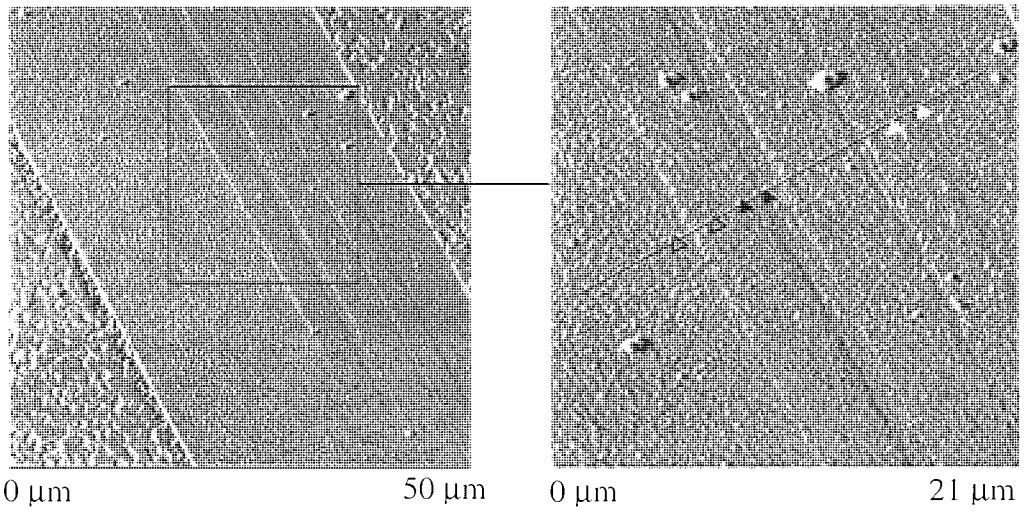

Figure 3.123 Right head assembly of a head after 5K passes of tape MP4 at 5°C, 10% RH with a close up of the pole area

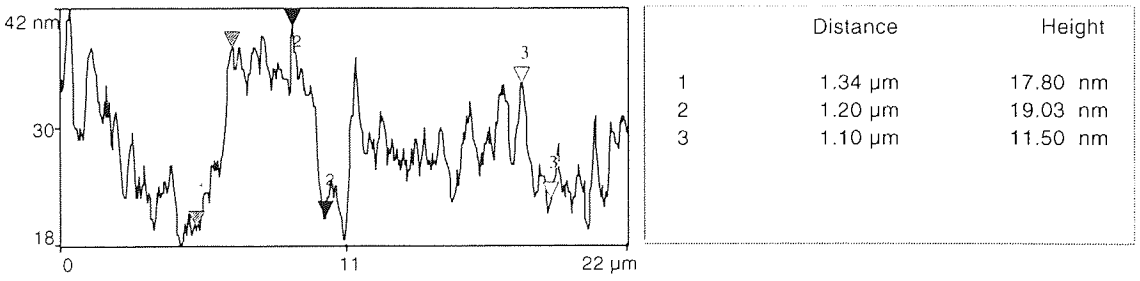

Figure 3.124 Line scan of the right head assembly of a head after 5K passes of tape MP4 at 5°C, 10% RH

AES analysis of this structure confirmed the presence of Fe, Ti and Al on all analysis positions, with the exception of the ceramic region (pole side).

3.5 Georgens Cycler with TR-5 Head Installed (Group B Tapes)

3.5.1 MP5

3.5.1.1 32°C, 80%RH

3.5.1.1.1 Dropout Measurement

After the completion of 10K passes (dropout cartridge) and 5K passes (three cartridges) with tape MP5 at 32°C 80% RH, cartridge failure had not occurred. Figure 3.125 show the 4 dB, 5 dB, 6 dB and 10 dB dropout growth as a function of increasing number of passes. The 4 dB x 50 µs and 10 dB x 50 µs class of dropout was seen to increase overall throughout the duration of the experiment as indeed did the 5 dB x 20 µs dropouts (Figure 3.125b).

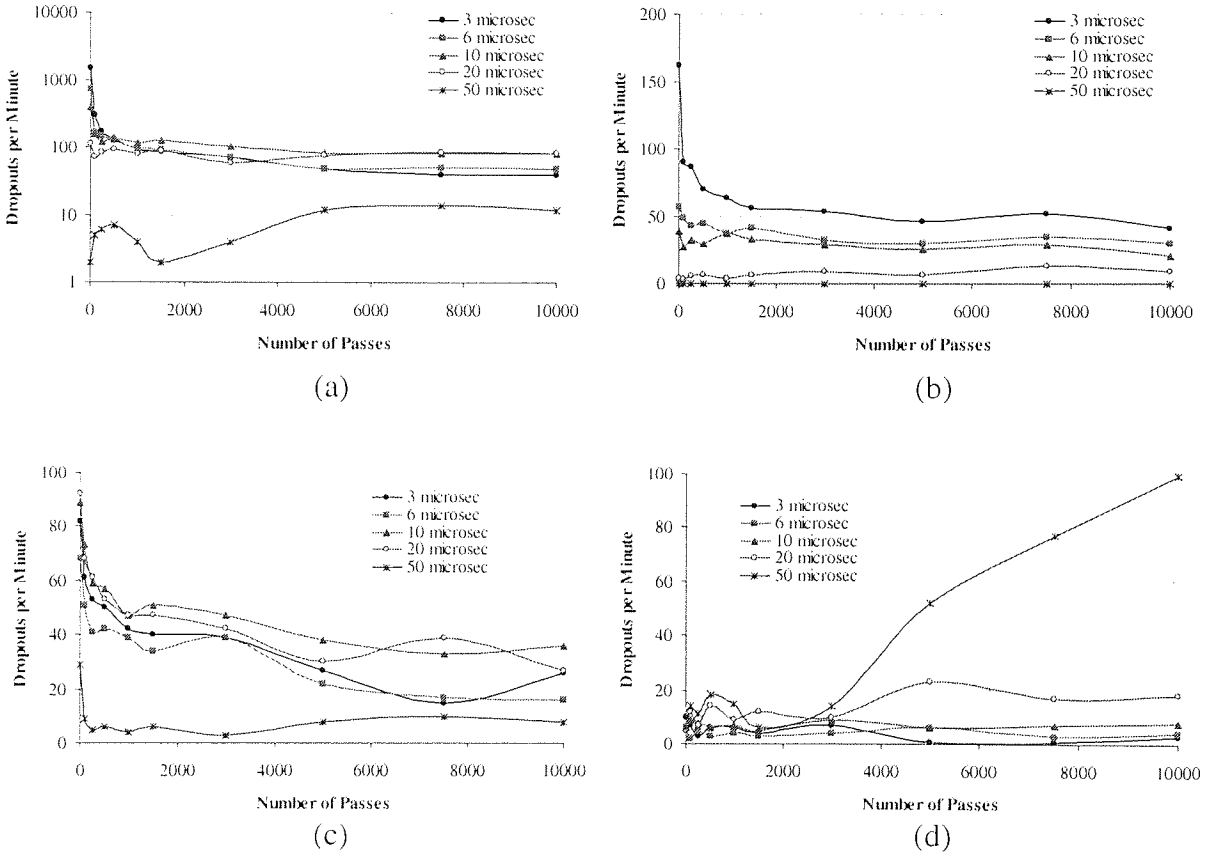

Figure 3.125 (a) 4 dB (b) 5 dB (c) 6 dB and (d) 10 dB Dropout Growth for Tape MP5 at 32°C, 80% RH

Unfortunately, possibly due to the running speed of 60ips being too high, tape MP6 broke before the completion of 2K passes. Comparison of tapes MP5 and MP6 (group B) was

therefore only possible up to 1500 passes, the predetermined number of passes completed before failure. Figure 3.126 shows how the dropout rate for tape MP6 compared to that of MP5 at 32°C, 80% RH after 1500 passes.

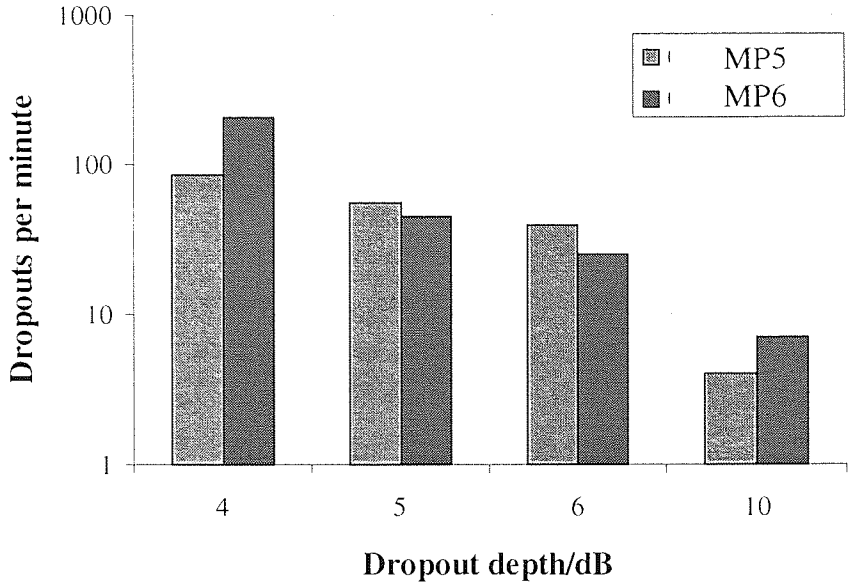

Figure 3.126 Comparison of the 3µs class of Dropout at 32°C, 80% RH for group B tapes after 1500 passes

The dropout magnitudes were similar after 1500 passes, this was not the case at the start of cycling where the two tapes differed. For MP6, the 4dB, 3µs class of dropout were an order of magnitude higher than MP5 for the virgin tape. The dropout magnitudes had converged by 1500 passes. As the dropout depth increased (4dB – 10dB) the initial difference in magnitudes decreased until, at the largest dropout depth of 10dB, the two tapes showed similar dropout profiles.

3.5.1.1.2 XPS Analysis

During cycling of the third of three cartridges for 500, 1500 and 3K passes, tape failure occurred after 1965 passes. This meant that the head had seen 4K passes instead of the required 5K.

XPS analysis at the centre and edge regions of tape MP5 at an increasing number of passes revealed the changes in elemental concentration presented in Figure 3.127 and Figure 3.128. The magnitudes of the N concentration were less than or equal to the group A tapes.

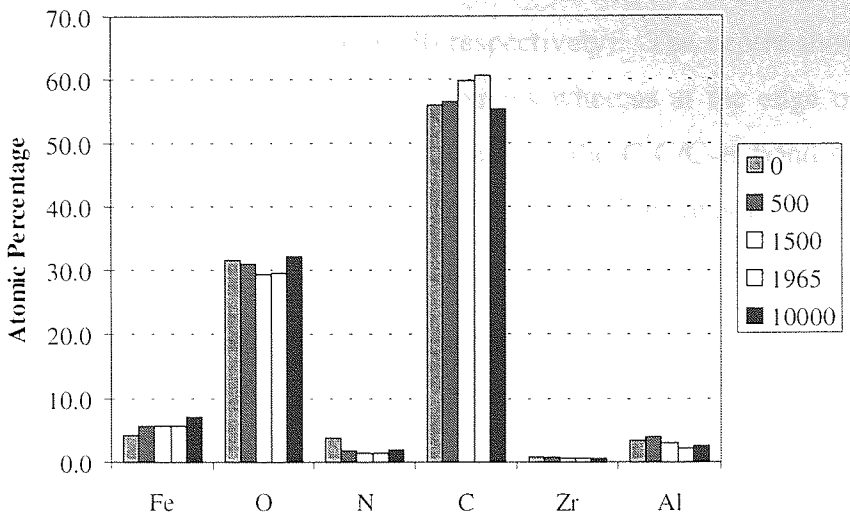

Figure 3.127 Atomic Concentration of Elements as a Function of Increasing Number of Passes for MP5 at 32°C, 80% RH – Centre

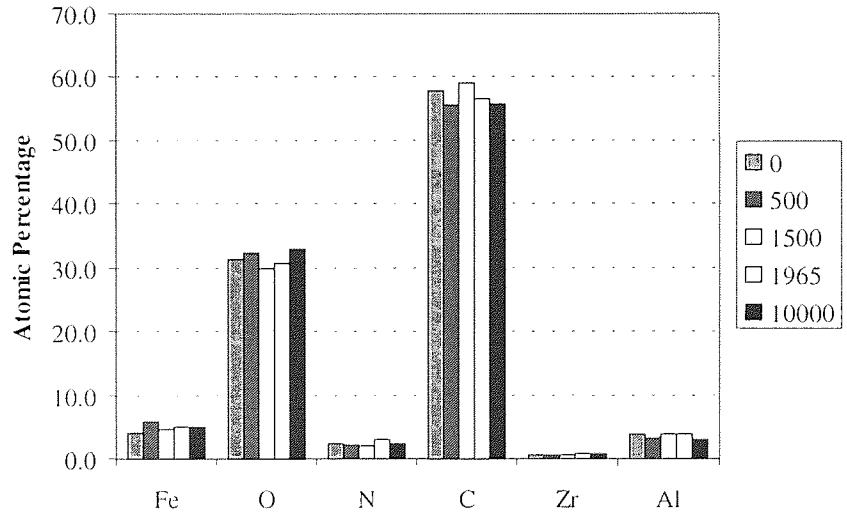

Figure 3.128 Atomic Concentration of Elements as a Function of Increasing Number of Passes for MP5 at 32°C, 80% RH – Edge

From Figure 3.127, it can be seen that at the tape centre, the Fe and C concentrations increased overall (except for the dropout cartridge) whilst the O concentration decreased with cycling. The N concentration decreased overall but the change was not as significant as for other elements. There were no distinguishable trends at the edge of the tape for all elements except Fe, which showed an overall increase (Figure 3.128).

Synthesis of the C peak confirmed the difference in the severity of changes between the centre and edge of tape (Figure 3.129 and Figure 3.130 respectively). The centre showed a definite increase in the C-C/C-H bond for the first 1500 passes whereas at the edge of the tape the change was of a more subtle nature. For both positions, the C-C/C-H bond decreased after 1500 passes being more severe at 10K passes. The C-N bond decreased at the centre of the tape but remained level at the edge. Both the C-N and C-O bonds showed an increase at 10K passes corresponding with the decrease in the C-C/C-H component.

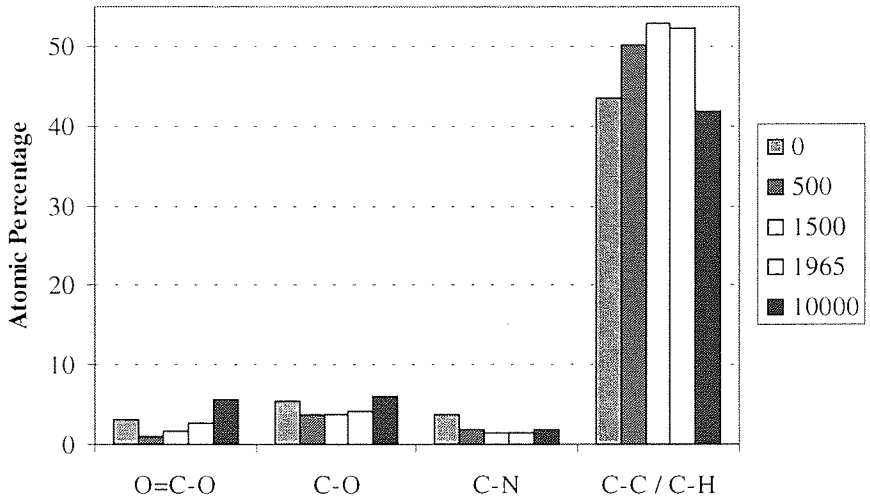

Figure 3.129 Synthesis of C for MP5 at 32°C 80% - Centre

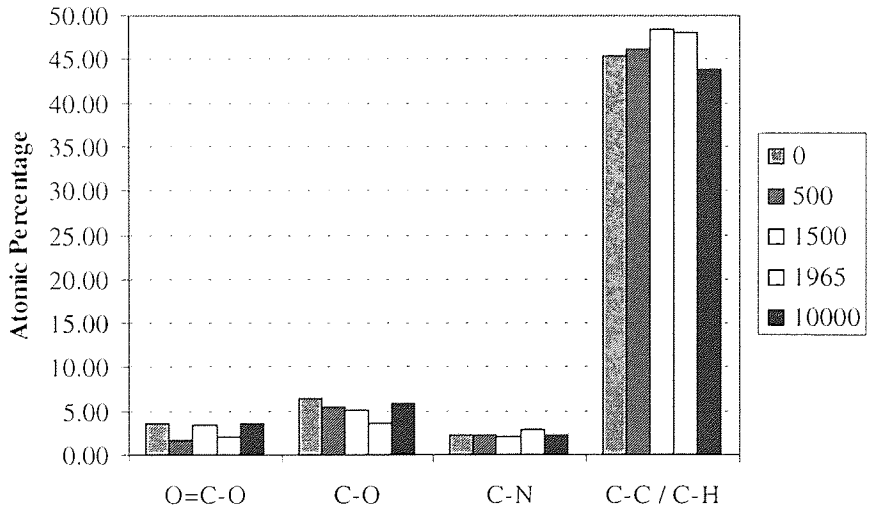

Figure 3.130 Synthesis of C for MP5 at 32°C 80% - Edge

Figure 3.131 shows the difference in elemental composition between the centre and edge regions at the surface of tape MP5 when cycled against a head at 32°C 80% RH. There is

clearly a higher percentage of Fe at the centre region of the tape compared to the edge. O appeared to be more abundant at the edge of tape, but considering the magnitude of O detected (~30%) the difference between the centre and edge, of 1% could be considered negligible. At the edge, there was an overall higher percentage of N when compared to the centre region. C seemed to be more prevalent at the centre of tape, but again as with the O concentration, the difference was mostly negligible. The tape sample analysed at 1965 passes showed a substantially greater concentration of C at the centre of tape compared to the edge. As this tape broke during cycling, it has to be considered that the cause of failure may have had some effect on the tapes surface.

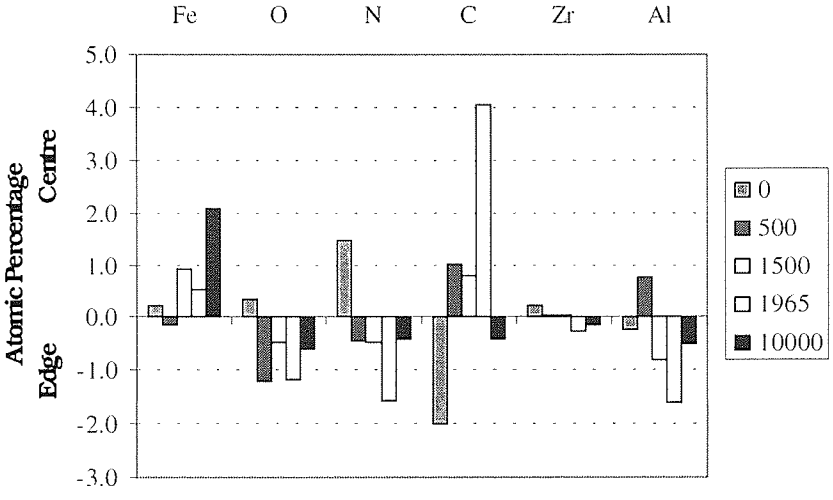

Figure 3.131 Difference between the Centre and Edge of MP5 with increasing number of passes at 32°C 80% RH

Comparison of single layer MP5 and dual layer MP6, which were of the same formulation, was made difficult since MP6 broke during both cycling experiments. The dropout cartridge tape broke after 2280 passes whereas during the second experiment, the third cartridge in the series of three (500, 1500, 3000 passes) failed due to a loss of tape tension after 2300 passes. This left two tape samples both having seen a similar number of passes.

Tape MP6 followed the exact same trends as tape MP5 at the centre of tape the only difference between tapes was the magnitudes of C and O. The amount of C detected was slightly higher and O slightly lower, in MP6 compared to MP5.

Figure 3.132 to Figure 3.134 inclusive, present the comparison of Fe:N, Fe:C and N:C ratios for tapes MP5 and MP6, centre and edge, when cycled against a head at 32°C, 80% RH.

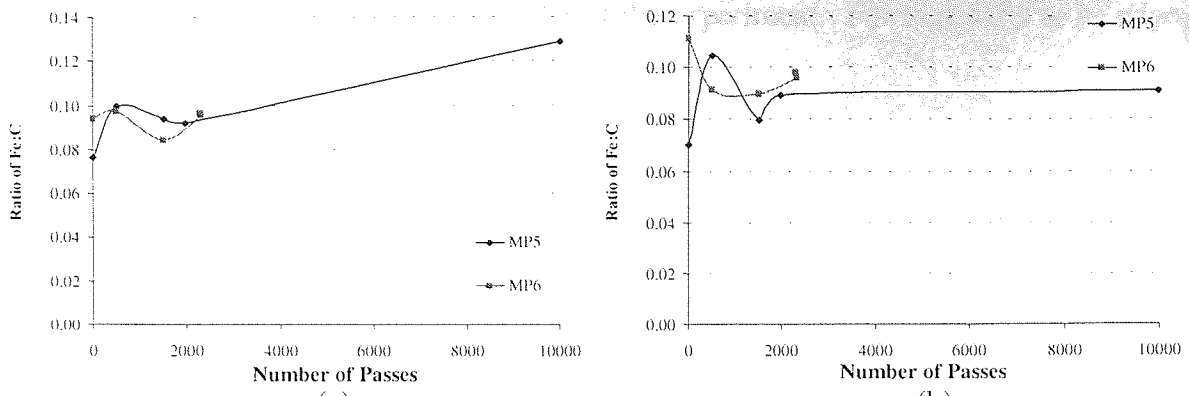

Figure 3.132 Ratio of Fe:C for MP5 and MP6 at 32°C, 80%
(a) Centre and (b) Edge

The ratio of Fe:C was very similar between tapes MP5 and MP6 (Figure 3.132) experiencing little change during cycling, the only difference between tapes was at the virgin stage where the ratio for MP6 was significantly higher than MP5 at the edge position.

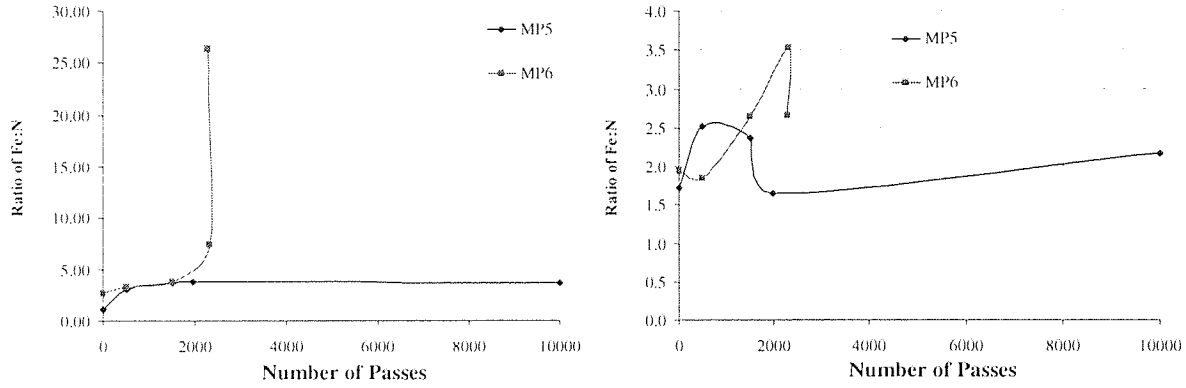

Figure 3.133 Ratio of Fe:N for MP5 and MP6 at 32°C, 80% RH
(a) Centre and (b) Edge

It was evident from the Fe:N ratios that severe N depletion had occurred at the centre of tape MP6 prior to failure. There was a difference between the two MP6 tapes that had reached approximately 2300 passes before failure (Figure 3.133). At the centre, the dropout tape exhibited a much larger Fe:N ratio compared to the tape cycled continuously. The reason for the large difference was that the N signal had fallen to below 0.5% at this stage. This difference was not as pronounced at the edge.

For the centre of tape MP5, the Fe:N ratio increased slightly during the first 2K passes and then remained unchanged for the remainder of the experiment. For tape MP5 at its edge the ratio neither increased nor decreased overall.

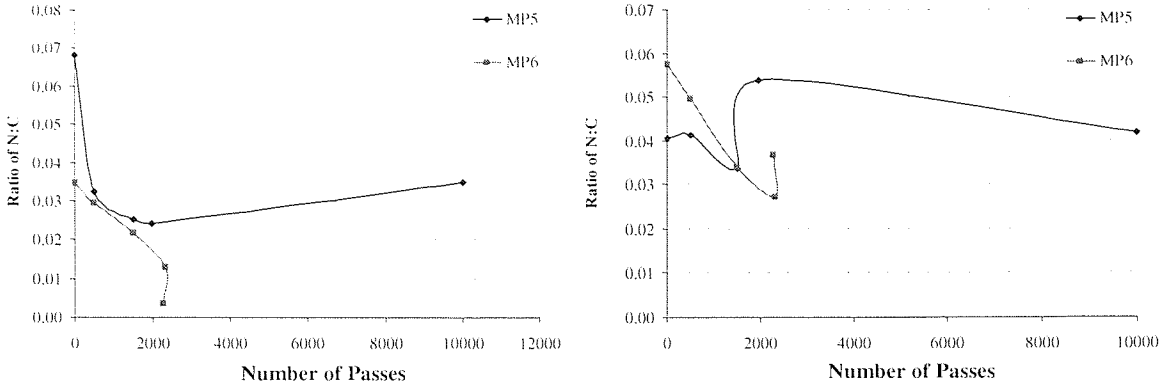

(a) (b)

Figure 3.134 Ratio of N:C for MP5 and MP6 at 32°C, 80% RH
(a) Centre and (b) Edge

The N:C ratio at the centre and edge of tape MP6 showed a dramatic change for the dropout cartridge sample (Figure 3.134) again due to the N signal having decreased dramatically. The situation at the edge of tape MP5 was different in that no real decrease was seen throughout cycling, the ratio was deemed more stable.

The overlayer thickness was calculated for MP5 at the centre and edge positions, these are presented in Figure 3.135. The overlayer thickness was seen to decrease with increased cycling at the centre of tape whereas at the edge of tape the thickness was more stable.

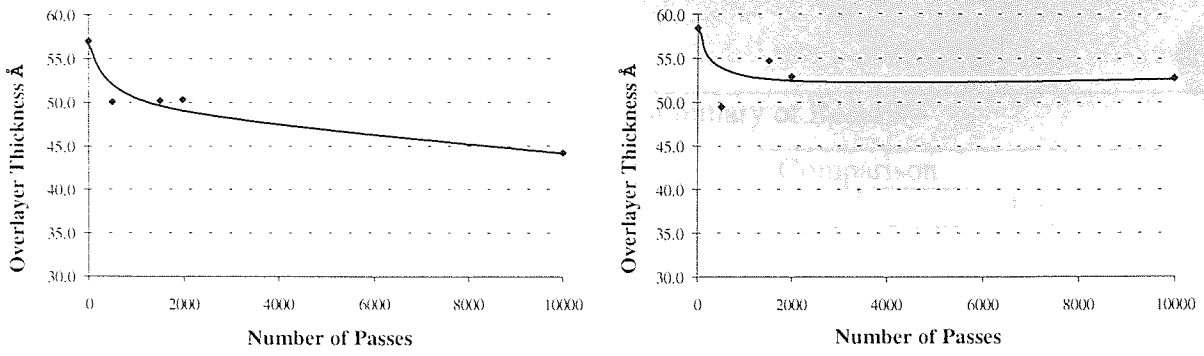

Figure 3.135 Variation in Overlayer Thickness as a Function of Increasing Number of Passes for MP5 at 32°C 80% RH – (a) Centre and (b) Edge

The Rms roughness of tapes MP5 and MP6 are presented in Table 3.16. No real difference was found between the centre and edge of tape MP5, for MP6 the centre was slightly rougher. Both tapes had worn smoother during cycling.

	MP5		MP6	
	Centre Rms/nm	Edge Rms/nm	Centre Rms/nm	Edge Rms/nm
virgin	7.5	7.5	10.1	10.1
10K passes	4.3	4.5		
2K passes			6.5	5.7

Table 3.16 Rms values for tapes MP5 and MP6 before and after cycling against a head at 32°C, 80% RH

The results for this section are summarised in Table 3.17.

Tape	Condition	Summary of Results		
			Comparison	
			Centre	Edge
MP5	32°C, 80% RH	XPS	Fe increased with cycling while N decreased. C increased up to 2K passes but had decreased at the 10K position.	As for the centre but with C being more stable.
		Synthesis of C	C-O and C-N decreased with cycling up to 2K passes but showed an increase at 10 K passes. C-C/C-H increased up to 2K and then decreased at the 10K point.	As for the centre
		Ratios	Fe:C and Fe:N increased while N:C decreased.	Fe:C stable, Fe:N increased slightly. N:C was relatively stable.
		Dropouts	Sharp decrease up to 1K passes and then stable. The exception was the 10 dB category which remained stable also the 50 μs class increased	
MP6	32°C, 80% RH (2K passes)	XPS	As for MP5 where comparison was possible*	As for MP5 where comparison was possible*
		Synthesis of C	As for MP5 where comparison was possible*	As for MP5 where comparison was possible*
		Ratios	Similar to MP5 except for ratios containing N. As N was severly depleted at the breaking point these ratios differ greatly.	As for centre.
		Dropouts	Similar to MP5 after 1500 passes	

*The same number of passes

Table 3.17 Summary of Results for the Georgens Cycler Experiments (TR-5 Head) using Group B Tapes at 32°C, 80%RH.

3.5.1.1.3 AFM and AES Analysis

The two read/write structures of each head were examined using AFM in order to investigate whether any staining and/or relative wear of the individual head components had resulted from the cycling experiments.

3.5.1.1.3.1 Single (Dropout) Cartridge

3.5.1.1.3.1.1 Left Structure

Figure 3.136 shows an AFM image of the left read/write structure of a head after 10K passes (dropout cartridge) of tape MP5 at 32°C, 80% RH. Stain was visible on the poles and possibly the ceramic areas, but not on the insulator regions.

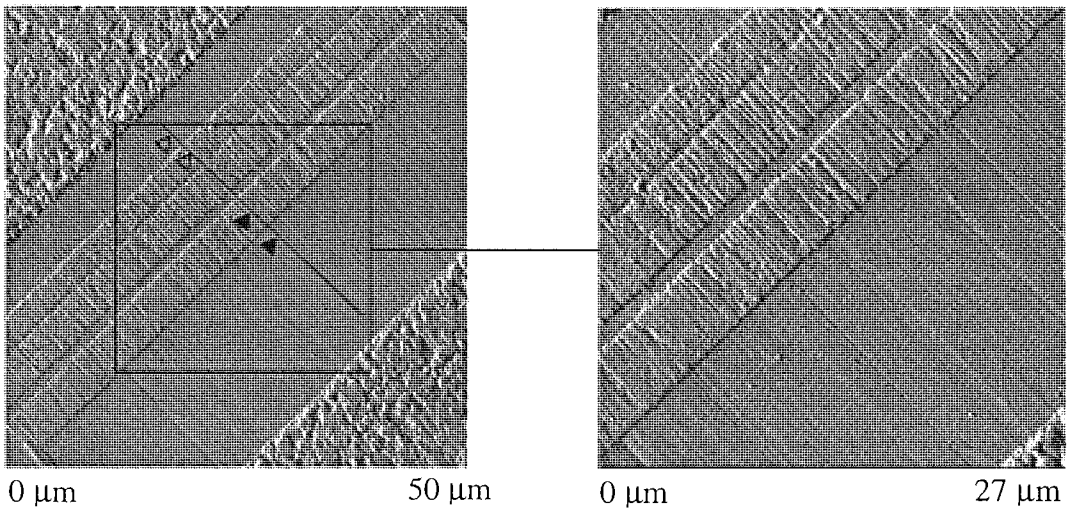

Figure 3.136 Left head assembly of a head after 10K passes of tape MP5 at 32°C, 80% RH with a close up of the pole area

Figure 3.137 shows a line scan across the pole and shield regions of the left head. No pole tip recession was evident on this structure although it is possible that any evidence of recession was obscured by stain formation. Pole to insulator region had a depth of approximately 30 nm. As the virgin poles were recessed by up to 15nm, the increase in pole height relative to the insulator is actually in the region of 45nm.

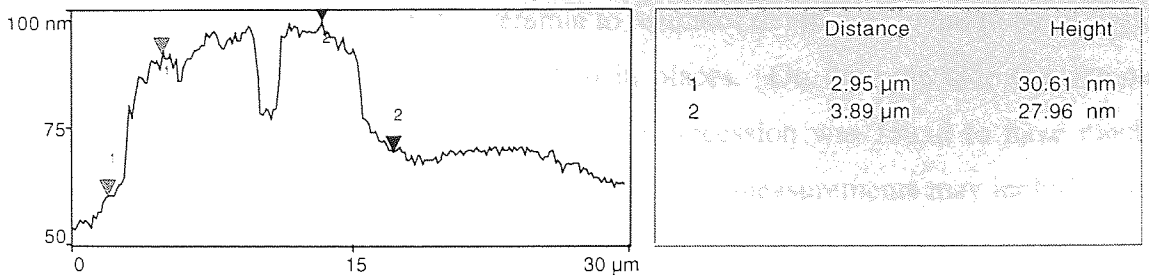

Figure 3.137 Line scan of the left head assembly of a head after 10K passes of tape MP5 at 32°C, 80% RH

The depth as measured from the ceramic (pole side) down to the insulator had a maximum value of ~74 nm with the TiC recession having a maximum value of ~60 nm. The TiC phase of the ceramic appeared to have undergone severe recession in relation to the Al_2O_3 phase. Similarly the ceramic (shield side) to insulator depths were measured at ~ 60nm with TiC recession being as high as ~ 57nm. It is possible that ceramic to insulator heights and TiC depths included stain which was present on the ceramic regions, giving erroneous results.

AES analysis of this structure confirmed the presence of Fe on all analysis positions with the exception of the insulator regions. Al was found on all areas.

3.5.1.1.3.1.2 Right Structure

Figure 3.138 shows an AFM image of the right read/write structure of a head after 10K passes (dropout cartridge) of tape MP5 at 32°C, 80% RH. As with the left-hand structure no immediate pole tip recession was evident. The heaviest staining was present on the pole regions but additional staining had also occurred on the ceramic regions.

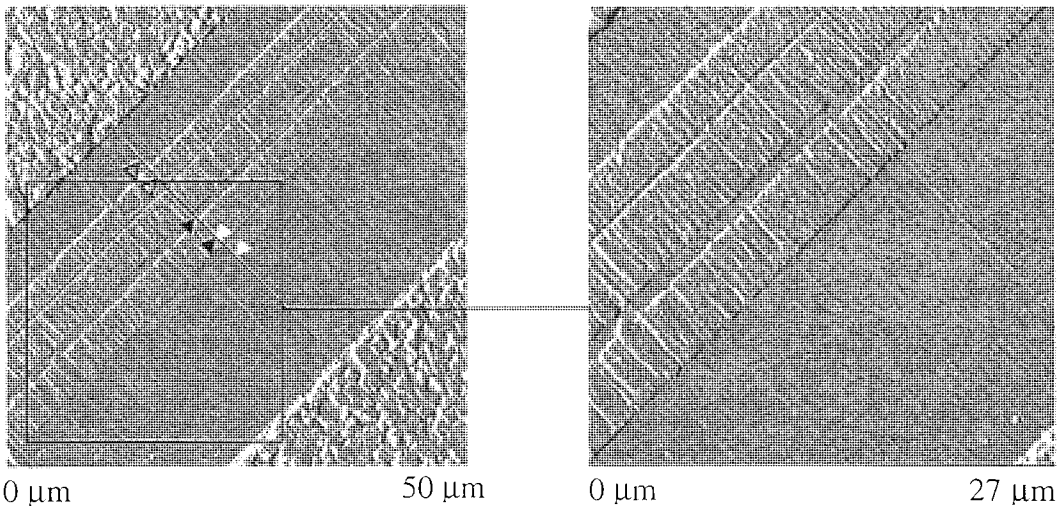

Figure 3.138 Right head assembly of a head after 10K passes of tape MP5 at 32°C, 80% RH with a close up of the pole area

On the shield side of the structure, the ceramic to insulator depth was found to be of the order of 80nm. TiC recession had reached ~ 70nm in places. On the pole side the ceramic to insulator depth was measured at ~70nm while TiC recession was found to have reached a maximum of ~ 67nm. Again, care must be taken as these measurements may include stain.

Figure 3.139 shows a line scan across the pole and shield regions of the left head. No pole tip recession was evident on this structure although it is possible that any evidence of recession will have been obscured by stain formation. For this right head structure, the total relative change between pole and insulator was approximately 39 nm.

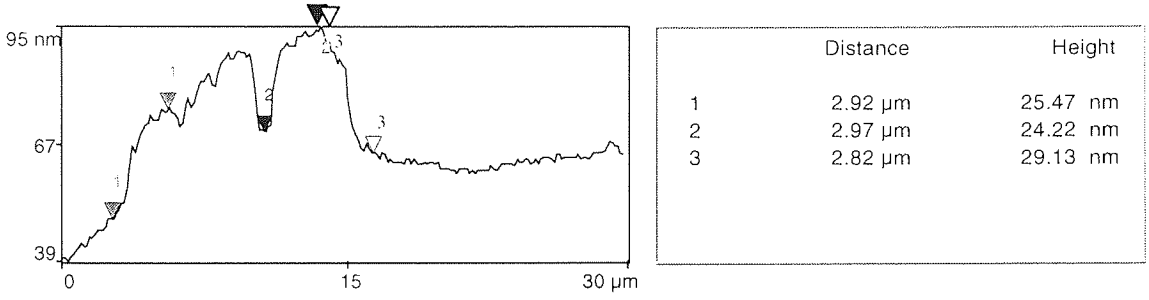

Figure 3.139 Line scan of the right head assembly of a head after 10K passes of tape MP5 at 32°C, 80% RH

AES analysis of this structure confirmed the presence of Fe on all component parts excluding the insulator regions. Al was detected on all areas without exception. Other than at expected areas (ceramic regions), Ti was detected on the shield, and on both insulators. Co was detected on the ceramic regions.

3.5.1.1.3.2 Multiple Cartridges

3.5.1.1.3.2.1 Left Structure

As mentioned earlier (3.5.1.1.2) the cartridge, which should have cycled up to 3000 passes failed after 1965 passes. The reason for tape failure is not known although it could be due to the running speed being too high. It is not known if the failure was instantaneous or if prior to breaking, the tape degenerated possibly depositing material onto the head and tape path components.

Figure 3.140 shows an AFM image of the left read/write structure of a head after 4K passes (three cartridges) of tape MP5 at 32°C, 80% RH. Heavy deposits were evident on all of the component parts although the insulator regions were not affected as much compared to other regions on the head. As with the group A tapes the deposited material was not like conventional stain, either in appearance or thickness.

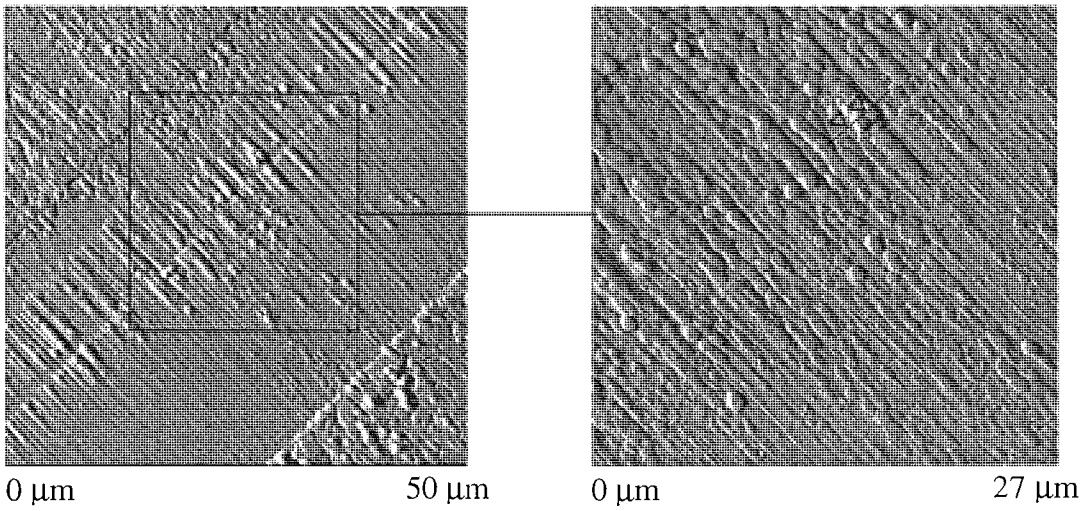

Figure 3.140 Left head assembly of a head after 4K passes of tape MP5 at 32°C, 80% RH with a close up of the pole area

Figure 3.141 shows a line scan across the highest area of deposited material, indicating that the height was 223nm. Due to heavy material formation, no pole tip recession was evident on this structure.

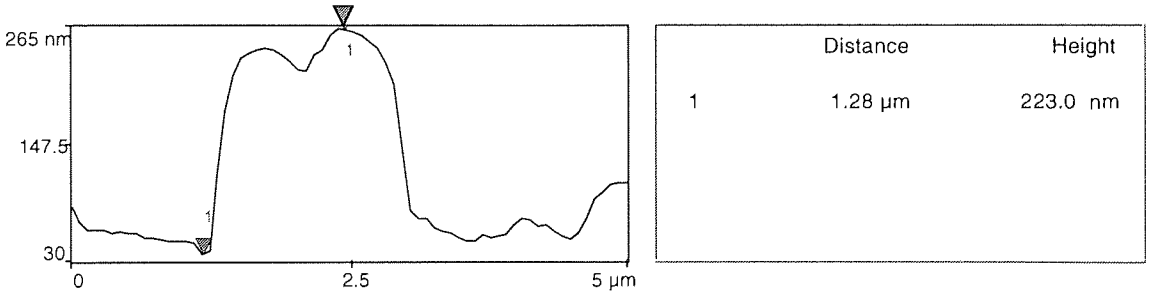

Figure 3.141 Line scan of the left head assembly of a head after 4K passes of tape MP5 at 32°C, 80% RH

Following AES analysis of this structure it was found that Fe and Al were present on all analysis positions.

3.5.1.1.3.2.2 Right Structure

Figure 3.142 shows an AFM image of the right read/write structure of a head after 4K passes (dropout cartridge) of tape MP5 at 32°C, 80% RH. As with the left-hand structure, no pole tip recession was detected due to heavy deposits.

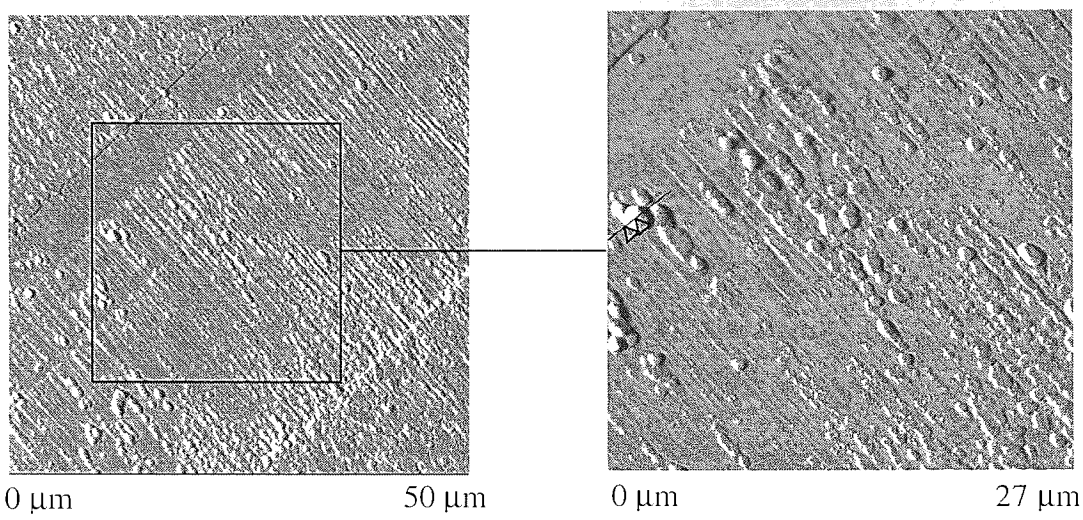

Figure 3.142 Right head assembly of a TR-5 head after 4K passes of tape MP5 at 32°C, 80% RH with a close up of the pole area

Figure 3.143 shows a line scan across the highest region of transferred material, which indicated a maximum thickness of 287.7 nm.

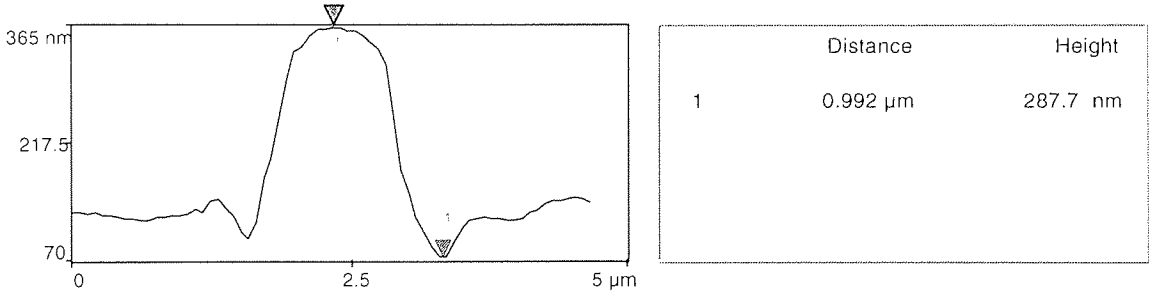

Figure 3.143 Line scan of the right head assembly of a TR-5 head after 4K passes of tape MP5 at 32°C, 80% RH

AES analysis of this structure confirmed the presence of Fe and Al on all component parts.

3.5.1.2 Comparison with Tape MP6

Comparison of head/tape interactions between the single and dual layer tapes of the same formulation was made difficult because the dropout cartridge broke after 2K passes. Similarly for the multiple cartridges experiment, the cartridge set to run for 3000 passes broke after 2K passes.

3.5.1.2.1.1.1 Left Structure

Figure 3.144 presents the left read/write structure of a head after 2K passes of tape MP6 at 32°C, 80% RH.

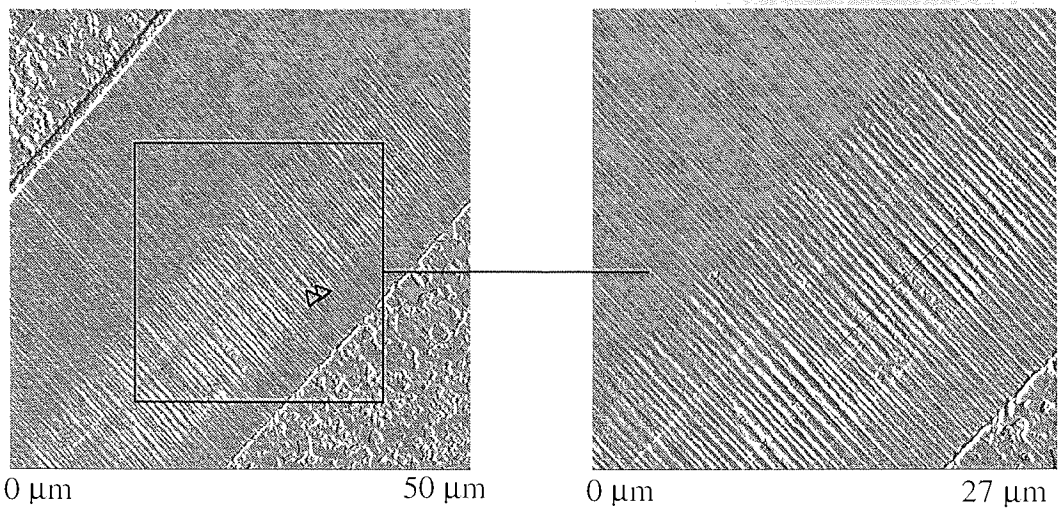

Figure 3.144 Left head assembly of a head after 2K passes of tape MP6 at 32°C, 80% RH with a close up of the pole area

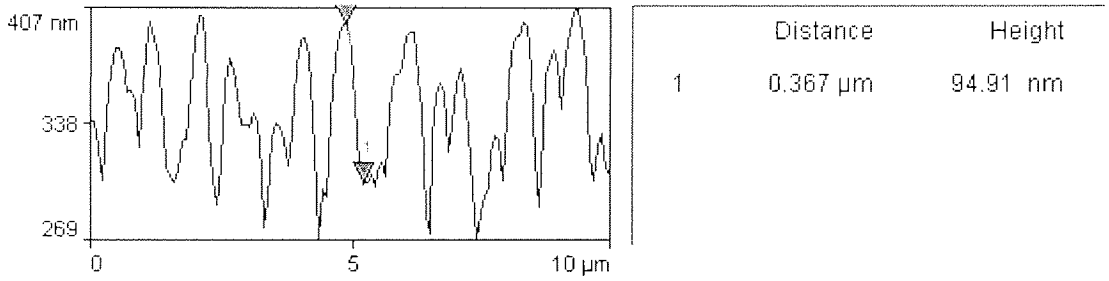

Figure 3.145 Line Scan of the left head assembly of a head after 2K passes of tape MP6 at 32°C, 80% RH

The head was visually very clean after 2K passes of tape. When compared with the virgin head (Figure 3.61), however, directional features were noted. A ridging effect (94nm, Figure 3.145) had appeared in the direction of tape motion indicating that either the head had worn by abrasive wear and/or a transfer of tape material had occurred.

On the shield side of the structure, the ceramic to insulator depth was found to be of the order of 62nm. TiC recession had reached ~ 157nm in places (Figure 3.146). On the pole side the ceramic to insulator depth was measured at ~ 73nm while TiC recession was found to have reached a maximum of ~ 156nm. The relative height between the insulator and ceramic regions had increased by around 35nm from the virgin condition (P.137), a height

corresponding roughly to known stain thickness. TiC recession had increased considerably indicating that either this particular tape and/or the environmental conditions were particularly aggressive toward the TiC phase of the ceramic.

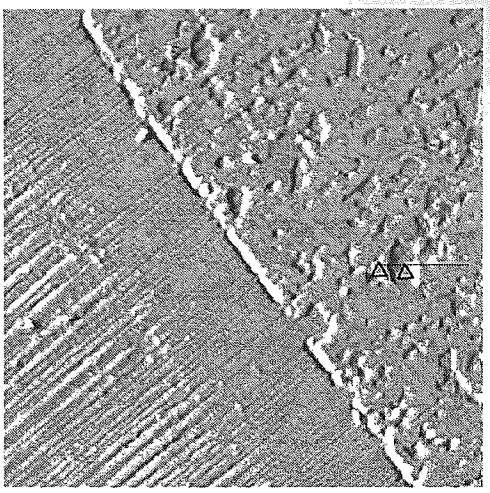

Figure 3.146 Left ceramic (shield side) on a head after 2K passes of tape MP6 at 32°C, 80% RH

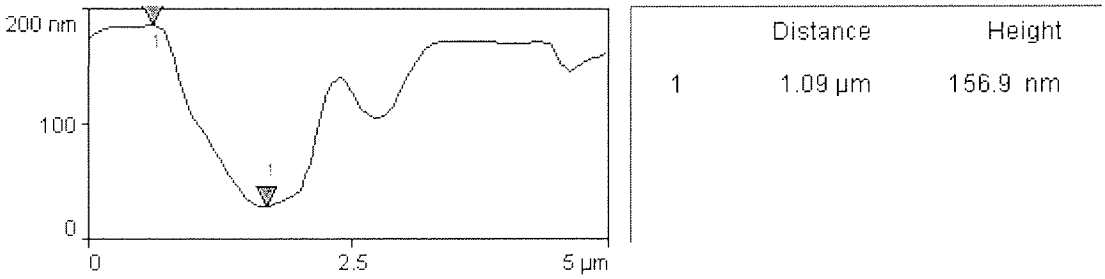

Figure 3.147 Line Scan of the left ceramic (shield side) of a head after 2K passes of tape MP6 at 32°C, 80% RH

AES analysis of this structure confirmed the presence of Fe on all component parts but the insulator regions.

3.5.1.2.1.1.2 Right Structure

Figure 3.148 shows an AFM image of the right read/write structure of a head after 2K passes (dropout cartridge) of tape MP6 at 32°C, 80% RH. The situation was the same as for the left head structure.

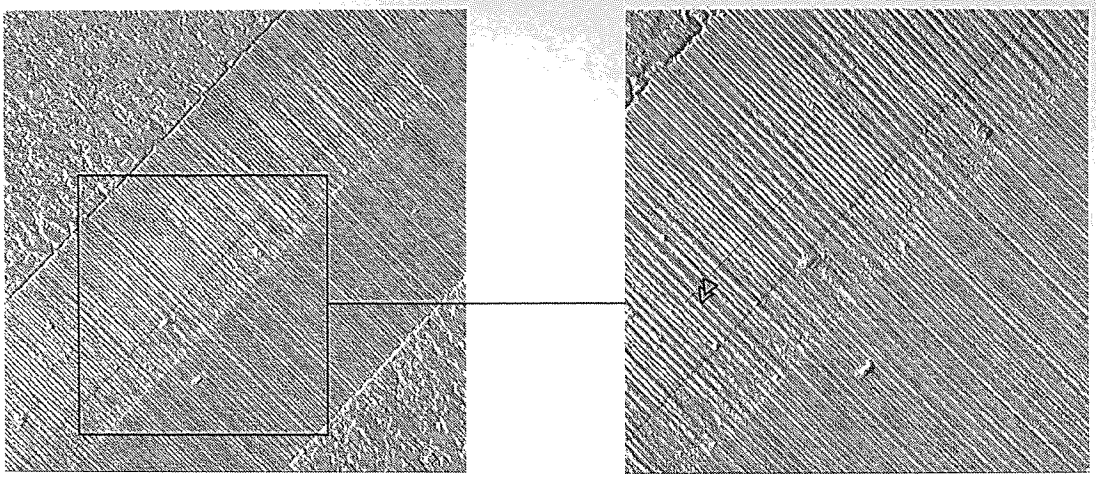

Figure 3.148 Right head assembly of a head after 2K passes
of tape MP6 at 32°C, 80% RH with a close up of the pole area

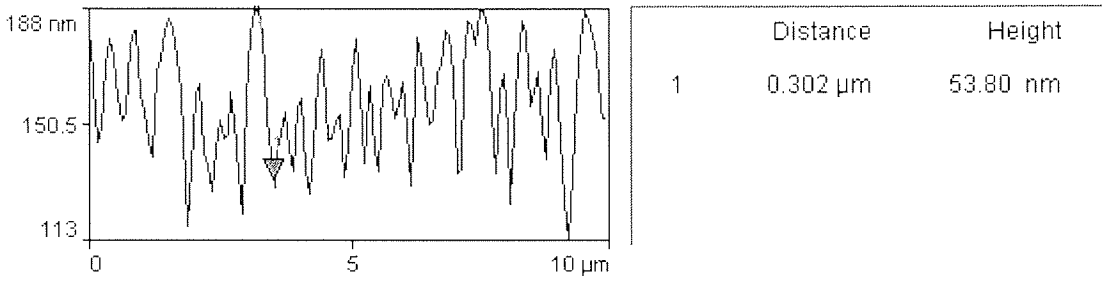

Figure 3.149 Line Scan of the right head assembly of a head after 2K passes
of tape MP6 at 32°C, 80% RH

On the shield side of the structure, the ceramic to insulator depth was found to be of the order of 73nm. TiC recession had reached ~ 125 in places. On the pole side the ceramic to insulator depth was measured at ~ 63nm while TiC recession was found to have reached a maximum of ~ 127nm. As with the left structure, the relative height between the insulator and ceramic regions had increased by around 27-45nm from the virgin condition (P.137). TiC recession had increased but not as significantly as on the left structure.

As with the left structure, AES analysis showed that Fe was present everywhere except the insulator regions

3.5.1.2.1.2 Multiple Cartridges

3.5.1.2.1.2.1 Left Structure

Figure 3.150 shows an AFM image of the left read/write structure of a TR-5 head after 4K passes of tape MP6 at 32°C, 80% RH. As with the dropout cartridge a ridging effect was present on the head. Ridges as large as 136nm were found (Figure 3.151).

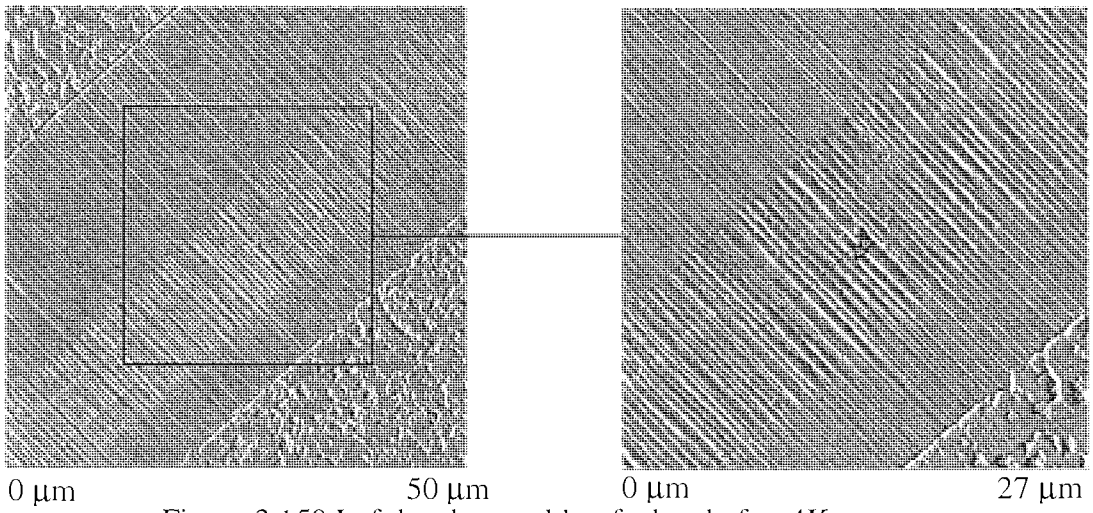

Figure 3.150 Left head assembly of a head after 4K passes of tape MP6 at 32°C, 80% RH with a close up of the pole area

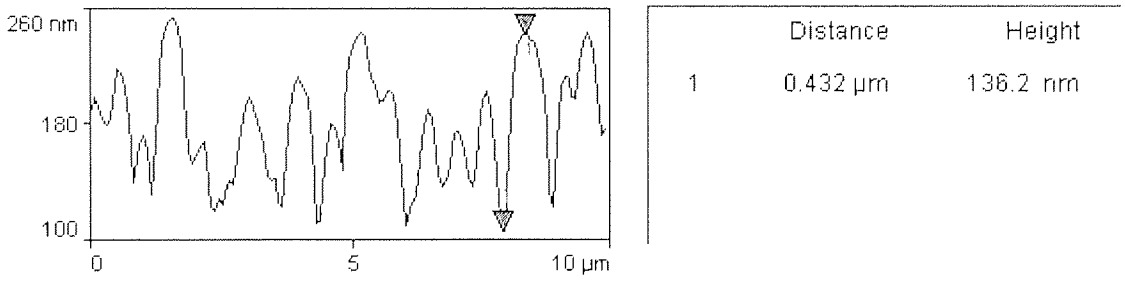

Figure 3.151 Line Scan of the left head assembly of a head after 4K passes of tape MP6 at 32°C, 80% RH

The ceramic (shield side) to insulator depth was found to be about 85nm whilst the TiC recession was measured at a maximum of 163nm. On pole side the ceramic to insulator was measured at 93nm and the TiC recession at a maximum of 136nm. The ceramic to insulator depth had increased by up to 60nm from the virgin head, also the TiC recession had increased by an extensive amount.

AES analysis of this structure confirmed the presence of Fe on all component parts but the insulator regions.

3.5.1.2.1.2.2 Right Structure

Figure 3.152 shows an AFM image of the right read/write structure of a head after 4K passes of tape MP6 at 32°C, 80% RH. As with the dropout cartridge a ridging effect was present on the head. Ridges as large as 94nm were found (Figure 3.151).

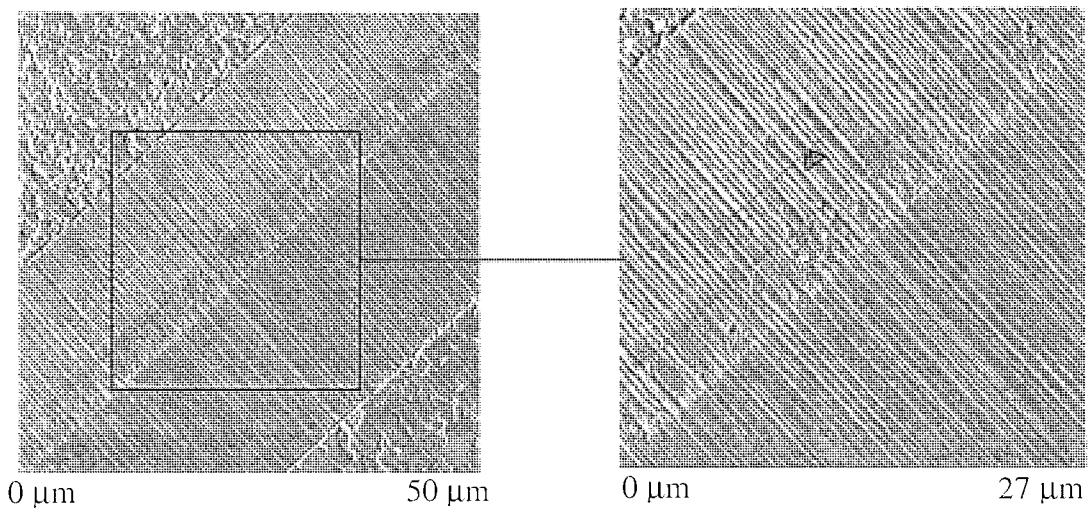

Figure 3.152 Right head assembly of a head after 4K passes of tape MP6 at 32°C, 80% RH with a close up of the pole area

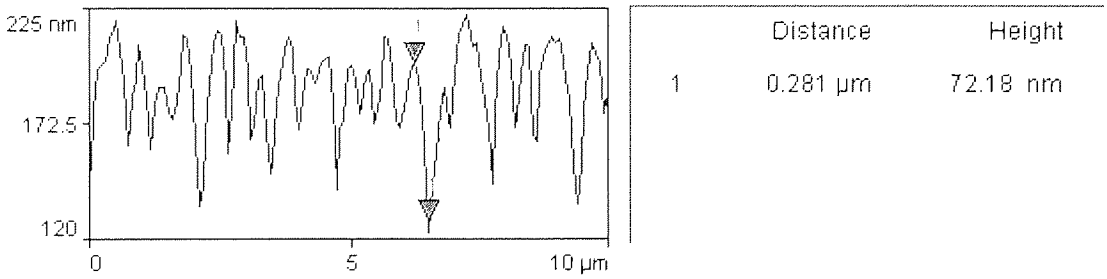

Figure 3.153 Line Scan of the right head assembly of a head after 4K passes of tape MP6 at 32°C, 80% RH

The shield side ceramic to insulator depth was measured at 90nm on average. The TiC recession was found to be as deep as 160nm at one position (Figure 3.154). The ceramic (pole side) to insulator depth was around 79nm. TiC recession on this ceramic was measure at a maximum 136nm.

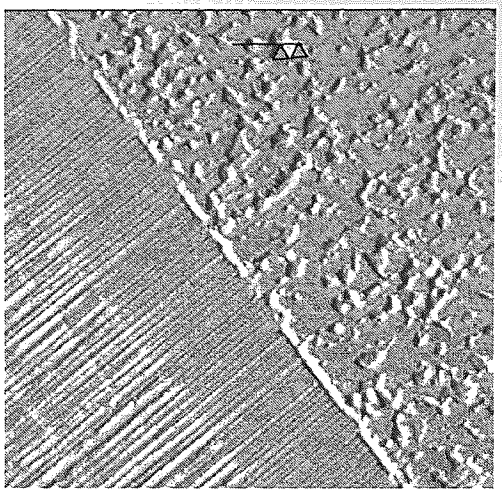

Figure 3.154 Left ceramic (shield side) on a head after 4K passes of tape MP6 at 32°C, 80% RH

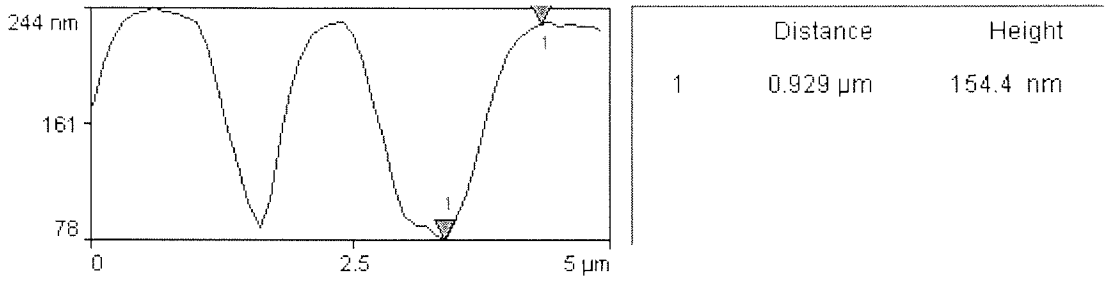

Figure 3.155 Line Scan of the left ceramic (shield side) of a head after 4K passes of tape MP6 at 32°C, 80% RH

AES analysis of this structure confirmed the presence of Fe on all component parts but the insulator regions.

3.5.2 MP5

3.5.2.1 5°C, 10%RH

3.5.2.1.1 Dropout Measurement

After the completion of 10K passes (dropout cartridge) and 5K passes (three cartridges) with tape MP5 at 5°C 10% RH, cartridge failure had not occurred. Figure 3.156 show the 4 dB, 5 dB, 6 dB and 10 dB dropout growth respectively as a function of increasing number of passes.

Most classes of remained relatively stable throughout cycling with only the 4 dB category having showed any real decrease before stabilising.

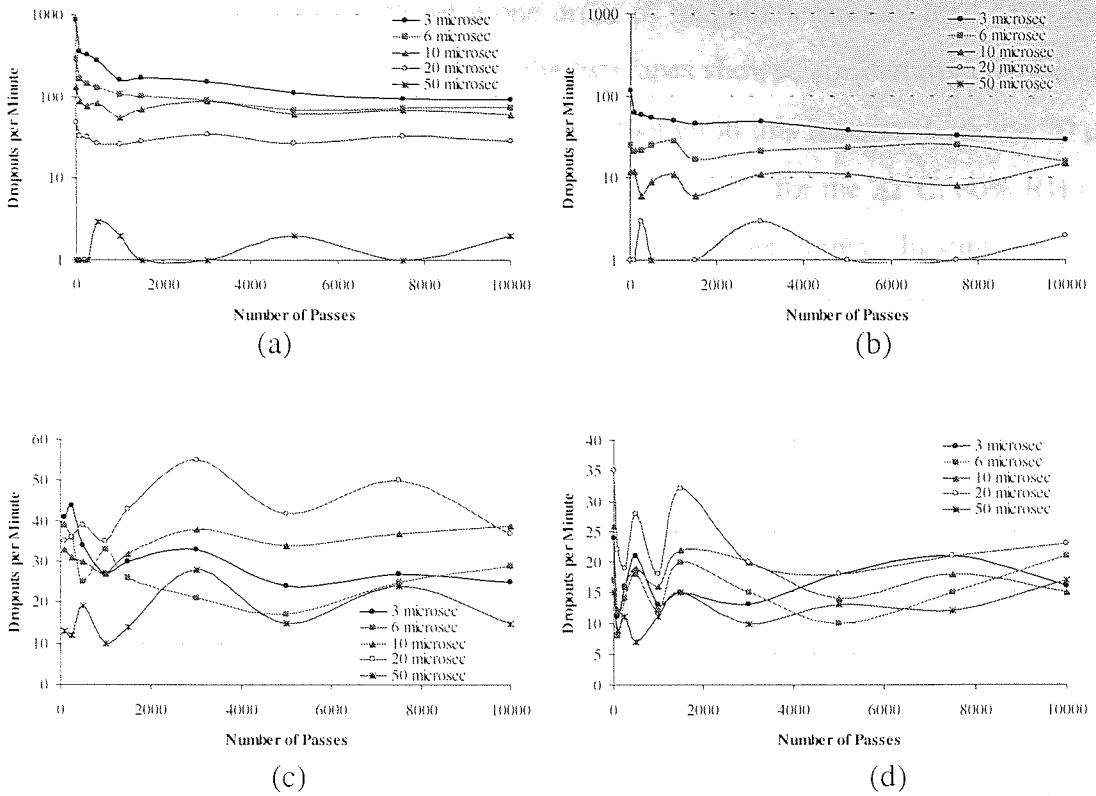

Figure 3.156 (a) 4 dB (b) 5 dB (c) 6 dB and (d) 10 dB dropout growth for tape MP5 at 5°C, 10% RH

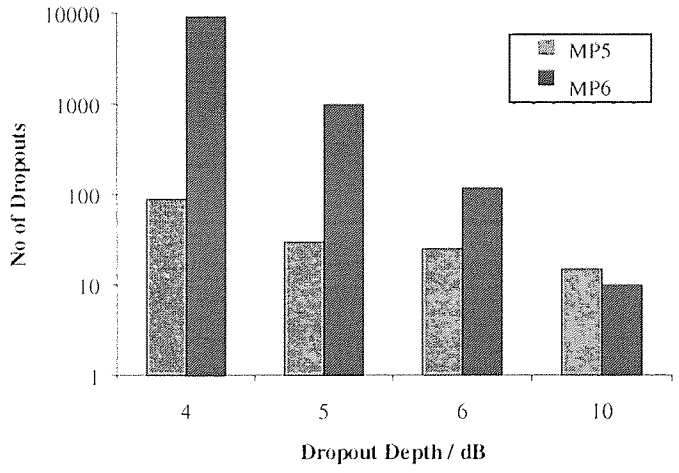

Figure 3.157 Comparison of the 3µs class of Dropout at 5°C, 10% RH for MP5 and MP6 after 10K passes

Whereas at 32°C, 80% RH after 1500 passes the two tapes showed similar dropout characteristics, at 5°C, 10% RH the difference between the two tapes was significant throughout cycling. For all time intervals in the 4dB class, the magnitude of dropouts for tape MP6 were two orders of magnitude greater than that of tape MP5. For the 5dB class the

magnitude of dropouts for MP6 were one order of magnitude greater than MP5 for all time intervals except for the 50μs class where the two tapes showed similar dropout characteristics. A similar situation was noted for the 6dB class though in this instance both the 20 μs and 50 μs intervals showed similar magnitudes for both tapes. As for the 32°C, 80% RH conditions the 10dB class was similar for both tapes up to comparable points. In summary the smaller the dropout depth, the greater the difference in magnitude between tapes MP5 and MP6, also the narrower the time interval the greater the difference between tapes.

3.5.2.1.2 XPS Analysis

At the tape centre, the concentration of Fe and O increased whilst N decreased with increased cycling, the C content decreased after the first 500 passes. The trends at the edge of the tape were the same as for the centre.

Figure 3.158 and Figure 3.159 present the synthesised C peaks for the centre and edge respectively, of tape MP5. The centre showed no change in the C-C/C-H bond but the C-O and C-N bonds decreased. At the edge of the tape, the changes were indeterminate due to a rogue result at 1500.

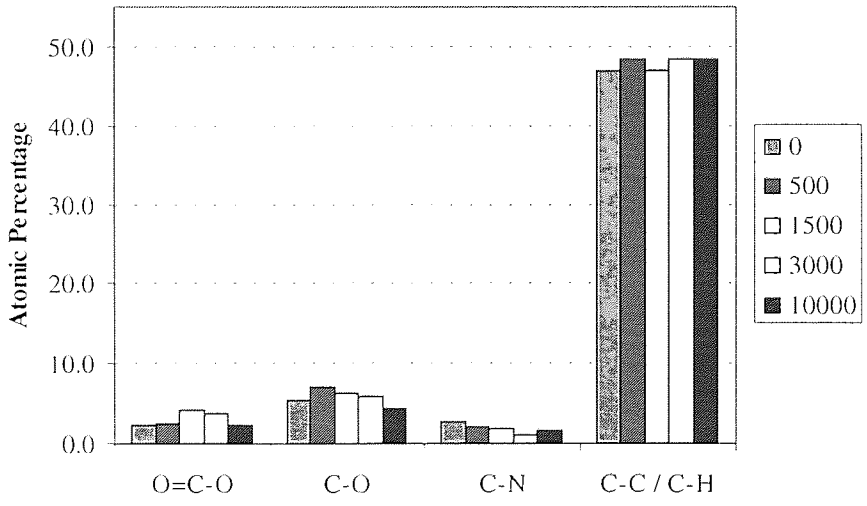

Figure 3.158 Synthesis of C for MP5 at 5°C 10% - Centre

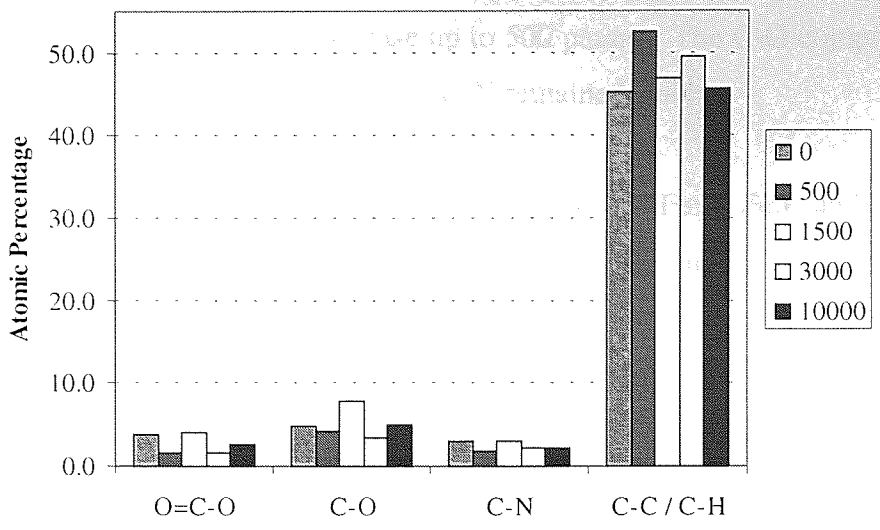

Figure 3.160 Synthesis of C for MP5 at 5°C 10% - Edge

Figure 3.161 shows the difference in elemental composition between the centre and edge regions at the surface of tape MP5 when cycled against a head at 5°C, 10% RH. The absolute divisions between centre and edge of tape are not present for this sample as with other tapes. Each of the elements can be said to be more abundant in either region according to the number of passes.

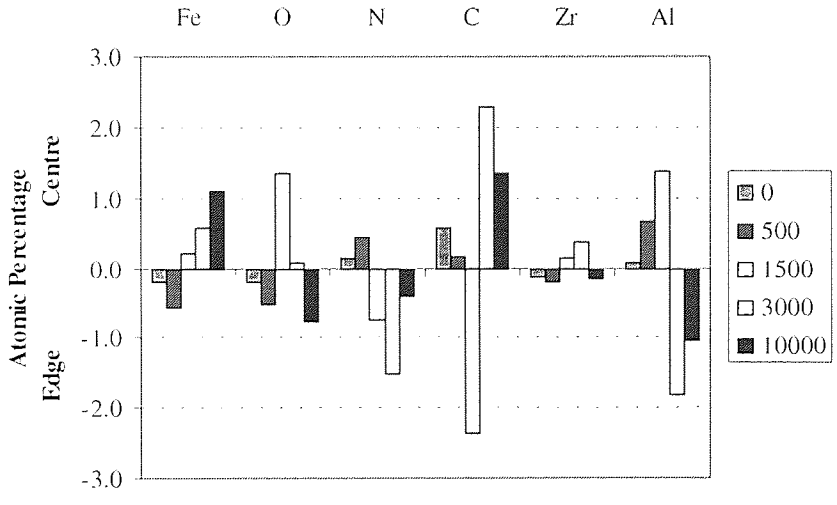

Figure 3.161 Difference between the Centre and Edge of MP5 with increasing number of passes at 5°C 10%

Tape MP6 followed near identical trends to MP5 at both tape positions, except the C concentration decreased at the 10K passes point as opposed to after 1500 passes. The synthesised C peak produced similar results at the centre of tape but with an increase in the C-

C/C-H component until decreasing at 10K passes. At the edge of tape MP6 the C-C/C-H component was stable after an initial increase up to 500 passes. The C-O component showed a gradual increase throughout cycling although C-N remained stable.

Figure 3.162 to Figure 3.164 inclusive, present a comparison of Fe:N, Fe:C and N:C ratios for tapes MP5 and MP6, centre and edge, when cycled against a head at 5°C, 10% RH.

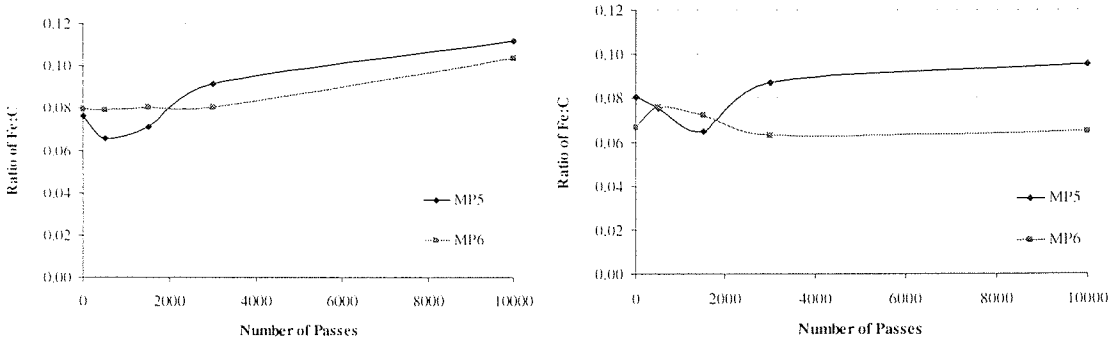

(a) (b)

Figure 3.162 Ratio of Fe:C for MP5 and MP6 at 5°C, 10% RH
(a) Centre and (b) Edge

The ratio of Fe:C was similar between tapes MP5 and MP6 (Figure 3.162), with tape MP5 being slightly higher than MP6 at the higher numbers of passes at both tape positions. Also at the higher number of passes, the centre of tape produced a greater Fe:C magnitude.

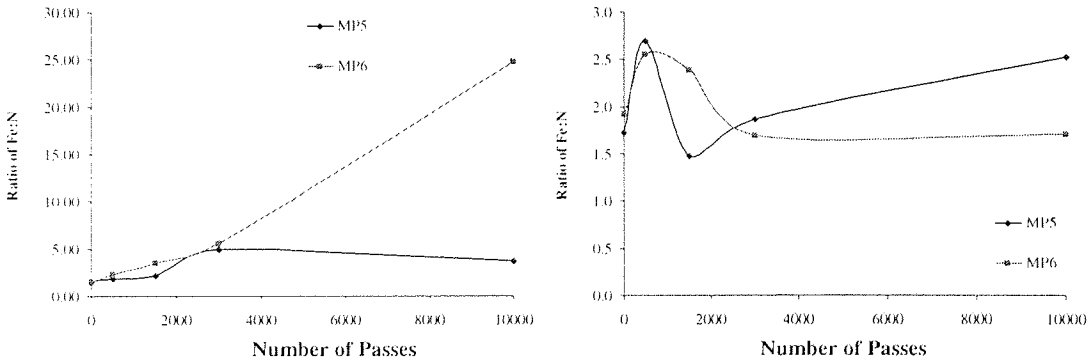

(a) (b)

Figure 3.162 Ratio of Fe:N for MP5 and MP6 at 5°C, 10% RH
(a) Centre and (b) Edge

It was evident from the Fe:N ratios that N depletion had occurred at the centre of tape MP6 (Figure 3.162) becoming severe at 10K passes. The reason for the large increase in the ratio

was that the N signal had fallen to below 0.5% at this stage while the Fe signal was at its largest value.

For the centre of tape MP5, the Fe:N ratio increased slightly during the first 3000 passes (very similar to tape MP6) and then remained unchanged for the remainder of the experiment. At the edge of both tapes the ratio remained relatively stable, the point at 1500 passes (tape MP6) was due to a low N signal.

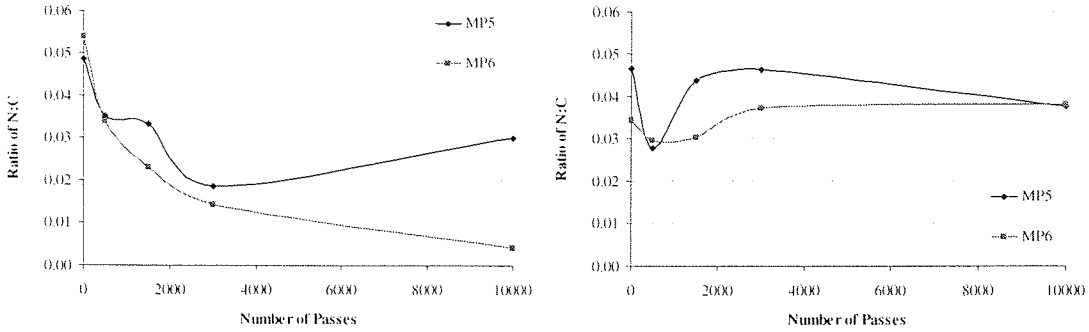

(a) (b)

Figure 3.164 Ratio of N:C for MP5 and MP6 at 5°C, 10% RH
(a) Centre and (b) Edge

The N:C ratio at the centre of tape MP6 showed a gradual decrease throughout cycling. As the C-O and C-N components of the synthesised C peak also decreased with cycling, binder depletion was indicated. Tape MP5 was very similar to tape MP6 up until 3000 passes after which the N:C ratio increased.

The overlayer thickness was calculated for MP5 at the centre and edge positions, these are presented in Figure 3.164. The overlayer thickness decreased overall with increased cycling at the centre of tape whereas at the edge of tape the thickness was more stable.

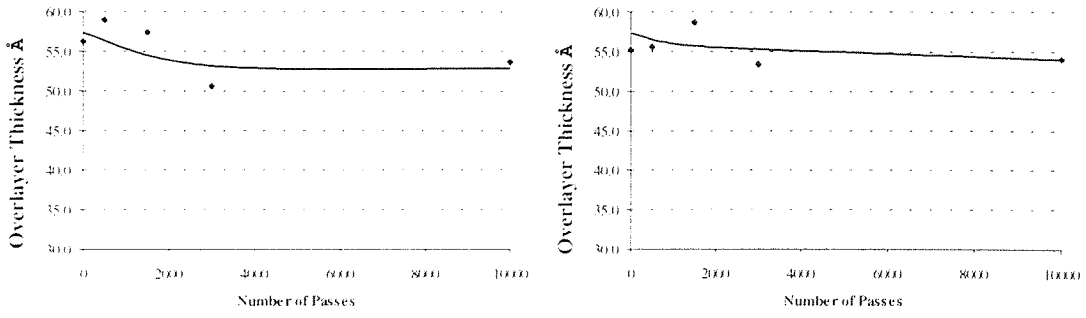

(a) (b)

Figure 3.164 Variation in Overlayer Thickness as a function of Increasing Number of Passes for MP5 a 5°C 10% RH – (a) Centre and (b) Edge

The Rms roughness' of tapes MP5 and MP6 are presented in. Table 3.18. A slight difference was found between the centre and edge of both tapes, the centre being slightly smoother. Both tapes had worn smoother during cycling.

	MP5		MP6	
	Centre Rms/nm	Edge Rms/nm	Centre Rms/nm	Edge Rms/nm
virgin	7.5	7.5	10.1	10.1
10K passes	4.8	5.4		
			5.9	6.4

Table 3.18 Rms values for tapes MP5 and MP6 before and after cycling against a head at 5°C, 10% RH

The results for this section are summarised in Table 3.19.

Tape	Condition	Summary of Results		
			Comparison	
			Centre	Edge
MP5	32°C, 80% RH	XPS	Fe increased while N decreased. C decreased after an initial decrease from the virgin state.	As for centre but N was more stable.
		Synthesis of C	C-O and C-N decreased with cycling, C-C/C-H was stable.	Indeterminate results
		Ratios	Fe:C and Fe:N increased while N:C decreased until 10k passes where an increase occurred.	Fe:C increased after an initial decrease whereas and Fe:N increased throughout. N:C decreased slightly overall
		Dropouts	Smaller categories decreased up to 1K passes then stabilised, larger dropouts remained stable with cycling.	
MP6	32°C, 80% RH (2K passes)	XPS	As for tape MP5	As for tape MP5
		Synthesis of C	C-O and C-N decreased with cycling, C-C/C-H increased up to 10K where a decrease was noted.	C-C/C-H stable after an increase up to 500 passes. C-O increased slightly with cycling whereas C-N remained stable.
		Ratios	Fe:C and Fe:N increased (Fe:N significantly at 10K) while N:C decreased.	Fe:C and Fe:N decreased while N:C increased slightly.
		Dropouts	The 4 dB category decreased up to 100 passes then stabilised, The remaining categories remained stable with cycling	

Table 3.19 Summary of Results for the Georgens Cycler Experiments (TR-5 Head) using Group B Tapes at 5°C, 10%RH.

3.5.2.1.3 AFM and AES Analysis

The two read/write structures of each head were examined using AFM in order to investigate whether any staining and/or relative wear of the individual head components had resulted from the cycling experiments.

3.5.2.1.3.1 Single (Dropout) Cartridge

3.5.2.1.3.1.1 Left Structure

Figure 3.165 shows an AFM image of the left read/write structure of a head after 10K passes (dropout cartridge) of tape MP5 at 5°C, 10% RH. Stain was visible on the poles, insulator and the ceramic areas.

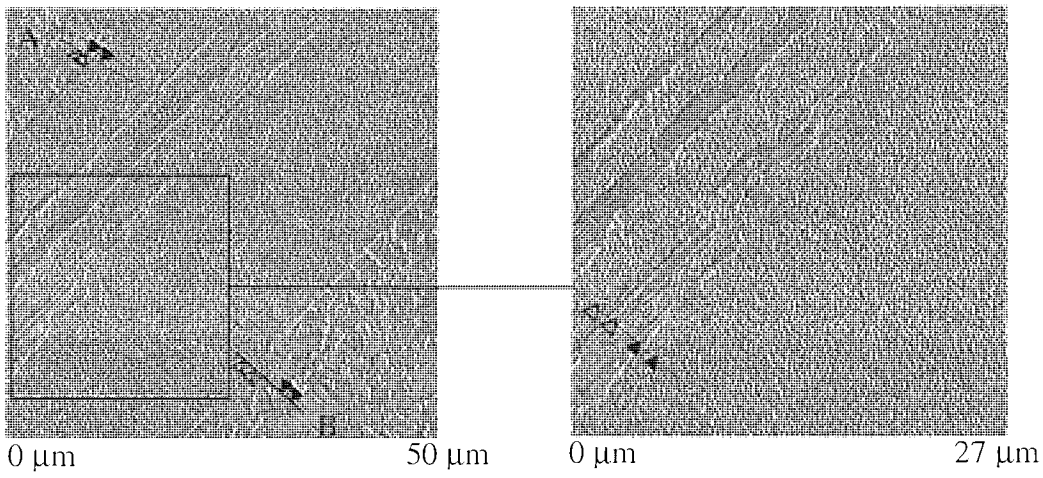

Figure 3.165 Left head assembly of a head after 10K passes of tape MP5 at 5°C, 10% RH with a close up of the pole area

AFM line scans from the ceramic to the insulator regions were produced to assess changes in the relative height of the two regions Figure 3.166 and Figure 3.167). Any changes to the relative height between the two phases of the ceramic material were also identified from the two line scans. The height between the ceramic (shield side) and insulator was measured as being between 19 and 33 nm, which was very similar to the virgin head (P.122). The situation was identical for the ceramic (pole side) to insulator heights. TiC recession on the ceramic (pole side) was found to be about 42nm whereas for the ceramic (shield side) it was measured at 30nm.

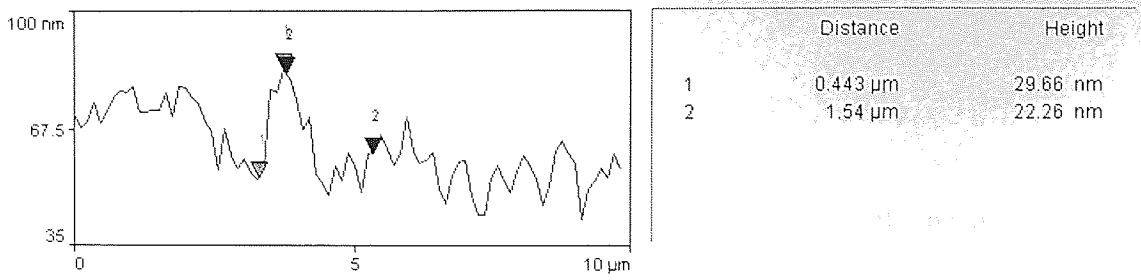

Figure 3.166 Line scan of ceramic (shield side) and insulator regions on the left head assembly of a head after 10K passes of tape MP5 at 5°C, 10% RH

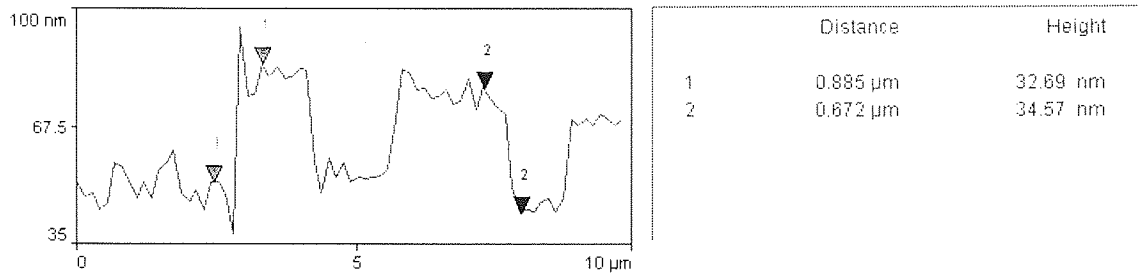

Figure 3.167 Line scan of ceramic (pole side) and insulator regions of the left head assembly of a head after 10K passes of tape MP5 at 5°C, 10% RH

Figure 3.169 shows a line scan across the pole and shield regions of the left head. No pole tip recession was evident from these scans although it is possible that any evidence of recession was obscured by stain formation. Stain was visible on the poles and insulator regions with only a small section of pole material being visible. From the unstained pole to the insulator was measured at around 25 nm (Figure 3.169). On the visible section of pole, there were recesses measured at up to 29 nm, similar to those seen on the virgin head (Figure 3.61). This would indicate that the pole had not suffered wear due to tape motion but had in fact been protected from such wear by stain formation.

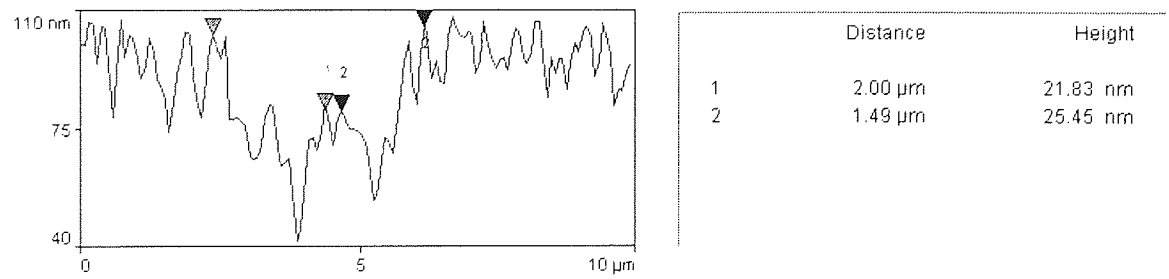

Figure 3.169 Line scan of the left head assembly of a head after 10K passes of tape MP5 at 5°C, 10% RH

AES analysis of this structure confirmed the presence of Fe on all analysis positions. Ti was detected on the shield.

3.5.2.1.3.1.2 *Right Structure*

Figure 3.170 shows an AFM image of the right read/write structure of a head after 10K passes (dropout cartridge) of tape MP5 at 5°C, 10% RH. As with the left-hand structure no immediate pole tip recession was evident. Visible staining was present on the pole and insulator regions. Evidence of PTR was found just out of range of the 50 μm scan (Figure 3.171)

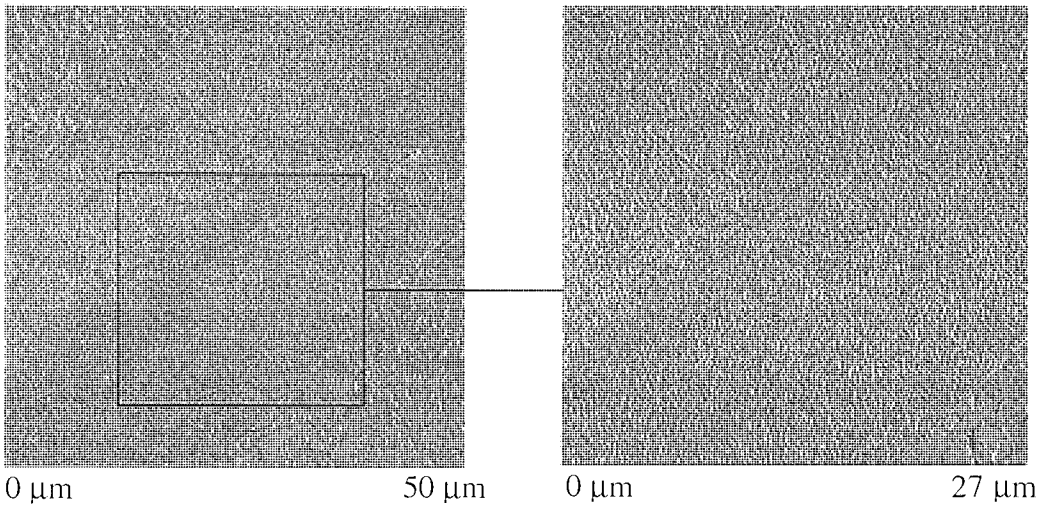

Figure 3.170 Right head assembly of a head after 10K passes of tape MP5 at 5°C, 10% RH with a close up of the pole area

From the ceramic (pole side) to the insulator, depths of 9 to 22 nm were measured. In addition, the depth of TiC recession was measured at a maximum of 42 nm. The ceramic (shield side) to insulator depths were found to be between 7 and 32 nm while the TiC recession was measured at a maximum 35 nm. The fact that lower depths were found between the ceramics and insulator regions tended to suggest either thick stain build up or ceramic wear or both. Recession of the TiC phase was greater than for the virgin head suggesting preferential wear of the TiC phase compared to the Al_2O_3 phase.

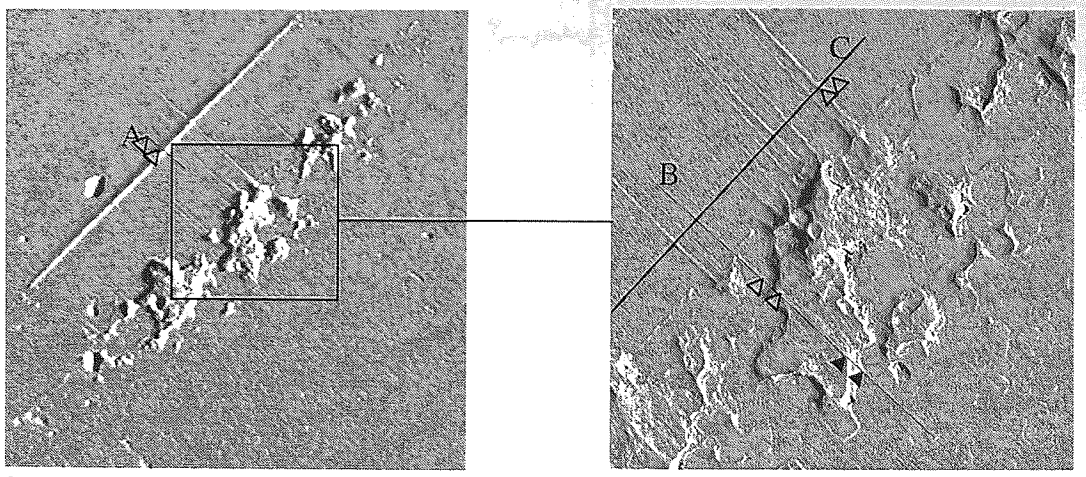

Figure 3.171 Close up of the pole and ceramic areas of the right head assembly of a head after 10K passes of tape MP5 at 5°C, 10% RH close up of the pole area

Figure 3.171 clearly shows how portions of the ceramic have been removed, dragged across the insulator and have become entrapped between the pole, and tape initiating PTR. Figure 3.172 gives depth information for the PTR (line 1 in Figure 3.171) whilst Figure 3.173 and Figure 3.174 (lines 2 and 3 respectively in Figure 3.171) show line scans across the damaged ceramic region.

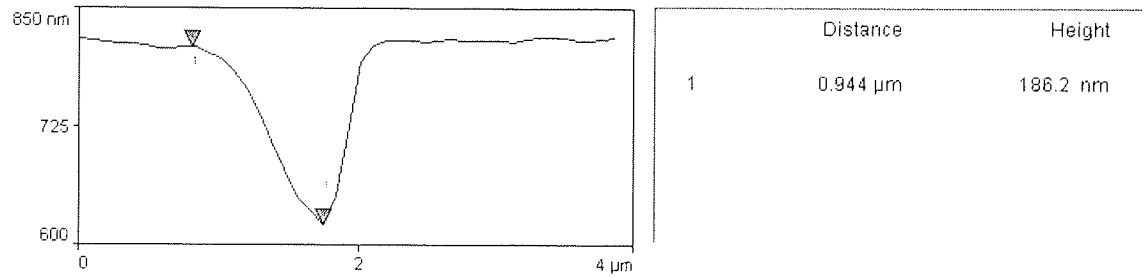

Figure 3.172 Line scan (A) of the recessed pole region of the right head assembly of a head after 10K passes of tape MP5 at 5°C, 10% RH

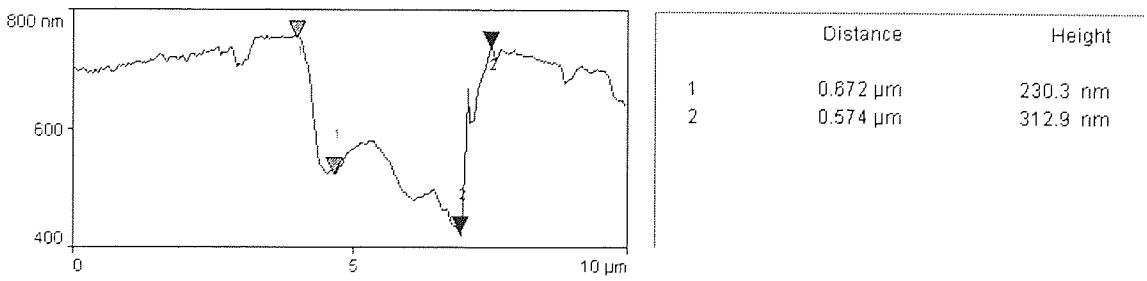

Figure 3.173 Line scan (B) of the right head assembly of a head after 10K passes of tape MP5 at 5°C, 10% RH

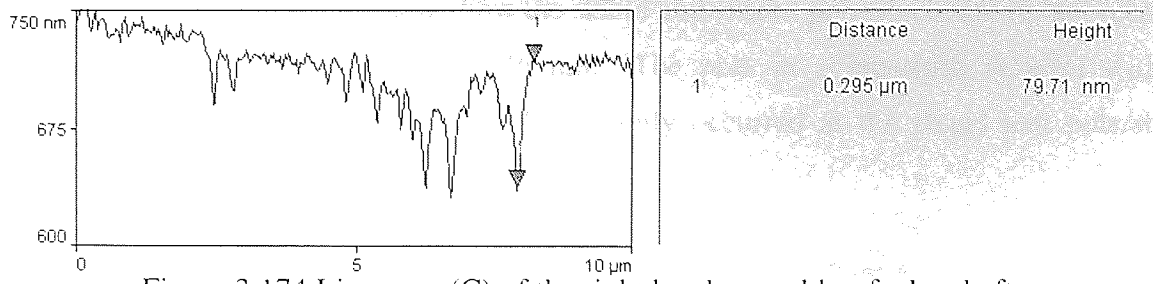

Figure 3.174 Line scan (C) of the right head assembly of a head after 10K passes of tape MP5 at 5°C, 10% RH

The fact that portions of the ceramic were removed would suggest that the lower ceramic to insulator depths for this head were due to ceramic wear.

AES analysis of this structure confirmed the presence of Fe on all analysis positions. Ti was detected on the shield and shared pole/shield which is where the PTR was evident. Al was detected on the shield.

3.5.2.1.3.2 Multiple Cartridges

3.5.2.1.3.2.1 Left Structure

Figure 3.175 shows an AFM image of the left read/write structure of a head after 5 000 passes of tape MP5 at 5°C, 10% RH. Little stain was visible on the head, which was remarkably clean with the pole regions being very similar in appearance to a virgin head (Figure 3.61). Evidence of abrasive wear was found across the structure. Two black stars mark the write gap in Figure 3.175 for ease of component identification.

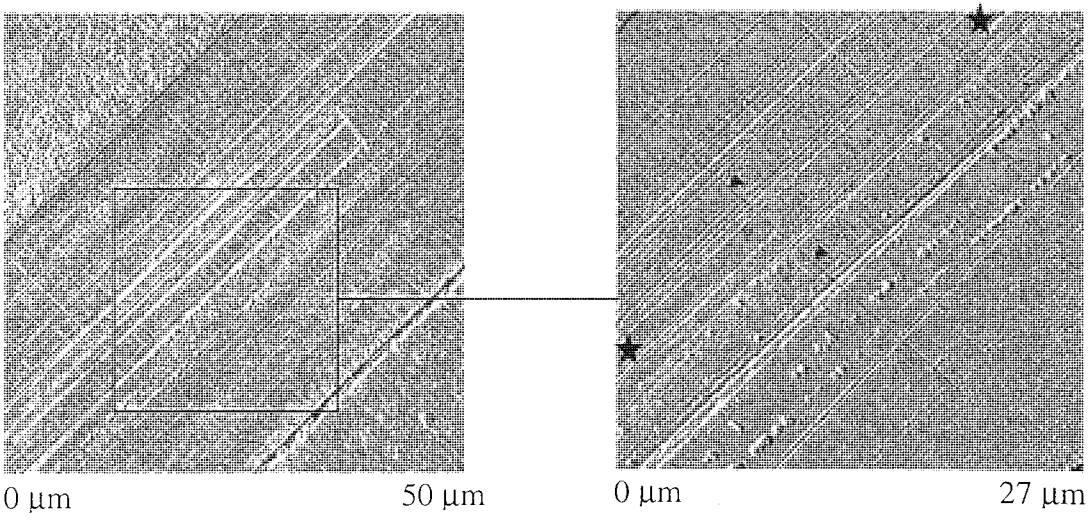

Figure 3.175 Left head assembly of a head after 5 000 passes of tape MP5 at 5°C, 10% RH with a close up of the pole area

The line scan in Figure 3.176 shows how the shield and shared pole/shield are in fact recessed from the insulator region by around 46 nm. The pole in comparison is level with its surrounding insulator indicating that PTR had only occurred at the shield and pole/shield regions.

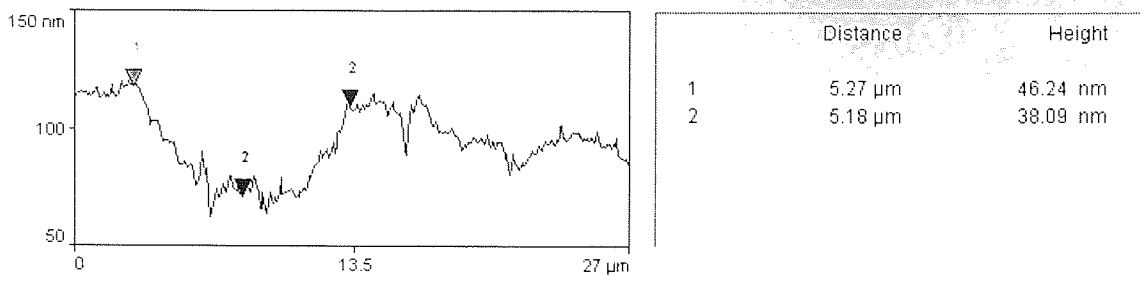

Figure 3.176 Line scan of the left head assembly of a head after 5K passes of tape MP5 at 5°C, 10% RH

The depth as measured from the ceramic (shield side) to the insulator ranged from 40 to 50 nm with the TiC recession having a maximum of 16 nm. The situation for the ceramic (pole side) was such that the depth to the insulator was so low that at some positions they could be considered to be level. The TiC recession was also very low, measured at around 5 nm.

AES analysis of this structure indicated that Fe was present on all pole positions showing preferential stain adhesion. Large amounts of Co were still detected indicating small amounts of stain were present, thus the AFM image appeared relatively clean.

3.5.2.1.3.2.2 Right Structure

Figure 3.177 shows an AFM image of the right read/write structure of a head after 5 000 passes of tape MP5 at 5°C, 10% RH. Contrary to the left structure, heavy staining had occurred across the poles and insulator regions. Portions of the poles were seen to be relatively stain free whereas the insulator regions were completely covered. Evidence of abrasive wear was also apparent.

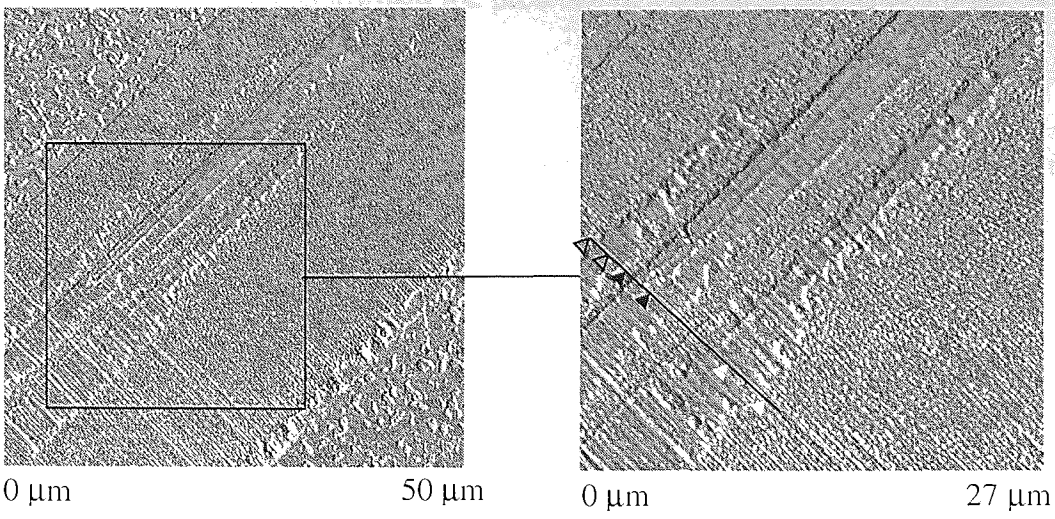

Figure 3.176 Right head assembly of a head after 5 000 passes of tape MP5 at 5°C, 10% RH with a close up of the pole area

The pole areas did not show signs of the ridges that were observed on a virgin head (Figure 3.61) indicating that they had either worn away or had been filled by stain. Figure 3.177 shows the pole to insulator depth as ~ 55nm which compared to the virgin head (~ 10nm) indicates a substantial increase of ~ 45nm. This again could be due to pole wear, and/or a substantial stain thickness on the insulator. The situation for the shield to insulator height was very similar.

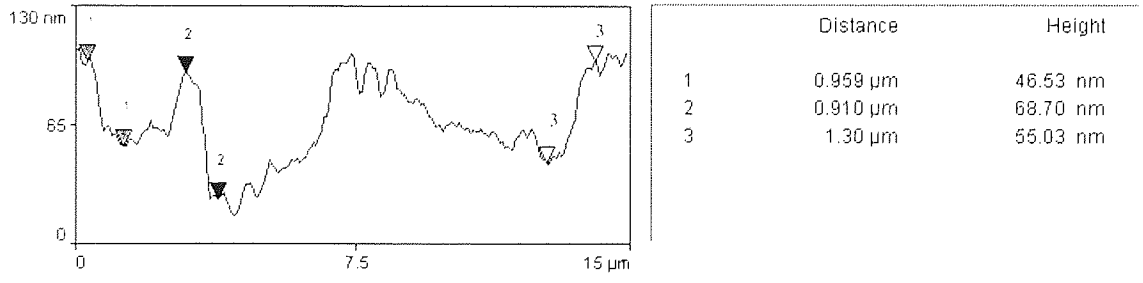

Figure 3.177 Line scan of the right head assembly of a head after 5K passes of tape MP5 at 5°C, 10% RH

The depth as measured from the ceramic (shield side) to the insulator ranged from 11 to 32 nm with the TiC recession having a maximum of 42 nm. The situation for the ceramic (pole side) was such that the depth to the insulator was a maximum of nearly 55 nm with the TiC recession being high measured at a maximum of 66 nm.

AES analysis of this structure confirmed the presence of Fe at all analysis positions. Ti was detected on both the pole and shield.

Figure 3.178 shows an SEM image of the right read/write structure after 10K passes of tape MP5 at 5°C, 10% RH. Damage to the ceramic region is evident. AES maps of the head confirmed the presence of Fe on all areas.

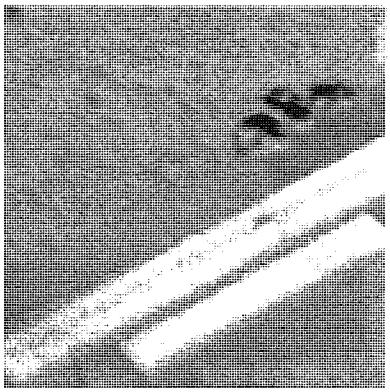

Figure 3.178 SEM Image of the right read/write structure after 10K passes of tape MP5 at 5°C, 10% RH (140μm).

3.5.2.2 Comparison with Tape MP6

Unlike during the experiments run at 32°C, 80% RH, tape MP6 finished the dropout and multiple cartridge experiments without failure at 5°C, 10% RH.

3.5.2.2.1.1.1 Left Structure

Figure 3.179 shows an AFM image of the left read/write structure of a head after 10K passes of tape MP6 at 5°C,10% RH. Even staining had occurred across the poles and insulator regions.

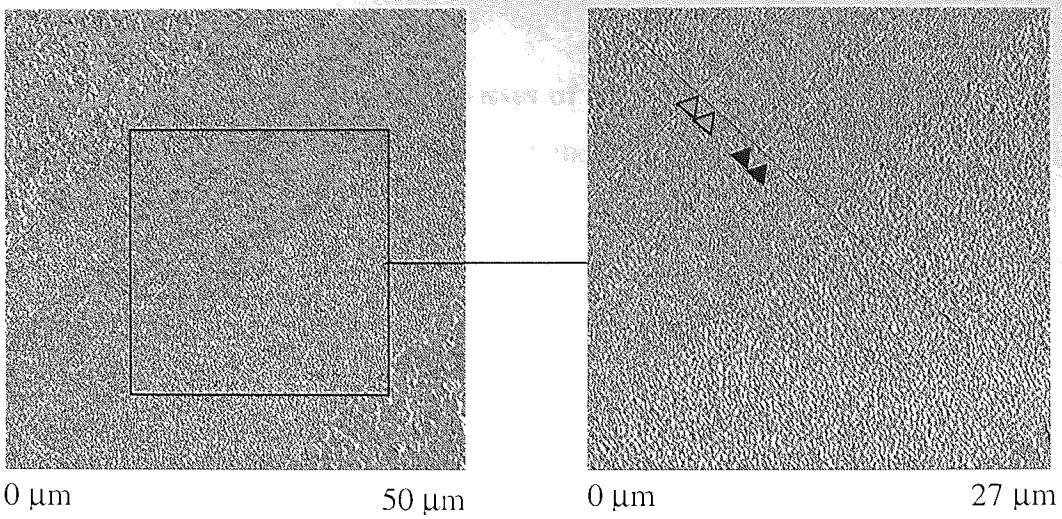

Figure 3.179 Left head assembly of a head after
10K passes of tape MP6 at 5°C, 10% RH and a close up of the poles

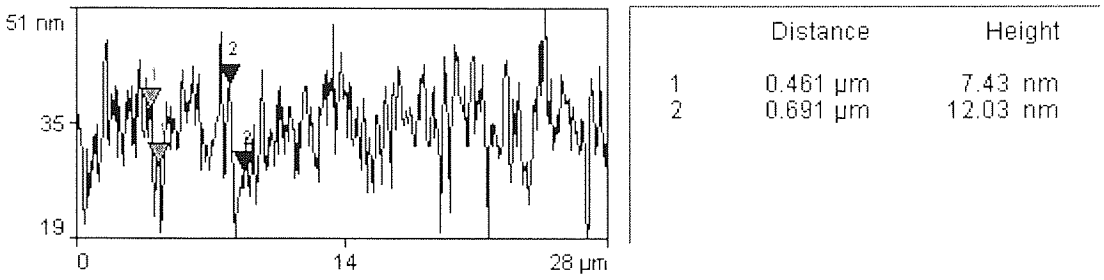

Figure 3.180 Line scan of the left head assembly of a head after
10K passes of tape MP6 at 5°C, 10% RH

The pole areas were level with the insulator regions at the end of the experiment (Figure 3.180), indicating that stain had adhered preferentially to the poles. Figure 3.180 shows the height from read gap to shield as being 7.4nm and write gap up to pole as being 12.0 nm, both depths indicating that the gaps were now recessed from the poles and surrounding insulator regions.

The ceramic (pole side) to insulator depth was measured at around 23nm, the TiC recession was found to be 30nm. The depth from ceramic (shield side) to insulator was found to be about 21nm while the TiC recession was measured at up to 40nm.

AES showed that Fe was detected at all positions whilst Ti was detected on the pole and one insulator region. Co although in very small quantities was detected on one insulator region.

3.5.2.2.1.1.2 Right Structure

The right hand head structure after 10K passes of tape MP6 at 5°C, 10% RH is presented in Figure 3.181. Severe damage to all areas of the structure is clearly visible. Portions of ceramic (shield side) had been removed and dragged, by tape motion, across the insulator region creating grooves. Some of the removed ceramic material became trapped between the tape and head where as a result of third body abrasive wear, PTR occurred. Other portions of the removed ceramic were dragged further across the pole regions where the grooves terminated at the next insulator region.

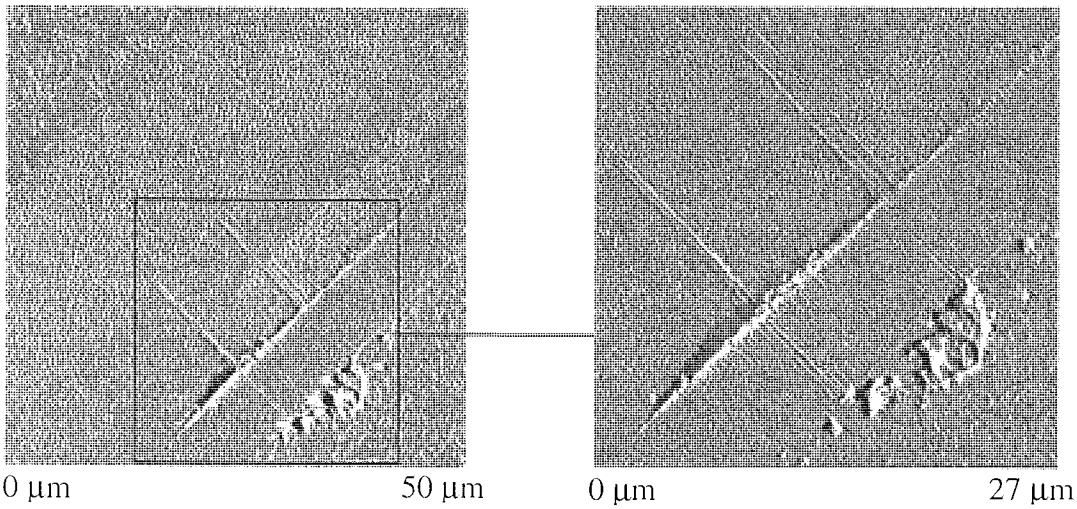

Figure 3.181 Right head assembly of a head after
10K passes of tape MP6 at 5°C, 10% RH and a close up of the poles

ceramic (pole side) to insulator depths were found to be around 20nm indicating little change from the virgin state. TiC recession was found to be in the region of 30nm, again little change from the virgin state. On the shield side of the head the cearmic to insulator depth was measured at around 30nm which was virtually unchanged from the virgin head. TiC recession of up to 42nm had occurred on the ceramic (shield side) showing an increase of about 20nm from the virgin state.

The damaged areas of the structure were examined with the AFM and the results are shown in Figure 3.182.

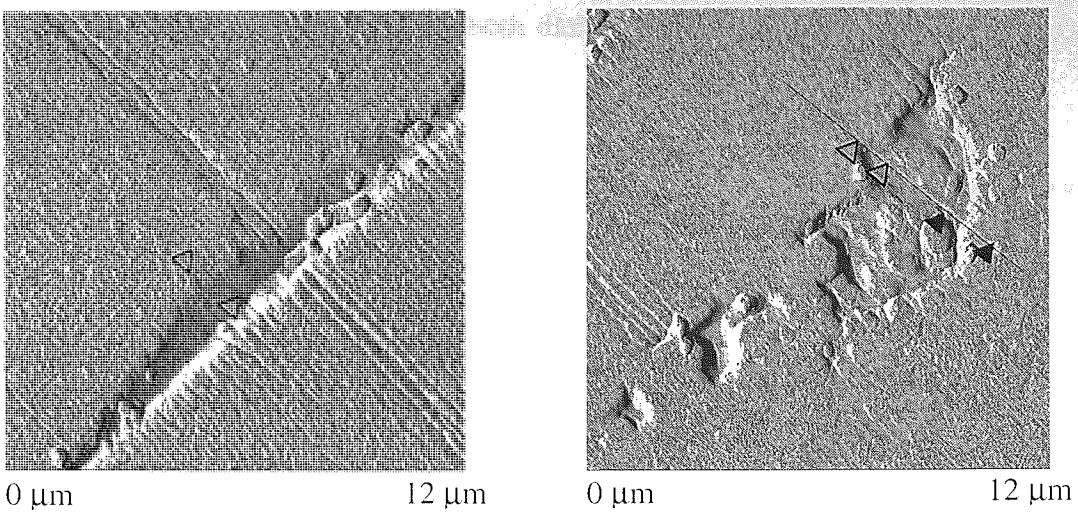

Figure 3.182 Right head assembly of a head after
10K passes of tape MP6 at 5°C, 10% RH, close up of the damaged ceramic

The AFM image of the PTR shows clearly that removed ceramic material is present in the recessed area. Depth information was found using the line scan option of the AFM and is shown in Figure 3.183 (PTR) and Figure 3.184 (damaged ceramic).

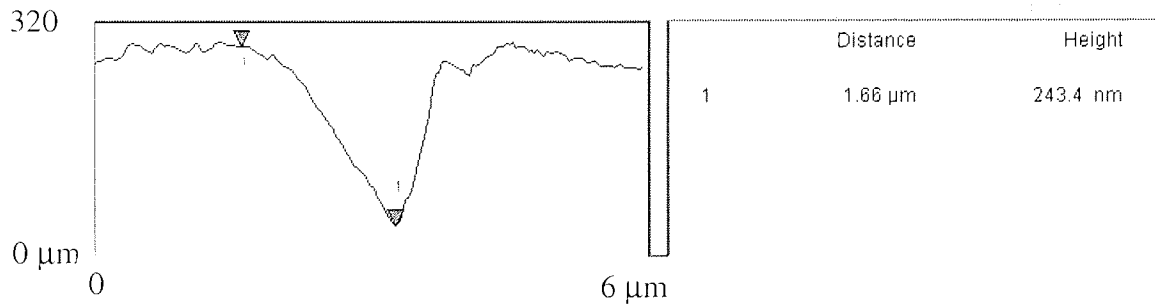

Figure 3.183 Line scan across the PTR on the right head assembly of a head after
10K passes of tape MP6 at 5°C, 10% RH

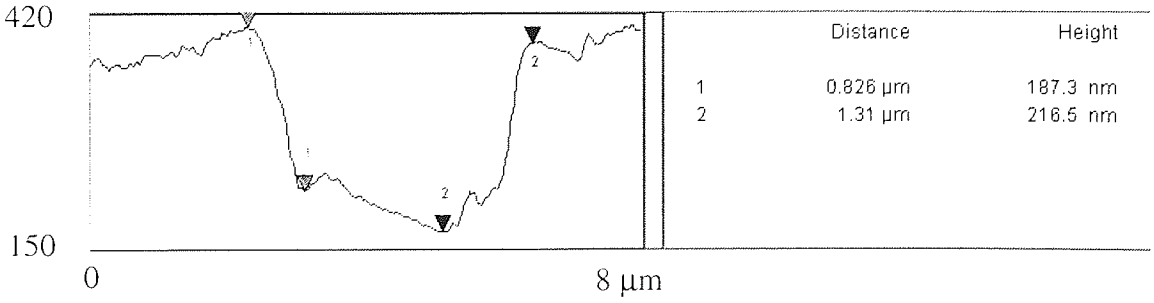

Figure 3.184 Line scan across the damaged ceramic on the right head assembly of a head after
10K passes of tape MP6 at 5°C, 10% RH

Depths of above 200nm were found for both damaged areas indicating severe damage that would probably render the head unusable.

Although evidence of ceramic material removal was found from AFM data (Figure 3.182) no such evidence was obtained from AES. Neither Ti or Al were detected on the pole regions.

3.5.2.2.1.2 Multiple Cartridges

3.5.2.2.1.2.1 Left Structure

After 5K passes of tape MP6 using multiple cartridges the poles on the left head structure was remarkably clean (Figure 3.185). The ceramic (shield side)and ceramic (pole side) regions showed visible signs of staining, as did the insulator adjacent to the ps-ceramic. A line of material was present at the junction between the pole and insulator.

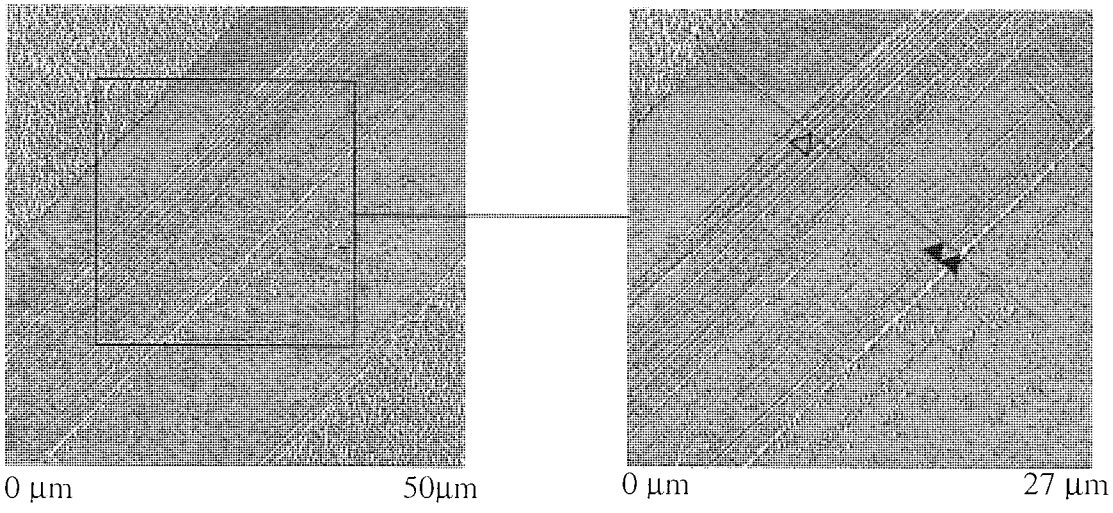

Figure 3.185 left head assembly of a head after
5K passes of tape MP6 at 5°C, 10% RH and a close up of the poles

From the ceramic (pole side) to the insulator, depths of around 30nm were measured. TiC recession could not be measured on the ceramic (pole side) due to the staining which had obscured the two phases of the ceramic. Depths of approximately 32nm were measured from the ceramic (shield side) to insulator, which showed little change from a virgin head. TiC recession on the ceramic (shield side) was between 14 – 25nm, again showing little change from the virgin state.

Grooves in the shared pole/shield were found to be up to 15nm deep (Figure 3.186), these were not in the direction of tape motion but were similar to those on the virgin head (Figure 3.61). This suggests that the grooves were an artefact of the processing techniques used. The material deposited at the junction between the pole and insulator was found to be about 45nm in height.

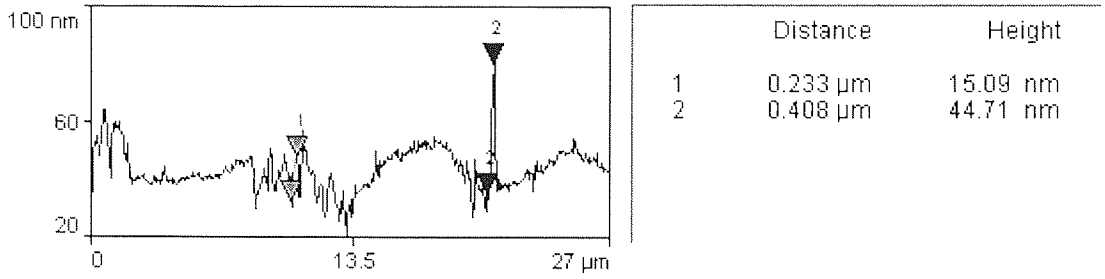

Figure 3.186 Line scan across the left head assembly of a head after 5K passes of tape MP6 at 5°C, 10% RH

Confirming the visual information gained from the AFM images, the poles were relatively stain free with Fe only being present on the pole.

3.5.2.2.1.2.2 Right Structure

The right structure after 5K passes of tape MP6 at 5°C, 10% RH was examined with AFM and the results are shown Figure 3.187. Similar to the left structure, the poles were extremely clean, with staining being confined to the ceramic (shield side) area.

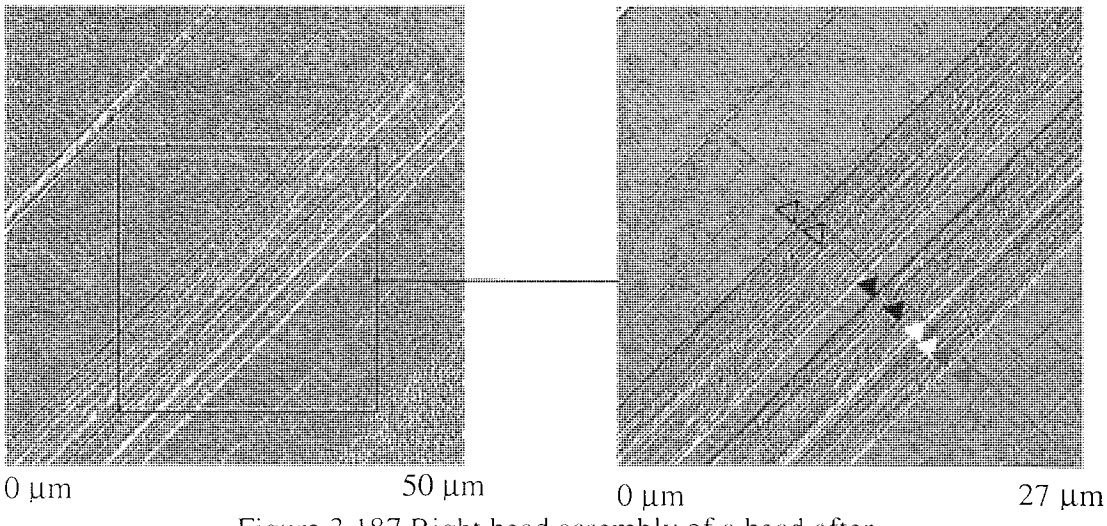

Figure 3.187 Right head assembly of a head after 5K passes of tape MP6 at 5°C, 10% RH and a close up of the poles

PTR was evident on this structure, the pole to insulator height was found to be 65.3 nm and the shield to insulator height 33.1nm (Figure 3.188). Both these heights were 10-15nm on the virgin head.

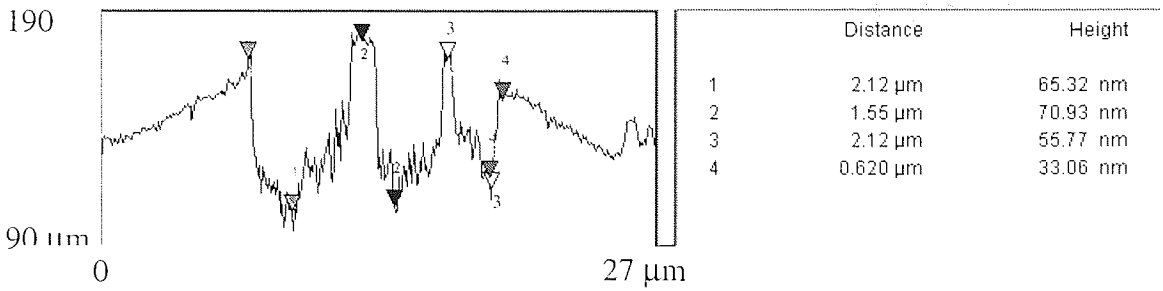

Figure 3.188 Line scan across the left head assembly of a head after 5K passes of tape MP6 at 5°C, 10% RH

The depth from the ceramic (pole side) to insulator was found to be around 22nm with the TiC being measured at 10nm and below. The ceramic (shield side) to insulator depths were very similar and were found to be around 21nm. The TiC recession on the ceramic (shield side) was measured at 10nm and below.

From AES analysis Fe was only detected on the ceramic (shield Side), Ti was found on the pole and shield.

CHAPTER 4 Discussion

4.1 Introduction

Four separate experimental procedures were followed incorporating several experimental tapes and three different tape cycling devices.

The first experiments involved an accelerated tape tester, consisting of a custom made cycler ("loop tester"), which enabled small lengths of tape (~ 1m) to run for up to several thousand passes in a relatively short period of time. The aim of the experiment was to ascertain if the loop tester produced results that were representative of a real tape drive system.

The second set of experiments used a modified tape drive (Georgens cycler), which allowed the effects of the tape transport system on the tape surface to be studied. To isolate any effects on the tape surface due to the head/tape interface, no read/write heads were fitted to the cycler.

For the third set of experiments a modified Georgens cycler, was fitted with a TR-4 head. This allowed the effects of the head/tape interface on the physical and chemical properties of the tape surface to be investigated. To investigate the significance of the environment on the head/tape interface, a more severe condition, likely to promote chemical/physical changes to the head and/or tape, was employed, namely 5°C, 10% RH.

For the final stage of the project, the TR-4 head was replaced by the next generation TR-5 head. It was also at this stage that the effect on the head/tape interface, of an energised MR element, was investigated.

4.2 Loop Tester Cycling Experiments

Cycling of the tape using the loop tester led to chemical changes to the surface of the tapes.

4.2.1 MP1

4.2.1.1 22°C, 40% RH

The initial reduction in the Fe signal was probably due to smearing of the top layer, which filled troughs in the surface of the tape and hence reduced the Fe signal detected by XPS.

Figure 3.4 (b) and Figure 3.5 both provide evidence of N and hence binder depletion with increasing number of passes. A reduction in binder should lead to a decrease in the C signal detected by XPS, an effect not substantiated by the results. Therefore there must be an increase in the C signal due to some other source.

Results showed that the increase was due to the increasing C-C/C-H component of the synthesised C peak. Any change in the magnitude of the C-C/C-H peak was probably due to a change in either the thickness of the hydrocarbon contamination layer and/or more likely to a change in the amount of lubricant present at the tape surface. This arises from the fact that the lubricant is a long chain hydrocarbon which would have a significant effect on the proportion of C-C/C-H detected, in the surface region of the tape. The fact that the C-C/C-H component increased with cycling would suggest that lubricant became more abundant at the surface and /or chain scission of the long chain hydrocarbon bonds occurred, allowing shorter C-H chains to migrate to the surface. The C-N and C-O components decreased with cycling which confirmed binder depletion.

The overlayer thickness was seen to initially increase, which was consistent with smearing of the overlayer (asperity removal) masking the Fe signal. Subsequent decrease was due to the removal of the overalyer and binder covering the magnetic pigment.

4.2.1.2 22°C, 80% RH

The largest change was for the Fe:N ratios, which showed a significant increase with increased cycling, due to greater binder depletion. As for the 22°C, 40% RH case the decreasing C-N and C-O components of the synthesised C peak confirmed binder depletion, whilst the increasing C-C/C-H component indicated lubricant enhancement at the surface.

4.2.2 Tape A

4.2.2.1 22°C, 40% RH

The N and Cl signals both decreased with increased cycling indicating binder depletion had occurred. As for tape MP1, the Fe:N (and Fe:Cl) ratios showed an increase with increased cycling, confirming binder depletion. This was also confirmed by decreasing C-N and C-Cl

components of the synthesised C peak. The C-C/C-H component increased with cycling after an initial decrease up to 100 passes. This suggested that lubricant migration to the tape surface occurred as cycling commenced.

A brief initial decrease of the overlayer thickness was noted before a stable situation occurred with increased cycling. If binder removal occurred throughout cycling then the overlayer thickness might be expected to decrease accordingly. For the stable situation found, it is possible that the lubricant enhancement occurred at the same rate as binder depletion producing a relatively constant overlayer thickness with cycling.

4.2.2.2 22°C, 80% RH

The trends for the elemental concentrations were similar to the ambient case. The largest change occurred for the Fe:N and Fe:Cl ratios, which showed a significant increase with increased cycling, due to greater binder depletion. Lubricant enhancement at the tape surface was indicated by the increasing C-C/C-H component of the synthesised C peak. The decreasing C-N and C-O components confirmed binder depletion.

4.3 Georgens Cycler (No Head)

Cycling of the tape in a Travan cartridge (in the absence of a head) led to chemical and physical changes to the surface of the tape.

For the experiments performed, the chemical changes were not sufficient to have a significant effect on the signal dropout rate. After a decrease, usually up to 1K passes, from an initial maximum, the dropout rate stabilised. Dropout level then remained constant for the remainder of the test. The initial decrease in the number of dropouts was considered to be due to the burnishing of tape asperities, decreasing the head/tape spacing and hence providing an improvement in the recorded signal according to the wallace equation (equation 20).

The best dropout performance was given by tape A followed by tape MP2 then tape MP1.

4.3.1 MP1

4.3.1.1 22°C, 40% RH

In a similar situation to the loop tester results, the initial reduction in the Fe signal was probably due to smearing of the top layer, which filled troughs in the surface and hence reduced detection of the Fe by XPS. The decreasing N signal was indicative of binder depletion. The synthesised C peak revealed that the C-N and C-O components decreased with cycling indicating that binder depletion had occurred while the C-C/C-H component increased indicating lubricant replenishment at the surface of the tape.

4.3.1.2 22°C, 80% RH

Figure 3.19 shows how the Fe signal remained constant until it increased at the higher number of passes, this was in conjunction with the C signal having increased overall up to 5K passes where a significant decrease was noted. The C-C/C-H component of the synthesised C peak showed that lubricant enhancement at the tape surface occurred until 5K passes where a slight decrease occurred. The decreasing N signal was indicative of binder depletion, which was confirmed by the synthesised C peak (Figure 3.20) which showed that the C-O and C-N components decreased with cycling particularly at the highest number of passes.

Lubricant depletion may have occurred at the higher number of passes (along with the continued binder depletion) which produced a relatively thin overlayer allowing more Fe to be detected.

4.3.1.3 32°C, 80% RH

At this condition the results were very similar to those from the 22°C, 80% RH tests. The Fe signal again increased while the N signal decreased but here at greater rates at the higher number of passes. As before binder depletion occurred whilst lubricant migration to the surface of the tape took place. The C-C/C-H component of the synthesised C peak did not show a decrease at the higher number of passes indicating that lubricant depletion did not occur at this condition. Since % RH is a measure of humidity relative to the current temperature of air, at 22°C, 80% RH there is less actual moisture in the system when compared to 32°C, 80% RH. Binder degradation is known to be accelerated by higher

moisture content[113]. Also the additional moisture may have acted as a lubricant at the tape surface, this would decrease the amount of lubricant lost from the tape.

4.3.1.4 40°C, 15% RH

The elemental XPS trends at this condition were similar to the 22°C, 80% RH and 32°C, 80% RH cases but to a lesser degree. The C signal was quite stable with increasing number of passes before decreasing at 5K and 10K passes. At this condition the synthesised C peak (Figure 3.21) showed that the C-C/C-H component of the C signal decreased initially, stabilised then increased at 10K passes. This would indicate that the amount of surface lubricant had decreased after 100 passes and was not able to recover until 10K passes. The C-O component remained relatively stable throughout cycling only exhibiting a decrease at 10K passes whereas the C-N component decreased with cycling indicating possible binder depletion.

4.3.2 Ratios

The change in the Fe:C ratios showed a slight increase with increased cycling (Figure 3.23 (a)). This was not the case for the ratios containing N, both provided evidence of N and hence binder depletion with increasing number of passes (Figure 3.23 (b) and Figure 3.24).

The elemental ratio plots suggest the change in surface concentration was dependent on the environmental operating conditions. In the case of Fe:N (Figure 3.23 (b)), the spread of data points for the virgin tape and the tape that had been cycled for just a few hundred passes was relatively small. However, at 10K passes the spread of data points for each condition was much wider. Indeed, Figure 3.23 (a), suggests that binder depletion is greater at high humidity than at ambient conditions of 22°C, 40% RH. The differences in the ratio of N:C (Figure 3.24) also suggested that the higher humidity conditions produced greater binder depletion. The N:C ratio produced at the low humidity condition of 40°C, 15% RH was of the highest magnitude and at the higher number of passes, similar to pseudo ambient conditions showing that with no head present the higher temperature did not adversely effect the tape. The ratio of Fe:C showed similarities when tape MP1 was cycled at the two high humidity conditions. However, when the tape was cycled at 40°C, 15% RH, the ratio of Fe:C

tended to a maximum, irrespective of the number of passes due to the greater Fe increase which occurred..

4.3.3 Overlayer

The overlayer which consisted of binder and lubricant (migrating to the surface during use) decreased overall with cycling which was consistent with a loss of binder material. The initial increase in overlayer thickness was probably as a result of smearing of the top layer as discussed earlier (4.2.1.1).

The overlayer thickness decreased as a function of temperature and/or relative humidity. The pseudo ambient condition of 22°C, 40% RH produced the thickest overlayer during cycling and remained relatively stable throughout. The remaining conditions all showed a decrease with increased cycling with the 40°C, 15% RH condition producing the thinnest overlayer of all the conditions.

4.3.4 Tape *MP2*

4.3.4.1 *22°C, 40% RH*

Two phases seemed to have occurred during cycling, initially, Fe and O decreased. This was consistent with smearing of the overlayer during running in of the tape. The next phase saw the O and Fe signals increasing for the remainder of cycling whilst C and N decreased. This would suggest the removal of binder material, which allowed a greater amount of magnetic pigment (γ-Fe_2O_3) to be detected. Figure 3.27 shows how the C-C/C-H component increased throughout cycling indicating that lubricant was renewed as cycling continued. The C-O and C-N components showed a slight increase and then decrease of binder material. Tape MP2 had a lower N content in its binder when compared to tape MP1 (Table 2.2) and as such the small amount detected was subject to greater error. It is possible that no increase occurred at the lower number of passes more that the signal was reasonably stable. However a decrease did occur at the higher number of passes.

The change in the Fe:C ratio showed a slight decrease in the initial stages of cycling, this was consistent with smearing of the overlayer. For the ratios containing N (Figure 3.28 b and c), both provided evidence of N and hence binder depletion at the higher number of passes.

Overall a decrease of the overlayer thickness was noted with increased cycling (Figure 3.29), this was consistent with a loss of binder material. The initial increase in overlayer thickness was probably as a result of smearing of the top layer as discussed earlier (4.2.1.1).

4.3.5 Tape A

4.3.5.1 22°C, 40% RH

Similar results were produced for the Georgens cycled tapes and those cycled on the loop tester. The Fe signal remained relatively stable with cycling, whereas the C signal increased up to 10K passes. The synthesised C peak showed that the C-C/C-H component had increased with cycling indicating lubricant migration to the surface of the tape. The C-N, C-Cl and C-O components had decreased as did the N and Cl signals, all indicative of binder depletion.

4.3.5.2 22°C, 80% RH

Similar results were produced for the condition of 22°C, 40% RH. Lubricant migration and binder depletion occurred with cycling.

4.3.5.3 Ratios

The change in the Fe:C ratios showed little change with increased cycling (Figure 3.36a). This was not the case for the ratios containing N and Cl, which provided evidence of N and Cl and hence binder depletion with increasing number of passes.

The elemental ratio plots suggested the change in surface concentration was dependent on the environmental operating conditions. For the cases of Fe:N and Fe:Cl (Figure 3.36b and c respectively), the spread of data points for the virgin tape and the tape that had been cycled for just a few hundred passes was relatively small. However, after 10,000 passes the spread of data points for each condition was much wider. The results suggest that binder depletion was greater at high humidity and/or high temperature than at the ambient conditions of 22°C, 40% RH. The same conclusions can be drawn from the N:C and Cl:C results in Figure 3.36d and e respectively.

4.3.5.4 Overlayer

The overlayer thickness decreased as a function of temperature and/or relative humidity (Figure 3.37). The ambient condition of 22°C, 40% RH produced the thickest overlayer during cycling and along with the conditions of 22°C, 80% RH was relatively stable throughout cycling. The conditions of 32°C 80% RH and 40°C, 15% RH produced a decrease in the overlayer thickness at the higher number of passes with the latter condition producing the thinnest overlayer of all the conditions. The results suggest that the increasing temperature produced a thinner overlayer. This means that more binder and/or lubricant were removed as the temperature increased. The synthesised C peak shows that lubricant was in fact increasing with cycling and so the removal of overlayer material must be due to the binder depletion.

4.4 Georgens Cycler with TR-4 Head

With the introduction of a head into the tape path (increasing tension at the guidepins) the role of the environment on the durability of the media was significant particularly for high temperature conditions. For both tapes (tape MP2 had been dropped), degradation of the backcoat was observed during cycling experiments at 40C°C, 15% RH and this sometimes led to cartridge failure due to the tape sticking to the cartridge guide pins.

As only one cartridge was cycled (due to availability of heads) there remained only two samples for analysis at the end of each experiment, a virgin tape and one which had reached the end of the designated number of passes.

The results suggest the addition of a (permanently unenergised) TR-4 head to the cycler did not lead to significant chemical changes to the surface of the tape. Indeed, for tape MP1 at 32°C, 80% the Fe:N ratio for the surface of the tape prior to the addition of a head was 12.5 whereas after the head had been included, the Fe:N ratio at the centre of the tape was 11.9. However, when comparing these values with those from the edge of the tape, there are significant differences. The percentage of Fe had reduced to 10.4 whereas the N content had increased to 2.1. This yielded an Fe:N ratio of 5.0 and indicated a greater amount of binder material at the edges of the tape. Note that for the virgin tape, the Fe:N ratio was 3.8 which shows that although the ratio is greater at the edge when compared to the centre of tape, a

reduction in N and/or an increase in Fe had occurred at both positions. Tape A produced similar results.

The difference between the centre and edge of tape was obvious from Table 3.4. There was clearly an abundance of Fe at the centre of tape whereas there was a higher N and C content at the edge. Therefore at the edge of the tape a greater amount of binder was present (in comparison to the centre) whereas at the centre the overlayer was thinner than at the edge allowing more of the pigment to be detected. The drive belt, probably through high contact pressure, had an effect on the chemical properties of the cycled tape.

No chemical reaction was ever found between the belt and the tape, from which we conclude that the effect on the tape is due to a physical interaction. Backcoat roughness may be transferred to the magnetic coating due to the pressure of the drive belt. This in turn would ensure that the magnetic coating under the belt is always rougher than the edge (off belt) region of the tape. During cycling, a tape would be worn smoother by contact with the head. If the centre region of a tape was always having its roughness renewed due to the backcoat/belt interaction, then the centre region would experience greater wear of its surface.

Comparison between environmental conditions was made difficult due to the different number of passes completed at each condition. At 40°C, 10% RH, tape failure for tape MP1, occurred after only 4K passes (2K for tape A). The experiment performed at 5°C, 10% RH (tapeMP1) was manually stopped after 20K passes (the extensive number of passes was an attempt to promote dropout growth).

In all cases the Fe signal increased at the centre and edge positions, also the magnitude was greater at the centre compared to the edge of tape. Conversely, the N and Cl signals decreased at the centre and edge in all cases and was of a higher magnitude at the edge of the tape.

Binder depletion was therefore occurring at both tape regions, for all conditions, but at a greater rate at the centre of tape.

Tape MP1 produced virtually identical dropout profiles at all three environmental conditions showing that temperature and humidity did not effect the signal performance of this tape. Tape A produced the lowest dropout levels at 32°C, 80% RH but the highest at 5°C, 10% RH. Although differences were noted between conditions the dropout performance improved with cycling.

PTR was in evidence at each condition for tape MP1. Ti was detected on the pole regions at 32°C, 80 % RH and 40°C, 15% RH. The removal of Ti particles from the Al_2O_3TiC ceramic of the ADR (1.5.2) and Travan (1.5.3) systems has been cited as a cause of PTR by Sourtey, Wild and Sullivan [99]. Similarly Harrison [98] cited the removal of Ti from the $CaTiO_3$ ceramic of the Hi-8 video system as a cause of three body wear.

4.5 Georgens Cycler with TR-5 Head

The series of experiments involving a TR-5 head were split into two sections. The first (Group A) used MP1 as the benchmark tape with two further MP tapes (MP3 and MP4), having slightly different formulations to MP1. The second section (Group B) involved the comparison of a single and dual layer tape (MP5 and MP6) having the same magnetic coating. Both the latter tapes were run at 1.5 ms^{-1} (60ips) as opposed to 2.3ms^{-1} (90ips) at which the previous experiments were run. This was due to the dual layer tape being thinner than the single layer tapes and hence more prone to damage at a faster running speed.

4.5.1 Environmental effects

4.5.1.1 Group A Tapes

4.5.1.1.1 XPS

4.5.1.1.1.1 32°C, 80% RH

Apart from differences in magnitudes the dropout trends were similar between tapes. The dropout rate stabilised after an initial decrease, usually up to 1K passes (again due to burnishing of tape asperities). Dropout levels then remained constant for the remainder of the test.

The only exceptions to this trend was for the larger dropout classes of 4dB × 50μs and 10dB × 50μs for tape MP1. At both environmental conditions, this tape displayed a slight increase at the higher number of passes. This was almost certainly caused by debris generated at the head tape interface and then becoming loosely bound to the head, although it may have been due to delaminative removal of pigment from the tape surface.

The process of removal of magnetic pigment would be of a gradual nature, starting with the removal of small areas, which would gradually increase in size with cycling. This would have been observed as an increase in the frequency of the smaller dropout classes preferentially to the larger 50μs class of dropout. This phenomenon was not observed, hence the growth of the 50μs class of dropout was thought to be due to debris. Since this never occurred in the Georgens cycler when no head was present, it was assumed that the presence of a head in the tape path system caused the growth of the 50μs class of dropout.

This was likely to be due to the transfer of magnetic tape to the head in the form of stain, or in some cases large areas of debris. It is possible that this debris could have been loosely attached to the head and therefore easily removed. Once removed the debris could attach itself to the magnetic surface of the tape and become entrapped in the tape pack. During dropout measurement the debris would pass underneath the head obscuring the magnetic signal from the tape and hence producing the increase in the 50μs class of dropout observed.

The dropout magnitudes at equilibrium showed that there were differences between tapes, due to differences in their formulations and structures. MP1 produced the highest initial and equilibrium dropouts of the group A tapes, with MP3 and MP4 yielding similar results. The higher lubricant content of MP3 and MP4 was considered to be responsible for reducing the occurrence of dropouts. Both tapes MP3 and MP4 had very similar dropout profiles (initial and equilibrium) indicating that at these conditions, the lower magnetic pigment loading of tape MP4 had no adverse effects on dropout performance.

Group A tapes produced very similar trends with respect to elemental changes at the tape surface. The Fe signal increased, as did O whereas N and C decreased. The C-C/C-H component of the synthesised C peak increased throughout cycling. Also from synthesis of

the C peak it was noted that the C-N and C-O components (both binder indicators) decreased throughout cycling.

Binder depletion was suggested by the decreasing N signal and the decreasing C-N and C-O signals. Lubricant migrating to the surface would increase the C-C/C-H signal as would chain scission in the binder resin resulting in phase segregation and low molecular weight short chain C-H polymers migrating to the surface of the tape. For tapes MP1 and MP3 the C-C/C-H component of the synthesised C peak increased up until 10K passes where a decrease occurred. The C-O component decreased up to the same point at which an increase occurred. This suggests that binder depletion and lubricant enhancement occurred until 10K passes where lubricant depletion was evident. Lubricant depletion never occurred for tape MP4. Also the C signal remained unchanged throughout cycling for tape MP4 at the edge, both effects were probably due to the proportionally larger amount of lubricant present in this tape.

The Fe:C ratios for the centre of the group A tapes showed an initial reduction before an increase for the remainder of the experiment (Figure 3.57). A close examination of the results showed that the Fe signal decreased at 500 passes before increasing for the remainder of cycling (Figure 3.52). This was consistent with polymeric material being smeared across the surface of the tape (due to asperity removal), masking the Fe signal. At the edge, a slight loss of Fe was observed along with a relatively stable C signal indicating that smearing of the overlayer was more prominent than for the centre of tape.

For tapes MP1 and MP3 the Fe:N ratios confirmed that binder depletion was occurring at both tape positions (Figure 3.58), but at a greater rate at the centre of the tapes. For tape MP4 the Fe:N ratio initially increased before stabilising at the centre and remaining virtually stable throughout cycling at the edge. The reason probably being the proportionally greater amount of lubricant present in this tape which would replenish the surface of the tape allowing the N signal to remain relatively stable.

All three tapes showed an initial decrease in the N:C ratios at both tape positions, showing a change in the nature of the overlayer in that binder depleted faster than lubricant enhancement for the first 1500 passes (Figure 3.59). At the centre of the tape the initial decrease was followed by an overall increase for the remainder of cycling. At the edge of tape the initial decrease was followed by a short increase then once again a decrease for the remainder of

cycling. All ratios containing N supported the prognosis of binder depletion with increased cycling with the exception of tape MP4, which only suffered binder depletion at the start of cycling.

4.5.1.1.1.2 5°C, 10% RH

Again, MP1 produced the highest dropouts of the group A tapes, but at these conditions, tape MP4 produced higher equilibrium dropouts than MP3. According to the relationship between the complex elastic modulus of a tape and its pigment loading, there is an optimum value for pigment loading. An increase or decrease from this value results in a decrease in the complex elastic modulus and hence a change in the wear properties of the tape. Without knowing where on the pigment loading/complex modulus graph curve, tape MP4 is situated relative to tape MP3, it is not possible to suggest reasons for the differences in dropout rates. It is not thought that the lower pigment loading would be significant enough to be the cause of the increased dropout rate.

This condition produced similar results to 32°C, 80% RH but less severe. The following trends were evident for tape MP4 at both the centre and edge of the tape. The Fe signal increased while the N signal decreased throughout cycling. Unusually the C and O signals remained relatively constant throughout the experiment. As for the condition of 32°C, 80% RH, there was a greater proportion of Fe and O at the centre of the tape with a greater proportion of N and C being detected at the edge. The amount of binder present at the surface was greater at the edge of tape (off belt) while the overlayer thickness was thinner at the centre due to higher contact pressure from the drive belt.

The fact that the C signal remained unchanged throughout cycling was probably due to two factors, the larger proportion of lubricant present in the tape and possible reduced tape wear at 5°C, 10% RH (larger amounts of material were transferred from tape to head at 32°C, 80% RH). The condition of 32°C, 80% RH produced relative differences between C and O, at the two tape positions of about 2% whereas the difference was 8% at 5°C, 10% RH. A decrease in tape wear could be the reason for the reduced difference between the centre and edge of the tape surface when compared to 32°C, 80% RH.

The stability of the C signal was reflected in the synthesised C peak where each component produced little variability with cycling with the exception of the C-N component which decreased at the centre and edge of tape (Figure 3.92 and Figure 3.93 respectively). The central tape position produced a definite decrease in the C-N bond throughout cycling indicating possible binder depletion although the C-O bond was stable. This illustrates the fact that the N signal, being very small, is more sensitive than other elements results, and therefore binder depletion should, if possible, be confirmed by a decreasing C-O bond.

Lubricant depletion occurred for tapes MP1 and MP3 at 10K passes but no such effect occurred for tape MP4. At the edge of tape, the C signal increased during cycling for tape MP4, both effects were probably due to the proportionally larger amount of lubricant present in this tape. Apart from this incident the three tapes produced similar trends at the edge of tape. Also it was found that for all three tapes there was a greater proportion of Fe and O at the centre of the tapes indicating a lower overlayer thickness and a greater proportion of C and N at the edge of the tapes indicating a greater amount of binder and lubricant.

There were differences between tapes at this condition and they are summarised below.

For tape MP1 the N and Fe signals remained relatively constant throughout cycling at both tape positions. The trend for the C signal was unusual in that it decreased up to 1500 passes and then increased for the remainder of cycling, again this was repeated at the edge of the tape. The synthesised C peak revealed that the C-C/C-H component increased throughout cycling (indicating lubricant migration to the surface).

Tape MP3 produced similar results to those at 32°C, 80% RH, in that at the centre of tape, the C and N signal decreased while the O and Fe signals increased. At the edge of tape C and O followed the same trend only not as severe. The N and Fe signals at the edge were considered to be stable. The C-C/C-H component of the synthesised C peak increased at both positions with the C-O and C-N components decreasing at both positions. Again lubricant enhancement and binder depletion were indicated.

There was a difference in the N:C trends between the centre and edge of each tape. At the centre of tape (Figure 3.95 (a)) there was an overall decrease in the N:C ratio whereas at the

edge of tape (Figure 3.95 (b)) there was an overall increase (tape MP1 remained stable). This suggests that binder depletion occurred at a greater rate than lubricant migration at the centre of tape, with the opposite effect occurring at the edge. The increase in the N:C ratio was due to the stable nature of the N and C signals at the edge.

The Fe:N ratios did not provided obvious trends, particularly at the edge, although each of the three comparable tapes did all give similar results. At the centre the ratio initially increased before decreasing slightly then increasing again. Fe increased overall and N decreased throughout cycling which was consistent with the initial and final increases in the Fe:N ratios. The decrease in the ratio was due to a decrease in the Fe signal rather than an increase in N (binder), possibly due to stain formation. This was confirmed by the Fe:C ratios which showed similar trends to the Fe:N ratios.

4.5.1.2 Group B Tapes

4.5.1.2.1 32°C, 80% RH

Tape MP5 consistently produced the lowest dropout rate of all tapes tested (groups A and B). It's comparable tape; MP6 gave similar results at this condition after 1500 passes.

At the centre and edge of tape MP5 the increasing Fe signal signified a removal of the overlayer (Figure 3.127 & Figure 3.128). C increased up until 10K passes where a decrease occurred while N decreased until 10K passes were reached and an increase was noted. This is consistent with lubricant depletion occurring at 10K passes allowing more binder to be detected. Synthesis of the C peak showed that the C-C/C-H component increased up to 1965 passes but then decreased at 10K passes (Figure 3.129). This fact, along with the C-O and C-N components having decreased with cycling until they increased at 10K passes, indicated that binder depletion initially occurred alongside lubricant enhancement. Following this, at some point between 1965 and 10K passes lubricant depletion occurred and as this occurred at the centre and edge of tape positions, it would indicate that tape MP5 suffered from poor lubricant enhancement with use.

Comparison of the centre and edge of tape MP5 showed that the Fe signal was greater at the centre whereas there was a larger amount of N at the edge of tape. This suggested that there

was more binder at the edge of tape with a thinner overlayer being present at the centre of tape.

XPS results for tape MP6 were similar to tape MP5 where comparison was possible, indicating that the single/dual layer fabrication did not create any elemental differences through cycling, although initial dropout measurements indicated a difference in performance.

For the centre of tape MP5, the Fe:N ratio increased with cycling but remained stable at the higher number of passes due to only a slight increase in N which kept the ratio low (Figure 3.133). At its edge the ratio neither increased nor decreased overall showing that the edge suffered less wear than the centre of tape. Similarly, The Fe:C ratios showed an increase at the centre but a stable ratio at the edge (Figure 3.132).

The N:C ratio at the centre of tape MP5 indicated that binder depletion had occurred with cycling. The situation at the edge was different in that no real decrease was seen throughout cycling, the ratio was deemed more stable. The higher contact pressure of the drive belt at the centre of tape had caused more binder to be removed than at the edge.

It was evident from the Fe:N ratios that binder removal occurred at the centre of tape MP6 (Figure 3.162) becoming severe at 10K passes. The reason for the large increase was that the N signal had fallen to below 0.5% at this stage while the Fe signal was at its largest value. This was confirmed by the N:C ratio at the centre and edge of tape MP6, which showed a dramatic change for the dropout cartridge sample (Figure 3.134) again due to the N signal having decreased dramatically, indicating severe binder depletion (C-N and C-O bonds decreased dramatically).

The N:C ratio at the centre of tape MP6 showed a gradual decrease throughout cycling. As the C-O and C-N components of the synthesised C peak also decreased with cycling, binder depletion was indicated.

There was very little difference between the Fe:C ratios for the two tapes being similar at both positions. The ratio was slightly higher in magnitude for virgin MP6. Both MP6 tapes that broke at about 2300 passes displayed very low N signals after failure, citing binder depletion as a possible cause of failure. Consequently any ratios involving N were grossly distorted.

As the dropout tape and tape destined for 3000 passes, both broke after 2300 passes, the comparison of MP5 and MP6 was made difficult at this condition. However, cartridge failure allowed the comparison of two MP6 tapes each having completed 2300 passes. The difference between them was that one was the dropout cartridge and had hence been removed at each predetermined number of passes for dropout analysis, while the other was to be cycled for 3000 passes without removal. Fe:N ratios were similar for both tapes at both positions indicating that the removal of a tape (disrupting the head/tape interface) did not affect the tape chemically at this number of passes.

4.5.1.2.2 5°C,10 %RH

Tape MP5 completed the experiment performed at 5°C, 10 RH without incident. It was noted that the Fe and C signals increased at the tape centre while N decreased. The O signal decreased initially but then remained stable. A similar situation was observed at the edge but to a lesser degree. Synthesis of the C peak revealed that at the tape centre, the C-C/C-H component increased during cycling while the C-O and C-N components decreased. Unfortunately there were no identifiable trends for any component at the edge of the tape. Unusually there were no obvious differences between the centre and edge of tape, with no one element being dominant at either the edge or centre.

Tape MP6 produced very similar results to tape MP5, at the tape centre the C and Fe signals increased with cycling while those of O and N decreased. The same trends occurred at the edge of tape for the C and O signal but the Fe and N signal remained fairly constant. In a very similar situation to the 32°C, 80% RH condition the N signal at the centre of tape MP6 decreased considerably at the higher number of passes.

Fe:C ratios were very similar for both tapes at the centre of tape. At the edge of tape, MP5 produced a higher ratio after 1500 passes, which continued up to 10K passes. Fe:N ratios at the tapes centres were very similar up to 3000 passes after which MP6 then produced a much higher ratio at 10K passes. At the edge of tape the situation was more stable and again similar results were recorded. At the centre of the tapes the N:C ratios were similar, an overall decease was noted which indicated binder (N) depletion had occurred. The edge produced less variation in the ratio with cycling and definite binder depletion could not be established.

For the cartridges used to measure the dropout rate (10K passes), both sets of results were similar. Stain was evident across both head structures and ceramic removal had occurred on the right structure. On the left structure, tape MP6 produced more Fe on the pole areas compared to MP5. The right structures produced very similar elemental concentrations with the only difference being the detection of Ti on the head run against tape MP5.

Differences were evident between the results for the multiple cartridge experiments, this despite both tapes having the same magnetic coating. Any differences therefore were due to the fact that tape MP5 is a single layer tape whilst tape MP6 is a dual layer tape. For tape MP5, Fe was only detected on the poles, for tape MP6 Fe was detected on the ceramic regions as well as the pole. Tape MP6 produced more stain material than tape MP5.

The overlayer thickness decreased with cycling this was true for the regions under the belt and away from the belt, for both tapes.

4.5.1.3 AFM

4.5.1.3.1 32°C, 80% RH

4.5.1.3.1.1 Group A Tapes

This condition was the most demanding on tape performance. The water content of the air at this condition was 30 times that of the second experimental condition (5°C, 10% RH) and excessive tape adhesion to the dropout cartridge heads occurred for all of group A tapes. The debris was not conventional stain material but more binder rich although Fe, the major constituent of stain was present in small amounts. It would appear that the high water content adversely affected the tapes causing them to deteriorate to the extent that large amounts of material were transferred to the head. For this reason the overlayer thickness for all tapes had reduced by a greater amount at this condition.

The debris adhered preferentially to the pole and ceramic regions of each head structure. Any debris present on the insulator regions appeared to have spread from the ceramic regions rather than have been deposited there outright. One possible reason for this is the smoothness of the insulator region compared to other areas on the head. The ceramic region had recessed

TiC phases while the poles were originally recessed. These recessed areas could be sites where transferred tape material was initially deposited. Alternatively, the moisture content at the conditions of 32°C, 80% RH was enough to saturate the insulator/tape interface (no recessed areas to dissipate the water) preventing a transfer of material to occur. A further reason could be the chemical bonds formed due to the electrical conductivity of the different areas of the head. The pole and TiC phase of the ceramic regions are both electrically conductive while the insulator regions are not. This would produce a difference in chemical bonding between the tape and conductive/non-conductive regions of the head.

For the heads that were run against multiple cartridges, Fe was detected at most positions analysed, indicating that stain had formed on the heads. The amount of Fe detected was always greatest on the pole areas, which were proud of the insulator rather than being recessed as in the virgin case. Further, larger amounts of debris were present around the energised left-hand MR element. An energised pole would be magnetic and therefore might influence deposition of pigment. The forces involved are considered to be too weak to produce adherent stain. Preferential formation of stain around the energised MR element was therefore thought to be due to current heating effects. The heat available could add energy to the adhesive bonding ensuring it occurred more readily and at a greater rate.

4.5.1.3.1.2 Group B Tapes

The transfer of material from tape to head was not as severe for the group B tapes in comparison with group A tapes. Comparison was made difficult due to the different number of tape passes each head had seen (cartridge failures occurred) although Fe was found on all heads run against these tapes. For the dropout heads and multiple cartridge heads, transferred material did not initially adhere to the insulator regions at this condition possibly due to the same reasons as the group A heads. The final cartridge in the multiple cartridge experiment failed after 1965 passes. This head was seen to have heavy tape deposits across all regions. It is thought the cause of the cartridge failure was also responsible for the gross adhesion.

4.5.1.3.2 5°C, 10 %RH

4.5.1.3.2.1 Group A Tapes

The water content was low at this condition and stain was present on most regions of the heads particularly on the poles. It is thought that the process of stain production occurs at the atomic level. Adhesive bonds formed between the tape and head materials are stronger than cohesive forces between binder resin and magnetic pigment, resulting in the removal and transfer of magnetic pigment from tape to head.

AES results showed that Fe was detected at most head positions and confirmed that Fe was predominant on the pole areas. Unusually, for tape MP1, Fe was not detected on the ceramic regions.

As for the case of 32°C, 80% RH an effect due to the active MR element was noted as larger amounts of debris were present around the energised left-hand MR element.

4.5.1.3.2.2 Group B Tapes

Stain was present on all regions of the heads particularly on the poles. Preferential formation of stain around the energised MR element was again evident and considered to be due to current heating effects.

The severe ceramic wear observed (particularly for tape MP6) gave an insight into the causes of PTR. Cyclic stressing of the TiC grains from repeated contact with passing tape causes inter-grain stresses below the TiC surface. At some point, the stress will be such that the grain (or part of it) shears and breaks free. These grains/flakes then become trapped between the head and tape, where they continually impact against the head in the manner of three-body abrasive wear.

The multiple cartridges experiment with tape MP6 at 5°C, 10% RH produced a head with virtually no stain (ceramic only), or apparent wear. It would appear that up to 3000 passes (500, 1500 and 3000) were not enough to promote the usual transfer of tape material for this tape at this condition possible due to improved lubricant properties.

CHAPTER 5 Conclusions

First and foremost is that cycling improved signal performance for all the tapes tested. After an initial decrease in the number of dropouts, usually up to 1K passes, they stabilised. Dropout level then remained constant for the remainder of the test. The initial decrease in the number of dropouts is considered to be due to the burnishing of asperities, decreasing the head/tape spacing and hence providing an increase in the recorded signal. Dropouts were found to vary with tape composition and physical properties by almost two orders of magnitude depending on media. These were an intrinsic property of a given tape and did not increase as a function of cycling except when tape degradation occurred.

The effect of environmental conditions on the dropout rate for tapes MP1, MP3 (group A) and MP5 (group B) was minimal. At both 32°C, 80% RH and 5°C, 10% RH the dropout profiles were similar. An environmental effect was noted for tapes MP4 (group A) and MP6 (group B) for which the condition of 5°C, 10% RH produced a higher dropout count. After considering various options such as overlayer thicknesses, amount of lubricant available at the interface and pigment loading of tape MP4 as well as the dual nature of tape MP6 no reason could be identified for the difference between the two conditions.

At 32°C, 80% RH tapes MP3 and MP4 had very similar dropout profiles indicating that at this condition, the lower magnetic pigment loading of tape MP4 had no adverse effects. This was not the case at 5°C, 10% RH, the condition for stain formation, where tape MP4 had a slightly higher dropout rate than that of tape MP3. The lower pigment loading was not considered to be the reason for the difference.

A difference in performance between tape formulations was noted wherein tape MP1 produced the highest and identical dropouts at 32°C, 80% RH and 5°C, 10% RH. The other two group A tapes had a higher lubricant content which had the effect of reducing the number of dropouts at each stage of cycling. A greater amount of lubricant would decrease the friction at the head/tape interface. Removal rate of magnetic pigment would also be reduced resulting in a reduction in dropouts.

The results show that no systematic significant damage to the tape surface occurred due to contact. However, chemical changes occurred at the surface of all the tapes studied and without exception there was a difference between the region of tape in contact with the drive belt (centre) when compared to that which was not in contact (edge). This usually manifested itself as a removal of binder from the region under the belt, producing a thinner overlayer to that at the edge of the tape and also a stronger Fe signal. At the edge of all the tapes, particularly at 32°C, 80% RH, there was a greater proportion of binder and lubricant present when compared to the centre of tape. The 32°C, 80% RH condition was responsible for heavy deposits being transferred from the tapes to the heads.

The drive belt, probably through high contact pressure, had an effect on the chemical properties of a cycled tape. It is possible that backcoat roughness may be transferred to the magnetic coating due to the pressure of the drive belt.

All the changes at the interface which were likely to affect signal output occurred at the head surface. Examination of AFM images of the Al_2O_3 /TiC ceramic showed that differential wear occured within the grains of the ceramic. This was most pronounced at high humidities. Under these conditions it appears that after prolonged contact with tape, the grains of TiC were seen to be recessed from the Al_2O_3 phase.

An active MR element encouraged the formation of stain probably as a result of current heating effects.

CHAPTER 6 Future Work

The future of linear tape systems is shifting to the use of multi-channel, narrow track read/write heads and high speed, thinner, smoother magnetic coating tapes. These changes alone will require investigation to determine how they affect the tribology at the head/tape interface. Will for instance the fact that multi-channels are being used exaggerate the energised MR effect reported in this thesis? Cycling experiments similar to those reported in this thesis could be used to analyse the head/tape interface in the presence of a multi-channel head with energised and non-energised MR elements. It would advantageous to be able to analyse the heads at various stages of cycling rather than at the conclusion of the experiment, as was the case for the reported experiments.

A new Thermomicroscopes AFM has the capacity to perform nano-indenting. Using this facility, the wear of the various head materials could be more easily monitored with cycling. Further, dummy heads manufactured from a single head material would be very useful for wear tests and to determine how a tape interacts with one particular head material.

During the experiments described in this thesis at no time was the signal monitored while cycling commenced. This would be extremely useful to determine when the interface is reaching a stage at which the system is becoming unusable. Heads and tapes could then be analysed to determine the reasons for such an occurrence.

To eliminate problems associated with spacing and spacing loss a very thin coating could be applied to the recording head. An ultra low wear coating would eliminate PTR and if the electrical resistivity is high enough also eliminate stain. Any spacing between head and tape would be the coating thickness. Recording head manufacturers are currently assesing such coatings (typically diamond like C (DLC)). Such a coating would cover the total head surface and would need to last the predicted lifetime of the head (15000 hours). The tribology of such systems is unknown and cannot be predicted.

Higher sensitivity Giant Magneto-Resistive read sensors will eventually be required to cope with smaller tracks (and hence less magnetic flux). These sensors are sensitive to corrosion and wear, for these reasons coatings would be beneficial to the system stability.

Experiments would need to be designed to identify the most important physical properties of the coatings, interface and substrate. Variables such as coating thickness, hardness and internal stress would be studied, these at various environmental conditions as a function of cycling.

If the written signal could be monitored during the experiments it would be possible to determine when signal degradation and error growth occurs and relate this to the physical state of the heads and tapes at such a time.

CHAPTER 7 Bibliography

[1] BWilson, "IBM unveils Largest ever Personal Hard-drive", IBM Homepage, http://www.storage.ibm.com/hardsoft/diskdrdl.htm, March 2000.

[2] Hewlett Packard Homepage, "Tape Backup", Internet address, http://www.products.storage.hp.com/eprise/main/storage/tapebackup/selectionPages/whyTapeBackup.htm, April 2001.

[3] C.D. Mee, "MRM' 95 Foreword", Journal of Magnetism and Magnetic Materials, Vol. 155, pp.1-5, 1996.

[4] H.N. Bertram, "Fundamentals of the Magnetic Recording Process", Proceedings of the IEEE,Vol.74, No.11, November, 1986, pp. 1494-1512.

[5] A.S.Hoagland, "Digital Magnetic Recording", John Wiley & Sons,Inc, 1963.

[6] J. Begun, "Magnetic Recording", Murry Hill Books, Inc, 1949.

[7] J.C. Mallinson, " The Foundations of Magnetic Recording", Academic Press, Inc, 1987.

[8] B. Gribstad, "New Data Storage Technology", Internet address, March 1995.

[9] C.D. Mee & E. Daniel, "Magnetic Recording Handbook: Technology and Applications", McGraw-Hill Publishing Company.

[10] Bhushan Tribology and mechanics of magnetic recording devices,

[11] H. J. Richter, "Recent advances in the recording physics of thin-film media", J. Phys. D: Appl. Phys. 32, pp.147–168, 1999.

[12] F.G.Pavuza and M. Wawra, "A PC-Controlled Instrument for the Evaluation of Magnetic Tapes a Base on Amplitude Statistics of the Output Signal", IEEE Electron Representatives Association, Vol. 1, pt. 3, pp. 278-283, 1989.

[13] K. O'Grady, H. Laidler, "The Limits to Magnetic Recording - Media Considerations", Journal of Magnetism and Magnetic Materials, Vol. 200, pp. 616-633, 1999.

[14] H. Jakusch, & R. J. Veitch, "Particles for Magnetic Recording", Journal of Information Recording Materials, Vol. 20, pp. 325-244, 1993.

[15] R.J. Veitch, A. Ilmer, W. Lenz, and V. Richter, "MP Technology for a New Generation of Magnetic Tapes", Journal of Magnetism and Magnetic Materials, Vol. 193, pp. 279-283, 1999.

[16] S. Iwasaki, Y. Nakamura, IEEE Trans. Magn. MAG-13 (1977) 1272.

[17] Yoshihisa Nakamura , "Perpendicular magnetic recording - progress and prospects" Journal of Magnetism and Magnetic Materials 200 pp.634-648, 1999.

[18] J.L. Sullivan, "The Tribology of Flexible Magnetic Recording Media", Journal of Magnetism and Magnetic Materials, Vol. 155, pp.312-317, 1996.

[19] Imation Homepage,

[20] H.J. Richter & R.J. Veitch, "MP Tape For High Density Digital Recording", Journal of Magnetism and Magnetic Materials, Vol. 155, pp. 80-82, 1996.

[21] S.B. Luitjens, W. Folkerts, H.W. Kesteren and J.J.M. Ruigrok, "Trends in Digital Magnetic Recording; The Application of Thin Film Heads for tape Recording", Philips Journal of Research, 51, pp. 5-19, 1998.

[22] K. Chiba et-al "Metal Evaporated Tape for High Band 8mm Video System", IEEE Transactions on Consumer Electronics, Vol. 35, No3, pp. 1989.

[23] S. Dasgupta, "Dispersion Characteristics of Magnetic Particles:Surface Charge, Surface Adsorption and acid-Base Interaction Behavior", Progress in Organic Coatings, 28, pp. 307-311, 1996.

[24] N. Sugita, et al, "Advances in Fine Magnetic Particles For High Density Recording", IEEE Transactions On Magnetics, Vol. 31, No. 6, pp 2854-2858 November 1995.

[25] K. Okamoto, et-al, "Advanced Metal Particle Technologies For Magnetic Tapes", Journal of Magnetism and Magnetic Materials, Vol. 155, pp. 60-66, 1996.

[26] D.E. Speliotis, "Advanced MP++ and BaFe++ Tapes", Journal of Magnetism and Magnetic Materials, Vol. 155, pp. 83-85, 1996.

[27] P.Glijer, "Advanced Multilayer Thin Films For Ultra-High Density Magnetic Recording", IEEE Transactions On Magnetics, Vol. 30, No. 6, pp 3957-3959, November 1994.

[28] S. Saitoh et al, " Developments and Advances in Thin Layer Particulate Recording Media", IEEE Transactions On Magnetics, Vol. 31, No. 6, pp 2859-2864, November 1994.

[29] Seiichi Hisano, Kazuhisa Saito, "Review Article Research and development of metal powder for magnetic recording", Journal of Magnetism and Magnetic Materials, Vol. 190, pp. 371-381, 1998.

[30] Kotera. H. et-al, "Behaviour of magnetic particles in compaction" IEEE Transactions on Magnetics Vol. 33. No. 2. March 1997.

[31] Hiroyuki Osaki, "Flexible Media — Recent Developments from the Tribology Point of View", Tribology International Vol. 33, pp. 373–382, 2000.

[32] Weick B.L. Bhushan.B, "Characterisation of magnetic tapes and substrates", IEEE transactions on magnetics vol. 32 No. 4 July.

[33] Gilson R.G., " Drying of particulate media coating", Journal of Magnetism and Magnetic Materials 120.

[34] Jung. C. et-al, "Interaction of a vinyl acetate - vinyl chloride based wetting binder with metal particles for magnetic recording" Physiochemical and engineering aspects 80.

[35] R .F. Hegel, "Tribological Comparisons of Particulate Magnetic Tape Coatings in Destructive Wear Testing", Tribology International, Vol. 31, No. 8, pp. 407-412, 1998.

[36] Jorgensen F. "The Complete Hand Book of Magnetic Recording" Tab Books Inc, 1980.

[37] S.B. Luitjens, "Metal Evaporated Tape: State of the Art and Prospects", Journal of Magnetism and Magnetic Materials, Vol. 155, pp. 261-265, 1996.

[38] M.Wright, "Recent Developments in the Production of Thin Film Magnetic Media by Electron Beam Evaporation", Journal of Vacuum Science & Technology A, Vol. 5, N0. 1, pp. 57-60, 1987.

[39] K. Sato et-al, "Noise Characteristics of Co-Ni Obliquly Evaporated Tape", Journal of Applied Physics, Vol. 69, o. 8, pp. 4736-4738, 1991.

[40] Z. G. Jiang et-al, "Nanotribological Evaluations of Hydrogenated Carbon-Films as Thin as 5 nm on Magnetic Rigid Disks", IEEE Transactions on Magnetics, Vol. 31, No. 6, Pt. 1, pp. 3015-3017, 1995.

[41] Y. Inoue et-al, "Atmospheric Corrosion of Thin-Film Recording Media in a lea Environment and its Evaluation", JSME International Journal Series I-Solid Mechanics Strength of Materials, Vol. 35, No. 4, pp. 428-433, 1992.

[42] M. S. Hempstock, "An Investigation of Thin Film Magnetic Recording Media", PhD Thesis, The University of Aston, September 1997.

[43] W. Goerlitz & A. Ito, "Substrates For Flexible Magnetic Recording Media: The Role of Base Films For Modern Performance Requirements", Journal of Magnetism and Magnetic Materials, Vol. 120, pp. 76-82, 1993.

[44] C. J. Pritchard & B. K. Middleton, "An Instrument for Detecting and Recording Drop-outs from Magnetic Tape", Mease. Sci. Technol. 2, pp. 684-685, 1991.

[45] H. Doshita, "Tribological Characteristics of Thin-Layer Magnetic Particulate Media", Triboligy International, Vol. 31, N0. 9, pp. 541-545, 1998.

[46] Saitoh. S. et-al, "Developments and advances in thin layer particulate recording media", IEEE Transactions on magnetics V 31 No 6 Nov 1995.

[47] K. H. J. Buschow et al, "High Density Digital Recording", Kluwer Academic Publishers, 1993, pp.261-266.

[48] J. Bain, "Next Generation Pole Materials for Magnetic Recording Heads", Carnegie Mellon University Homepage, Sept, 1996.

[49] S. T. Patton, B. Bhushan, "Micromechanical and Tribological Characterization of Alternate Pole Tip Materials for magnetic Recording Heads", Wear, Vol. 202, pp. 99-109, 1996.

[50] R.H.Dee and J.C.Cates, "Advanced MR Read/Inductive Write Heads for High performance, High Density Tape Applications", IEEE Transactions On Magnetics, Vol. 34, No. 4, pp 1866-1871, July 1998.

[51] Talke. F. "Talke Laboratory Head/Tape Interface Research" Talke Group Homepage.

[52] Maegawa T. et al, "Optimum Magnetic - Head Shape Design for High Density Recording" IEEE transactions on magnetics Vol. 28 No 5 september 1992.

[53] K. Hayashi, "Soft Magnetic Properties of FeRuGaSi Alloy Films:SOFMAX", Journal of Applied Physics Vol. 64, No. 2, 15 July, 1988.

[54] H. Sakakima, "Properties of amorphous Alloy Films Mainly Composed of Co-Nb", IEEE Transactions On Magnetics, Vol. 19, No. 2, pp 131-135, March 1983.

[55] F. Roozeboom, "Rapid thermal annealing of Soft-Magnetic Metal Alloys", Philips.

[56] T. Okumura et al, "Read / Write Characteristics For Laminated High Moment Fe-Ta-N Film Heads For HDTV VTR", IEEE Transactions On Magnetics, Vol. 28, No. 5, pp 131-135, September 1992.

[57] H. Dong et al, "Comparison of Mechanical and Tribological Properties of Permalloy and High Moment FeTaN Thin Film Heads for Tape Recording Heads", IEEE Transactions on Magnetics, Vol. 32, No5, September 1996.

[58] T. Suzuki et al, "Offtrack Characteristics of Shielded Magnetoresitve Head", IEEE Transactions on Magnetics, Vol. 27, No. 6 pp. 4690-4692, 1991.

[59] R. H. Dee, "Read Heads for Magnetic Tapes", Spie, Vol. 2604 pp. 181-191 ?

[60] Growchowski E. "The era of magnetoresistive heads" IBM Homepage 1997.

[61] J.A. Brug et al, "Impact on new Magnetoresistive Materials on Magnetic Recording Heads", Journal of Applied Physics Vol. 79, No. 8, Pt. 2A, pp. 4491-4495, 1996.

[62] W. Folkerts & Prof. Holstlaan, "Magnetoresistive Thin Film Heads For Tape Recording", the C.A.M.S.T. Record, Issue 18, March 1994, pp. 8-11.

[63] Fortuna Poweresystems, "HP Surestore DAT 40 DDS-4 Tape Drive" Internet Address – http://www.data-storage.co.uk/hpdat40.htm, February, 2001.

[64] Onstream homepage,

[65] Onstream homepage, "Desktop Solutions", internet address- http://www.onstream.com/desktop/index.asp, February 2001.

[66] M. Ferelli, Travan - from concept to product Computer technology review, 1995.

[67] Travan Technology Backgrounder , Imation Homepage, http://www.imation.com/ about/news/newsitem/0,1233,186,00.html, February 2001.

[68] Dave Smith Tisd 97.

[69] M.S.Hempstock, M.A.Wild, J.L.Sullivan, A study of the durability of flexible magnetic media in a linear tape system. Tribology International, Vol.31, No.8, pp. 435-441, 1998.

[70] M.S.Hempstock, M.A.Wild, J.L.Sullivan, Interactions at the head-tape interface of a linear tape system. Tribology International, Vol.33, pp. 391-399, 2000.

[71] D. Tabor, " Tribology- The Last 25 Years: A Personal View", Tribology International Vol. 28, No. 1, pp. 7-10, 1995.

[72] William W. Scott, B. Bhushan, "Corrosion and wear studies of uncoated and ultra-thin DLC coated magnetic tape-write heads and magnetic tapes", Wear 243 pp. 31–42, 2000.

[73] B. Pugh, "Friction and Wear – A Tribology Text For Students", Newnes-Butterworth, London, 1973.

[74] E. Sourty, J. L. Sullivan and M. D. Bijker, "The tribology of advanced digital recording (ADR) systems", Tribology International, Volume 33, Issue 9, pp. 629-637 September 2000.

[75] J. Halling, "Principles of Tribology", McMillan Press Ltd, pp. 22-35, 1983.

[76] R.J. Anderson, "High Speed Tape Mechanics" NML Technical Report, December 1996.

[77] R.F. Hegal, "Tribology Transactions", 36, 1993, 67

[78] E. Rabinowicz, "Friction and Wear of Materials", Wiley, New York,1965.

[79] B. Bhushan and S. Sundararajan, "Micro/Nanoscale Friction and Wear Mechanisms of Thin Films using Atomic Force and Friction Force Microscopy", Acta mater. Vol. 46, No. 11, pp. 3793-3804, 1998.

[80]Elford, C.L. and Reed, D.A., "Technology trends and Disk Array Performance", Journal of Paralel and Distributed Computing, Vol. 46, pp. 136-147, 1997.

[81] Anderson. R.M. Bhushan. B. "Concurrent Measurement of In Situ Friction Force and Head Signal Amplitude During Dropouts in Rotary Head Tape Drives" Wear V.202 1996.

[82] C. J. Pritchard & B. K. Middleton, "An Instrument for Detecting and Recording Drop-outs from Magnetic Tape", Mease. Sci. Technol. 2, pp. 684-685, 1991.

[83] Patton. S. T. Bhushan. B."Tribological Evaluation of the Streaming Mode Performance of Metal Evaporated and Metal Particle Tapes" IEEE Transactions on Magnetic Recording, V 32 No 5 Sept 1996.

[84] J.R.Hone, " The Automatic Dropout Analysis Instrument", PhD Thesis, Uniuversity College of Swansea, 1991.

[85] Stek. A. Stupp. S. E. Luitjens S.B, "Some Aspects of Overwrite in Thick Magnetic Media" IEEE Transactions on Magnetics Vol. 32. No. 5. Sept 1996.

[86] R. L. Arudi J. A. Mc Cracken, "Metal in Gap Head Staining" Minutes of THIC Meeting, October 3 1989.

[87] Bhushan. B. Hahn. W. H. Jr, "Stains on Magnetic Tape Heads "Wear V. 184 1995.

[88] Kamei, T. et al, "Removal of brown stain on magnetic head by a chelating agent on magnetic tapes.", Journal of Magnetism and Magnetic Materials, Vol. 193, pp 291-295, 1999.

[89] J. Lauer P. M. Blanc, "Friction Polymer Buildup on a Tape Head by Ellipsometry and Infrared Emission", Polym. Prepr. Am. Chem. Soc. Div. Polym. Chem., 29 (2) 1988, P 275 - 276.

[90] R. J. Owen, 2Magnetic Head/Tape Interface Study for Satellite Tape Recorders", IIT Reasearch Institute, Chicago, lL, IITRI/NASA Goddard Contract NAS5-11622, Vol. 2, 1970, pp. 132 - 137.

[91] N. Ishiwata et al, "Narrow Track MR Head Technology", IEEE Transactions On Magnetics, Vol. 32, No. 1, pp 38-42, January 1996.

[92] Tian. H. Lee. J. "Electrostatic Discharge Damage of MR Heads" IEEE Transactions on Magnetics Vol. 31. No. 6. Nov 1995.

[93] B. Bhushan. V. Khatavkar, "Role of Water Vapour on the Wear of Mn-Zn Ferrite Heads Sliding against Magnetic Tapes" Wear 202, pp. 30-34,1996.

[94] Jianghong Gong, Zhe Zhao, Hezhuo Miao and Zhenduo Guan, :*R*-Curve behaviour of TiC Particle Reinforced Al_2O_3 Composites", Scripta materialia, 43, pp 27-31, 2000.

[95] Jianghong Gong *, Zhe Zhao, Zhenduo Guan, Hezhuo Miao, "Load-dependence of Knoop hardness of $Al_2 O_3$ -TiC composites", Journal of the European Ceramic Society 20 pp. 1895-1900, 2000.

[96] J. Li et al "A fine Al_2O_3–TiC–Co ceramic and its erosion behaviour", J. Phys. D: Appl. Phys. 30 pp. 2234–2239, 1997.

[97] S.Y. Guo et al, "The Friction-Wear Behaviour of Al_2O_3–TiC-Co Advanced Ceramic during in-situ SEM", Wear 203-204, pp.319-324, 1997.

[98] Harrison, M.J.K., Sullivan, J.L. and Theunissen, G.S.A.M., "Wear mechanisms of sandwich-type video heads". Procedure of the Institute of Mechanical Engineers, Part J, Journal of Engineering Tribology, Vol. 211, pp.263–277, 1997.

[99] E. Sourtey, M. Wild, J.L. Sullivan, "?" Aston University Unpublished work.

[100] B.Bhushan & D.V. Khatavkar, "Rle of Wator Vapor on the Wear of Mn-Zn Ferrite Heads Sliding against Magnetic Tapes" Wear, Vol, 202, pp. 30-34, 1996.

[101] Morioka. Y. et-al, "An Analysis of Tape to Head Spacing by Three Dimensional Computer Stimulation" IEEE Transactions on Magnetics Vol. 27. No. 6. Nov 1991.

[102] B. Bhushan. J.A lowry, "Friction and Wear Studies of Various Head Materials and Magnetic Tapes in a Linear Mode Accelerated Test using a New Nano-Scratch Wear Measurement Technique." Wear 190, pp. 1-15,1995.

[103] B.Bhushan and S.T.Patton, "Friction and Wear of Ultra High Density Magnetic Tapes", Journal of Applied Physics, Vol. 75, No. 10, pp. 5771-5773, 1994.

[104] B. Bhushan & S.T. Patton, "Friction and Wear of Metal Particle, Barium Ferrite and Metal Evaporated Tapes in Rotary Head Recorders", Journal of Tribology, Vol. 118, January, 1996, pp. 21-32.

[105] M.S. Hempstock & J.L. Sullivan, "A Study of the Mechanical and Magnetic Performance of Metal Evaporated Tape", Journal of Magnetism and Magnetic Materials, Vol. 115, pp. 323-328, 1996.

[106] B. Bhushan & V.N. Koinkar, "Microtribology of Metal Particle, Barium Ferrite and Metal Evaporated Magnetic Tapes", Wear, Vol. 181-183, 1995, pp. 360-370.

[107] Fujiwara. I. Kamei. T. Tanaka. K, "Friction Force Microscopy (FFM) Study of Lubricant Thin Films on Thin Magnetic Recording Media" Journal of Applied Physics Vol. 78 No 6 1995.

[108] Bhushan. B. Khatavkar. V, "Role of Tape Abrasivity on Friction, Wear, Staining and Signal Degradation in Audio Tapes" Wear 190, 1995.

[109]Xu, J. et-al, "The Effect of Temperature and Humidity on the Friction and Wear of Magnetic Tape", Wear, 203-204, pp.642-647, 1997.

[110] Hempstock. M.S. Wild. M.A. Sullivan. J.L. "Interactions at the Head–Tape Interface of a Linear Tape System", Tribology International, Vol. 33 pp.391–399, 2000.

[111] Bhushan.B. Hahn. F. "Stains on Magnetic Tape Heads", Wear, 184, pp.193-202, 1995.

[112] J.K.Lancaster, "A review of the Influence of Environmental Humidity and Water on Friction, Lubrication and Wear", ASME Journal od Tribology, Vol. 29. No. 6, pp.371-389, 1990.

[113] E.F. Cuddihy, "Hygroscopic Properties of Magnetic Recording Tape", IEEE Transactions on Magnetics, Vol. MAG-12, No. 2, 1976.

[114] Harrison. M. J. K. Sullivan J. L. and Theunissen G. S. A. M. "Pole Tip Recession in Sandwich Heads incorporating a FeTaN Soft Magnetic Track", Tribology International Vol. 31, No. 9, pp. 491–500, 1998.

[115] Li. Y, Talke. F.E, " a Model for the Effect of Humidity on Stiction of the Head/Disk Interface", Tribology International Vol. 35, pp. 429–434, 1992.

[116]Hempstock. M. S. and Sullivan. J. L, "Characterization of Surface Changes to Metal evaporated and Metal Particle Media Following Durability Tests in Helical Scan Hi-8 Recorders at Ambient and High Humidity Conditions". Tribology International, Vol. 31, No. 8, pp. 419–424, 1998.

[117] Smith, G.C., "Quantitative surface analysis for materials science.", The Institute of Metals, 1991, pp All.

[118] Watts, John F., "An introduction to surface analysis by electron spectroscopy.", Oxford University Press, Royal Microscopical Society, 1990, pp All.

Appendix

Tribology International Vol. 31, No. 8, pp. 435–441, 1998

Printed in Great Britain
0301-679X/98/$19.00 + 0.00

PII: S0301-679X(98)00065-6

A study of the durability of flexible magnetic media in a linear tape system

ELSEVIER

Tribology International 33 (2000) 391–399

TRIBOLOGY INTERNATIONAL

www.elsevier.com/locate/triboint

Interactions at the head–tape interface of a linear tape system

M.S. Hempstock, M.A. Wild, J.L. Sullivan *

Surface Science Research Group, School of Engineering and Applied Science, Aston University, Birmingham, B4 7ET, UK

The Tribology of Flexible Magnetic Recording Media in Linear Tape Systems and its Impact on Signal Performance

JOHN L. SULLIVAN, MIKE S. HEMPSTOCK & MARK A. WILD, *Aston University, Birmingham, UK*

Pole tip recession and staining at the head to tape interface of linear tape recording systems

E. Sourty*, M. Wild and J.L. Sullivan

Surface Science Research Group, School of Engineering and Applied Science,

University of Aston, Birmingham B4 7ET